1993

An improved technique to determine the controlling unstable equilibrium point in a power system

Roger Thomas Treinen
Iowa State University

Order Number 9414026

An improved technique to determine the controlling unstable equilibrium point in a power system

Treinen, Roger Thomas, Ph.D.

Iowa State University, 1993

U·M·I
300 N. Zeeb Rd.
Ann Arbor, MI 48106

An improved technique to determine the controlling unstable equilibrium point in a power system

by

Roger Thomas Treinen

A Dissertation Submitted to the
Graduate Faculty in Partial Fulfillment of the
Requirements for the Degree of
DOCTOR OF PHILOSOPHY

Department: Electrical Engineering and Computer Engineering
Major: Electrical Engineering (Electric Power Systems)

Approved:

Signature was redacted for privacy.

In Charge of Major Work

Signature was redacted for privacy.

For the Major Department

Signature was redacted for privacy.

For the Graduate College

Members of the Committee:

Signature was redacted for privacy.

Iowa State University
Ames, Iowa

1993

TABLE OF CONTENTS

LIST OF FIGURES

LIST OF TABLES

ABSTRACT

In the past fifteen years considerable progress has been made in first swing power system transient stability assessment using the transient energy function (TEF) method.

The accuracy of stability assessment provided by the TEF method depends on the determination of the controlling unstable equilibrium point (UEP). The technique that determines the controlling UEP in the current commercial version (Version 3.0) of the TEF method program is based on the so-called 'exit point method' and has also been recently labeled the 'BCU method.'

The exit point method consists of two basic steps. They are the detection of the exit point θ^e and detection of the minimum gradient point θ^o. The controlling UEP is solved for by using θ^o as an initial guess.

It has been observed that this method lacks robustness in the sense that the following two problems may occur.

Problem 1: There may be no detection of the point θ^o.

Problem 2: If θ^o is found, it may not be in the domain of convergence of θ^u for the particular solving algorithm used. Hence, another equilibrium point, not the controlling UEP will be located.

The result of this research has been the development of a new numerical technique for determining the controlling UEP. With the exit point as an initial starting point this technique efficiently produces a sequence of points. A significant part of this dissertation was the formulation of an analytical foundation which shows that under certain assumptions this sequence will converge to the controlling UEP. Hence this new technique exhibits a substantial improvement over the exit point method because of the following reasons

- The technique does not attempt to detect the point θ^p.
- The technique can produce a point that is close to θ^u thus avoiding a domain of convergence problem.

This technique was applied to two realistic, large-scale power systems. In every case an accurate stability assessment was provided.

1. INTRODUCTION

1.1 The Need for Transient Stability Analysis of Power Systems

Transient stability analysis involves the study of electric power system characteristics and parameters under the effect of large disturbances so that a stability assessment can be made. These large disturbances may be caused by such events as: a sudden change in load, a three-phase fault on a major transmission facility, and line outages in which the lines are heavily loaded. The system parameters that are usually monitored are synchronous generator angle, voltage at various buses, power flow over transmission lines and the apparent impedance seen by out-of-step relays. Typically, the stability assessment can be made by examining the relative angles of the synchronous generators during the transient period and stability is maintained if the generators remain in synchronism.

Transient stability of a power system is a concept that is part of power system security. In turn, the concept of power system security is encompassed by power system reliability. The North American Reliability Council (NERC) defines reliability in a power system as [1]:

> ***Reliability,*** *in a bulk electric system, is the degree to which the performance of the elements of that system results in electricity being delivered to customers within accepted standards and in the amount desired. The degree of reliability may be measured by the frequency, duration, and magnitude of adverse effects on the electric supply (or service to customers).*
>
> *Bulk electric system reliability can be addressed by considering two basic and functional aspects of the bulk electric system - adequacy and security.*

Thus, it is important that the power system retain this sense of reliability at all times. As the definition implies, reliability criteria need to be met both at steady-state operating conditions and through transient periods.

Reliability can be approached by considering two basic and functional aspects of the electric power system, adequacy and security. This suggests that one very important criterion is that the bulk power supply in North America be planned and operated with security in mind. NERC defines power system security as [1]:

> ***Security*** *is the ability of the bulk electric system to withstand sudden disturbances such as electric short circuits or unanticipated loss of system components.*

For a power system to be secure it must be stable (either steady-state or transient); this implies that power system transient stability is a vital concern in power system security. Transient stability of a power system is defined as [2]:

> *A power system is transiently stable for a particular steady-state operating condition and for a particular disturbance if, following that disturbance, it reaches an acceptable steady-state operating condition.*

Transient stability analysis studies usually involve time simulation in which numerical integration of the differential equations that govern the dynamics of synchronous generators as well the solution of the algebraic equations that describe the network are performed. These studies are performed off-line and are performed on a limited number of contingency scenarios. One outcome of the studies is the determination the critical clearing time of each of these contingencies. The critical clearing time is the maximum clearing time of a disturbance such that the power system still remains stable. In the North American interconnection, a large majority of the utilities do not set operating guidelines based on critical clearing times. Since most disturbances are cleared by relays or circuit breakers with preset

clearing times, the guidelines are normally based on stability limits and these limits are important to determine through these studies. Stability limits are usually limits on power flow across certain high voltage transmission lines and generation output of certain plants such that if the power system was being operated at these limits and a disturbance did occur somewhere in the system the clearing time of the preset relays would result in the system being unstable.

Power system operators are interested in such studies since it is their responsibility that the power system remain secure at all times in the sense that not only does the system need to remain stable but all reliability criteria need to be met. If reliability criteria are violated, then remedial actions must be taken and these actions will be manifested through such things as proper operation of controls and protective equipment, adequate sources of real and reactive power when needed and so on. Since the operating point of the electric power system is an ever changing entity due to such occurrences as load changes and economical dispatching of generation the operator is not only concerned about the security of the system at the present moment but also the security of the system as it moves and settles to a new operating point. Information compiled from these off-line studies are available to the operator so operating decisions can be made with security in mind. Planning engineers also conduct many transient stability studies in planning further additions to the power system. Their primary concern is that new additions to the power system do not decrement the stability properties of the system and to make sure all of the reliability criteria, which apply to dynamic system performance, are met.

In today's modern power system there is not only a need for transient stability analysis but a need for a much more diverse type of transient stability analysis by the operators and planners. The reason is that modern power systems such as the North American interconnected power system are becoming more stressed in the sense that in certain areas generation as well as transmission facilities are loaded at or above their rated capability or operating limits. There are many reasons why these stressed conditions exist and power systems are operating at or near their limits:

- Heavier use of existing transmission facilities because of the policy to conserve oil and natural gas which has resulted in limited operation of oil-fired and gas-fired power plants. The increased dependence on other types of plants has resulted in shipment of large blocks of economy power to load centers over high capacity transmission lines.

- Fewer high voltage transmission lines are being built because of: right of way restrictions, regulatory delays, and the high capital costs incurred.

- Heavier loading of transmission lines has become so common that some transmission lines which had been built for emergency use are now often being used for normal operation. Because of this heavy loading, the transmission network operates in a stressed condition.

If the power system is stressed and thus displays the above mentioned conditions, it may exhibit very different dynamic behavior from an unstressed system during a transient. For example, in the case of an unstressed system, the transient behavior of the system due to a disturbance is easy to analyze because the behavior is dominated by the effects of location and duration of the disturbance itself. For the reliability criteria to be upheld in this case, limits may be placed on the duration of the disturbance and on the power being generated by units close to the disturbance.

In contrast, a stressed system may behave quite differently and manifest a complex dynamic behavior. These stressed conditions arise from the large power transfers and heavy loading of the transmission network as stated earlier. Typically, when a disturbance, such as a large three-phase fault, occurs in the stressed case, the dynamic behavior is initially controlled by the generators electrically close to the disturbance. As the transient progresses, the behavior may be dominated by generators that are remote from the disturbance. In fact, situations may arise in stressed systems in which the post-disturbance system is not even steady-state stable [2]. It follows directly that the analysis of this situation becomes more complex than that of the unstressed case.

1.2 Need for Direct Methods of Transient Stability Assessment

It is quite clear that the power system operator and planner are faced with a power system that is quite large and complex. In particular, the operator is faced with the problem that a large disturbance can occur at a great number of locations in the system and there are almost an infinite number of possible operating states. Also, since in many stressed situations the dynamic performance of the system can be quite complex and even unpredictable there is no guarantee that the off-line analysis can give any help to the system operators in making decisions concerning system security. Faced with this dilemma, it might be in the best interest of the system operator to have a near real-time transient stability analysis tool that provides the means of assessing transient stability on-line. Also, since the power system is usually operating near its limits a qualitative measure of the degree of stability of the power system would also be of great help. In this way the operator does not have to rely entirely on off-line studies to make decisions.

Realistically there are only a few transient stability analysis tools that the operator or planner could use. Four possible types of analysis tools, realistic or not, that might be of assistance if the operator is confronted with the problems stated above are given below.

i) The dynamics of a power system are governed by a coupled set of nonlinear algebraic and differential equations. If the operator had available the explicit closed form solution to these differential and algebraic equations that describe the power system then the transient stability problem can be easily dealt with. A simple calculation could determine the system conditions at the end of clearing and then using this point another calculation would be needed to see if the system is stable or not. A measure to determine the degree of stability would be just as simple to calculate. The problem with this is that up to now no explicit form of a solution has been found.

ii) The transient stability problem could also be easily dealt with if the operator had available an analysis tool that did the following: at any point along the disturbed system trajectory a calculation could be made which provided explicit information for the assessment of transient stability. The assessment would be made under the assumption that the disturbance would be cleared at that point. Also a measure for the degree of stability could be easily obtained. Again the problem with this is that no such tool exist.

iii) The operator does have time simulation techniques but these techniques are time consuming since the equations need to be simulated for a relatively long period of time for transient stability assessment to be made. Also, this analysis does not provide any measure for the degree of stability.

iv) If the operator had a tool that would provide a good approximation to the assessment of transient stability, not be computationally burdensome and provide a measure of the degree of stability then this tool based on the above discussion would fulfill the needs of the operator. Such a tool does exist in the form of direct methods of transient stability assessment.

Direct methods of transient stability analysis offer alternative means of assessing transient stability when compared to time simulation. Direct methods have the potential to provide a near-real time assessment of transient stability, and in addition, can provide information regarding relative degrees of stability at different operating configurations.

The direct stability analysis based on the transient energy function (TEF) method is a potential candidate to meet requirements of near real-time transient stability evaluations. Therefore the TEF method is a potential candidate for near real-time transient stability assessment since it avoids time consuming step-by-step time domain simulation and provides a qualitative measure of the degree of system stability via an energy margin.

1.3 Review of Direct Methods of Transient Stability Analysis

Direct methods consist of two primary groups. Methods that are based on some energy criterion that is used for transient stability analysis and methods that are based on the second or direct method of Lyapunov [3] which use this Lyapunov theory for transient stability analysis. These methods are related since nearly all the Lyapunov functions used are energy based.

1.3.1 Early Work on Energy Functions

The early work on direct methods was concerned with an energy criterion for transient stability analysis. The earliest energy method for transient stability analysis is the well-known *equal area criterion* for a single machine-infinite bus system. This criterion simply states that if all the kinetic energy acquired by the generator during the disturbed period can be converted into potential energy, after the disturbance is cleared, the system will be stable. Kimbark [4] gives a detailed treatment of this subject.

Since the time of the equal area criterion many attempts have been made to extend this idea of an energy criterion to multi-machine systems. Overall, in the investigations of direct stability analysis there have been two main categories of interest: 1) development of functions which accurately represent the system energy, and 2) correctly identifying the *critical value* of this energy. The following is an overview of the main contributions to the area of direct stability analysis starting from the equal area criterion to the present day.

In 1930 Gorev [5] (from the former Soviet Union) used the first integral of energy to obtain a criterion for power system stability for a three-machine system with zero transfer conductances. This criterion used a solution method equivalent to the determining of a region of stability for the stable equilibrium point.

In 1947 Magnusson [6] developed a technique very similar to Gorev in which a three-machine system with zero transfer conductances were used. The significant difference between Magnusson's formulation and that of

Gorev's is that Magnusson derived a potential energy function with respect to the post-disturbance stable equilibrium point.

In 1958 Aylett [7] proposed an *energy integral criterion* for multi-machine systems. He analyzed the phase-plane trajectories of a multi-machine system in which the classical model was employed and transfer conductances were omitted. Aylett points out by using a two-machine system, that there is a critical phase-plane trajectory which passes through the saddle point, which he called the separatrix (i.e., a manifold). A criterion for system stability was developed by examining the phase-plane trajectory. If the phase-plane trajectory started outside of the separatrix, it becomes unbounded, hence the system becomes unstable. Aylett also developed an energy integral for the system. He shows that the energy versus angle curve has two regions separated by a curve which passes through the saddle point. The stable situation corresponds to the region inside of the curve for which kinetic energy is less than potential energy. The unstable situation corresponds to the region outer to the curve for which the kinetic energy is greater than the potential energy. These regions introduce the concept of *region of stability*. The most significant aspect of this work is the formulation of a system of equations based on the inter-machine motion.

In 1972 Tavora and Smith [8] dealt with the transient energy of a multi-machine system and examined equilibrium points. They used the classical model with zero transfer conductances as well as the center of angle (now referred to as center of inertia) formulation for the swing equations. Using this model Tavora and Smith obtained an expression for the transient kinetic energy which the authors say determines stability. The authors suggested that for stability to be maintained, the trajectory, after the last phase of the disturbance, be confined to what they called a *potential well*. Thus they concluded that for stability to be maintained, the total energy of the disturbed motion must be less than that needed to escape from the potential well.

1.3.2 Application of Lyapunov's Direct Method

The work reported in Section 1.3.1 used the concept of an energy criterion in the analysis of transient stability for the power system and by the middle 1960's most work on power system stability analysis was refocused on direct methods consisting of Lyapunov functions. Lyapunov direct methods then emerged as a solution to the power system stability problem. Earlier work in this area was done by Gless [9] and El-Abiad and Nagappan [10].

Gless used an example of a single machine-infinite bus without transfer conductances and matched the results obtained by direct methods to those obtained by using the equal area criterion and Aylett's phase-plane technique.

In Section 1.3.1 it was stated that an important issue in an energy criterion method was to determine the critical value of the energy. This idea of a critical value can also be applicable when a Lyapunov direct method based on energy is used. The critical value in this setting is usually the largest value of energy such that the conditions for stability as stated in the theorems of Lyapunov's direct method are satisfied. In 1966 El-Abiad and Nagappan developed a valid Lyapunov function for a multi-machine system without transfer conductances. They identified the unstable equilibrium point with the lowest potential energy as the unstable equilibrium which gave the critical energy. The stability region that resulted was bounded and all conditions from Lyapunov's direct method theory were satisfied. This procedure however, generally produced conservative estimates for transient stability assessment. They also developed a function with transfer conductances which they claim is a valid Lyapunov function since when the norm of the state vector is larger than some small constant the time derivative of the function is negative semi-definite. However this cannot be considered a true Lyapunov function.

Gupta and El-Abiad [11] worked on this problem and they showed that the unstable equilibrium point with the least potential energy may not be near the disturbed system trajectory at all. They used an unstable equilibrium point that was close to the disturbed trajectory for the critical value.

Up to this point nearly all of the power system models for which a valid Lyapunov function can be constructed neglected transfer conductances. It was shown by Sastry [12] that since the power system is reduced to the internal generator nodes the model is not realistic if the transfer conductances are neglected. In most situations if the transfer conductances are present then the resulting Lyapunov-like function has a path dependent integral where the path is the trajectory of the post-disturbance system. In fact, Willems [13] claims that the Lyapunov method cannot be applied when transfer conductances are present since this results in an indefinite time derivative of the candidate function.

An attempt has been made by Uemura [14] to approximate the path dependent terms due to the transfer conductances by linear approximations.

1.3.3 Improvements to the Direct Methods

Because of the difficulties transfer conductances present the focus in late 1970's on direct methods was again on developing a suitable energy function which could be expressed in terms of physical energy components but had a Lyapunov-like structure.

Athay, Podmore et al. [15], in 1979 at System Control, Inc. (SCI) made significant progress towards the development of the so called *transient energy function (TEF) method* which is the basis of the method used at Iowa State University today. Notable accomplishments of this work are:

- incorporation of the COI formulation and approximation of path dependent terms in the energy function,

- determination of the relevant UEP in the direction of the system trajectory, and hence the determination of the critical transient energy,

- investigation of the potential energy boundary surface (PEBS) which was first developed by Kakimoto et al. [16],

- use of extensive computer simulations to investigate energy behavior as well as other system functions at different instants in the transient.

Although the work from SCI was a tremendous breakthrough, drawbacks were still evident. The procedure developed still provided conservative results for a wide range of faults locations. Intensive work by Fouad et al. [17, 18] at Iowa State University led to the following findings:

- Not all the excess kinetic energy at the instant of fault clearing contributes directly to the separation of critical machines from the rest of the system. This component of kinetic energy which accounts for the other inter-machine swings should be subtracted from the energy that need to be absorbed by the system for stability to be maintained. This gave way for what is known as the corrected kinetic energy.

- When more than one generator tends to lose synchronism, instability is determined by the gross motion of these machines, i.e., by the motion of their center of inertia.

- The concept of a *controlling UEP* for a particular system trajectory is a valid concept.

- Not all the machines that are advanved (i.e., have angles greater than *90°*) at the controlling UEP loss synchronism.

Fouad et al. [19] also developed a criterion known as the *mode of disturbance (MOD) method* to identify the controlling UEP among several candidate UEPs. This innovative criterion accounts for two aspects of the transient dynamic behavior of the system namely:

- the effect of the disturbance on various generators (i.e., fault location),

- the energy absorbing capacity of the post-disturbance network.

Chiang et al. [20] verified the foundations of this procedure and presented a theoretical foundation for the direct method by providing a mathematical and physical reasoning for the existence of the controlling UEP.

Chiang et al. [21] then showed that for a power system without transfer conductances the stability boundary is composed of the union of stable manifolds. A numerical scheme was suggested in order to determine the controlling UEP. In this method the associated gradient system was utilized along with a computational scheme suggested by Kakimoto [16]. The constant energy surface which passed through the controlling UEP was used to approximate the relevant stability boundary of the power system. The relevant stability boundary is the part of the stability boundary where the disturbed trajectory passes. This method is referred to as the *exit point method* but has recently also been called the *BCU method* [22]. This scheme consists of detecting the exit point of the associated gradient system along the projected disturbed trajectory. In actuality, this consists of finding the first maximum of potential energy that the disturbed trajectory encounters when projected into angle-space. The gradient system, with the exit point as the initial condition, is integrated to a point x, which is very close to the controlling UEP. Finally, the UEP is solved for with x as the starting point. The critical energy is then the potential energy at the controlling UEP.

This exit point method described above is employed for identifying the controlling UEP, and hence the critical energy, in the TEF method.

In 1982, Vittal [23] and Michel et al. [24] developed an individual machine energy function in order to identify the transient energy pulling a particular machine from the rest of the system. Michel et al. [24] have concluded that system separation does not depend on the total system energy, but rather on the transient energy of individual machines or groups of machines. However, the individual machine energies along the faulted trajectories need to be evaluated at each time step, thus increasing the computation time.

There are two survey papers available on direct methods applied to power systems , Fouad [25, 1975] and Ribbens-Pavella, [26, 1985] and three

books on this subject, Fouad and Vittal [27, 1992] and Pai [28, 1988] and [29, 1981].

1.4 Motivation for the Present Work

In the TEF method the exit point method is used to determine the controlling UEP. The reason for this is that this method is computationally straightforward. It has been observed, however, while applying the TEF method to certain cases that the exit point method does not work correctly. There seems to be two problems that occur:

1. The method does not produce an UEP but instead the stable equilibrium point.

2. The method may not determine the controlling UEP but instead another unstable equilibrium point in which case an incorrect critical energy would result.

1.5 Scope of this Research Work

The main objectives of this research work are:

1. develop a numerical procedure that when incorporated into the exit point method eliminates the above mentioned problems,

2. under certain assumptions analytically justify the use of the procedure,

3. apply the TEF method with this new procedure incorporated to large-scale realistic power systems to obtain transient stability assessment results and compare these with time simulation,

2. MATHEMATICAL MODEL

The contents of this chapter consists of three sections with each having the following description.

Section 2.1 The mathematical equations in center of inertia that model the dynamics of a generator for the classical model of a power system are presented.

Section 2.2 The transient energy function is derived in the center of inertia.

Section 2.3 A presentation of how the transient stability assessment is performed using the transient energy function.

2.1 System Equations

The simplest model representing a multi-machine power system, called the classical model [30, Chapter 2], is used throughout this research project. This model is based on the following assumptions.

1. Mechanical power input remains constant for each machine during the transient period.
2. Damping or asynchronous torque is negligible.
3. The synchronous machine can be represented by a constant voltage source behind the transient reactance.
4. The motion of the machine rotor coincides with the angle of the voltage behind the transient reactance.
5. Loads are represented by passive impedances.

The classical model of a synchronous machine may be used to study the stability of a power system in an inertial transient, during which the system dynamic response is dependent largely on the stored kinetic energy in the rotating masses and the synchronizing torques. For many power systems, the length of time of this transient is on the order of one second or less [30, Chapter 2].

With the loads represented by constant impedances, the load nodes and the terminal voltage nodes of the machines are eliminated. The resulting network contains only the internal machine nodes. The machine reactances and the constant impedance loads are included in the network admittance matrix ($\boldsymbol{Y}_{bus}$).

Throughout the rest of this chapter variables to be defined such as δ, θ, ω, and ϖ are taken to be vectors unless they are subscripted with a i, j or k in which denotes the corresponding element in the vector. Based on the above assumptions, the nonlinear differential equations which are referred to as the swing equations that govern the dynamics of the n machine system are given by the following equations and the point δ^s will denote the stable equilibrium point (SEP) for these equations

$$\frac{2H_i}{\omega_r}\dot{\omega}_i = P_i - P_{ei} \tag{2.1}$$

$$\dot{\delta}_i = \omega_i - \omega_r \qquad i = 1, 2, \ldots, n$$

where

$$P_i = P_{mi} - E_i^2 G_{ii} \tag{2.1b}$$

$$P_{ei} = \sum_{\substack{j=1 \\ j \neq i}}^{n} \left[C_{ij} \sin\left(\delta_i - \delta_j\right) + D_{ij} \cos\left(\delta_i - \delta_j\right)\right] \tag{2.1c}$$

$$C_{ij} = E_i E_j B_{ij} \text{ and } D_{ij} = E_i E_j G_{ij}$$

and

n - number of machines in the power system,
G_{ii} - driving point conductance,
P_{mi} - mechanical power input,
E_i - internal voltage behind the transient reactance,
H_i - normalized inertia constant,
ω_i - absolute machine rotor speed,
ω_r - speed of the synchronously rotating reference frame,
δ_i - machine angle deviation with respect to a synchronously rotating reference frame,
G_{ij} - the real part of the transfer admittance in the system reduced to the internal nodes between machines i and j.
B_{ij} - the imaginary part of the transfer admittance in the system reduced to the internal nodes between machines i and j.

Note, since damping is neglected for all machines the minimal order of the state-space of the n machine power system described by equation (2.1) is $2(n-1)$ [31].

Transforming equations (2.1) into the center of inertial (COI) reference frame, provides a better physical insight to the transient stability problem formulation. This formulation conveniently removes the kinetic energy associated with the acceleration of the inertial center of the system during a transient [8]. In order to transform equations (2.1) to the COI reference frame, the following must be done.

Define M_i and M_T as follows.

$$M_i \equiv \frac{2H_i}{\omega_r}$$

$$M_T \equiv \sum_{i=1}^{n} M_i$$

Let δ_o be the center of inertia (COI) angle and define it as

$$\delta_o = \frac{1}{M_T} \sum_{j=1}^{n} M_j \, \delta_j \tag{2.2}$$

Then

$$\omega_o = \dot{\delta}_o = \frac{1}{M_T} \sum_{j=1}^{n} M_j \, \dot{\delta}_j \Rightarrow \dot{\omega}_o = \ddot{\delta}_o = \frac{1}{M_T} \sum_{j=1}^{n} M_j \, \ddot{\delta}_j = \frac{1}{M_T} \sum_{j=1}^{n} M_j \, \dot{\omega}_j$$

Define the new COI angles and speeds as

$$\theta_i = \delta_i - \delta_o$$

$$\varpi_i = \dot{\delta}_i - \dot{\delta}_o$$

Then

$$\theta_i = \delta_i - \delta_o \Rightarrow \varpi_i = \dot{\theta}_i = \dot{\delta}_i - \dot{\delta}_o \Rightarrow \dot{\varpi}_i = \ddot{\theta}_i = \ddot{\delta}_i - \ddot{\delta}_o = \dot{\omega}_i - \dot{\omega}_o$$

$$\dot{\varpi}_i = \dot{\omega}_i - \dot{\omega}_o \Rightarrow M_i \, \dot{\varpi}_i = M_i \, \dot{\omega}_i - M_i \, \dot{\omega}_o$$

$$M_i \, \dot{\varpi}_i = P_i - P_{ei} - M_i \, \dot{\omega}_o = P_i - P_{ei} - \frac{M_i}{M_T} \sum_{j=1}^{n} (P_j - P_{ej})$$

Define P_{COI} as below, where P_i and P_{ei} are taken from equations (2.1b) and (2.1c).

$$P_{COI} = \sum_{i=1}^{n} (P_i - P_{ei}) = \sum_{i=1}^{n} P_i - 2 \sum_{i=1}^{n-1} \sum_{j=i+1}^{n} D_{ij} \cos(\delta_i - \delta_j)$$

It is evident that

$$M_T \, \dot{\omega}_o = \sum_{i=1}^{n} M_i \, \dot{\omega}_i = \sum_{i=1}^{n} (P_i - P_{ei}) = P_{COI} \tag{2.3}$$

Since M_T is the total inertia of the system and δ_o is the center of inertia angle, P_{COI} is then the power that accelerates the center of inertia of the system.

Note that the vectors, θ and ϖ, always satisfy the constraints of the inertial center reference frame. This can be seen as

$$\sum_{i=1}^{n} M_i \theta_i = \sum_{i=1}^{n} M_i \delta_i - \sum_{i=1}^{n} M_i \delta_o = \sum_{i=1}^{n} M_i \delta_i - \frac{M_T}{M_T} \sum_{i=1}^{n} M_i \delta_i = 0 \qquad (2.4a)$$

$$\sum_{i=1}^{n} M_i \varpi_i = \sum_{i=1}^{n} M_i \dot{\delta}_i - \sum_{i=1}^{n} M_i \dot{\delta}_o = \sum_{i=1}^{n} M_i \dot{\delta}_i - \frac{M_T}{M_T} \sum_{i=1}^{n} M_i \dot{\delta}_i = 0 \qquad (2.4b)$$

The n^{th} machine angle and the n^{th} machine speed terms, θ_n and ϖ_n derived from equations (2.4) are:

$$\theta_n = -\frac{1}{M_n} \sum_{i=1}^{n-1} (M_i \theta_i) \qquad (2.5a)$$

$$\varpi_n = -\frac{1}{M_n} \sum_{i=1}^{n-1} (M_i \varpi_i) \qquad (2.5b)$$

In the inertial center reference frame the nonlinear differential equations that govern the dynamics of the power system are shown below.

$$M_i \dot{\varpi}_i = P_i - P_{ei} - \frac{M_i}{M_T} P_{COI} \qquad (2.6a)$$

$$\dot{\theta}_i = \varpi_i \qquad i = 1, 2, \ldots, n-1 \qquad (2.6b)$$

The point δ^s is transformed into the point θ^s which denotes the SEP of the power system in the COI reference frame.

Equation (2.6a) is very similar to equation (2.1), but in equation (2.6a) a fraction of P_{COI} which is based on that machine's inertia is subtracted from

the right hand side. This subtraction over all the machines results in a total subtraction of P_{COI}. Note that because of equations (2.4) the minimal order of the state-space of equations (2.6) is $2(n-1)$. Thus, throughout the rest of this research project, the order of the state-space representation will be $(\theta, \varpi) = (\theta_1, \theta_2, \ldots, \theta_{n-1}, \varpi_1, \varpi_2, \ldots, \varpi_{n-1})$. Equations (2.6) with equation (2.5a) substituted in can be written explicitly as

$$\begin{aligned}
M_i \dot{\varpi}_i = {} & P_{mi} - E_i^2 G_{ii} - \sum_{\substack{j=1 \\ j \neq i}}^{n-1} \left[C_{ij} \sin(\theta_i - \theta_j) + D_{ij} \cos(\theta_i - \theta_j) \right] \\
& - C_{in} \sin\left(\theta_i + \frac{1}{M_n} \left(M_1\theta_1 + M_2\theta_2 + \cdots + M_{n-1}\theta_{n-1} \right) \right) \\
& - D_{in} \cos\left(\theta_i + \frac{1}{M_n} \left(M_1\theta_1 + M_2\theta_2 + \cdots + M_{n-1}\theta_{n-1} \right) \right) \\
& - \frac{M_i}{M_T} \sum_{k=1}^{n} \left(P_{mk} - E_k^2 G_{kk} \right) \\
& + 2 \frac{M_i}{M_T} \sum_{k=1}^{n-1} \sum_{j=k+1}^{n-1} D_{kj} \cos(\theta_k - \theta_j) \\
& + 2 \frac{M_i}{M_T} \sum_{k=1}^{n-1} D_{kn} \cos\left(\theta_k + \frac{1}{M_n} \left(M_1\theta_1 + M_2\theta_2 + \cdots + M_{n-1}\theta_{n-1} \right) \right)
\end{aligned}$$

$$\dot{\theta}_i = \varpi_i \qquad i = 1, 2, \ldots, n-1 \qquad (2.7)$$

The right-hand side of equation (2.6a) is referred to as f_i,

$$f_i = P_i - P_{ei} - \frac{M_i}{M_T} P_{COI} \qquad (2.8)$$

and note that

$$\sum_{i=1}^{n} f_i = \sum_{i=1}^{n} (P_i - P_{ei}) - \frac{P_{COI}}{M_T} \sum_{i=1}^{n} M_i = P_{COI} - P_{COI} = 0$$

2.2 Transient Energy Function in the Center of Inertia Formulation

As noted in Section 1.3.3 the TEF used at Iowa State University and in this dissertation is based on the function derived by Athay, Podmore et. al. [15]. This function is derived on the basis of the physical energy of the system. The contents of this section is a presentation of the derivation. It is shown that derivation can be put into a vector matrix form but for simplicity it is not derived in this fashion.

Equation (2.6a) can be written as

$$M_i \dot{\omega}_i = P_{ai} = P_i - P_{ei} - \frac{M_i}{M_T} P_{COI}$$

where P_{ai} is the accelerating power in per-unit. In reality though, the right hand side of equation (2.6a) should be accelerating torque T_{ai} in per-unit. The reason equation (2.6a) is accelerating power is that since the speed ω is nearly constant during the first part of the transient period P_{ai} is numerically equal to T_{ai} in per-unit.

The transient energy function which will be denoted as $V(\theta, \omega)$ can be derived as follows. First it must be noted that for a machine, $\int T\,(d\theta(t)/dt)\,dt$ = energy, where $\theta(t)$ is the angle of the rotor and T is the torque on the rotor and because $P_{ai} = T_{ai}$ in per-unit $\int P\,d\theta(t)/dt)\,dt$ = energy in per-unit. For each of the machines in the system the following equation always hold true with P_{ei} and P_{COI} functions of the variable $\theta(t)$.

$$M_i \dot{\omega}_i(t) - \left[P_i - P_{ei}(\theta(t)) - \frac{M_i}{M_T} P_{COI}(\theta(t)) \right] = 0 \qquad (2.9)$$

Let $\Theta(\tau)$, $\Omega(\tau)$ and τ be the variables of integration corresponding to the variables $\theta(t)$, $\omega(t)$ and t respectively. Multiply both sides of equation (2.9) by

$((d\Theta_i(\tau)/d\tau)\, d\tau)$ and integrate the left hand side from $\tau = 0$ to $\tau = t$ and sum over all machines in the power system. This integration depends on the path taken by $\Theta(\tau)$ and $\Omega(\tau)$ as τ varies. Let this path be denoted by C. Let $(\Theta(0),\Omega(0)) = (\theta^s,0)$ and $(\Theta(t),\Omega(t)) = (\theta,\varpi)$ so that $V(\theta, \varpi) = V(\Theta(t),\Omega(t))$. The integral takes the form

$$V(\Theta(t),\Omega(t)) = \sum_{i=1}^{n} \int_{\tau=0}^{\tau=t} \left[M_i\, \dot{\Omega}_i(\tau) - P_i + P_{ei}(\Theta(\tau)) + \frac{M_i}{M_T} P_{COI}(\Theta(\tau)) \right] \frac{d\Theta_i(\tau)}{d\tau} d\tau \quad (2.10)$$

This can be written in the form

$$V(\Theta(t),\Omega(t)) = \sum_{i=1}^{n} \int_{\tau=0}^{\tau=t} \left[M_i\, \dot{\Omega}_i(\tau) - f_i(\Theta(\tau)) \right] \frac{d\Theta_i(\tau)}{d\tau} d\tau$$

This also can be written as

$$V(\Theta(t),\Omega(t)) = \sum_{i=1}^{n-1} \int_{\tau=0}^{\tau=t} M_i\, \dot{\Omega}_i(\tau)\, \frac{d\Theta_i(\tau)}{d\tau} d\tau + \int_{\tau=0}^{\tau=t} M_n\, \dot{\Omega}_n(\tau)\, \frac{d\Theta_n(\tau)}{d\tau} d\tau$$

$$- \sum_{i=1}^{n-1} \int_{\tau=0}^{\tau=t} f_i(\Theta(\tau)) \frac{d\Theta_i(\tau)}{d\tau} d\tau - \int_{\tau=0}^{\tau=t} f_n(\Theta(\tau)) \frac{d\Theta_n(\tau)}{d\tau} d\tau$$

Since

$$\dot{\Omega}_i(\tau)\, \frac{d\Theta_i(\tau)}{d\tau} d\tau = \Omega_i(\tau) \frac{d\Omega_i(\tau)}{d\tau} d\tau$$

the above equation can be written as

$$V(\Theta(t),\Omega(t)) = \sum_{i=1}^{n-1} \int_{\tau=0}^{\tau=t} M_i\, \Omega_i(\tau)\, \frac{d\Omega_i(\tau)}{d\tau} d\tau + \int_{\tau=0}^{\tau=t} M_n\, \Omega_n(\tau)\, \frac{d\Omega_n(\tau)}{d\tau} d\tau$$

$$-\sum_{i=1}^{n-1}\int_{\tau=0}^{\tau=t} f_i(\Theta(\tau))\frac{d\Theta_i(\tau)}{d\tau}d\tau - \int_{\tau=0}^{\tau=t} f_n(\Theta(\tau))\frac{d\Theta_n(\tau)}{d\tau}d\tau \quad (2.11a)$$

Because of the following two COI constraint equations

$$\frac{d\Theta_n(\tau)}{d\tau} = \frac{-1}{M_n}\left(M_1\frac{d\Theta_1(\tau)}{d\tau} + \cdots + M_{n-1}\frac{d\Theta_{n-1}(\tau)}{d\tau}\right)$$

$$f_n(\Theta(\tau)) = -\left(f_1(\Theta(\tau)) + \cdots + f_{n-1}(\Theta(\tau))\right)$$

the previous equation for $V(\Theta(t),\Omega(t))$ can be written in vector matrix form as

$$V(\Theta(t),\Omega(t)) = \int_{\tau=0}^{\tau=t}\left[\left[M^{\varpi}\Omega(\tau)\right]\cdot\frac{d\Omega(\tau)}{d\tau}\right] - \left[\left[M^{\theta}f(\Theta(\tau))\right]\cdot\frac{d\Theta(\tau)}{d\tau}\right]d\tau \quad (2.11b)$$

with $\Omega(\tau) = (\Omega_1(\tau), \ldots, \Omega_{n-1}(\tau))^T$, $\Theta(\tau) = (\Theta_1(\tau), \ldots, \Theta_{n-1}(\tau))^T$ and $f(\Theta(\tau)) = (f_1(\Theta(\tau)), \ldots, f_{n-1}(\Theta(\tau)))^T$. The matrices M^{θ} and M^{ϖ} are defined as

$$M_{ij}^{\theta} = \begin{cases} \left(1+\dfrac{M_i}{M_n}\right) & \text{if } i=j \\ \dfrac{M_i}{M_n} & \text{if } i\neq j \end{cases}$$

$$M_{ij}^{\varpi} = \begin{cases} M_i\left(1+\dfrac{M_i}{M_n}\right) & \text{if } i=j \\ \dfrac{M_i M_j}{M_n} & \text{if } i\neq j \end{cases}$$

A partial closed form solution for the function $V(\theta,\varpi)$ can be produced if the previous time integral is transformed into a line integral. In equation (2.11a) the $d\tau$'s can be canceled and the integration is taken over the path C from the SEP $(\theta^s,0)$ to the point (θ,ϖ). The differential $d\Theta_n$ can be taken as

$$d\Theta_n = d\left(\frac{-1}{M_n}\left(M_1\Theta_1 + M_2\Theta_2 + \cdots + M_{n-1}\Theta_{n-1}\right)\right)$$

If f_i from equation (2.8) is explicitly used the term by term expression of equation (2.11a) takes the form as shown below. The first term has the form

$$\sum_{i=1}^{n} \int_{(\theta^s,0)\ C}^{(\theta,\varpi)} M_i\ \Omega_i\ d\Omega_i = \frac{1}{2} \sum_{i=1}^{n} M_i\ \varpi_i^2$$

The second term takes the form

$$-\sum_{i=1}^{n} \int_{(\theta^s,0)\ C}^{(\theta,\varpi)} P_i\ d\Theta_i = -\sum_{i=1}^{n} P_i\left(\theta_i - \theta_i^s\right)$$

The two integral terms above are path independent. The third term takes the form

$$\sum_{i=1}^{n} \int_{(\theta^s,0)\ C}^{(\theta,\varpi)} P_{ei}\ d\Theta_i = \sum_{i=1}^{n} \sum_{\substack{j=1 \\ j\neq i}}^{n} \int_{(\theta^s,0)\ C}^{(\theta,\varpi)} \left[C_{ij}\ sin\left(\Theta_i - \Theta_j\right) + D_{ij}\ cos\left(\Theta_i - \Theta_j\right)\right] d\Theta_i$$

Since $C_{ij} = C_{ji}$ and $sin(\Theta_i - \Theta_j) = -\ sin(\Theta_j - \Theta_i)$

$$\sum_{i=1}^{n} \sum_{\substack{j=1 \\ j\neq i}}^{n} C_{ij}\ sin\left(\Theta_i - \Theta_j\right) d\Theta_i = \sum_{i=1}^{n-1} \sum_{j=i+1}^{n} C_{ij}\ sin\left(\Theta_i - \Theta_j\right) d(\Theta_i - \Theta_j)$$

The first part of the third term becomes

$$\sum_{i=1}^{n-1} \sum_{j=i+1}^{n} \int_{(\theta_i^s - \theta_j^s)\ C}^{(\theta_i - \theta_j)} C_{ij}\ sin\left(\Theta_i - \Theta_j\right) d(\Theta_i - \Theta_j)$$

$$= - \sum_{i=1}^{n-1} \sum_{j=i+1}^{n} C_{ij} \left[\cos\left(\theta_i - \theta_j\right) - \cos\left(\theta_i^s - \theta_j^s\right) \right]$$

and this term is path independent. Since $D_{ij} = D_{ji}$ and $\cos(\Theta_i - \Theta_j) = \cos(\Theta_j - \Theta_i)$

$$\sum_{i=1}^{n} \sum_{\substack{j=1 \\ j \neq i}}^{n} D_{ij} \cos\left(\Theta_i - \Theta_j\right) d\Theta_i = \sum_{i=1}^{n-1} \sum_{j=i+1}^{n} D_{ij} \cos\left(\Theta_i - \Theta_j\right) d(\Theta_i + \Theta_j)$$

The second part of the third term can then be formed as

$$\sum_{i=1}^{n} \sum_{\substack{j=1 \\ j \neq i}}^{n} \int_{(\theta_i^s + \theta_j^s)\ C}^{(\theta_i + \theta_j)} D_{ij} \cos\left(\Theta_i - \Theta_j\right) d\Theta_i$$

$$= \sum_{i=1}^{n-1} \sum_{j=i+1}^{n} \int_{(\theta_i^s + \theta_j^s)\ C}^{(\theta_i + \theta_j)} D_{ij} \cos\left(\Theta_i - \Theta_j\right) d(\Theta_i + \Theta_j)$$

As noted above, the integral term associated with the term C_{ij} is path independent, however, the integral term associated with the term D_{ij} is path dependent. The limits of integration are also changed to reflect the differential $d(\cdot)$.

Because of equation (2.4) the fourth and final term can be shown to be

$$\sum_{i=1}^{n} \int_{(\theta^s,0)\ C}^{(\theta,\varpi)} \frac{M_i}{M_T} P_{COI}\, d\Theta_i = \int_{(\theta^s,0)\ C}^{(\theta,\varpi)} \sum_{i=1}^{n} \frac{M_i}{M_T} P_{COI}\, d\Theta_i$$

$$= \int_{(\theta^s,0)\ C}^{(\theta,\varpi)} \sum_{i=1}^{n} \frac{M_i}{M_T} \sum_{j=1}^{n} \left(P_j - P_{ej}\right) d\Theta_i = \int_{(\theta^s,0)\ C}^{(\theta,\varpi)} \sum_{j=1}^{n} \left(P_j - P_{ej}\right) M_T \sum_{i=1}^{n} M_i\, d\Theta_i = 0$$

The reason that the term associated with D_{ij} is path dependent is the following. Integration of the vector field f_i is path independent if there exist a scalar function W, such that $f_i = \partial W/\partial\theta_i$. If this W can be found the Hessian of W must be symmetric. It then follows that $\partial f_j/\partial\theta_i = \partial f_i/\partial\theta_j$, but since $\partial\cos(\theta_i - \theta_j)/\partial\theta_j \neq \partial\cos(\theta_j - \theta_i)/\partial\theta_i$ this violates the symmetry condition. Therefore, W cannot be found and hence, there is path dependence.

Integration of the right hand side in equation (2.9) results in a constant of integration which can be taken as $V(\theta,\varpi)$ when evaluated at some point (θ,ϖ). Combining the above terms it can be seen that the transient energy function $V(\theta,\varpi)$ has two distinct components which are kinetic energy and potential energy, hence,

$$V(\theta,\varpi) = V_{KE}(\varpi) + V_{PE}(\theta)$$

where

$$V_{KE}(\varpi) = \frac{1}{2}\sum_{i=1}^{n} M_i\,\varpi_i^2$$

and

$$V_{PE}(\theta) = -\sum_{i=1}^{n} P_i\left(\theta_i - \theta_i^s\right)$$

$$-\sum_{i=1}^{n-1}\sum_{j=i+1}^{n} C_{ij}\left(\cos\theta_{ij} - \cos\theta_{ij}^s\right)$$

$$+\sum_{i=1}^{n-1}\sum_{j=i+1}^{n}\int_{(\theta_i^s + \theta_j^s)\,C}^{(\theta_i + \theta_j)} D_{ij}\cos\left(\Theta_i - \Theta_j\right)d(\Theta_i + \Theta_j) \qquad (2.12)$$

where $\theta_{ij} = \theta_i - \theta_j$.

The terms in the TEF have physical meaning and can be interpreted as follows.

$$\frac{1}{2}\sum_{i=1}^{n} M_i \varpi_i^2$$

represents the total change in kinetic energy of all machine rotors relative to COI.

$$\sum_{i=1}^{n} P_i\left(\theta_i - \theta_i^s\right)$$

represents the total change in positional energy of all rotors relative to the COI.

$$- C_{ij}\left(\cos\,\theta_{ij} - \cos\,\theta_{ij}^s\right)$$

represents the change in the stored magnetic energy of each branch ij.

$$\int_{(\theta_i^s + \theta_j^s)\,C}^{(\theta_i + \theta_j)} D_{ij} \cos\left(\Theta_i - \Theta_j\right) d(\Theta_i + \Theta_j)$$

represents the change in the dissipation energy of branch ij due to the transfer conductance.

When the power system experiences a transient there are usually three stages in which the system evolves. The first stage is the pre-disturbance stage in the which the power system is at equilibrium. The second stage is the disturbed stage in which the state of the power system moves away from the equilibrium due to the disturbance. The final stage is the post-disturbance stage. An initial condition is imposed on this post-disturbance power system due to the removal of the disturbance. Thus, given an initial condition it is this final stage for which transient stability is to be analyzed.

The TEF (2.11) was derived for this post-disturbance system. The lower limit of integration for the derivation was the post-disturbance SEP. The upper limit of integration represents the initial condition put on this system through the clearing of the disturbed trajectory. The TEF evaluated at this initial condition then represents the energy with respect to the post-disturbance SEP that is injected into the system by the disturbance. As noted earlier, the last term of the TEF is path dependent and relies on a explicit path C from the post-disturbance SEP to the point (θ,ϖ). Uemura, et. al. [14] developed a path that approximates this term which is based on a linear angle trajectory assumption. It has become standard practice in the TEF method to incorporate this linear angle trajectory.

With this linear approximation employed, the TEF becomes

$$V(\theta,\varpi) = \frac{1}{2}\sum_{i=1}^{n} M_i \varpi_i^2 - \sum_{i=1}^{n} P_i\left(\theta_i - \theta_i^s\right) - \sum_{i=1}^{n-1}\sum_{j=i+1}^{n} C_{ij}\left(\cos\theta_{ij} - \cos\theta_{ij}^s\right) + \sum_{i=1}^{n-1}\sum_{j=i+1}^{n} D_{ij}\frac{\theta_i - \theta_i^s + \theta_j - \theta_j^s}{\left(\theta_{ij} - \theta_{ij}^s\right)}\left(\sin\theta_{ij} - \sin\theta_{ij}^s\right) \qquad (2.13)$$

There are two important points to note with regard to the TEF method.

- The TEF, formulated relative to the COI, is of great advantage. The components of both the rotor kinetic energy and position energy contributing to the motion of the COI are subtracted. This removes the component of energy that has no effect on system stability. This aspect of the formulation improves the description of the transient energy used in stability assessment and accounts for the components of energy responsible for stability (or instability) more accurately [27].

- The direct method of Lyapunov is often used to determine stability of a dynamical system and this method can lead to an approximation of the

stability region of the system. However, the TEF is not a Lyapunov function because of the indefiniteness of the time derivative of V along the system trajectory.

2.3 Transient Stability Assessment Using the TEF Method

The assessment of transient stability through the application of the TEF method is performed by comparing two values of the transient energy, V, (V will now denote $V(\theta,\varpi)$ without loss of generality). The values of transient energy compared are the transient energy injected into the system through the disturbance and the critical energy of the post-disturbance system. In other words, the TEF is evaluated at $(\theta^{cl},\varpi^{cl})$, which is the state of the system at the clearing of the last disturbance, to measure the transient energy V^{cl} injected into the system. The TEF is then evaluated at θ^u where θ^u denotes the controlling UEP, to measure the critical energy of the post-disturbance system, V^{cr}. These TEF evaluations are shown below in equation (2.14).

$$V^{cl} = V\Big|_{(\theta^s,0)}^{(\theta^{cl},\varpi^{cl})}, \quad V^{cr} = V\Big|_{(\theta^s,0)}^{(\theta^u,0)} \tag{2.14}$$

Transient stability assessment is then performed by comparing these two values. If $V^{cl} < V^{cr}$, the system is stable and if $V^{cl} > V^{cr}$, the system is unstable. When $V^{cl} = V^{cr}$ the system is considered critically stable. In other words, if the post-disturbance system can absorb the energy that is injected into the system through the disturbance, the system will be stable, otherwise instability will occur.

Alternatively, transient stability assessment can be made by evaluating the energy margin ΔV which is

$$\Delta V = V^{cr} - V^{cl} = V\Big|_{(\theta^{cl},\varpi^{cl})}^{(\theta^u,0)} \tag{2.15}$$

The energy margin ΔV in terms of the TEF is

$$\Delta V = -\frac{1}{2}\sum_{i=1}^{n} M_i\left(\varpi_i^{cl}\right)^2 - \sum_{i=1}^{n} P_i\left(\theta_i^u - \theta_i^{cl}\right)$$

$$-\sum_{i=1}^{n-1}\sum_{j=i+1}^{n} C_{ij}\left(\cos\theta_{ij}^u - \cos\theta_{ij}^{cl}\right)$$

$$+\sum_{i=1}^{n-1}\sum_{j=i+1}^{n} D_{ij}\frac{\theta_i^u - \theta_i^{cl} + \theta_j^u - \theta_j^{cl}}{\left(\theta_{ij}^u - \theta_{ij}^{cl}\right)}\left(\sin\theta_{ij}^u - \sin\theta_{ij}^{cl}\right) \quad (2.16)$$

Again, if $\Delta V > 0$ the system is stable, otherwise instability occurs. The corrected kinetic energy is normally used in the energy margin calculation and this will be presented in a later chapter.

The TEF method is said to assess the *first swing transient stability* of a power system. If a disturbance is such that the angle trajectory does not go unstable in the first swing the TEF method is thought to assess this situation as stable. However, this does not truly imply that the system is stable since instability can occur after two or more swings.

Determining the critical value of the transient energy is the next step in the process of assessing transient stability. The contents of Chapter 4 is a description of a numerical method called the exit point method for determining the controlling UEP. The next chapter contains a description of two dynamical systems that are related to the system given in equation (2.6).

3. RELATED DYNAMICAL SYSTEMS

The exit point method for determining the controlling UEP is based on an underlying analytical foundation as given by Chiang et. al. [20] and [21]. Also a numerical procedure for implementing this method was given by Chiang et. al. [21]. This analytical formulation is based on two dynamical systems and their relationship with each other. The first dynamical system is that describing an unrealistic multi-machine power system and will be referred to as the *swing system*. The second dynamical system is that of the associated gradient of the potential energy and will be referred to as the *gradient system*.

The results from [20] and [21] need to be applied to this dissertation but cannot be applied directly. The reason for this is that the analytical formulation in [20] and [21] employed a multi-machine power system model that has no transfer conductances, damping present and an infinite bus present for a reference frame. The presence of the damping and the absence of the transfer conductances is necessary because a valid Lyapunov function can be found and this Lyapunov function is necessary in the analytical foundation. The model given by equation (2.6) has transfer conductances included, no damping and the system is in the COI reference frame. The transfer conductances can be omitted and the damping added to equation (2.6), but there is still a difference in the reference frame. Thus, the theory in [20] and [21] needs to be shown to hold when the multi-machine power system is in the COI reference frame.

The swing system is actually the modification of equations (2.6). The modification is the absence of the transfer conductances and the addition of damping in equations (2.6). Therefore, due to the absence of transfer conductances the swing system describes the dynamics of an unrealistic power system but this system is needed so that the analytical foundation shown in this chapter can be made.

This chapter consists of three sections. The main results of the first section are the following.

Section 3.1 The swing system is presented. The characterization of the stability boundary for the swing system is given. An approximation to the relevant stability boundary of the swing system is shown. Finally, a mathematical definition for the energy margin is given.

Section 3.2 The associated gradient system and the characterization of the stability boundary for the gradient system are given.

Section 3.3 The relationship between the swing system and the gradient system is presented.

Throughout this chapter references [20] and [21] will be referred to quite frequently. When there needs to be a change made due to the equations being in the COI reference frame it will be given explicitly.

3.1 The Swing System

The material in this section is concerned with assumptions on and properties of the swing system which is the dynamical system generated by the set of nonlinear differential equations (3.1). This system is derived from the equations (2.1) and the derivation is given in Appendix A, Section A.1. This swing system will be considered to represent the post-disturbance power system. Note the damping coefficient D_i and the absence of the transfer conductances.

$$M_i \dot{\varpi}_i = h_i = P_i - D_i \varpi_i - \sum_{\substack{j=1 \\ j \neq i}}^{n-1} C_{ij} \sin\left(\theta_i - \theta_j\right)$$

$$- C_{in} \sin\left(\theta_i + \frac{1}{M_n}\left(M_1\theta_1 + M_2\theta_2 + \cdots + M_{n-1}\theta_{n-1}\right)\right)$$

$$\dot{\theta}_i = \varpi_i \qquad i = 1, 2, \ldots, n-1 \qquad (3.1)$$

Let

$$g_i = P_i - \sum_{\substack{j=1 \\ j \neq i}}^{n-1} C_{ij} \sin\left(\theta_i - \theta_j\right)$$

$$- C_{in} \sin\left(\theta_i + \frac{1}{M_n}\left(M_1\theta_1 + M_2\theta_2 + \cdots + M_{n-1}\theta_{n-1}\right)\right)$$

Then equations (3.1) become

$$M_i \dot{\varpi}_i = h_i = g_i - D_i \varpi_i$$

$$\dot{\theta}_i = \varpi_i \qquad i = 1, 2, \ldots, n-1 \qquad (3.2)$$

Note that $g_i = f_i$ (2.8) when $D_{ij} = 0$. It was also shown in Appendix A, Section A.1 that

$$\sum_{i=1}^{n} P_{ei} = 0 \text{ and } \sum_{i=1}^{n} P_i = 0 \qquad (3.3)$$

and that these equations (3.3) imply that

$$g_n = - \sum_{i=1}^{n-1} g_i$$

It is obvious that equations (3.1) have continuous first order partial derivatives. Hence, there exist a solution to equations (3.1) and this solution

is unique. In order to present an analytical foundation the following terminology is defined as in [31] , [32] and [33].

$(\theta^s,0)$ $\in R^{(n-1)} \times R^{(n-1)}$, the swing system SEP.

$\phi(\theta,\varpi,t)$ $R^{(n-1)} \times R^{(n-1)} \times R \rightarrow R^{(n-1)} \times R^{(n-1)}$, the solution of the swing system with initial condition (θ,ϖ) and $\phi(\theta,\varpi,0) = (\theta,\varpi)$.

$A(\theta^s,0)$ $\subset R^{(n-1)} \times R^{(n-1)}$, the stability region of the swing system. This is defined as $\{ (\theta,\varpi) : \phi(\theta,\varpi,t) \rightarrow (\theta^s,0)$ as $t \rightarrow \infty \}$

$\partial A(\theta^s,0)$ the stability boundary of the swing system.

E the set of all equilibrium points for the swing system.

EB the set which is the intersection of the set E and the stability boundary of the swing system, (i.e., $EB = \partial A(\theta^s,0) \cap E$).

$W^s(\theta^i,0)$ $\subset R^{(n-1)} \times R^{(n-1)}$, the stable manifold for the hyperbolic equilibrium point $(\theta^i,0)$ defined as $\{ (\theta,\varpi) : \phi(\theta,\varpi,t) \rightarrow (\theta^i,0)$ as $t \rightarrow \infty \}$.

$W^u(\theta^i,0)$ $\subset R^{(n-1)} \times R^{(n-1)}$, the unstable manifold for the hyperbolic equilibrium point $(\theta^i,0)$ defined as $\{ (\theta,\varpi) : \phi(\theta,\varpi,t) \rightarrow (\theta^i,0)$ as $t \rightarrow -\infty \}$.

3.1.1 Characterization of the Stability Boundary of the Swing System

The following will lead to the characterization of the stability boundary of the swing system.

Property 3.1.1

The Jacobian of the swing system is a $2(n-1) \times 2(n-1)$ matrix of the form

$$J_{ss} = \begin{bmatrix} \frac{\partial \varpi}{\partial \theta} & \frac{\partial \varpi}{\partial \varpi} \\ \frac{\partial \left[M^{-1} \left(g - D\, \varpi \right) \right]}{\partial \theta} & \frac{\partial \left[M^{-1} \left(g - D\, \varpi \right) \right]}{\partial \varpi} \end{bmatrix} = \begin{bmatrix} 0 & I \\ M^{-1} \frac{\partial g}{\partial \theta} & - M^{-1} D \end{bmatrix}$$

and the matrices M and D are diagonal matrices with elements M_i and D_i respectively. Assuming the matrix $\partial g / \partial \theta$ is nonsingular at the equilibrium points of the swing system then these equilibrium points are hyperbolic.

The proof is given in [20]. ■

Assumption 3.1.2

Let $(\theta^i,0), (\theta^j,0) \in EB$. The intersection of $W^s(\theta^i,0)$ and $W^u(\theta^j,0)$ satisfies the transversality condition for all $(\theta^i,0), (\theta^j,0) \in EB$. Here i may equal j. This simply means that the tangent spaces of the corresponding manifolds at the intersection point must span the space $R^{(n-1)} \times R^{(n-1)}$.

Property 3.1.3

There does exist a function $V(\theta,\varpi)$ for the swing system so that

i) $\dot{V}(\phi(\theta,\varpi,t)) \leq 0 \quad \forall (\theta,\varpi) \notin E$

ii) If $(\theta,\varpi) \notin E$ then the set $\{ t \in R : \dot{V}(\phi(\theta,\varpi,t)) = 0 \}$ has measure 0 in R. In other words there is no interval $[T_1, T_2]$, $T_1 < T_2$, with $t \in [T_1, T_2]$ such that $\dot{V}(\phi(\theta,\varpi,t)) = 0$. If $(\theta,\varpi) \notin E$ and if $\dot{V}(\theta,\varpi) = 0$ for some t_1 then the instant before t_1, $\dot{V} < 0$ and the instant after t_1, $\dot{V} < 0$.

iii) $V(\phi(\theta,\varpi,t))$ is bounded implies $\phi(\theta,\varpi,t)$ is bounded.

The proof to parts ii) and iii) are given in [20]. Part i) can be shown by employing the energy function (2.12) with $D_{ij} = 0$. The energy function now takes the form

$$V = \frac{1}{2}\sum_{i=1}^{n} M_i \varpi_i^2 - \sum_{i=1}^{n} P_i\left(\theta_i - \theta_i^s\right) - \sum_{i=1}^{n-1}\sum_{j=i+1}^{n} C_{ij}\left(\cos\theta_{ij} - \cos\theta_{ij}^s\right) \qquad (3.4)$$

With ϖ_n and θ_n explicitly substituted in, equation (3.4) becomes

$$\begin{aligned} V = {} & \frac{1}{2}\sum_{i=1}^{n-1} M_i \varpi_i^2 + \frac{1}{2}\frac{1}{M_n}\left(\varpi_1 M_1 + \cdots + \varpi_{n-1} M_{n-1}\right)^2 \\ & - \sum_{i=1}^{n-1} P_i\left(\theta_i - \theta_i^s\right) + \frac{P_n}{M_n}\left(\left(\theta_1 - \theta_1^s\right)M_1 + \cdots + \left(\theta_{n-1} - \theta_{n-1}^s\right)M_{n-1}\right) \\ & - \sum_{i=1}^{n-1}\sum_{j=i+1}^{n-1} C_{ij}\left(\cos\theta_{ij} - \cos\theta_{ij}^s\right) \\ & - \sum_{i=1}^{n-1} C_{in}\cos\left(\theta_i + \frac{1}{M_n}\left(\theta_1 M_1 + \cdots + \theta_{n-1} M_{n-1}\right)\right) \\ & + \sum_{i=1}^{n-1} C_{in}\cos\left(\theta_i^s + \frac{1}{M_n}\left(\theta_1^s M_1 + \cdots + \theta_{n-1}^s M_{n-1}\right)\right) \end{aligned} \qquad (3.5a)$$

The energy function (3.4) is similar to the energy function given equation (2.12) and can be written simply as

$$V = V_{KE} + V_{PE}$$

with

$$V_{KE} = \frac{1}{2}\sum_{i=1}^{n-1} M_i \varpi_i^2 + \frac{1}{2}\frac{1}{M_n}\left(\varpi_1 M_1 + \cdots + \varpi_{n-1} M_{n-1}\right)^2 \qquad (3.5b)$$

$$V_{PE} = -\sum_{i=1}^{n-1} P_i\left(\theta_i - \theta_i^s\right) + \frac{P_n}{M_n}\left(\left(\theta_1 - \theta_1^s\right)M_1 + \cdots + \left(\theta_{n-1} - \theta_{n-1}^s\right)M_{n-1}\right)$$

$$-\sum_{i=1}^{n-1}\sum_{j=i+1}^{n-1} C_{ij}\left(\cos\theta_{ij} - \cos\theta_{ij}^s\right)$$

$$-\sum_{i=1}^{n-1} C_{in}\cos\left(\theta_i + \frac{1}{M_n}\left(\theta_1 M_1 + \cdots + \theta_{n-1}M_{n-1}\right)\right)$$

$$+\sum_{i=1}^{n-1} C_{in}\cos\left(\theta_i^s + \frac{1}{M_n}\left(\theta_1^s M_1 + \cdots + \theta_{n-1}^s M_{n-1}\right)\right) \qquad (3.5c)$$

The derivation of the time derivative of $V(\theta,\omega)$ is shown in Appendix A, Section A.2.1 and is shown to be

$$\dot{V} = \sum_{i=1}^{n}\left[\frac{\partial V}{\partial\theta_i}\dot{\theta}_i + \frac{\partial V}{\partial\omega_i}\dot{\omega}_i\right] = -\omega^T M^v \omega \qquad (3.6)$$

where M^v is defined by matrix equation (A.9)

It is also shown in Appendix A, Section A.2.2 that

$$\dot{V} = -\omega^T M^v \omega < 0 \;\forall\, \omega \neq 0 \qquad (3.7)$$

■

The inequality (3.7) along with the fact that for an open region around $(\theta^s,0)$, $V(\theta,\omega) > 0$ for $(\theta,\omega) \neq (\theta^s,0)$ implies that V qualifies as a Lyapunov function.

Also from the inequality (3.7) it is evident that every trajectory of the swing system must either go to infinity or converge to one of the equilibrium points, which implies there are no limit cycles or chaotic motion.

Theorem 3.1.4

Assume that $\overline{int(A(\theta^s,0))} = A(\theta^s,0)$ where *int* denotes interior of a set and the bar denotes closure of a set. With this assumption, Assumption 3.1.2, Properties 3.1.1 and 3.1.3, the stability boundary of the swing system can be characterized as

$$\partial A(\theta^s,0) = \bigcup_{(\theta^i,0) \in EB} W^s(\theta^i,0) \tag{3.8}$$

The proof can be found in Chiang et. al. [21] and Zaborsky et. al. [35], however the energy function in property 3.1.3 must be substituted for the proofs given in [21 and 35]. It has also been shown in [20 and 35] that the stability boundary can be expressed as

$$\partial A(\theta^s,0) = \bigcup_{(\theta^i,0) \in EB\text{-}1} \overline{W^s(\theta^i,0)}$$

where *EB-1* is the set of all equilibrium points on the stability boundary which are of type-*1*. A type-*1* equilibrium point is such that the Jacobian evaluated at that point has only one eigenvalue with a positive real part. In fact, it has been shown Zaborsky et. al. [35] that

$$\bigcup_{(\theta^i,0) \in EB\text{-}k} \left[\overline{W^s(\theta^i,0)} - int\left(W^s(\theta^i,0)\right)\right] = \bigcup_{(\theta^j,0) \in EB\text{-}(k+1)} \overline{W^s(\theta^j,0)}$$

Where *EB-k* denotes the set of all equilibrium points on the stability boundary that are of type-*k*. It is assumed that there is a $(\theta^i,0) \in$ *EB-k* and a $(\theta^j,0) \in$ *EB-(k+1)* such that $(\theta^i,0) \in \partial\overline{W^s(\theta^j,0)}$. The right-hand side of the above equation may be empty.

The assumption that $\overline{int(A(\theta^s,0))} = A(\theta^s,0)$ is given by Zaborsky et. al. [36] and is shown to be needed if the proofs given in [20 and 21] are to be valid. This assumption implies that there are no unstable equilibrium points interior to $\overline{A(\theta^s,0)}$. ■

Theorem 3.1.5

The stability region, $A(\theta^s,0)$, for the swing system is unbounded. This is due to the fact that there are no equilibrium points of the swing system which are sources.

The proof is given in [20]. ■

3.1.2 An Approximation to the Relevant Stability Boundary

When a disturbance occurs in a power system the state of the system will start to move from the initial equilibrium position. When the disturbance is cleared the state of the system is the initial state or initial condition for the post-disturbance system. If the disturbance is sustained the state may leave the stability region for the post-disturbance system. In doing so the state will intersect with the stability boundary and because of equation (3.8) will intersect a stable manifold. The intersection point is referred to as an exit point and will be described in Chapter 4. This gives rise to the definition of the controlling UEP as used in this dissertation work.

Definition 3.1.6

Define the controlling UEP as the UEP which anchors the stable manifold intersected by the disturbed system state.

The stability of the post-disturbance system is preserved if the disturbance is cleared before the disturbed state intersects the stability boundary. Therefore, stability can be assessed if the intersection point can be determined. This is, however, one of the proposed tools stated in Section 1.2 that did not work because the intersection point is difficult to detect. There is a way out of this difficulty in that an approximation to this stable manifold by a constant energy surface can be made. The constant energy surface is associated with the energy of the UEP that corresponds to the stable manifold

that is intersected. Hence, this constant energy surface only approximates the part of the stability boundary that is relevant to the disturbance specified.

The following two theorems will illustrate the effectiveness of the above idea, but first the following definitions must be given

$(\theta^{s1},0) \subset R^{(n-1)} \times R^{(n-1)}$, the pre-disturbance system SEP.

$V_c(\theta^1,\varpi^1) \subset R^{(n-1)} \times R^{(n-1)}$, $\{ (\theta,\varpi) : V(\theta,\varpi) < V(\theta^1,\varpi^1)$ and connected and containing $(\theta^s,0) \}$.

$\partial V(\theta^1,\varpi^1)$ $\{ (\theta,\varpi) : V(\theta,\varpi) = V(\theta^1,\varpi^1)$ and connected to $(\theta^1,\varpi^1) \}$.

$\phi^d(\theta,\varpi,t)$ $R^{(n-1)} \times R^{(n-1)} \times R \rightarrow R^{(n-1)} \times R^{(n-1)}$, the solution of the disturbed system with initial condition (θ,ϖ) and $\phi^d(\theta,\varpi,0) = (\theta,\varpi)$.

Theorem 3.1.7

Let $(\theta^u,0) \in EB$.

i) The connected constant energy surface $\partial V(\theta^u,0)$ intersects the stable manifold, $W^s(\theta^u,0) \in \partial A(\theta^s,0)$ only at the point $(\theta^u,0)$. The set $V_c(\theta^u,0)$ does not contain any point which belongs to the stable manifold $W^s(\theta^u,0)$.

ii) Suppose $(\theta^1,\varpi^1) \in W^s(\theta^u,0)$ with $(\theta^1,\varpi^1) \neq (\theta^u,0)$. The set $V_c(\theta^1,\varpi^1)$ does contain points which belong to the stable manifold $W^s(\theta^u,0)$.

The proof is given in [21] ■

Theorem 3.1.8

Let $(\theta^{s1},0)$ be the initial condition for the disturbed trajectory. Let this disturbed trajectory intersect the stable manifold $W^s(\theta^u,0) \subset \partial A(\theta^s,0)$ at

the point $(\theta^e, \varpi^e) \neq (\theta^u, 0)$ at the time t_2. In other words $(\theta^e, \varpi^e) = \phi^d(\theta^{s1}, 0, t_2)$. Assume that $(\theta^{s1}, 0) \in A(\theta^s, 0) \cap V_c(\theta^u, 0)$.

The disturbed trajectory must pass through the constant energy surface $\partial V(\theta^u, 0)$ before it intersects the stable manifold $W^s(\theta^u, 0)$.

Proof:
From the assumption, $V(\theta^{s1}, 0) < V(\theta^u, 0)$. At the intersection point $V(\theta^e, \varpi^e) > V(\theta^u, 0)$. The energy function (3.5a) is continuous along the disturbed system and hence, continuous with respect to t. The application of the Intermediate-Value Theorem guarantees there is a t_1, $0 < t_1 < t_2$, such that $V(\phi^d(\theta^{s1}, 0, t_1)) = V(\theta^u, 0)$. ■

From Theorems 3.1.7 and 3.1.8, $\partial V(\theta^u, 0)$ seems to approximate $W^s(\theta^u, 0)$ and the approximation is conservative in nature. The second part of Theorem 3.1.7 simply states that if any other constant energy surface that intersects with the stable manifold is taken to approximate the stability boundary then this approximation may be poor. If the energy surface has an energy larger than that at the UEP then holes may appear in this approximate stability boundary. Also if some other energy surface that has energy smaller than that at the UEP is taken as an approximation then the stability assessment may be too conservative.

3.1.3 A Mathematical Definition for the Energy Margin

The concept of the energy margin for the transient stability assessment was given in Section 2.4. This margin is based on the mathematically founded idea presented in Theorem 3.1.8. Similarly the energy margin defined in this section is

$$\Delta V = V(\theta^u, 0) - V(\theta^{cl}, \varpi^{cl})$$

where $(\theta^{cl}, \varpi^{cl})$ is the initial condition put on the post-disturbance system. If $\Delta V > 0$ the system is stable and if $\Delta V \leq 0$ the system will be considered unstable.

Figure 3.1 depicts part of the stability boundary for the post-disturbance system. In particular, note the controlling UEP $(\theta^u,0)$, the corresponding stable manifold $W^s(\theta^u,0)$; the constant energy surface $\partial V(\theta^u,0)$ and the disturbed trajectory $\phi^d(\theta^{s1},0,t)$. The disturbed trajectory intersects the stable manifold at the point A (i.e., an exit point). Note, this figure is shown in two dimensions and some parts are exaggerated to illustrate the point intended.

In Figure 3.1 the initial condition that is placed on the post-disturbance system must lie on the disturbed trajectory. For example three different initial conditions are denoted by the points 1, 2 and 3. By using the previously defined energy margin, the stability of the post-disturbance system can be assessed. The system is stable with point 1 as the initial condition. With point 2 as the initial condition the system is unstable in terms of the energy margin but in reality the system is stable. This points out the conservativeness of this procedure. With point 3 as the initial condition the system is unstable.

As noted earlier the point of intersection of the faulted trajectory and the stable manifold $W^s(\theta^u,0)$ is nearly impossible to detect. However, this part of the stability boundary can be approximated by the constant energy surface. This constant energy surface is defined by the energy at the UEP which anchors the stable manifold that was intersected. So the problem then lies with finding $(\theta^u,0)$. One suggested way of doing this is to make use of the associated gradient system.

3.2 The Associated Gradient System

The associated gradient of the potential energy system is given by

$$\dot{\theta} = - \nabla V_{PE} = \frac{- \partial V_{PE}}{\partial \theta} \tag{3.9}$$

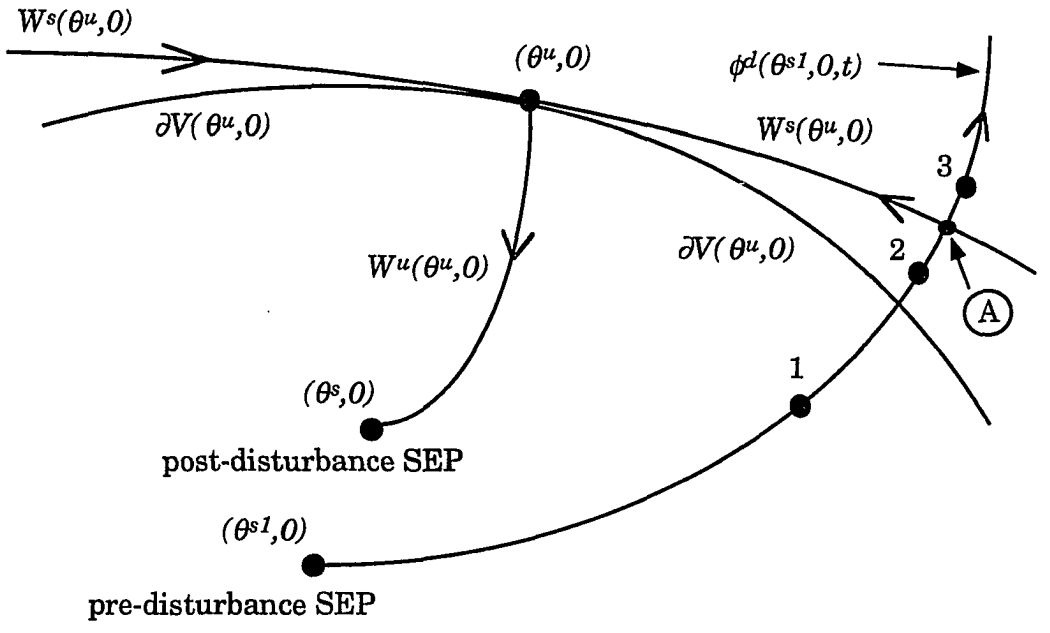

Figure 3.1 Illustration of the approximate stability boundary

where V_{PE} is given by equation (3.5b). Equation (3.9) can also be written as

$$\dot{\theta}_i = \frac{-\partial V_{PE}}{\partial \theta_i} = z_i \qquad i = 1, \ldots, n\text{-}1 \qquad (3.10)$$

From matrix equation (A.7), z_i can be written as

$$z = M^{\theta} g$$

$$\begin{bmatrix} z_1 \\ \vdots \\ z_{n-1} \end{bmatrix} = \begin{bmatrix} 1 + \frac{M_1}{M_n} & \cdots & \frac{M_1}{M_n} \\ \vdots & \ddots & \vdots \\ \frac{M_{n-1}}{M_n} & \cdots & 1 + \frac{M_{n-1}}{M_n} \end{bmatrix} \begin{bmatrix} g_1 \\ \vdots \\ g_{n-1} \end{bmatrix} \qquad (3.10)$$

Then the gradient system can be written in vector-matrix notation as

$$\dot{\theta} = - \nabla V_{PE} = \frac{- \partial V_{PE}}{\partial \theta} = z = M^{\theta} g \tag{3.11}$$

Define the following terminology for the gradient system.

$\phi_{gs}(\theta,t)$ $R^{(n-1)} \times R \rightarrow R^{(n-1)}$, the solution of the gradient system with initial condition (θ) and $\phi_{gs}(\theta,0) = (\theta)$.

$A(\theta^s)$ $\subset R^{(n-1)}$, the stability region of the gradient system.

$\partial A(\theta^s)$ the stability boundary of the gradient system.

H the set of all equilibrium points for the gradient system.

HB the set which is the intersection of the set H and the stability boundary of the gradient system, (i.e., $HB = \partial A(\theta^s) \cap H$).

The following will lead to the characterization of the stability boundary of the gradient system along with an important property on the gradient system.

Theorem 3.2.1

Let θ^s be an isolated minimum of V_{PE}, then θ^s is an asymptotically stable equilibrium point of the gradient system.

The proof is given in [32, pg. 200] and is based on the fact that V_{PE} can be taken as a Lyapunov function and it is immediately seen that

$$\dot{V}_{PE} = \frac{\partial V_{PE}}{\partial \theta} \cdot \dot{\theta} = - \left(\frac{\partial V_{PE}}{\partial \theta} \right)^2 < 0 \text{ for } \theta \notin H$$

Hence V_{PE} decreases along trajectories of the gradient system. ■

Theorem 3.2.2

Let y be an α-limit point or an ω-limit point of a trajectory of the gradient system. Then y is an equilibrium point of the gradient system. This implies that a trajectory of the gradient system must either run off to infinity or else tend to an equilibrium point.

The proof is given in [32, pg. 203]. ■

Property 3.2.3

The Jacobian of the gradient system is of the form

$$J_{gs} = \frac{\partial}{\partial \theta_j}\left[\frac{-\partial V_{PE}}{\partial \theta_i}\right] = -\frac{\partial^2 V_{PE}}{\partial \theta_j \, \partial \theta_i} = \frac{\partial z_i}{\partial \theta_j} \quad i, j = 1, \cdots, n\text{-}1$$

Assume that this Jacobian is nonsingular at the equilibrium points of the gradient system. This Jacobian is symmetric since

$$\frac{\partial^2 V_{PE}}{\partial \theta_i \, \partial \theta_j} = \frac{\partial^2 V_{PE}}{\partial \theta_j \, \partial \theta_i}$$

Since there are no zero eigenvalues all are hyperbolic. The right eigenvectors of the Jacobian also form an orthogonal basis [32].

Assumption 3.2.4

Let θ^i, $\theta^j \in HB$. The intersection of $W^s(\theta^i)$ and $W^u(\theta^j)$ satisfy the transversality condition for all θ^i, $\theta^j \in HB$. Here i may equal j

Theorem 3.2.5

The stability of the gradient system can also be formulated in a manner similar to that of the swing system as shown in Section 3.1.1. Assume

that $\overline{int(A(\theta^s))} = A(\theta^s)$. With this assumption, Theorems 3.2.1, 3.2.2, Properties 3.2.3 and Assumption 3.2.4 the stability boundary of the gradient system can be described as

$$\partial A(\theta^s) = \bigcup_{(\theta^i) \in HB} W^s(\theta^i)$$

The proof is given in [21].

It has also been shown [20 and 35] that the stability boundary can be expressed as

$$\partial A(\theta^s) = \bigcup_{(\theta^i) \in HB\text{-}1} \overline{W^s(\theta^i)}$$

where *HB-1* is the set of all equilibrium points on the stability boundary which are of type-*1*. Also the theory given in [35] can be applied to the gradient system so that

$$\bigcup_{(\theta^i) \in HB\text{-}k} \left[\overline{W^s(\theta^i)} - int\left(W^s(\theta^i)\right)\right] = \bigcup_{(\theta^j) \in HB\text{-}(k+1)} \overline{W^s(\theta^j)}$$

Where *HB-k* denotes the set of all equilibrium points on the stability boundary that are of type-*k*. It is assumed that there is a $(\theta^i) \in$ *HB-k* and a $(\theta^j) \in$ *HB-(k+1)* such that $(\theta^i) \in \partial\overline{W^s(\theta^j)}$. The right-hand side of the above equation may be empty. ■

Theorem 3.2.6

At regular points of the gradient system the vector field is perpendicular to the level surfaces of V_{PE}. Which can also be stated as, at regular points, the trajectories of the gradient system $\phi_{gs}(\theta,t)$ cross

level surfaces of V_{PE} orthogonally. Regular points of the gradient system are points such that $z \neq 0$.

The proof is given in [32, pg. 201]. ■

Assumption 3.2.7

Consider the unloaded gradient system which is defined as the gradient system with $P_i = 0$, $i = 1, ..., n-1$. Assume that the stability region of the unloaded gradient system is bounded.

3.3 The Connection Between the Swing System and the Associated Gradient System

This section contains a description of the connection between the swing system and the gradient system.

Theorem 3.3.1

θ is an equilibrium point of the gradient system if and only if $(\theta,0)$ is an equilibrium point of the swing system.

Proof:

Assume that θ is an equilibrium point of the gradient system, then $z = 0$. It was shown in Proposition A.2.1 in Appendix A that the matrix M^{θ} is positive definite which implies that it is nonsingular. Since $z = 0$ this implies that $g = 0$ and in turn $(\theta,0)$ is an equilibrium point of the swing system. Assume that $(\theta,0)$ is an equilibrium point of the swing system. Since $g = 0$ it is seen immediately that $z = 0$. ■

Proposition 3.3.2

The assumption in Property 3.2.3 that the Jacobian matrix J_{gs} is nonsingular at equilibrium points of the gradient system is equivalent to the assumption in Property 3.1.1 that the matrix $\partial g / \partial \theta$ is nonsingular at the equilibrium points of swing system.

Proof:

It is seen from Theorem 3.3.1 that an equilibrium point of the gradient system corresponds to an equilibrium point of the swing system. If the matrix $\partial g / \partial \theta$ is nonsingular at an equilibrium point of the swing system then it is nonsingular at an equilibrium point of the gradient system. From equation (3.11) the Jacobian matrix J_{gs} can be written as

$$J_{gs} = \frac{\partial z}{\partial \theta} = M^{\theta} \frac{\partial g}{\partial \theta}$$

It was shown in Appendix A, Proposition A.1.1 that M^{θ} is positive definite which implies that $det(M^{\theta}) \neq 0$ and since $\partial g / \partial \theta$ is nonsingular $det(\partial g / \partial \theta) \neq 0$. From the well known property of determinants $det(M^{\theta} \partial g / \partial \theta) \neq 0$; hence, since $\partial g / \partial \theta$ is nonsingular so is J_{gs}. ■

Theorem 3.3.3

A type-k equilibrium point is one in which there are k number of eigenvalues with positive real parts. θ is a type-k equilibrium point of the gradient system if and only if $(\theta,0)$ is a type-k equilibrium point of the swing system. An immediate result of this is that θ^s is the SEP of the gradient system if and only if $(\theta^s,0)$ is the SEP of the swing system.

Proof:

The proof is given in Appendix A, Section A.3. ■

Assumption 3.3.4

Assume that there are a finite number of equilibrium points on the stability boundaries of both the swing system and the associated gradient system.

Theorem 3.3.5

θ is an equilibrium point on the stability boundary of the gradient system if and only if $(\theta,0)$ is an equilibrium point on the stability boundary of the swing system.

Proof:

With Assumption 3.3.2, the proof is given in Theorem 6-3 in [21]. The proof will follow if the variable z in this work is substituted for the variable f in Theorem 6-3 in [21]. ■

The connection between the gradient system and the swing system is contained in Theorem 3.3.5 which again states that an equilibrium point on the stability boundary of the gradient system corresponds to an equilibrium point on the stability boundary of the swing system.

4. THE EXIT POINT METHOD

The exit point method (also known as the BCU method [22]) is a numerical procedure used to determine a starting point relatively close to the controlling UEP. This method is based on the connection between the swing system and the gradient system which were presented in Chapter 3, Section 3.3. The contents of this chapter is a discussion of the exit point method. The following is a brief description of each section in this chapter.

Section 4.1: The exit point is defined and a fundamental assumption of the exit point method is given.

Section 4.2: A Taylor series expansion of the function V_{PE} (3.5.c) is shown in order that a description of the equipotential energy surfaces can be made.

Section 4.3: Examples of the equipotential energy surfaces derived from the Taylor series expansion and of an unloaded 3-machine system are given.

Section 4.4: A 3-dimensional illustration of the energy well of the function V_{PE} for the unloaded 3-machine system is given.

Section 4.5: A discussion of how the exit point is detected is given.

Section 4.6: The numerical algorithm of the exit point method is given.

Section 4.7: An interpretation of the exit point method is given in the form of two scenarios.

Section 4.8: Three problems associated with the exit point method are discussed.

Section 4.9: The results of the application of the exit point method to the unloaded 3-machine system are presented.

Section 4.10: The issue of the equality in $\partial A(\theta^s,0) \cap \{(\theta,\varpi) : \varpi = 0\} = \partial A(\theta^s)$ is addressed.

Section 4.11: A summary of Chapter 4 is presented.

4.1 The Fundamental Assumption of the Exit Point Method

The *exit point* is a term defined to be the point that is the intersection of the stability boundary of a dynamical system and a trajectory that starts within the stability region and then leaves it. It is assumed that this trajectory will not intersect the stability region again. The notation that is used here and through out this chapter can be found in Chapter 3, Sections 3.1, 3.1.2 and 3.2. Let $(\theta^{s1},0) \in A(\theta^s,0)$ and let the disturbed trajectory intersect $\partial A(\theta^s,0)$ at the point $(\theta^{ess},\varpi^{ess})$. In other words, $(\theta^{ess},\varpi^{ess}) = \phi^d(\theta^{s1},0,t) \cap \partial A(\theta^s,0)$ and is the exit point with respect to the swing system. Since the disturbed trajectory intersects the stability boundary it must then intersect a stable manifold as stated in Theorem 3.1.4 and by the mathematical definition of the controlling UEP, Definition 3.1.6, $(\theta^{ess},\varpi^{ess}) \in W^s(\theta^u,0)$. Accordingly, the exit point with respect to the gradient system is denoted by θ^{egs}. Define $Ang(\theta,\varpi) = \theta$. The disturbed trajectory is in the $2(n-1)$-dimensional ϖ-θ-space. The trajectory $Ang(\phi^d(\theta^{s1},0,t))$ is the projection of the disturbed trajectory into the $(n-1)$ dimensional θ-space. The exit point θ^{egs} is defined to be $\theta^{egs} = Ang(\phi^d(\theta^{s1},0,t)) \cap \partial A(\theta^s)$ and since $\partial A(\theta^s)$ is composed of stable manifolds, then $\theta^{egs} \in W^s(\theta^i)$, where $\theta^i \in HB$. It is not known at this time, that $(\theta^{ess},\varpi^{ess}) \in W^s(\theta^u,0)$ implies that $\theta^{egs} \in W^s(\theta^u)$. However, there is numerical evidence that suggests this may be true for a considerable number of cases. In fact, there is an example given in Section 4.9 where this is shown

to be true. Since there is a lack of an analytical foundation, the following fundamental assumption will be made.

Assumption 4.1

$(\theta^{ess}, \varpi^{ess}) \in W^s(\theta^u,0)$ implies that $\theta^{egs} \in W^s(\theta^u)$.

Figure 4.1 is an illustration of the idea put forth by Assumption 4.1. In this figure the disturbed trajectory intersects the partially shown stable manifold $W^s(\theta^u,0)$ at the exit point $(\theta^{ess}, \varpi^{ess})$. The point B denotes the flow on the manifold that goes toward $(\theta^u,0)$. The dashed line, which is the projection in θ-space of the disturbed trajectory, intersects the partially shown stable manifold $W^s(\theta^u)$ at the exit point θ^{egs}. It is seen in Figure 4.1 that the exit point $(\theta^{ess}, \varpi^{ess})$ is detected before the exit point θ^{egs} is. The reason it is illustrated this way is because through the numerous cases where the exit point method was applied to a realistic power system this order usually appeared. The viewer must be cautious when looking at Figure 4.1. This figure is not the result of any analysis of a specific system; it is to illustrate the idea of Assumption 4.1 and is not to be taken literally. For example, in this figure the θ-space is two-dimensional and it seems that the ϖ-space is one-dimensional which cannot be.

The exit point $(\theta^{ess}, \varpi^{ess})$ is difficult to detect, however the situation of detecting the point θ^{egs} is different. If, for example, a point on $W^s(\theta^u)$ may be found then $W^s(\theta^u)$ can be utilized to determine θ^u and this is why the gradient system is used. The computational scheme suggested by Chiang et. al. [21] does not in general detect the exact exit point θ^{egs} but does detect a point that is relatively close to the point θ^{egs}. The shape of the equipotential energy contours of the function V_{PE} that are connected to the stable manifold $W^s(\theta^u)$ is the key behind this computational scheme. The next section contains a discussion which expands on the shape these equipotential energy contours.

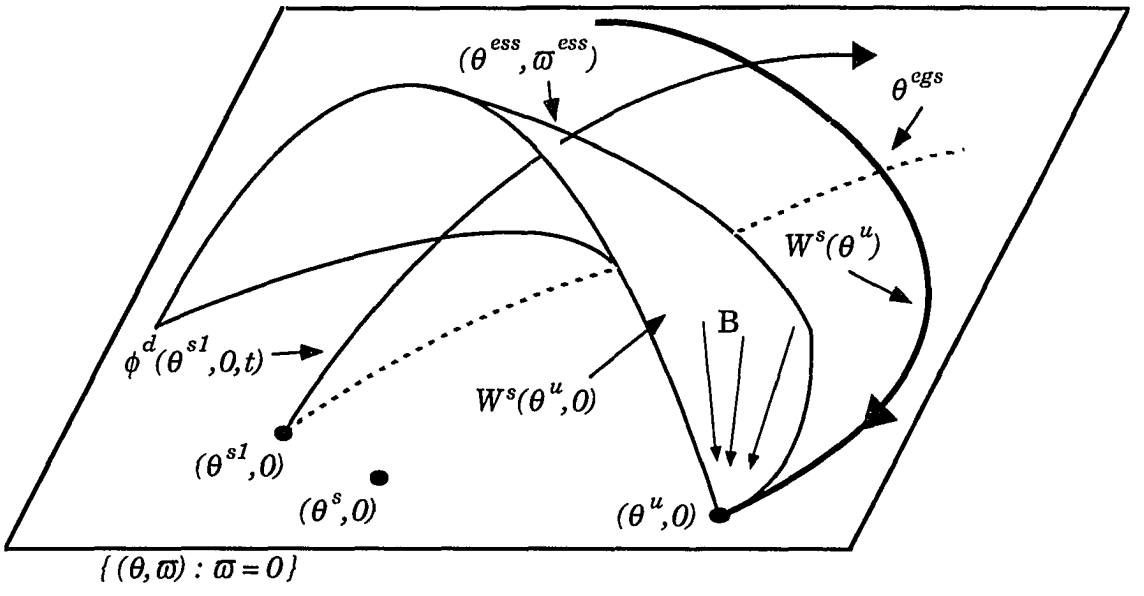

Figure 4.1 Illustration of Assumption 4.1

A point of interest that is shown in Figure 4.1 is that $\partial A(\theta^s,0) \cap \{(\theta,\varpi) : \varpi = 0\} \neq \partial A(\theta^s)$. Since $(\theta^u,0) \in \partial A(\theta^s,0)$, Theorem 3.3.6 of Section 3.3 implies $(\theta^u) \in \partial A(\theta^s)$ and this is shown in Figure 4.1. There are however, points $\theta \in \partial A(\theta^s)$ such that $(\theta,0) \notin \partial A(\theta^s,0)$ and this is also shown in Figure 4.1. An example based on a specific system will be given in Section 4.10 that indicates that $\partial A(\theta^s,0) \cap \{(\theta,\varpi) : \varpi = 0\} \neq \partial A(\theta^s)$.

4.2 Taylor Series Expansion of the Function V_{PE}

A Taylor series expansion of the function V_{PE} around θ^u is one way of determining the shape of the equipotential energy contours in a neighborhood of θ^u. The extent of the truncation of the series might indicate how far from θ^u that the remaining shape is valid. The Taylor series expansion [37] of V_{PE} around θ^u will take the form

$$V_{PE}(\theta) = V_{PE}(\theta^u) + \sum_{i=1}^{n-1} \frac{\partial V_{PE}(\theta^u)}{\partial \theta_i} (\theta_i - \theta_i^u)$$

$$+ \frac{1}{2} \sum_{i=1}^{n-1} \sum_{j=1}^{n-1} \frac{\partial^2 V_{PE}(\theta^u)}{\partial \theta_i \, \partial \theta_j} (\theta_i - \theta_i^u)(\theta_j - \theta_j^u)$$

$$+ \frac{1}{6} \sum_{i=1}^{n-1} \sum_{j=1}^{n-1} \sum_{k=1}^{n-1} \frac{\partial^3 V_{PE}(\theta^u + s(\theta - \theta^u))}{\partial \theta_i \, \partial \theta_j \, \partial \theta_k} (\theta_i - \theta_i^u)(\theta_j - \theta_j^u)(\theta_k - \theta_k^u) \quad (4.1)$$

where $s \in (0, 1)$. The last term in equation (4.1) is the third order remainder term denoted by

$$R_3(\theta) = \frac{1}{6} \sum_{i=1}^{n-1} \sum_{j=1}^{n-1} \sum_{k=1}^{n-1} \frac{\partial^3 V_{PE}(\theta^u + s(\theta - \theta^u))}{\partial \theta_i \, \partial \theta_j \, \partial \theta_k} (\theta_i - \theta_i^u)(\theta_j - \theta_j^u)(\theta_k - \theta_k^u)$$

Assuming that $R_3(\theta)$ is relatively small near θ^u, it may be ignored. From equation (3.12) the first order term can be eliminated. From equation (3.10) $-\partial V_{PE} / \partial \theta = z = 0$ at an equilibrium point , hence

$$\sum_{i=1}^{n-1} \frac{\partial V_{PE}(\theta^u)}{\partial \theta_i} (\theta_i - \theta_i^u) = \sum_{i=1}^{n-1} - z_i (\theta_i - \theta_i^u) = 0$$

The truncated series can be written as

$$V_{PE}(\theta) = V_{PE}(\theta^u) + \frac{1}{2} \sum_{i=1}^{n-1} \sum_{j=1}^{n-1} \frac{\partial^2 V_{PE}(\theta^u)}{\partial \theta_i \, \partial \theta_j} (\theta_i - \theta_i^u)(\theta_j - \theta_j^u) \quad (4.2)$$

This equation (4.2) can be expressed in vector - matrix notation as

$$V_{PE}(\theta) = V_{PE}(\theta^u) + \frac{1}{2} (\Delta\theta)^T H(\theta^u) (\Delta\theta) \quad (4.3)$$

where $H(\theta^u)$ is the Hessian of V_{PE} and $\Delta\theta = (\theta - \theta^u)$. From Property 3.2.3 it is seen that $H(\theta^u)$ is a nonsingular symmetric matrix. There exist an orthonormal matrix Q (i.e., $Q^{-1} = Q^T$) such that $Q^T H(\theta^u) Q = E$ [38]. The matrix E is a diagonal matrix of the eigenvalues of $H(\theta^u)$ and it can be immediately seen that this equation implies $H(\theta^u) = Q E Q^T$. In fact, the columns of the matrix Q are the right eigenvectors of $H(\theta^u)$. Equation (4.3) becomes

$$V_{PE}(\theta) = V_{PE}(\theta^u) + \frac{1}{2}(\Delta\theta)^T Q E Q^T (\Delta\theta) \tag{4.4}$$

Let $\Delta\theta = Q\ \vartheta$ so that $\vartheta = Q^{-1}\ \Delta\theta = Q^T\ \Delta\theta$ and $\theta = Q\ \vartheta + \theta^u$. Equation (4.4) becomes

$$V_{PE}(Q\ \vartheta + \theta^u) = V_{PE}(\theta^u) + \frac{1}{2}\vartheta^T E\ \vartheta \tag{4.5}$$

Notice that the Hessian matrix of V_{PE} is equivalent to the negative of the Jacobian of the gradient system equations (i.e., $J_{gs} = -H$). The eigenvalues of J_{gs} are hyperbolic and then so are the eigenvalues of H, which are the elements of E. It must also be noted that the matrix Q is now the basis for the new variables ϑ and this basis is based at the UEP, θ^u. If u_i is the i^{th} right eigenvector of H then u_i is the new coordinate axis for ϑ_i.

Let the eigenvalues of J_{gs} evaluated at the UEP be $\lambda_1, \lambda_2, \ldots, \lambda_k, -\lambda_{k+1}, \ldots, -\lambda_{n-1}$ with $\lambda_i > 0$. The first k eigenvalues of J_{gs} are positive while the last $(n-1-k)$ eigenvalues are negative. The elements of the diagonal matrix E are then $-\lambda_1, -\lambda_2, \ldots, -\lambda_k, \lambda_{k+1}, \ldots, \lambda_{n-1}$. Equation (4.5) can then be expanded into

$$V_{PE}(Q\ \vartheta + \theta^u) = V_{PE}(\theta^u) + \frac{1}{2}(-\lambda_1 \vartheta_1^2 - \cdots - \lambda_k \vartheta_k^2 + \lambda_{k+1} \vartheta_{k+1}^2 + \cdots + \lambda_{n-1} \vartheta_{n-1}^2)$$

The energy at any point on the stable manifold $W^s(\theta^u)$ has equal or higher energy that of $V_{PE}(\theta^u)$. The equipotential energy contours in question will have the form $\{\ \vartheta : V_{PE}(Q\ \vartheta + \theta^u) - V_{PE}(\theta^u) = \varepsilon,\ \varepsilon > 0\ \}$. Close to the

controlling UEP these equipotential energy contours will take the form in the Q basis as

$$\varepsilon = \frac{1}{2}(- \lambda_1 \vartheta_1^2 - \cdots - \lambda_k \vartheta_k^2 + \lambda_{k+1} \vartheta_{k+1}^2 + \cdots + \lambda_{n-1} \vartheta_{n-1}^2) \qquad (4.6)$$

Equation (4.6) takes the form of a higher dimensional hyperboloid.

4.3 Equipotential Energy Contours of the Function V_{PE}

Two examples are given in this section to illustrate the shape of the equipotential energy contours of V_{PE} around θ^u. The first is an example to show the hyperbolic contours which are a result of the Taylor series expansion of V_{PE}. The second example illustrates the actual equipotential contours of a 3-machine system.

4.3.1 Two-dimensional Example of the Hyperbolic Contours of the Function V_{PE}

As an example to illustrate the hyperbolic contours, let V_{PE} be a function of two variables θ_1 and θ_2. Let $+\lambda_1$ and $-\lambda_2$ be the eigenvalues of J_{gs} and let u_1 and u_2 be the corresponding eigenvectors. The eigenvalues of $H(\theta^u)$ are then $-\lambda_1$ and $+\lambda_2$. Figure 4.2 is an illustration of the equation

$$\varepsilon = \frac{1}{2}(-\lambda_1 \vartheta_1^2 + \lambda_2 \vartheta_2^2)$$

for $\varepsilon > 0$, $\varepsilon < 0$ and $\varepsilon = 0$. Three different contours levels for $\varepsilon > 0$, one for $\varepsilon < 0$ and one for $\varepsilon = 0$ are shown. These contour levels look more like parabaloids than hyperboloids, but these levels are supposed to represent hyperboloids. The eigenvectors u_1 and u_2 are shown and note the symmetry of the contours around these eigenvectors. The stable and unstable manifolds of the gradient

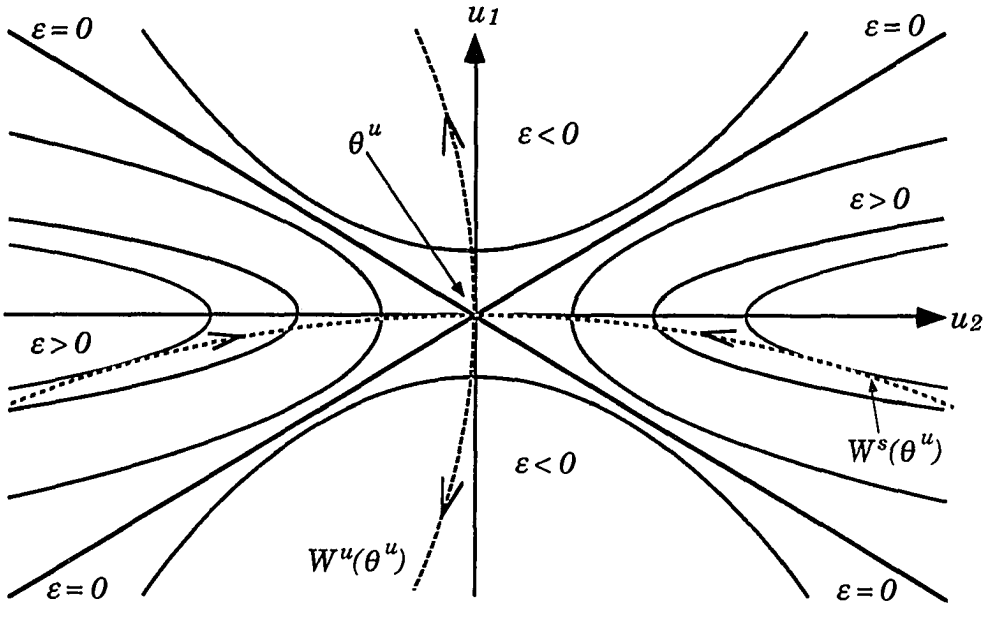

Figure 4.2 Hyperbolic equipotential energy curves

system are shown and note that the corresponding eigenvectors are tangent to these.

4.3.2 Energy Contours of the Function V_{PE} for the Unloaded 3-machine System

In this section four figures which illustrate the equipotential contours of the function V_{PE} for the unloaded 3-machine system will be given. The data for the 3-machine system as well as an one-line diagram is given in Appendix B, Sections B.1 and B.2. This system contains transfer conductances. In order to illustrate the equipotential contours of V_{PE} (3.5c) for this system the transfer conductances need to be eliminated and hence the name unloaded 3-machine system. The unloaded 3-machine system is a modified version of the 3-machine system and is given in Appendix B, Section B.3.

The purpose of showing these figures is to show: i) the stability boundary of the associated gradient system, ii) the equilibrium points on this stability boundary and iii) the shape of the equipotential energy levels near an UEP and around the stable manifold.

The potential energy function V_{PE} given by equation (3.5c) is shown by equation (4.7) with explicit numerical values for C_{ij} and M_i from Appendix B, Section B.3. It must first be noted that from the internal generator angles given in Table B.9, $\delta^s = 0$ and hence, the SEP, $\theta^s = 0$. The values of P_i are also zero.

$$V_{PE} = - C_{12}\left(\cos\left(\theta_1 - \theta_2\right) - 1\right) - C_{13}\cos\left(\theta_1 + \frac{1}{M_3}\left(\theta_1 M_1 + \theta_2 M_2\right)\right)$$

$$- C_{23}\cos\left(\theta_2 + \frac{1}{M_3}\left(\theta_1 M_1 + \theta_2 M_2\right)\right) + C_{13} + C_{23}$$

Substituting C_{ij} and M_i for explicit values

$$V_{PE} = - 1.1712\cos\theta_{12} - 1.4096\cos\left(\theta_1 + \frac{1}{0.1254}\left(0.0160\,\theta_1 + 0.0340\,\theta_2\right)\right)$$

$$- 1.7384\cos\left(\theta_2 + \frac{1}{0.1254}\left(0.0160\,\theta_1 + 0.0340\,\theta_2\right)\right) + 4.3192$$

Simplifying, the above equation becomes

$$V_{PE} = - 1.1712\cos\left(\theta_1 - \theta_2\right) - 1.4096\cos\left(1.1276\,\theta_1 + 0.2711\,\theta_2\right)$$

$$- 1.7384\cos\left(0.1276\,\theta_1 + 1.2711\,\theta_2\right) + 4.3192 \qquad (4.7)$$

The associated gradient system is defined in Chapter 3, Section 3.2 and is

$$\dot{\theta}_1 = z_1 = \frac{- \partial V_{PE}}{\partial \theta_1} = - 1.1712\sin\left(\theta_1 - \theta_2\right) - 1.5895\sin\left(1.1276\,\theta_1 + 0.2711\,\theta_2\right)$$

$$- .2218\sin\left(0.1276\,\theta_1 + 1.2711\,\theta_2\right) \qquad (4.8a)$$

$$\dot{\theta}_2 = z_2 = \frac{-\partial V_{PE}}{\partial \theta_2} = 1.1712 \sin(\theta_1 - \theta_2) - 0.3821 \sin(1.1276\,\theta_1 + 0.2711\,\theta_2)$$

$$- 2.2097 \sin(0.1276\,\theta_1 + 1.2711\,\theta_2) \qquad (4.8b)$$

Figure 4.3 is a contour plot of the equipotential curves of V_{PE} (4.7). The range of the axes is from $-350°$ to $350°$ for θ_1 and from $-300°$ to $300°$ for θ_2. There are many features of Figure 4.3 and are noted in the following paragraphs.

Theorem 3.2.6 states that the trajectories of the gradient system cross equipotential surfaces orthogonally. Therefore, the flow or phase-plane portrait can immediately be observed from Figure 4.3.

The SEP of this unloaded gradient system is $\theta^s = (0.0°, 0.0°)$ and this correlates to the low point of energy denoted by L. The stability region is shaped as a bowl since by moving away from θ^s the energy of the equipotential surfaces increase. Figure 4.4 is similar to Figure 4.3 except that the stability boundary of the gradient system has been drawn in. There are twelve unstable equilibrium points on the stability boundary. Six of these are high points of energy each denoted by H. These high points are actually unstable equilibrium points of the gradient system and are sources (i.e., all eigenvalues of J_{gs} evaluated at this equilibrium point have a positive real part) in which the flow always moves away from this type of equilibrium point. The other six equilibrium points are saddle points (i.e., at least one eigenvalue has a positive real part and at least one eigenvalue has a negative real part when J_{gs} is evaluated at this point). These saddles are denoted by the black dots in Figure 4.4. Table 4.1 contains a list of the twelve equilibrium points on the stability boundary.

The stability boundary that is drawn into Figure 4.4 is composed of the stable manifolds of the twelve equilibrium points on the stability boundary. Note that these stable manifolds were not numerically calculated. As noted, if the equipotential contours are known the flow can be observed immediately, hence, the stable manifolds were drawn in such that the equipotential surfaces were perpendicular to the flow. The saddle points are type-*1* and have an one-dimensional stable manifold that can be distinguished in Figure

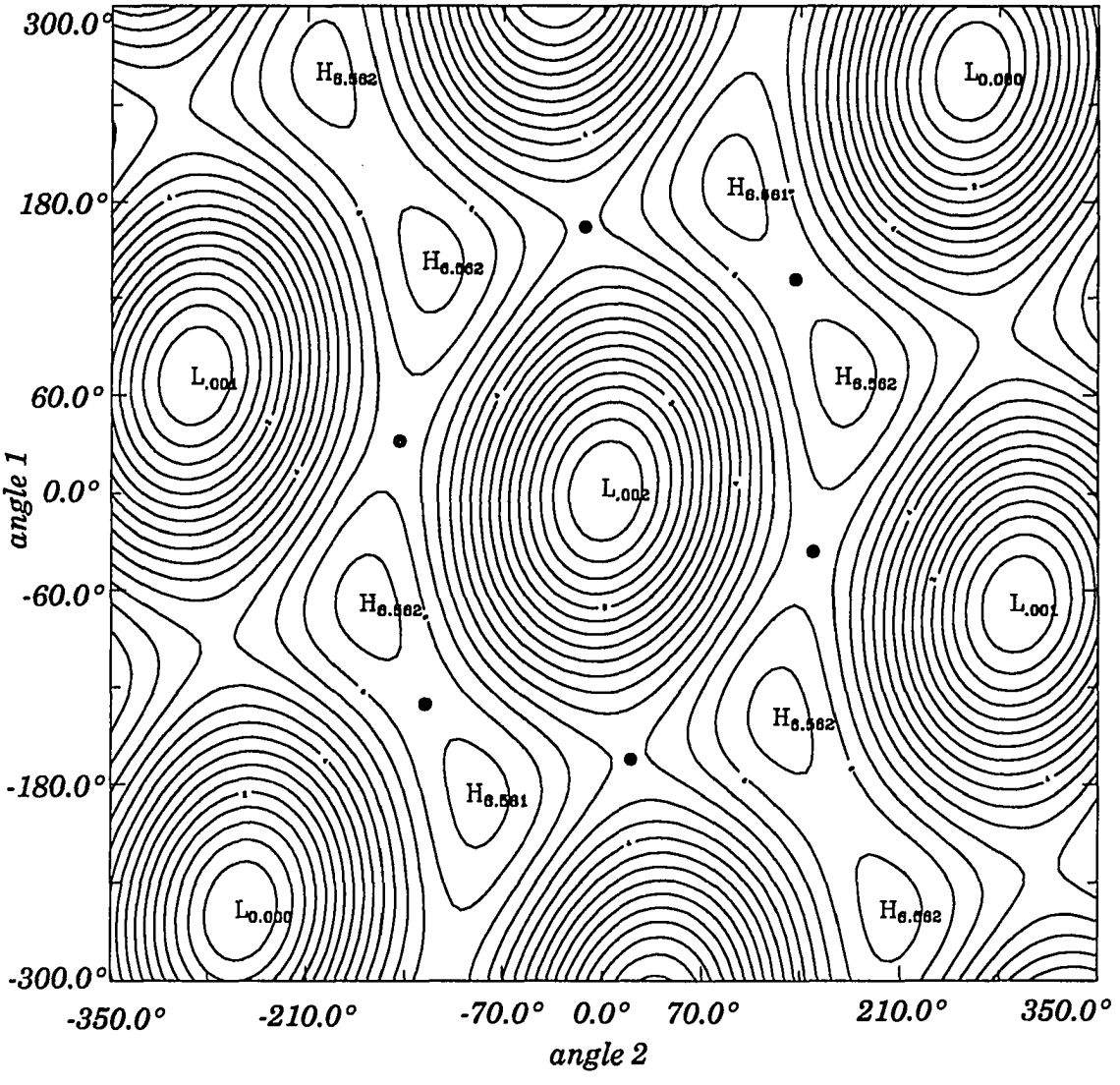

Figure 4.3 Equipotential contours of V_{PE}

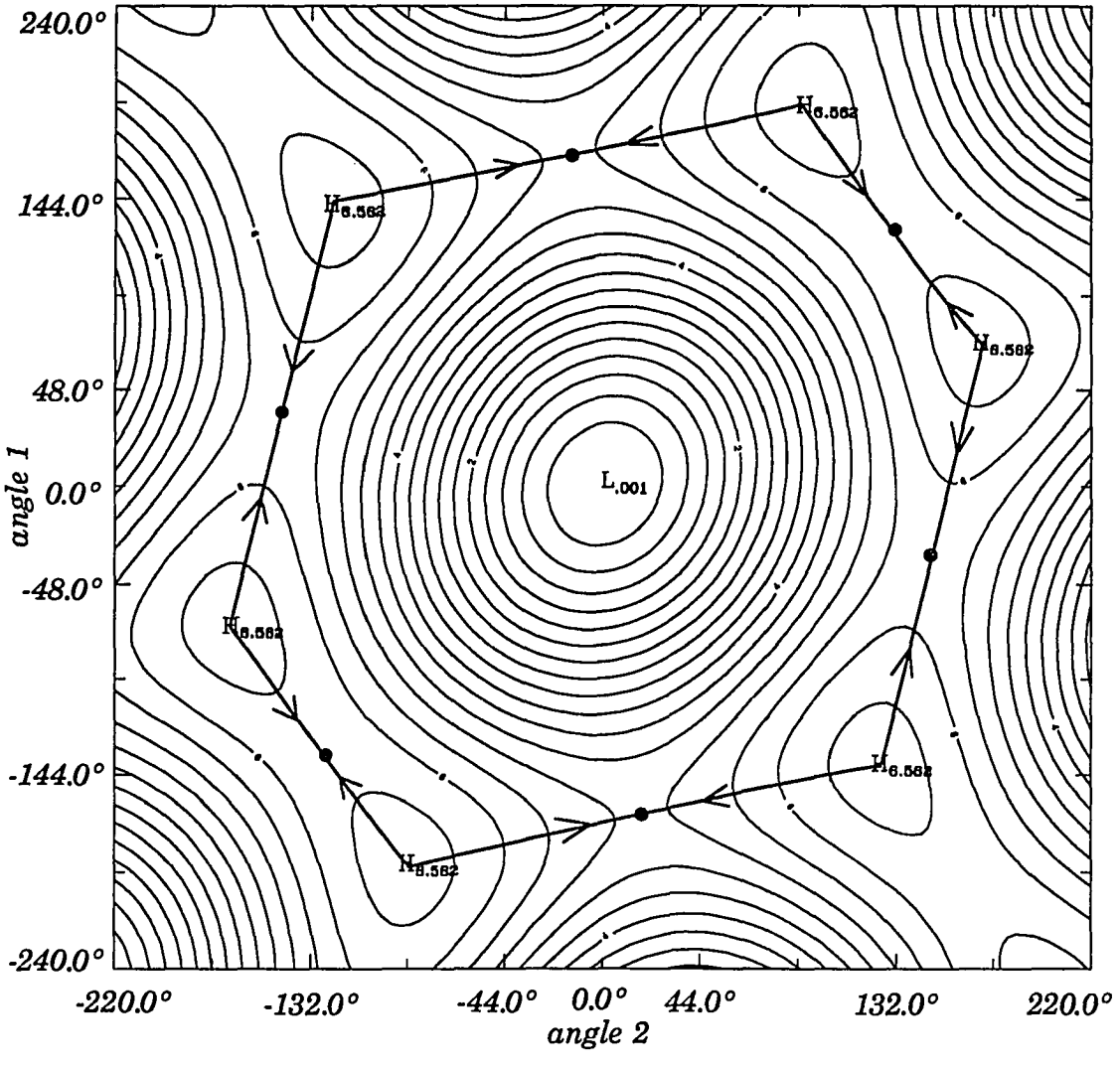

Figure 4.4 Equipotential contours of V_{PE} with stability boundary

Table 4.1 Equilibrium points on the stability boundary of the gradient system

Equilibrium points (θ_1,θ_2)	
Sources	Saddles
(139.92°, -122.68°)	*(163.58°, -16.42°)*
(187.23°, 89.83°)	*(128.69°, 128.69°)*
(70.14°, 167.55°)	*(-34.89°, 145.11°)*
(-139.92°, 122.68°)	*(-163.58°, 16.42°)*
(-187.23°, -89.83°)	*(-128.69°, -128.69°)*
(-70.14°, -167.55°)	*(34.89°, -145.11°)*

4.4 by the arrows denoting the flow direction. The source points are type-*2* and have a zero-dimensional stable manifold and this stable manifold is just the source point itself.

These twelve unstable equilibrium points are also unstable equilibrium points on the stability boundary of the four-dimensional swing system as stated in Theorem 3.3.5. Let an equilibrium of the swing system have the form $(\theta_1, \varpi_1 = 0, \theta_2, \varpi_2 = 0)$, then for example, *(163.58°, 0, 16.42°, 0)* is an unstable equilibrium points swing system. As noted in Theorem 3.3.3 the type-*1* unstable equilibrium points of the gradient system (i.e., saddle points) are type-*1* unstable equilibrium points of the swing system (i.e., saddle points). Type-*2* unstable equilibrium points of the gradient system (i.e., source points) are type-*2* unstable equilibrium points of the swing system (i.e., saddle points).

Figure 4.5 contains an illustration of a detailed contour plot of the equipotential surfaces around the saddle point *(163.58°, -16.42°)* and the stable manifold of this saddle point. These equipotential surfaces are similar to the ones shown in Figure 4.2. It seems obvious that the equipotential surfaces look hyperbolic in shape even when they are not relatively close to the saddle point. In other words, the equipotential surfaces whose energy is not

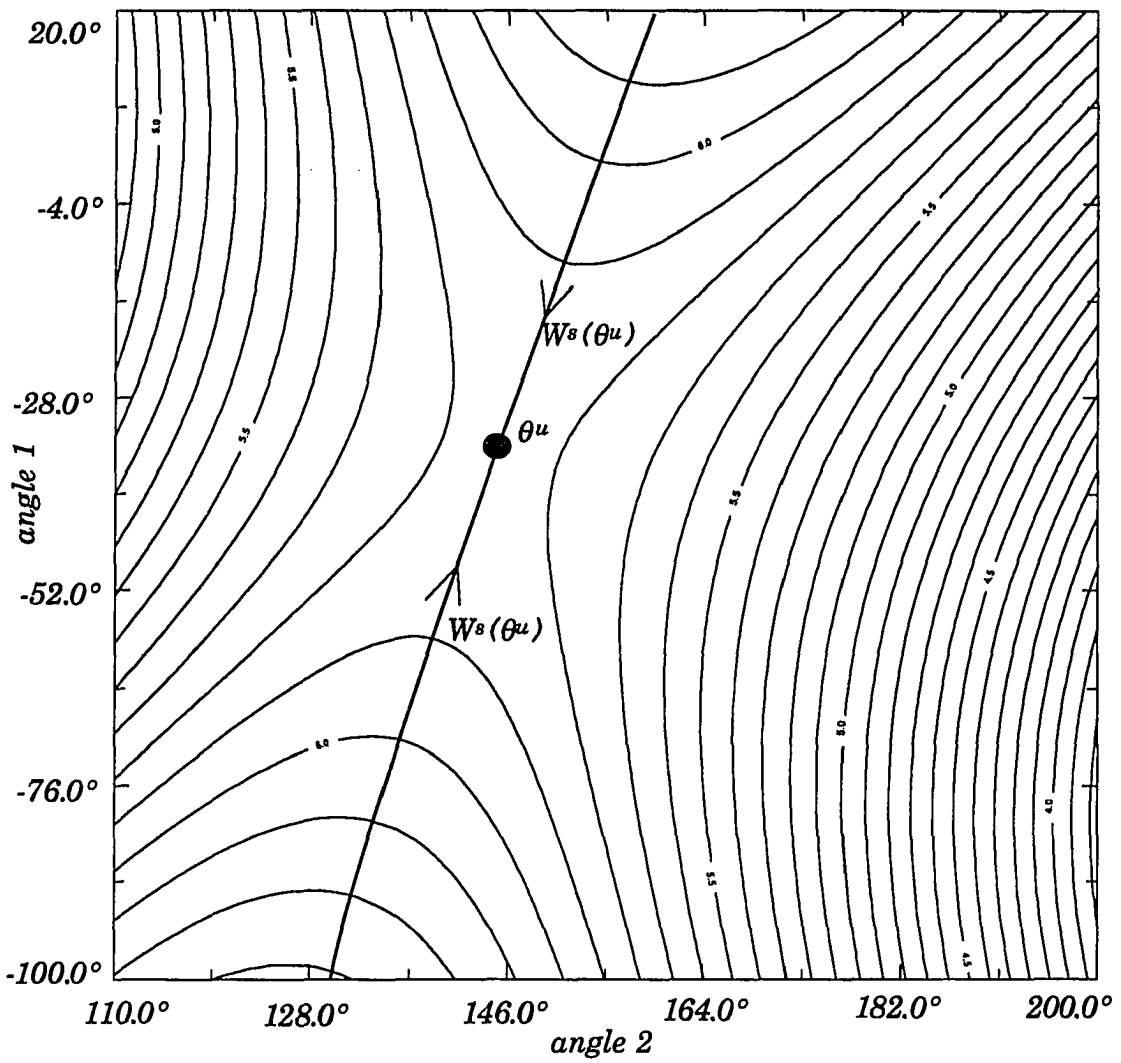

Figure 4.5 Close-up of the equipotential contours of V_{PE}

relatively close to the energy of the saddle point still keep there hyperbolic shape around the stable manifold.

All of the points denoted by L in Figure 4.1 are low points. The low points are stable equilibrium points of the gradient system and each low point has a region of attraction. However only one of these low points is the stable equilibrium point that is of interest. Similarly, all points denoted by H in Figure 4.1 are source points.

Also, symmetry can be seen in Figure 4.3 and in the unstable equilibrium points given in Table 4.1. This symmetry is due to the fact that the *cosine* terms in the function V_{PE} are periodic with period 2π. Reference [39] contains a further investigation into this symmetry.

4.4 Energy Well of the function V_{PE} for the 3-machine System

Figure 4.6 contains a better perspective of the depth of the equipotential surfaces of the function V_{PE} that cannot be fully illustrated by Figures 4.3 and 4.4. This shows that the equipotential surfaces of the function V_{PE} do indeed form an energy well. The ridge around the top of the energy bowl can be seen as stability boundary and the dips in this ridge are the saddle points. Note that units on both axis are in radians.

4.5 Detecting the Exit Point of the Gradient System

The purpose of the discussion in the last two sections was to illustrate the shape of the equipotential surfaces around the stable manifold of a saddle point. It may be concluded that not only do the equipotential surfaces around the stable manifold close to saddle point have a hyperbolic like shape but that they retain this type of shape when they are not relatively close to the saddle point.

Under Assumption 4.1 the projection into θ-space of the disturbed trajectory intersects the stable manifold $W^s(\theta^u)$ at the exit point θ^{egs}. This situation is depicted in Figure 4.7.

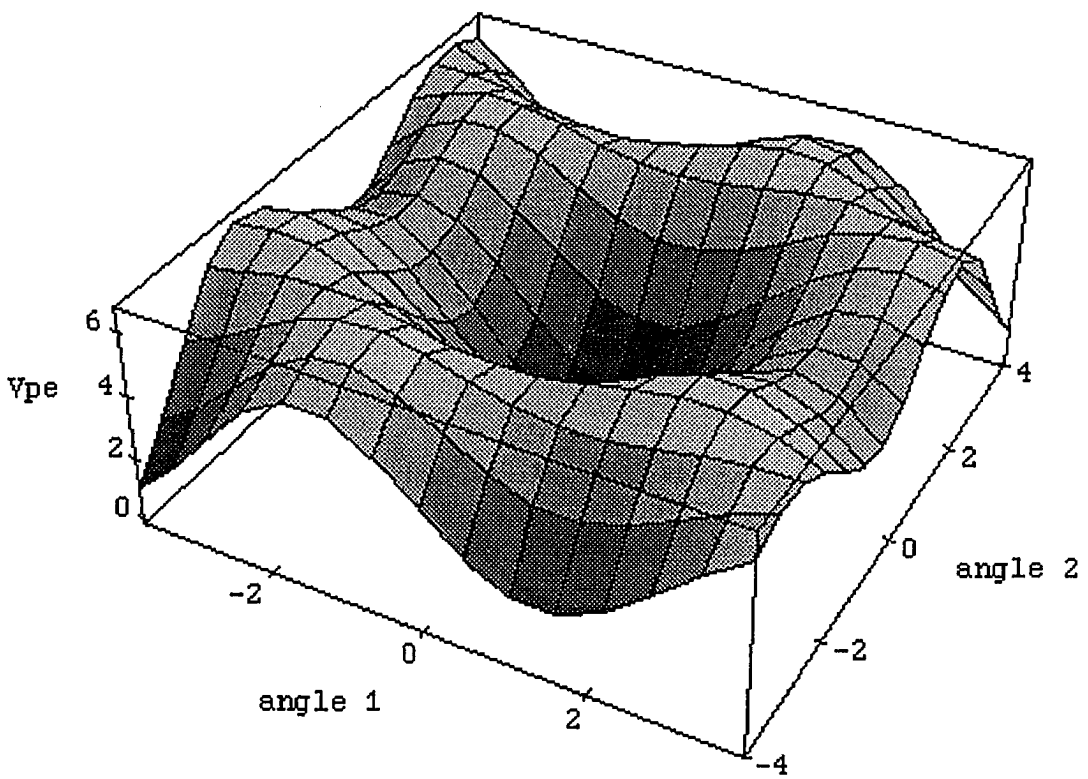

Figure 4.6 Energy well of the function V_{PE}

Figure 4.7 is an illustration of four typical hyperbolic like energy curves around the stable manifold of the controlling UEP which is assumed to be a saddle point. These equipotential curves have values of $0 < C_1 < C_2 < C_3 < C_4$. The exit point θ^{egs} is rarely numerically detectable but a close approximation to this point can be made. This approximation results in the point $\theta^{egs\alpha}$. The point $\theta^{egs\alpha}$ is numerically detected by evaluating

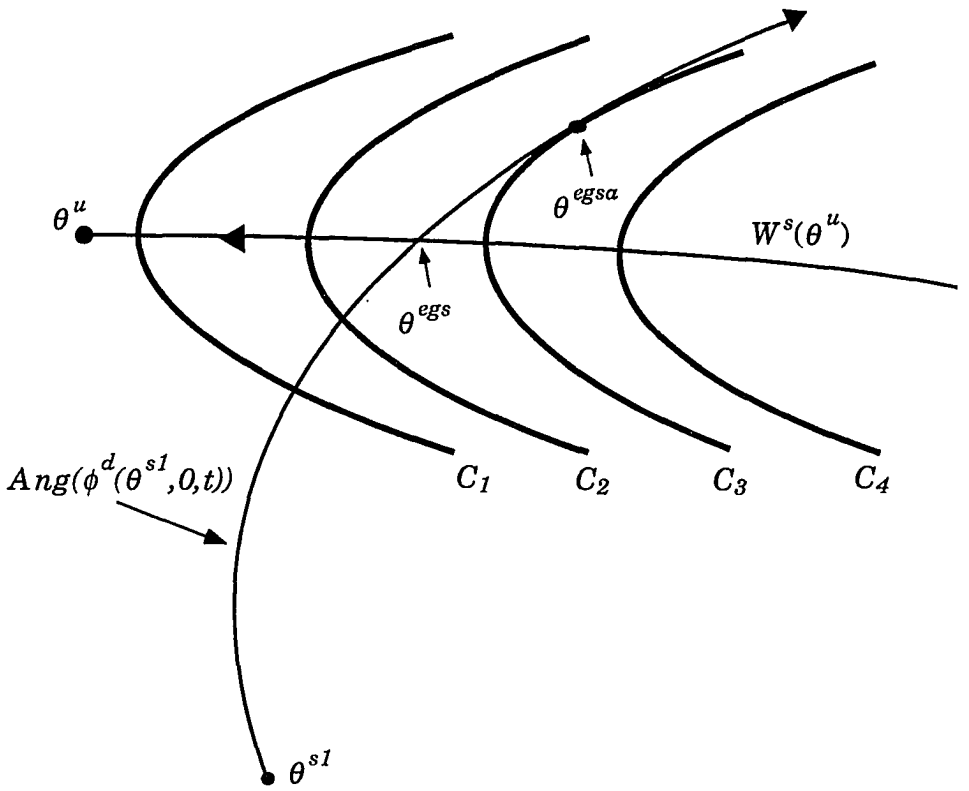

Figure 4.7 Approximating the exit point of the gradient system

$$\frac{dV_{PE}}{dt} = \frac{\partial V_{PE}}{\partial \theta}\frac{d\theta}{dt} = - z \cdot \varpi = 0 \tag{4.9}$$

along the disturbed trajectory. The vector z is the negative gradient of the function V_{PE} as defined in Chapter 3, Section 3.2 and $\varpi = \dot{\theta}$. The reason that equation (4.9) is satisfied in Figure 4.7 can explained in two ways.

Before $Ang(\phi^d(\theta^{s1},0,t))$ gets to the point θ^{egsa}, the values of V_{PE} along this trajectory are less than C_3, at θ^{egsa}, $V_{PE} = C_3$ and after this $V_{PE} < C_3$. Hence, V_{PE} goes through a maximum at the point θ^{egsa}.

The second method of visualizing equation (4.9) is shown in Figure 4.8.

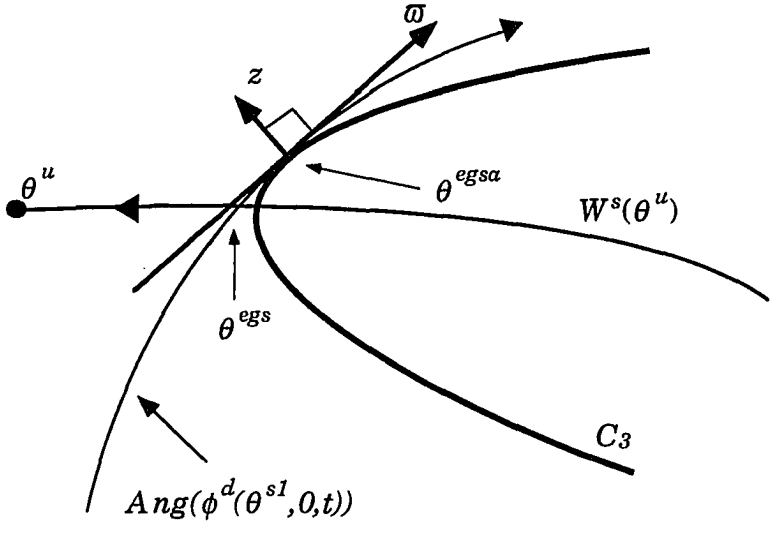

Figure 4.8 Detecting the approximate exit point of the gradient system

Since the vector z is the negative gradient of V_{PE} it is perpendicular to the equipotential surface at the point at which it is based. The vector $\varpi = \dot{\theta}$ is tangent to the projection into θ-space of the disturbed trajectory. At the point $\theta^{egs\alpha}$ it is seen that the vectors z and ϖ are perpendicular to each other which is exactly what is stated by equation (4.8). Note that the only way the exit point θ^{egs} is detected is if $Ang(\phi^d(\theta^{s1},0,t))$ intersects $W^s(\theta^u)$ perpendicularly and this makes detecting this point virtually numerically impossible. In both Figures 4.7 and 4.8 the point $\theta^{egs\alpha}$ was outside the stability region of the gradient system. In general, this point can be either in the stability region or outside of the region. Note that there can be other points along $Ang(\phi^d(\theta^{s1},0,t))$ where $dV_{PE}/dt = 0$. For example if $Ang(\phi^d(\theta^{s1},0,t))$ passes near and by θ^s, a point where $dV_{PE}/dt = 0$ may be encountered and this may be a minimum point. Since $\theta^{egs\alpha}$ is a point where V_{PE} goes through a maximum, dV_{PE}/dt will go from being positive to being negative. However, it is assumed that the point $\theta^{egs\alpha}$ will be encountered somewhere relatively close to the stability boundary of the gradient system.

4.6 Numerical Algorithm of the Exit Point Method

The numerical algorithm of the exit point method is a computational scheme that determines a point relatively close to the controlling UEP. The numerical algorithm of the exit point method is given below in two steps and this algorithm is denoted *algorithm-EP*. For some dynamical system with solution ϕ, define $N(\phi)$ to be the numerical approximation to ϕ.

algorithm-EP

i) Detect the point $\theta^{egs\alpha}$ along the numerical trajectory $N(Ang(\phi^d(\theta^{s1},0,t)))$. It was assumed in Section 4.1 that $(\theta^{s1},0) \in A(\theta^s,0)$. Let θ^{lu} be the UEP on the stability boundary of the gradient system with lowest energy. Assume that $\theta^{s1} \in V_c(\theta^{lu})$ where the definition of $V_c(\theta^{lu})$ follows from a similar definition given in Section 3.1.2.

ii) Define

$$\psi(t) = \sum_{i=1}^{n-1} \left| z_i(N(\phi_{gs}(\theta^{egs\alpha},t))) \right|$$

$\psi(t)$ is then the 1-norm of z along $N(\phi_{gs}(\theta^{egs\alpha},t_2))$. .Let $\theta^{mgp} = N(\phi_{gs}(\theta^{egs\alpha},t_2))$ where $t_2 > 0$ is the first time such that $\psi(t_2)$ reaches a local minimum. The point θ^{mgp} is referred to as the *minimum gradient point.*

Find the minimum gradient point θ^{mgp}.

After these two steps are completed the controlling UEP θ^u is simply solved for by solving the nonlinear algebraic equations $z = 0$ with θ^{mgp} as the initial guess.

When the controlling UEP is determined, transient stability can be assessed as described in Section 3.1.3.

4.7 Interpretation of the Steps in the Exit Point Algorithm

The reasoning behind algorithm-EP can be explained through the following two scenarios. These scenarios follow the same three step format in which algorithm-EP is explained.

Scenario 1:

i) The exit point of the gradient system $\theta^{egs} \in W^s(\theta^u)$ is detected.

ii) Assume that the numerical integration technique has infinite precision and thus exactly traces the trajectory $\phi_{gs}(\theta^{egs},t)$. Since $\theta^{egs} \in W^s(\theta^u)$, $\phi_{gs}(\theta^{egs},t) \rightarrow \theta^u$ as $t \rightarrow \infty$. However, along $\phi_{gs}(\theta^{egs},t)$, $\psi(t)$ may or may not go through a local minimum, but it can see that $\psi(t) \rightarrow 0$ as $t \rightarrow \infty$; If T is taken large enough, the point $\phi_{gs}(\theta^{egs},T)$ should be relatively near θ^u. If the point $\phi_{gs}(\theta^{egs},T)$ is taken as the initial guess, the nonlinear algebraic solver should converge to θ^u which is the desired result. Note that any numerical integration has finite precision and if the initial condition were on the stable manifold the numerical trajectory would soon depart from this manifold due to numerical error.

iii) The controlling UEP θ^u is solved for using $\phi_{gs}(\theta^{egs},T)$ as an initial starting guess.

Scenario 2:

i) The approximate exit point θ^{egsa} is detected and this point is assumed to be relatively close to the stable manifold $W^s(\theta^u)$ for the following reasons. It can be observed that if the equipotential contours have a

sufficient curvature near $W^s(\theta^u)$ and if the projection into θ-space of the disturbed trajectory intersects the stable manifold in a near perpendicular fashion the point $\theta^{egs\alpha}$ will most likely be relatively close to $W^s(\theta^u)$. Note that this point may or may not be in the stability region of the gradient system.

ii) It is assumed that there is a finite precision in the numerical approximation. It seems reasonable that if $\theta^{egs\alpha}$ is relatively close to $W^s(\theta^u)$, $N(\phi_{gs}(\theta^{egs\alpha},t))$ should stay relatively close to $W^s(\theta^u)$ for a certain period of time and near the end of this time period $N(\phi_{gs}(\theta^{egs\alpha},t))$ should be relatively close to θ^u. After the end of this period $N(\phi_{gs}(\theta^{egs\alpha},t))$ will tend to flow away from $W^s(\theta^u)$ and θ^u. As $N(\phi_{gs}(\theta^{egs\alpha},t))$ approaches closer to θ^u, $\psi(t)$ should get smaller since this quantity is based on the vector field z. At the UEP $z = 0$, therefore, close to the UEP the 1-norm of z must be relatively small. As $N(\phi_{gs}(\theta^{egs\alpha},t))$ passes by θ^u, $\psi(t)$ should begin to get larger. Therefore, $\psi(t)$ will go through a local minimum when $N(\phi_{gs}(\theta^{egs\alpha},t))$ is relatively close to θ^u.

iii) The initial guess point θ^{mgp} will be relatively close to θ^u so that the nonlinear algebraic solver will produce θ^u.

Figure 4.9 is an illustration of the three steps of the numerical algorithm of the exit point method. The system that is used is the unloaded 3-machine system that was first utilized in Section 4.3.2. The controlling UEP θ^u has the coordinates $(-34.89°, 145.11°)$ which are in the form (θ_1,θ_2). It is assumed that $W^s(\theta^u)$ is intersected by $Ang(\phi^d(\theta^{s1},0,t))$ and that the approximate exit point $\theta^{egs\alpha}$ has been found and is relatively close to $W^s(\theta^u)$ as shown in the Figure 4.9. There is no actual disturbed trajectory simulated. The point $\theta^{egs\alpha}$ is just placed in the relative vicinity of $W^s(\theta^u)$ and notice that this point is in the stability region of the gradient system. The point $\theta^{egs\alpha}$ has the coordinates $(-87.00°, 131.17°)$. The numerical trajectory $N(\phi_{gs}(\theta^{egs\alpha},t))$ is shown in this figure and was actually simulated by the integration of equations (4.8). Note that this trajectory does indeed stay relatively close to

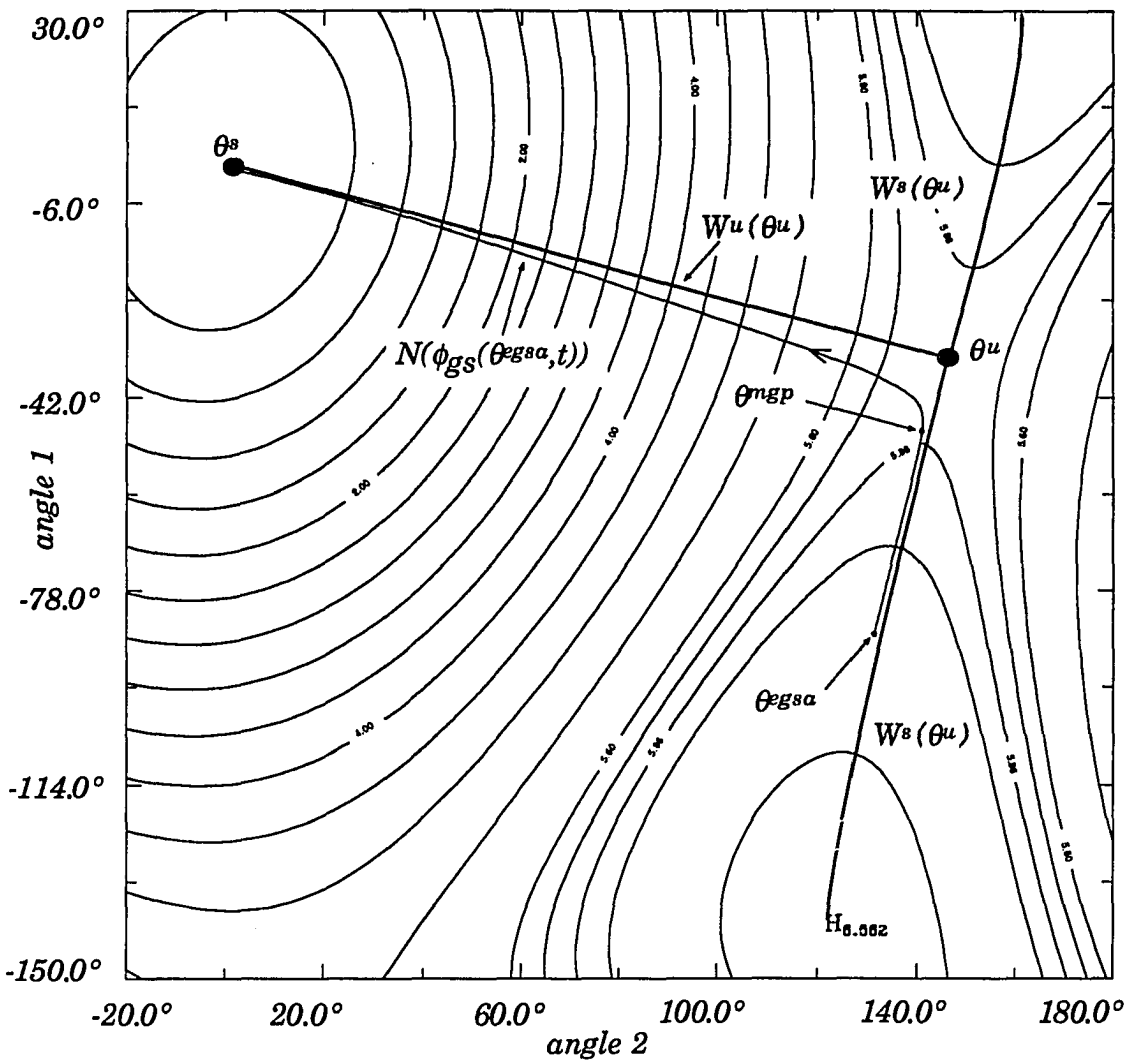

Figure 4.9 Illustration of the minimum gradient point

$W^s(\theta^u)$ for some time. The minimum gradient point was found as indicated and is located at *(-46.40°, 141.13°)*. Note that this point is relatively close to θ^u. At the point before θ^{mgp} on the numerical trajectory, the 1-norm of z is $|z_1| + |z_2| = 0.2112$, at θ^{mgp}, $|z_1| + |z_2| = 0.2109$, and at the point after θ^{mgp}, $|z_1| + |z_2| = 0.2147$, which shows that a minimum of $\psi(t)$ was found at θ^{mgp}.

Figure 4.10 is similar to Figure 4.9 except that the approximate exit point $\theta^{egs\alpha}$ is not in the stability region of the gradient system. The coordinates for the point $\theta^{egs\alpha}$ are *(-87.00°, 131.19°)*. The minimum gradient point was determined to be at the coordinates *(-56.46°, 140.86°)* and is in a similar position with respect to θ^u as the θ^{mgp} in Figure 4.9. The numerical trajectory converges to the point *(-69.78°, 290.22°)* which can be seen in Figure 4.3.

4.8 Issues of the Exit Point Method

Section 4.7 contained an interpretation of the ideas behind the exit point method. These ideas where heuristic and no formal analytical justification exist which states that through the application of this method the controlling UEP will be determined. Since this method does not have a strict analytical foundation, problems with the method may arise. In fact, problems have been observed in certain systems when the exit point algorithm was applied. This section contains a list of the problems observed and a discussion of each.

Problem 1

One problem may be that no minimum of $\psi(t)$ is encountered along $\phi_{gs}(\theta^{egs\alpha},t)$ which implies that there is no minimum gradient point. This idea is illustrated in Figure 4.11. It is assumed that $W^s(\theta^u)$ is intersected by $Ang(\phi^d(\theta^{s1},0,t))$. The approximate exit point is located at *(-87.00°, 128.00°)*. The numerical trajectory $N(\phi_{gs}(\theta^{egs\alpha},t))$ is also shown. Along $N(\phi_{gs}(\theta^{egs\alpha},t))$ there is no minimum of $|z_1| + |z_2|$. In this particular situation a reason that there is no minimum of $|z_1| + |z_2|$ might be that the numerical trajectory does not approach θ^u and this is due to the fact that $\theta^{egs\alpha}$ is not

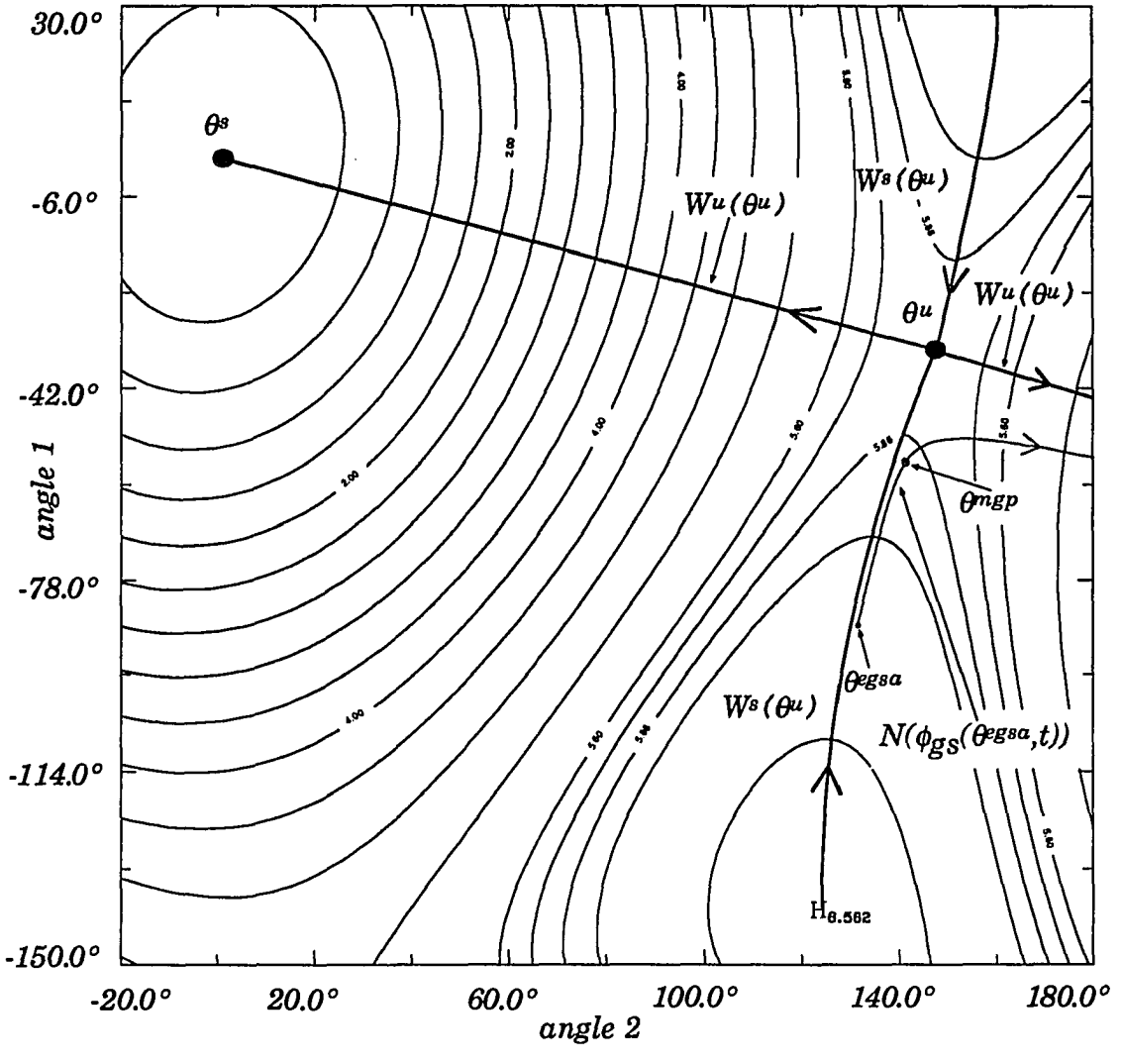

Figure 4.10 Illustration of the minimum gradient point outside of the stability region

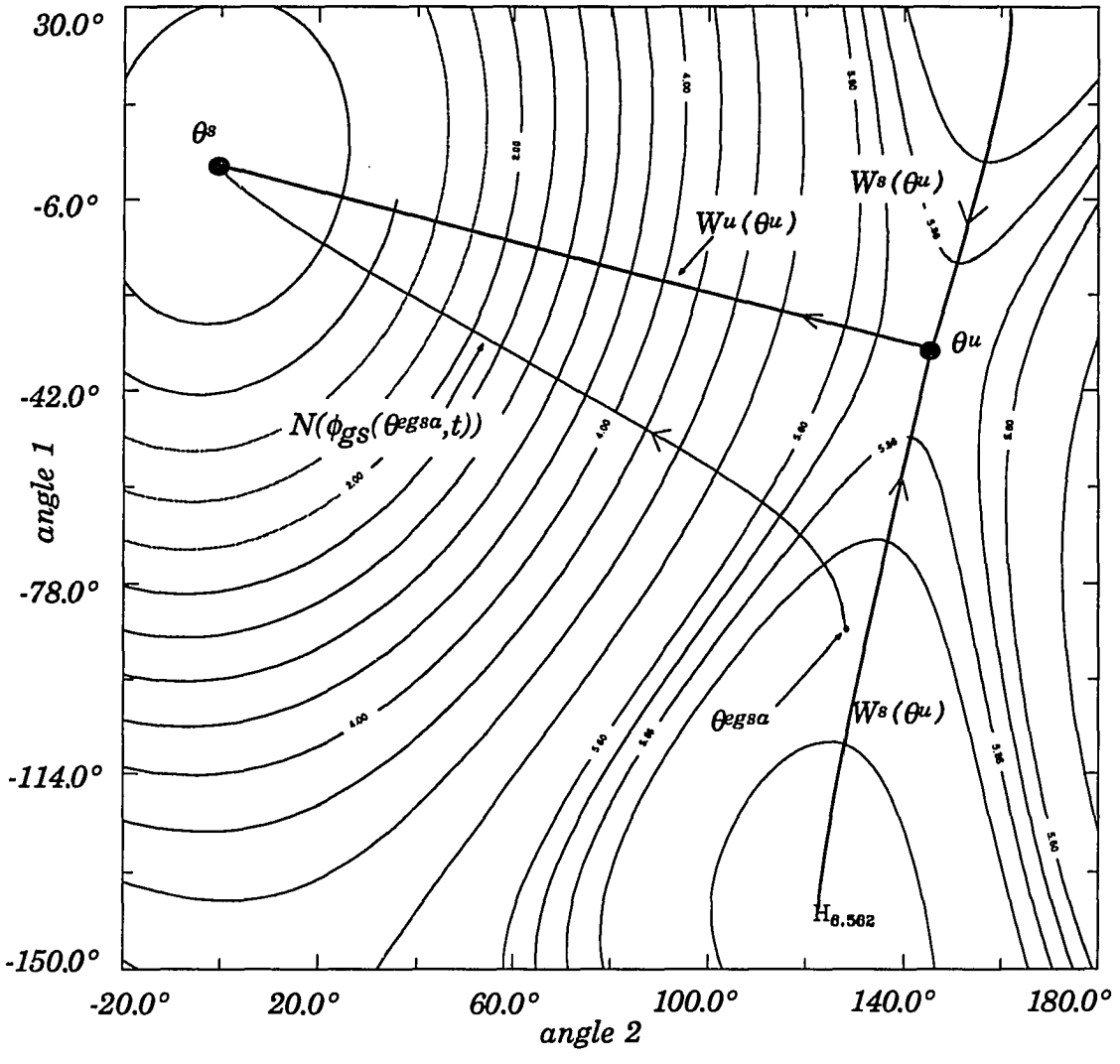

Figure 4.11 No minimum gradient point found

relatively close to $W^s(\theta^u)$. Therefore, it may be plausible to conclude that the closer θ^{egsa} is to $W^s(\theta^u)$ the better the chances are that $N(\phi_{gs}(\theta^{egsa},t))$ will pass near θ^u and a resultant minimum gradient point will be encountered.

The existence of the minimum gradient point may also depend on the fact that the true solution $\phi_{gs}(\theta^{egsa},t)$ is approximated by a numerical trajectory $N(\phi_{gs}(\theta^{egsa},t))$. Assume that there is no local minimum of $\psi(t)$ along the true trajectory $\phi_{gs}(\theta^{egsa},t)$. Since there is a difference between $\phi_{gs}(\theta^{egsa},t)$ and $N(\phi_{gs}(\theta^{egsa},t))$, even though this difference may be relatively small, there may be a local minimum of $\psi(t)$ along $N(\phi_{gs}(\theta^{egsa},t))$. The same can be claimed for the reverse situation. There may be a local minimum of $\psi(t)$ along the trajectory of the true solution but along the numerical trajectory there may be no local minimum of $\psi(t)$ encountered.

In the case where there is not a local minimum of $\psi(t)$ encountered along the numerical trajectory, a change in the step size may or may not result in an encountered minimum gradient point. If a minimum gradient point is encountered with the change in the step size this does not imply that the true solution encounters a minimum gradient point.

There are no hard-and-fast rules that can be applied to the above situations. One guideline may be to try to keep the numerical approximation as close to the true solution as possible while keeping in mind that too much accuracy in the numerical solution might be too costly in terms of computation.

If it happens that no minimum of $\psi(t)$ is encountered along the numerical trajectory, then by Theorem 3.2.2, the trajectory will converge to an equilibrium point or go off to infinity. If the trajectory converges to an equilibrium point, this point will be a low point (i.e., a stable equilibrium point). In this case there needs to be a check put into the numerical algorithm so that this situation may be detected. The application of the nonlinear algebraic solver will result in a stable equilibrium point and the exit point method will fail. Note that the stable equilibrium point which the numerical trajectory is converging to may or may not be the stable equilibrium point of the gradient system but is always a low point.

Problem 2

If a local minimum of $\psi(t)$ is encountered along the numerical trajectory then this point θ^{mgp} is used as an initial guess when the nonlinear algebraic equations are solved. It may happen that the equilibrium point determined by the application of the nonlinear algebraic solver is not the controlling UEP θ^u. The point θ^{mgp} is then not in the domain of convergence of θ^u for the particular nonlinear algebraic solving algorithm.

It seems reasonable to assume that if θ^u is not produced by the application of the nonlinear algebraic solver then what is produced is another unstable equilibrium point on the stability boundary of the gradient system or a low point.

Assume that a low point is produced. An assessment of transient stability is fruitless since the energy at a low point is zero.

Assume that another unstable equilibrium point on the stability boundary is produced. This situation is shown in Figure 4.12. It is assumed $W^s(\theta^u)$ is intersected by $Ang(\phi^d(\theta^{s1},0,t))$ and that $\theta^{egsa} \in Ang(\phi^d(\theta^{s1},0,t))$. The point θ^{egsa} is located at *(-120.00°, 123.41°)*. The resultant minimum gradient point θ^{mgp} is located at *(-102.47°, 125.05°)*. When a nonlinear algebraic solving algorithm is applied with θ^{mgp} as the initial guess point, the source point, which is denoted by the symbol H and is located at *(-139.92°, 122.68°)*, is produced. The application of the exit point algorithm was supposed to produce θ^u located at *(-34.89°, 145.11°)*. One reason θ^u is not produced may be that the point θ^{egsa} was located relatively close to the source point and the minimum gradient point which was encountered was not that relatively far from θ^{egsa}. This implies that θ^{mgp} may be relatively close to the source point. The nonlinear algebraic solver algorithm that was used in this case was FindRoot from Mathematica [40].

The source point *(-139.92°, 122.68°)* has a higher energy value than that of the point θ^u and because of this the assessment of transient stability through the evaluation of the energy margin may not be conservative. Since it was assumed that $W^s(\theta^u)$ was intersected by $Ang(\phi^d(\theta^{s1},0,t))$ then by Assumption 4.1, $W^s(\theta^u,0)$ is intersected by $\phi^d(\theta^{s1},0,t)$. It was shown in Theorem 3.1.8 that the trajectory $\phi^d(\theta^{s1},0,t)$ must pass through the constant

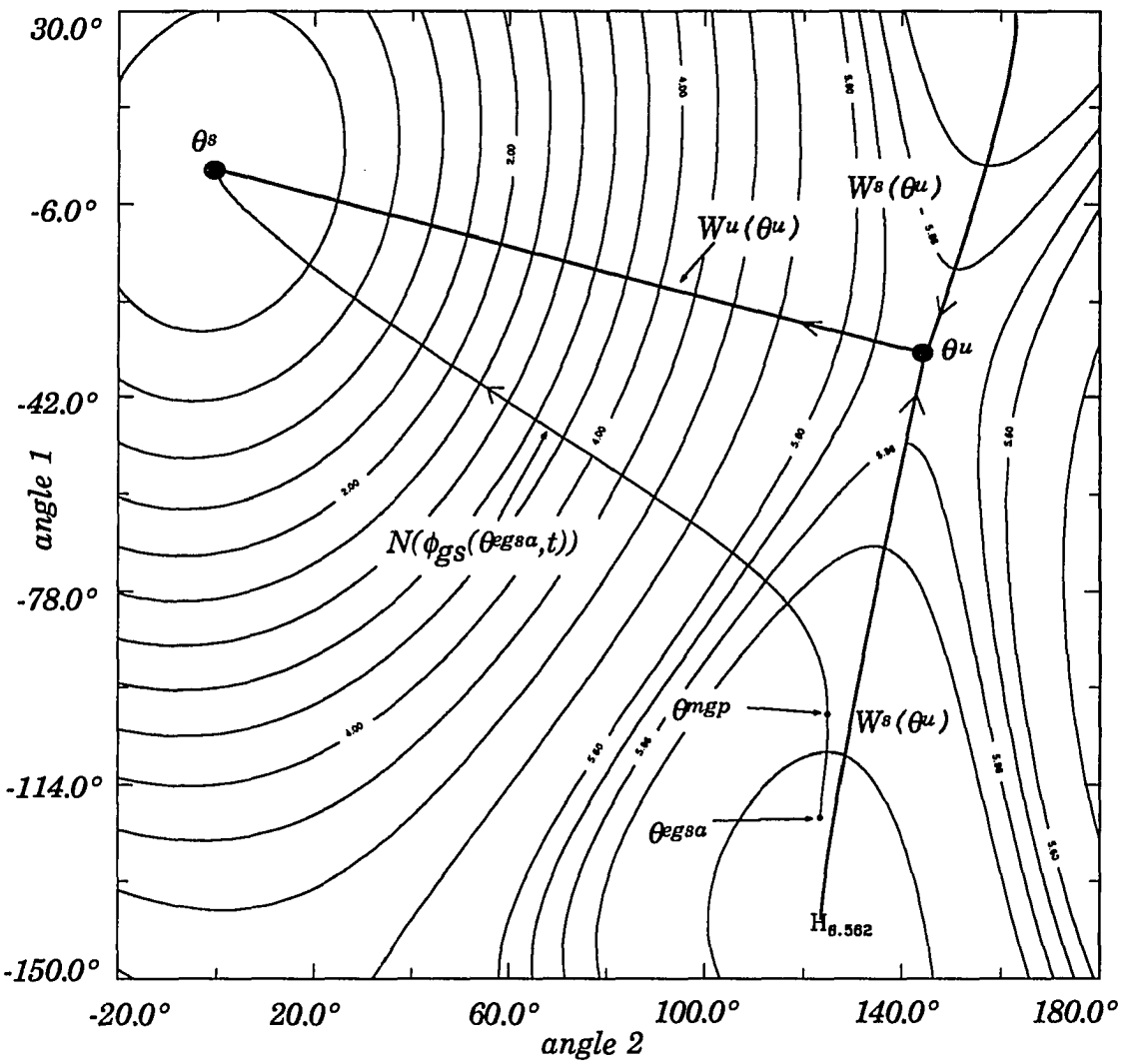

Figure 4.12 Incorrect unstable equilibrium point found

energy surface defined by the energy value at $(\theta^u,0)$ before it intersected $W^s(\theta^u,0)$. However, if the relevant stability boundary is approximated by the constant energy surface, which is defined by the source point, there may be a clearing point $(\theta^{cl},\varpi^{cl})$ that is not in the stability region of the swing system but when assessment is made system is deemed stable.

Assume that through the application of the exit point method a UEP is found which is not the controlling UEP and not a low point. It seems likely that this UEP will have a higher energy value than the controlling UEP θ^u. The reason this might be the case is motivated through Figure 4.12. Take any $\theta^x \in W^s(\theta^u)$, $\theta^x \notin HB$, then $\phi_{gs}(\theta^x,t) \rightarrow \theta^y \in HB$ as $t \rightarrow -\infty$. This follows directly from Theorem 3.2.7. Therefore, this can be interpreted as the stable manifold $W^s(\theta^u)$ "starting at" one or more unstable equilibrium points on the stability boundary of the gradient system and "ending at" θ^u. In Figure 4.12 the stable manifold $W^s(\theta^u)$ "starts at" the two source points *(-139.92°, 122.68°)* and *(70.14°, 167.55°)* and "ends at" θ^u. Both of these unstable equilibrium points have a higher energy than the energy at θ^u. Therefore, if $\theta^{egs\alpha}$ is close to $W^s(\theta^u)$ and one of the higher energy UEPs, θ^{mgp} may also be near one of these higher energy UEPs.

Suppose that θ^{mgp} is encountered. If θ^{mgp} is not encountered near one of the higher energy UEPs or θ^u then it must be relatively far inside the stability region $A(\theta^s)$ or in one of the regions of attraction of another low point. The reason for this is that $\phi_{gs}(\theta^{egs\alpha},t)$ will flow into one of these regions. Therefore, it is most likely in this situation that a low point will be produced by the application of the nonlinear algebraic solver.

Problem 3

The reason Assumption 4.1 was put forth is because there is no analytical justification that $(\theta^{ess},\varpi^{ess}) \in W^s(\theta^u,0)$ implies that $\theta^{egs} \in W^s(\theta^u)$. The reason there is no justification is that the exit points are produced by the disturbed trajectory and this trajectory usually cannot be related to the post-disturbance system. It may be the case that $(\theta^{ess},\varpi^{ess}) \in W^s(\theta^u,0)$ and $\theta^{egs} \in W^s(\theta^j)$ where $\theta^u \neq \theta^j$. In situations like these the method could produce UEPs whose energy values may be higher or lower than the energy at θ^u. It has

been shown in Theorems 3.1.7 and 3.1.8 that the transient stability assessment through the energy margin calculation which is based on the controlling UEP θ^u will be a conservative one. However, with the energy margin calculation based on other UEPs the assessment may be too conservative or even over estimated.

4.9 Application of the Exit Point Method to the Unloaded 3-machine System

In the previous sections of this chapter the associated gradient system of the unloaded 3-machine power system model was analyzed. In this section the results of the application of the exit point method to the unloaded 3-machine swing system are given. Also, transient stability results are shown. For this application the post-disturbance system is taken to be equal to the pre-disturbance system and this system is given in Appendix B, Section B.2. The differential equations of the swing system given by equation (3.1) are.

$$\dot{\varpi}_1 = (- C_{12} \sin(\theta_1 - \theta_2) - C_{13} \sin\left(\theta_1 + \frac{1}{M_3}(\theta_1 M_1 + \theta_2 M_2)\right) - D_1 \varpi_1) / M_1$$

$$\dot{\theta}_1 = \varpi_1$$

$$\dot{\varpi}_2 = (- C_{21} \sin(\theta_2 - \theta_1) - C_{23} \sin\left(\theta_2 + \frac{1}{M_3}(\theta_1 M_1 + \theta_2 M_2)\right) - D_2 \varpi_2) / M_2$$

$$\dot{\theta}_2 = \varpi_2$$

The values of M_i and C_{ij} are given in Section B.2 of Appendix B. The damping is uniform with $D_1 = 2 M_1$ and $D_2 = 2 M_2$.

The disturbed system is taken as

$$\dot{\varpi}_1 = (0.0464 - 0.3 C_{12} \sin(\theta_1 - \theta_2)$$

$$- 0.1\, C_{13} \sin\left(\theta_1 + \frac{1}{M_3}\left(\theta_1 M_1 + \theta_2 M_2\right)\right) - D_1\, \varpi_1 \,) / M_1$$

$$\dot{\theta}_1 = \varpi_1$$

$$\dot{\varpi}_2 = (0.4726 - 0.3\, C_{21} \sin\left(\theta_2 - \theta_1\right) - D_2\, \varpi_2 \,) / M_2$$

$$\dot{\theta}_2 = \varpi_2$$

The disturbed system is similar to the post-disturbance system except for two changes. A small term similar to an increase in mechanical power is added to the right hand side of $\dot{\varpi}_1$ and $\dot{\varpi}_2$. Also, the parameters C_{ij} are scaled which is similar to changes in the power system network configuration. However, it is not claimed that this disturbed system can be realized.

The three steps of the numerical algorithm of the exit point method are illustrated in Figure 4.13. The following observations can be made.

- The projection into θ-space of the numerically calculated disturbed trajectory $N(Ang(\phi^d(\theta^{s1},0,t)))$ is shown. This trajectory starts at $\theta^s = \theta^{s1} = (0.0°, 0.0°)$. It is easily seen that this trajectory intersects the stable manifold $W^s(\theta^u)$ where the coordinates for θ^u are $(128.69°, 128.69°)$.

- As noted earlier, the exit point of the gradient system will probably not be detected, but a point that is relatively close to the stable manifold $W^s(\theta^u)$ will. In this example this point is the approximate exit point $\theta^{egs\alpha} = (102.33°, 146.11°)$ and is shown in the figure. This point does indeed seem to be relatively close to the stable manifold $W^s(\theta^u)$.

- The numerical trajectory of the gradient system $N(\phi_{gs}(\theta^{egs\alpha},t))$ is shown. The minimum gradient point is found and $\theta^{mgp} = (105.27°, 140.66°)$. When the nonlinear algebraic solver routine FindRoot is

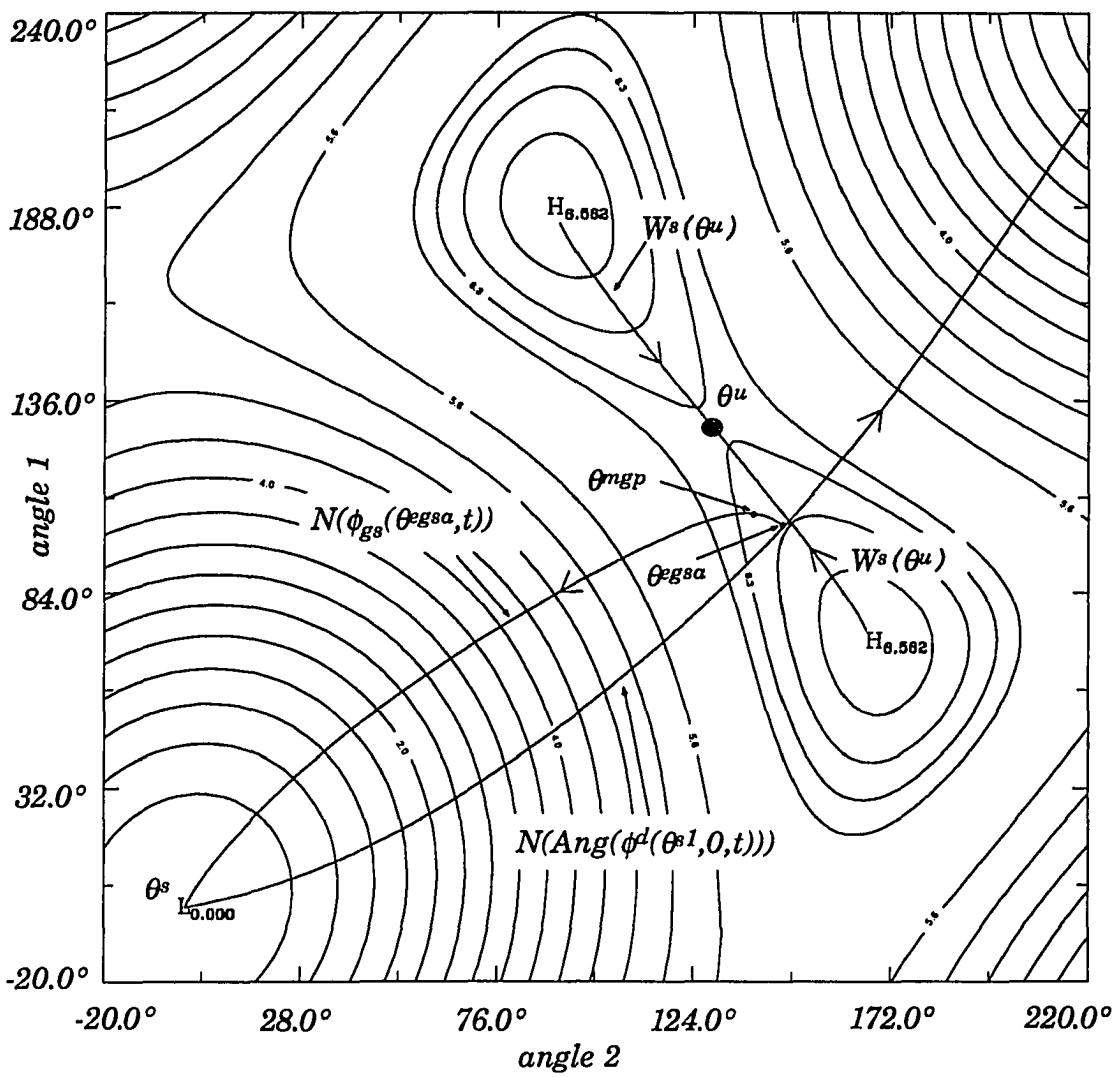

Figure 4.13 Disturbed trajectory, exit point and minimum gradient point

applied the point θ^u is produced. Considering Assumption 4.1 the UEP $\theta^u = (128.69°, 128.69°)$ will be taken as the controlling UEP, which is the desired result, and the transient stability assessment through the evaluation of the energy margin will be based on the energy value at θ^u.

Figure 4.14 shows there is numerical support for Assumption 4.1. The following can be observed in Figure 4.14 and it must be noted that the swing system is in a four-dimensional space in this example while the figure only shows two dimensions. $N(Ang(\phi^d(\theta^{s1},0,t)))$ is shown and this trajectory starts at $\theta^s = \theta^{s1} = (0.0°, 0.0°)$ and ends at the point $(\theta^{cl},\varpi^{cl})$ which happens to lie just inside the stability region of the swing system. This point is taken as the critical clearing state on the disturbed trajectory and corresponds to a critical clearing time of $t^{cl} = 0.8244$ seconds. The critical clearing time was determined through time simulation. The point θ^{cl} is shown in the figure. In order to show that Assumption 4.1 holds in this particular case a similar technique as described in scenario 2 of Section 4.7 will be used. Since $(\theta^{cl},\varpi^{cl})$ is just inside the stability region, it is relatively close to the stability boundary and hence, relatively close to a stable manifold in the stability boundary. Since $(\theta^{cl},\varpi^{cl})$ is close to a stable manifold of the swing system, the swing system trajectory $\phi(\theta^{cl},\varpi^{cl},t)$ and hence the numerical trajectory $N(\phi(\theta^{cl},\varpi^{cl},t))$ should approach relatively close to the UEP which anchors this stable manifold.

The projection into θ-space of the numerical approximation to the solution of the swing system $N(Ang(\phi(\theta^{cl},\varpi^{cl},t)))$ is shown in Figure 4.14. This trajectory starts at θ^{cl} and seems to go very near to the UEP θ^u, goes by θ^u, then turns and goes toward the UEP again and finally heads toward θ^s. The numerical trajectory $N(\phi(\theta^{cl},\varpi^{cl},t))$ is in four-dimensional space and does not go directly through $(\theta^u,0)$ because $\varpi \neq 0$ at that point. Figure 4.15 is plot of all four states variables of $N(\phi(\theta^{cl},\varpi^{cl},t))$ versus time. The time axis starts at $t^{cl} = 0.8244$ seconds. When $t \approx 1.2$ seconds, $\theta_1 \approx \theta_2 \approx 128°$ which are close to the coordinates of θ^u which are $(128.69°, 128.69°)$. This time of $t \approx 1.2$ seconds corresponds to the first time $N(Ang(\phi(\theta^{cl},\varpi^{cl},t)))$ passes by θ^u. Again, When $t \approx 1.75$ seconds, $\theta_1 \approx \theta_2 \approx 128°$ and this corresponds to the second time

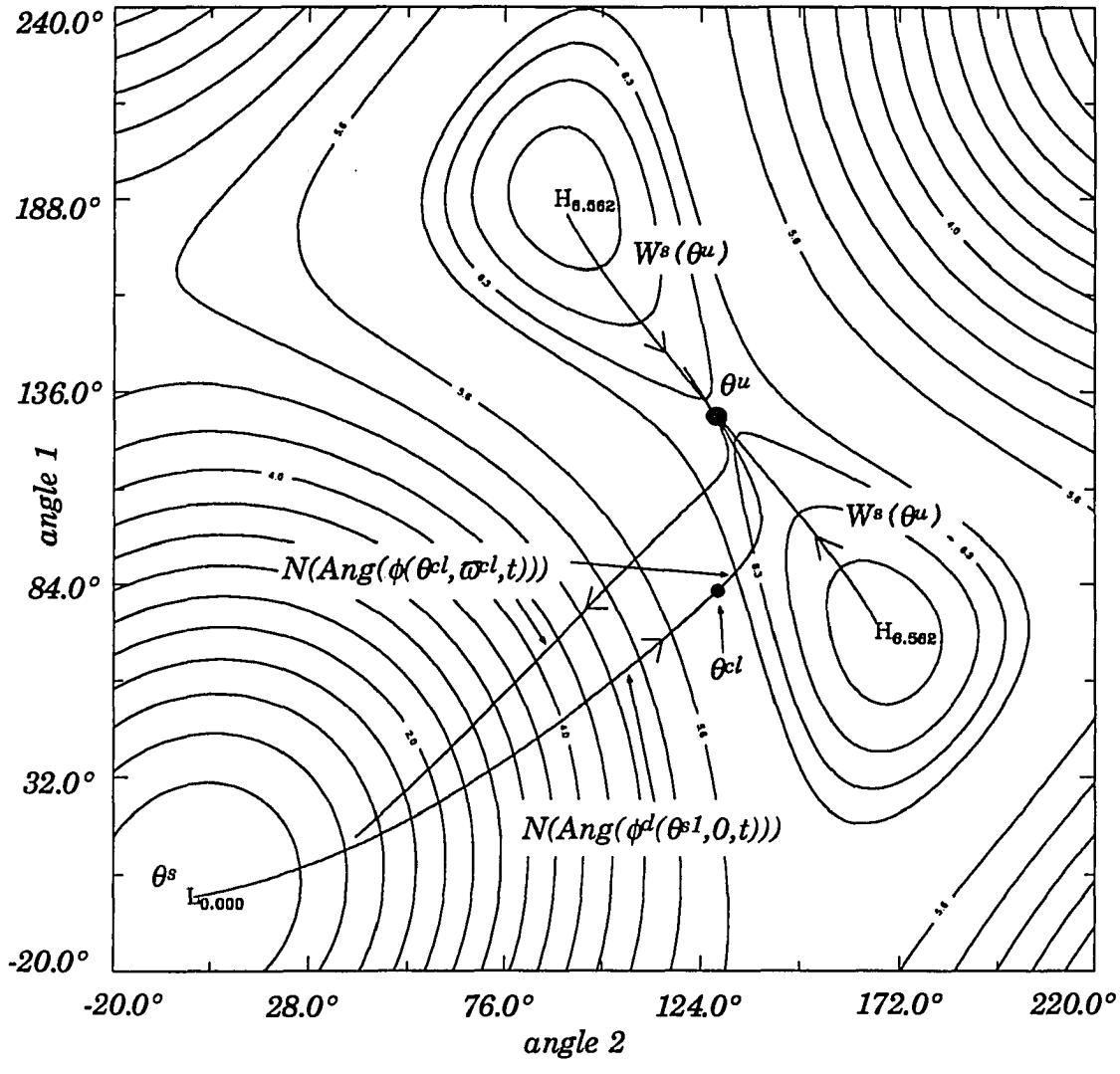

Figure 4.14 Numerical support of Assumption 4.1

$N(Ang(\phi(\theta^{cl},\varpi^{cl},t)))$ passes by θ^u. At these two times the speeds ϖ_1 and ϖ_2 are relatively small which indicates that $\phi(\theta^{cl},\varpi^{cl},t)$ travels relatively close to $(\theta^u,0)$. The result of this is that the stable manifold that is intersected by $\phi^d(\theta^{s1},0,t)$ is indeed $W^s(\theta^u,0)$ and Assumption 4.1 does hold in this case.
The part of the stability boundary that is relevant to the disturbed trajectory is $W^s(\theta^u,0)$ and can now be approximated by the constant energy surface $\partial V(\theta^u,0) = \{ (\theta,\varpi) : V(\theta,\varpi) = V(\theta^u,0) = V_{PE}(\theta^u) = V_{PE}(128.69°, 128.69°) = 6.296 \}$. This constant energy surface is precisely what the energy margin, which was defined in Chapter 3, Section 3.1.3, is based on. . Figure 4.16 is a plot of V_{PE}, V_{KE}, $V = V_{PE} + V_{KE}$ and $V_{PE}(\theta^u)$ all evaluated along the disturbed trajectory. The graph of $V = V_{PE} + V_{KE}$ intersects the constant graph of $V_{PE}(\theta^u)$ at the time of *0.8018* seconds. This time of *0.8018* seconds would then be the critical clearing time as evaluated through the application of the energy margin. The percent error is $(0.8244 - 0.8108) / 0.8244 = 2.75\%$ and is relatively small thus displaying the credibility of using $\partial V(\theta^u,0)$ to approximate $W^s(\theta^u,0)$.

4.10 Addressing the Issue of the Equality in $\partial A(\theta^s,0) \cap \{(\theta,\varpi) : \varpi = 0\} = \partial A(\theta^s)$

This section is presented as a side note to address the issue of whether or not $\partial A(\theta^s,0) \cap \{(\theta,\varpi) : \varpi = 0\} = \partial A(\theta^s)$. This was also addressed in [21] where it was stated that the equality in the above equation is uncertain.

The differential equations in matrix form for the swing system and the associated gradient system are repeated here for convenience.

The swing system which is defined in Section 3.1 is

$$\dot{\varpi} = M^{-1} g - M^{-1} D \varpi$$

$$\dot{\theta} = \varpi$$

The associated gradient system is defined in Section 3.2 and is

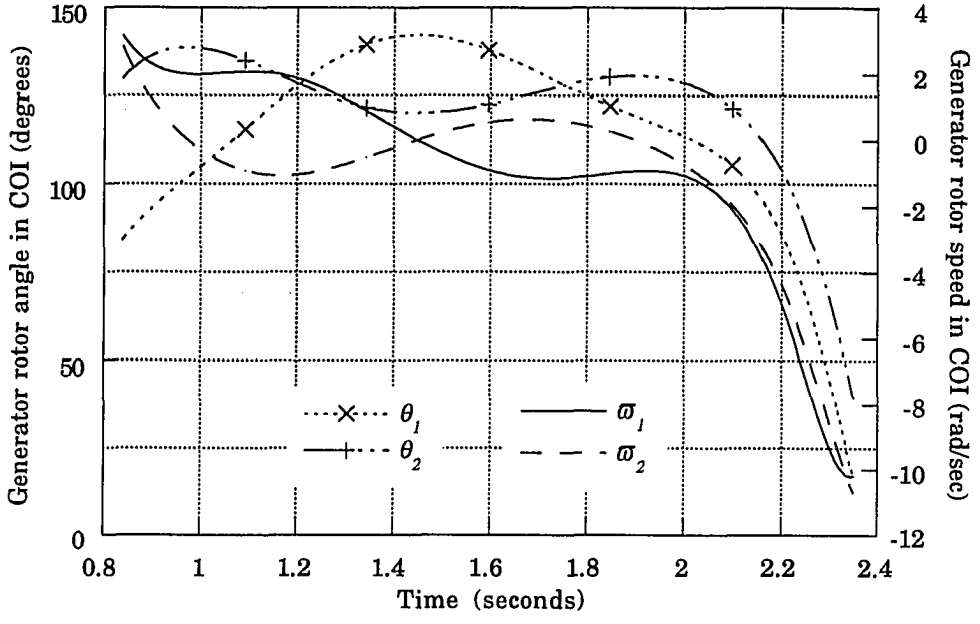

Figure 4.15 State variables curves of the swing system

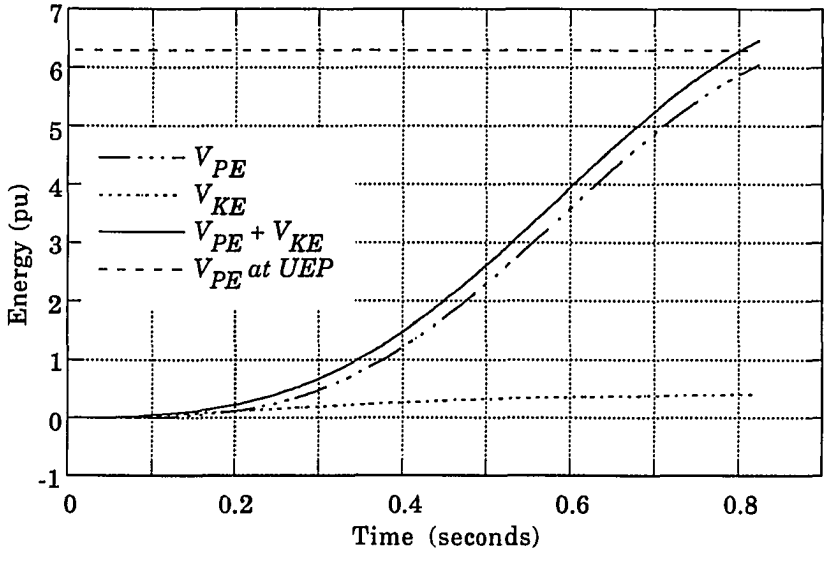

Figure 4.16 Energy quantities along the disturbed trajectory

$$\dot{\theta} = M^{\theta} g$$

From an observation of these two dynamical systems there does not seem to be any immediate reason why $\partial A(\theta^s,0) \cap \{(\theta,\varpi) : \varpi = 0\} = \partial A(\theta^s)$ is true.

The numerical example below shows that $\partial A(\theta^s,0) \cap \{(\theta,\varpi) : \varpi = 0\} \neq \partial A(\theta^s)$. The stability boundary of the associated gradient system of the unloaded 3-machine system is shown in Figure 4.4. Figure 4.17 is an illustration of part of $W^s(\theta^u) \subset \partial A(\theta^s)$ and part of $\partial A(\theta^s,0) \cap \{(\theta,\varpi) : \varpi = 0\}$ around the UEP $\theta^u = (-34.89°, 145.11°)$. The part of $W^s(\theta^u)$ that is shown is determined by integrating the gradient system backwards in time with the initial condition relatively close to θ^u. The part of $\partial A(\theta^s,0) \cap \{(\theta,\varpi) : \varpi = 0\}$ that is shown is determined as follows. The differential equations of the swing system are integrated forward in time with the initial condition of the form $(\theta,0)$. The initial condition is selected as follows. For this particular example select a point (θ_1^1, θ_2^1) that is near $W^s(\theta^u)$ and inside $A(\theta^s)$ and create a sequence of points $\theta_2^1, \theta_2^2, \cdots$ with $\theta_2^{i+1} > \theta_2^i$ and $\theta_2^{i+1} - \theta_2^i$ relatively small. Take the point $(\theta_1^1, \theta_2^1, 0, 0)$ as the initial condition and solve the swing system. If the trajectory converges to θ^s then keep θ_1 the same and use the next element in the sequence for θ_2 and repeat with this new initial condition. If the trajectory did not converge to θ^s for the initial condition $(\theta_1^1, \theta_2^i, 0, 0)$,take $(\theta_1^1, (\theta_2^{i-1} + \theta_2^i)/2)$ as the point on $\partial A(\theta^s,0) \cap \{(\theta,\varpi) : \varpi = 0\}$. Increment θ_1 to a suitable value and repeat the process over again. With enough points determined to be relatively close to $\partial A(\theta^s,0)$ they can be connected together as shown in the figure.

4.11 Summary

Sections 4.1 through 4.4 contained a prelude to the description of the exit point method. Section 4.1 contained the fundamental assumption of the exit point method which was numerically supported when the unrealistic, unloaded 3-machine system was analyzed in Section 4.9. Sections 4.2, 4.3 and

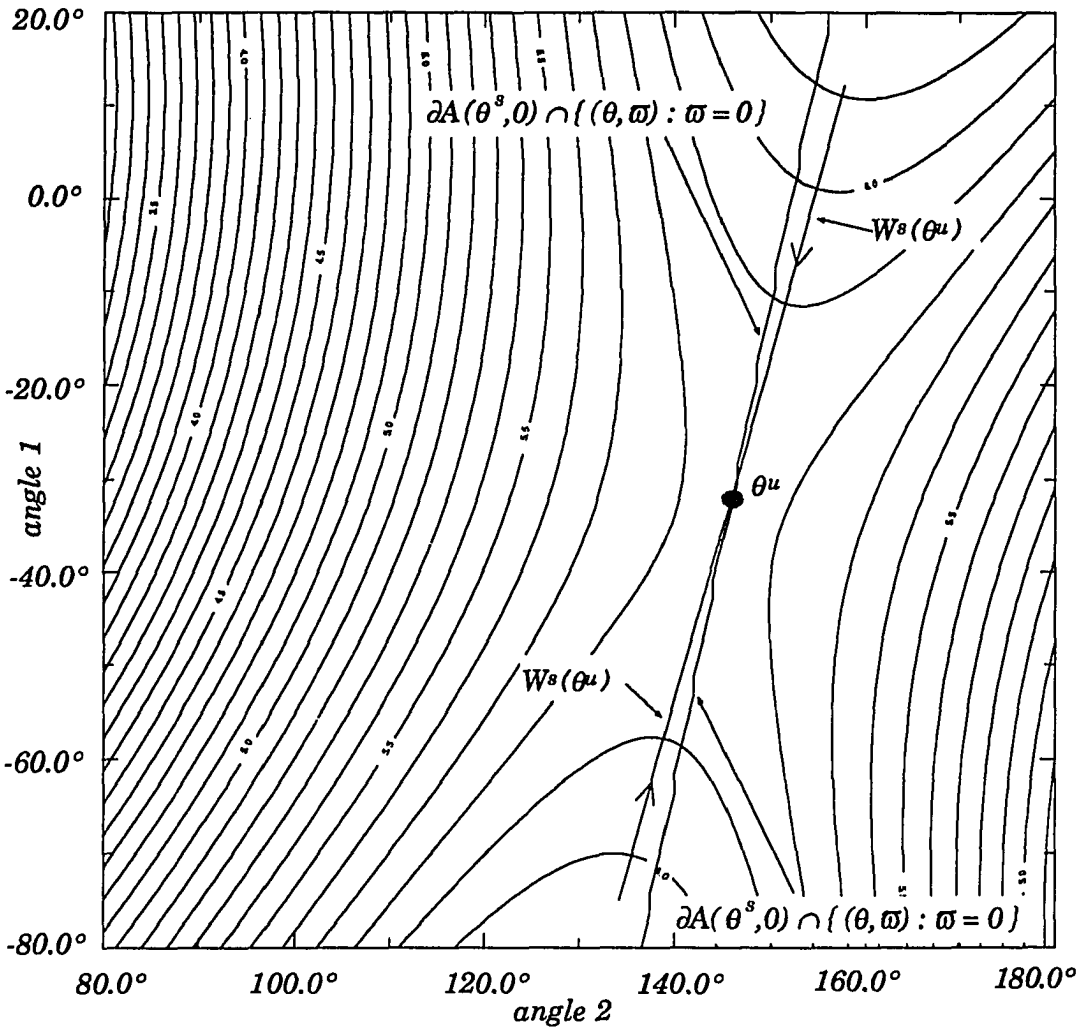

Figure 4.17 Stability boundaries of the two systems

4.4 contained a discussion on the description of the equipotential surfaces as well as the potential energy well. It was noted that the shape of these equipotential surfaces play a crucial role in the detection of the exit point.

Section 4.5 contained a discussion of how the approximate exit point is detected. Section 4.6 contained the description of the three step numerical algorithm of the exit point method. Section 4.7 contained the reasoning why this method may work for determining the controlling UEP. It was shown that there is an analytical foundation for this method as presented in scenario 1. However, in the numerical setting the idea underlying foundation is not valid and this leads into the problems of the exit point method as presented in Section 4.8. Problem 1 illustrated that there may be no minimum gradient point. The idea in Problem 2 was that if there was a minimum gradient point found the resulting equilibrium point may not be the intended unstable equilibrium point (i.e., the controlling UEP). The idea of Problem 3 was that there is no analytical proof that the implication stated in Assumption 4.1 is true and this is precisely why it is assumed.

Section 4.9 contained the results of the application of the exit point method to the unloaded 3-machine system. In this case the exit point method worked correctly in the sense that it indeed determined the controlling UEP. The concept of the constant energy surface, defined by the controlling UEP, approximating the relevant stability boundary was substantiated.

Section 4.10 contained an example whose result addresses the issue of the extended connection of the stability boundaries of the swing and gradient systems.

The case that was analyzed in Section 4.9 seemed to be a "good" case since Problem 1, Problem 2 and Problem 3 were avoided. However, these problems can occur and it seems likely that as the dimension of the problem becomes larger there may be more probability that problems such as the ones mentioned will occur.

Chapter 5 contains a description of a new numerical method that when applied will prevent conditions described in Problem 1 and Problem 2 from happening. This method is referred to as *shadowing the stable manifold.*

5. SHADOWING A STABLE MANIFOLD OF THE GRADIENT SYSTEM

The contents of this chapter is a presentation of a new numerical method known as *shadowing the stable manifold* and the foundations of this new method are based on the exit point method. The underlying idea of the exit point method is to utilize $W^s(\theta^u)$ in order to determine the controlling UEP θ^u as defined in Definition 3.1.6. In step (i) of this numerical method a point $\theta^{egs\alpha}$ is found and it is hoped that this point is relatively close to $W^s(\theta^u)$. Then in step (ii), when the trajectory $\phi_{gs}(\theta^{egs\alpha},t)$ is numerically approximated each of the resulting approximated points $N(\phi_{gs}(\theta^{egs\alpha},t_i))$ will be relatively close to the stable manifold $W^s(\theta^u)$ up to a certain time t_k. The minimum gradient point is hoped to be close to θ^u so that the resulting equilibrium point from the application of the nonlinear solver is θ^u.

As discussed in Section 4.8 there are three problems associated with the exit point method. Problem 3 is concerned with the validity of Assumption 4.1. Problems 1 and 2 are a direct result of the failure of step (i) and step (ii) of the numerical method. The issue in Problem 1 is that no minimum gradient point is found and this situation may happen regardless of where $\theta^{egs\alpha}$ is located with respect to $W^s(\theta^u)$. The issue of Problem 2 is that an incorrect equilibrium point is produced. This problem can generally be attributed to the location of $\theta^{egs\alpha}$ with respect to θ^u and other unstable equilibrium points on the stability boundary of the gradient system.

The shadowing method algorithm is substituted for the existing exit point method algorithm. Upon the application of the shadowing method a finite sequence of points $\{\theta^{mi}\}_{i=0}^{N}$ is produced with the point θ^{m0} being relatively close to the point $\theta^{egs\alpha}$ and an initial condition for the algorithm. An advantage of the shadowing method over the exit point method is that under certain conditions there is a guarantee that θ^{mN} is relatively close to θ^u. With the point θ^{mN} relatively close to θ^u it would be likely that θ^u would result from the application of the nonlinear algebraic solver with θ^{mN} as the

initial guess. Therefore, Problem 1 and Problem 2 associated with the exit point method are eliminated.

The term shadowing comes from Definition 6.6.3 in [41]. A sequence $\{x^i\}_{i=-\infty}^{\infty}$ is said to Δ-shadow the sequence $\{y^i\}_{i=-\infty}^{\infty}$ if $d(x_i, y_i) < \Delta \ \forall i$. Where $d(x_i, y_i)$ is some suitable distance function.

This definition cannot be directly applied to the method described here since the sequence $\{\theta^{mi}\}_{i=0}^{N}$ is finite. So, in this situation the definition can be indirectly applied if a finite sequence $\{\theta^{Wi}\}_{i=0}^{N}$ can be found with $\theta^{Wi} \in W^s(\theta^u)$ along with some $\Delta > 0$ so that $d(\theta^{Wi}, \theta^{mi}) < \Delta \forall\, i \in [0, ..., N]$. In other words, the sequence $\{\theta^{mi}\}_{i=0}^{N}$ Δ-shadows a sequence from $W^s(\theta^u)$.

The following is a description of the four sections in this chapter.

Section 5.1 This section contains a description of the shadowing method in the form of a numerical algorithm.

Section 5.2 This section contains the results of the application of the shadowing method to two examples. These are the same two examples which the exit point method failed when applied to in Section 4.8.

Section 5.3 This section contains an analytical foundation for this shadowing method when applied to the unloaded gradient system model (i.e., $P_i = 0$, $i = 1, ..., n-1$).

Section 5.4 This final section contains a conclusion to the chapter along with three important remarks concerning this shadowing method.

Most of the notation used in this chapter was defined in Chapter 3, Sections 3.1, 3.1.2 and 3.2. When convenient a small description will be added to clarify the notation.

5.1 A Description of the Shadowing Method Algorithm

Before giving a description of the shadowing method algorithm a fact about the periodicity of the function V_{PE} (3.5c) needs to be given.

Take any $\theta^r \in R^{(n-1)}$ and define the set $S_{ray}(\theta^r) = \{ \theta : \theta = (\theta^r - \theta^s)\ \alpha + \theta^s,\ \alpha \geq 0 \}$ which represents an affine ray (i.e., a ray which does not necessarily pass through the origin) which passes through the point θ^r and starts at the SEP θ^s. The function V_{PE} (3.5c) for the unloaded gradient system takes the following form on the ray. This derivation is similar to the derivation of $dg((\theta^1 - \theta^s)\ \alpha + \theta^s)/d\alpha$ as shown in Appendix A, Section A.3.

$$V_{PE}((\theta^r - \theta^s)\ \alpha + \theta^s) = - \sum_{i=1}^{n-1} \sum_{j=i+1}^{n-1} C_{ij} \cos\left(\Omega_{ij}\ \alpha + \theta_i^s - \theta_j^s\right)$$

$$- C_{in} \cos\left(\Delta_i\ \alpha + \theta_i^s + m^s\right) + C^{PE} \qquad (5.1)$$

where Ω_{ij}, Δ_i and m^s are defined in Appendix A, Section A.3 and these three terms are fixed when given fixed θ^s and θ^r. The constant term C^{PE} is defined by evaluating the part of V_{PE} which is only a function of θ^s. It can be seen that the function V_{PE} (5.1) is only a function of α along the ray. This function V_{PE} takes the form of an almost periodic function as defined in [42, Chapter 12]. This function V_{PE} seems as if it were periodic but this is not the case in general. If the terms Ω_{ij}, and Δ_i, which resemble frequency terms, are incommensurable, that is, the frequency terms Ω_{ij}, and Δ_i do not have a common frequency, the function V_{PE} (5.1) is not periodic, but almost periodic. Note that a periodic function is an almost periodic function. From the definition of an almost periodic function the following is stated. Given any $\chi > 0$ and $\alpha^* \geq 0$ there exist a scalar $\iota(\chi) > 0$ which depends on χ such that in any interval $I \subset R^+$ of length $\iota(\chi)$ there is a $\alpha^{**} \in I$ such that

$$\left| V_{PE}((\theta^r - \theta^s)\ \alpha^* + \theta^s) - V_{PE}((\theta^r - \theta^s)\ (\alpha^{**} + \alpha^*) + \theta^s) \right| \leq \chi$$

The numerical algorithm of the shadowing method consists of a basic three step cycle. Each time a cycle is executed a point θ^{mi} of the sequence is produced. Hence, in order to produce the finite sequence $\{\theta^{mi}\}_{i=0}^{N}$ the cycle needs to be executed N times. The value of what N should be is discussed later in this section.

Figure 5.1 is similar to Figure 4.7 except that two cycles (i.e., six steps) of the shadowing method are shown. The application of these two cycles produces the points θ^{m1} and θ^{m2} as shown. The six steps that are shown in the figure need to be described and these six steps will be referred to as *s-1* through *s-6*.

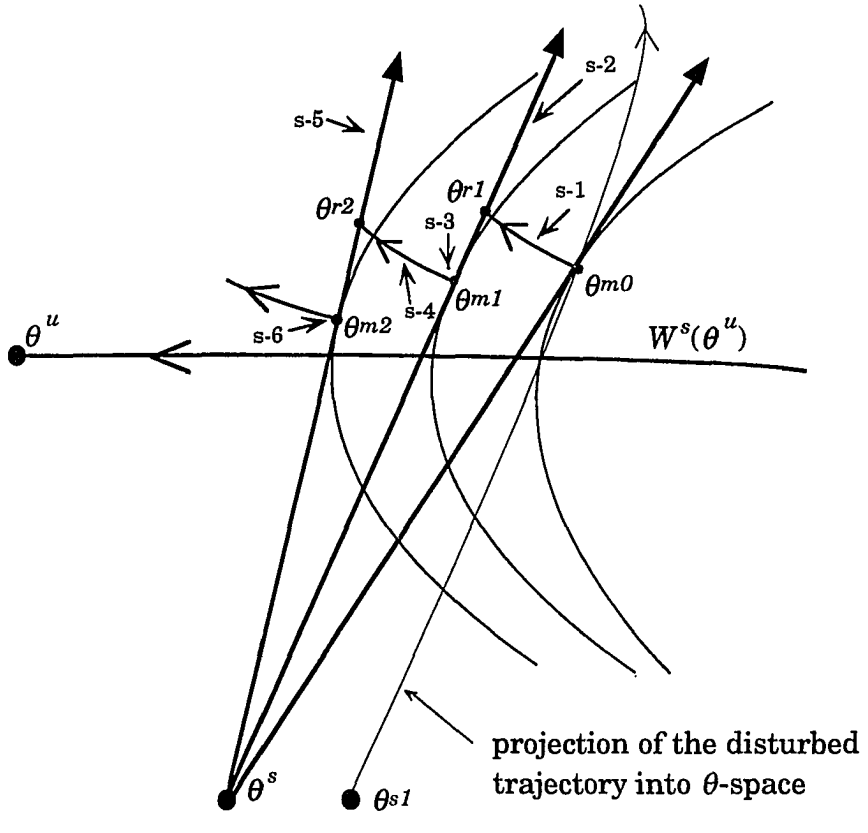

Figure 5.1 Illustration of the shadowing method

The point θ^{m0} is determined in a similar manner to the detection of the approximate exit point θ^{egsa}. Along the projection of the disturbed trajectory the point θ^{m0} is detected where $-z(\theta^{m0}) \cdot (\theta^{m0} - \theta^{s}) = 0$. This detection is explained in step *s-3* below.

s-1 Let $\theta^{r1} = \phi_{gs}(\theta^{m0}, t_1)$ with t_1 relatively small. $\phi_{gs}(\theta^{m0}, t_1)$ is the solution for the gradient system as defined in Chapter 3, Section 3.2.

s-2 Create an affine ray that starts at θ^{s} and passes through the point θ^{r1}. This ray would consist of the set $S_{r1} = \{ \theta : \theta = (\theta^{r1} - \theta^{s})\ \alpha + \theta^{s},\ \alpha \geq 0 \}$.

s-3 This step consists of finding a local maximum of V_{PE} on the ray in the vicinity of θ^{r1}. This point will be denoted as $\theta^{m1} \in S_{r1}$. This point θ^{m1} satisfies the following equation.

$$\frac{dV_{PE}}{d\alpha} = \frac{\partial V_{PE}}{\partial \theta}\frac{d\theta}{d\alpha} = -z(\theta^{m1}) \cdot (\theta^{r1} - \theta^{s}) = 0 \qquad (5.2)$$

As shown earlier in this section, V_{PE} is an almost periodic function of α along the ray, so, the problem of determining the point θ^{m1} can be formulated in terms of determining the value of α such that $dV_{PE}((\theta^{r1} - \theta^{s})\ \alpha + \theta^{s})/d\alpha = 0$. It will not be shown here, but because of the fact that V_{PE} (5.1) is almost periodic there are an infinite number of local maximums and local minimums of V_{PE} along the ray.

Newton's Method may be applied and the iterative scheme is

$$\alpha_{j+1} = \alpha_j - \frac{dV_{PE}((\theta^{r1} - \theta^{s})\ \alpha_j + \theta^{s})/d\alpha}{d^2V_{PE}((\theta^{r1} - \theta^{s})\ \alpha_j + \theta^{s})/d\alpha^2} \qquad j = 1, 2, \cdots$$

Since $z = M^{\theta} g$, as shown in Chapter 3, Section 3.2, this can be written as

$$\alpha_{j+1} = \alpha_j - \frac{\left[- M^{\theta} g((\theta^{r1} - \theta^{s})\,\alpha_j + \theta^{s})\right] \cdot (\theta^{r1} - \theta^{s})}{\left[- M^{\theta} dg((\theta^{r1} - \theta^{s})\,\alpha_j + \theta^{s})/d\alpha\right] \cdot (\theta^{r1} - \theta^{s})} \qquad j = 1, 2, \cdots$$

The derivation $dg((\theta^{r1} - \theta^{s})\,\alpha + \theta^{s})/d\alpha$ is given in Appendix A, Section A.3. The starting point for the iterative scheme is $\alpha_1 = 1$ which corresponds to θ^{r1} on the ray. The Newton Method may be iterated until for some α_k, $k > 1$, $|[- M^{\theta} g((\theta^{r1} - \theta^{s})\,\alpha_k + \theta^{s})] \cdot (\theta^{r1} - \theta^{s})|$ is relatively small which can be written as

$$\left|\left[- M^{\theta} g((\theta^{r1} - \theta^{s})\,\alpha_k + \theta^{s})\right] \cdot (\theta^{r1} - \theta^{s})\right| < \eta$$

For example, the value of η may be picked as

$$\eta = c\left|\left[- M^{\theta} g(\theta^{r1})\right] \cdot (\theta^{r1} - \theta^{s})\right|$$

Where $c > 0$ is a relatively small number. The point θ^{m1} is then $\theta^{m1} = (\theta^{r1} - \theta^{s})\,\alpha_k + \theta^{s})$. It seems likely that by keeping t_i relatively small $\alpha_1 = 1$ will be a good starting guess for the Newton Method.

s-4 Repeat step s-1 with θ^{m1} replacing θ^{m0} and let $\theta^{r2} = \phi_{gs}(\theta^{m1}, t_2)$ with t_2 relatively small.

s-5 Repeat step s-2 with θ^{r2} replacing θ^{r1}.

s-6 Repeat step s-3 and find $\theta^{m2} \in S_{r2}$ by the previously defined Newton scheme, where $S_{r2} = \{\, \theta : \theta = (\theta^{r2} - \theta^{s})\,\alpha + \theta^{s},\ \alpha \geq 0 \,\}$. In this scheme the value 2 would now replace the value 1 (e.g. $\theta^{r1} \Rightarrow \theta^{r2}$).

In Figure 5.1 the points θ^{m0}, θ^{m1} and θ^{m2} are relatively close to $W^{s}(\theta^{u})$. The point θ^{m1} is closer to θ^{u} than θ^{m0}; also, θ^{m2} is closer to θ^{u} than θ^{m1}. It seems likely that if a few more cycles of the shadowing method are performed θ^{mN} will be relatively close to θ^{u}.

Steps s-1 through s-3 are one cycle and steps s-4 through s-6 are another cycle. Therefore, the shadowing method can be described by a generic cycle of three steps, *sc-1* through *sc-3*. The following describes the start of the i^{th} cycle, $i \in [1, ..., N]$.

sc-1 Let $\theta^{ri} = \phi_{gs}(\theta^{m(i-1)}, t_i)$ with t_i relatively small.

sc-2 Form an affine ray such that this ray consists of the set $S_{ri} = \{ \theta : \theta = (\theta^i - \theta^s)\ \alpha + \theta^s,\ \alpha \geq 0 \}$.

sc-3 Determine the point $\theta^{mi} \in S_{ri}$ by applying the previously mentioned Newton scheme. In this scheme the value of i would now replace the value *1* (e.g. $\theta^1 \Rightarrow \theta^{ri}$).

Step sc-1 is similar to a predictor type of step. Starting at some point $\theta^{m(i-1)}$ the flow of the gradient system goes away from $W^s(\theta^u)$ and thus a relatively small t_i is required to keep θ^{ri} in the vicinity of $W^s(\theta^u)$.

Step sc-3 is similar to a corrector type of step. The situation of detecting the point θ^{mi} is similar to the situation of detecting the approximate exit point $\theta^{egs\alpha}$. The shape of the equipotential surfaces around $W^s(\theta^u)$ is the key to detecting the respective points in both situations. As shown in Figure 5.1 the equipotential surfaces have a hyperboloid like shape around $W^s(\theta^u)$ and this is a necessity for step sc-3 to work as intended. In higher dimensions (i.e., $(n-1) > 2$) the shape will be that of a higher dimensional hyperboloid.

The application of the shadowing method will produce the finite sequence $\{\theta^{mi}\}_{i=0}^{N}$. The value of N will not be determined before the shadowing method is applied. What will determine the value of N is a criterion that will be checked during the shadowing process. This criterion is similar to the one that is checked when the minimum gradient point is to be found. The criterion for determining the value of N is as follows. At the end of the i^{th} cycle the following sequence of points will have been produced, θ^{m0}, θ^{m1}, ..., θ^{mi}. If, for a relatively small $\beta > 0$, the following inequality holds, let $N = i$.

$$\sum_{j=1}^{n-1} \left| z_j(\theta^{mi}) \right| < \beta$$

In other words, let $N = i$ when the 1-norm of z, evaluated at θ^{mi}, is smaller than β. If the approximate exit point is close to an unstable equilibrium point which is not θ^u the 1-norm of z may be relatively small when evaluated at or near this approximate exit point. Therefore, a value for β may be for example

$$\beta = c \sum_{j=1}^{n-1} \left| z_j(\theta^{m0}) \right|$$

where $c > 0$ is a relatively small number.

Again, the idea behind this criterion is that $z = 0$ at θ^u and along any path starting in a neighborhood of θ^u and going toward θ^u the 1-norm of z will eventually get smaller.

5.2 Examples of the Shadowing Method

In Section 4.8 there were two examples given in which the application of the exit point method failed. In this section the results from the application of the shadowing method to these two examples are given. The detection of the point θ^{m0} was explained in Section 5.1, however, in order to compare the results from the application of these two methods the point θ^{m0} will be taken as θ^{egsa}.

Example 1

In section 4.8 there was an example of the application of the exit point method to the unloaded 3-machine system in which there was no minimum gradient point found. This example is illustrated in Figure 4.11 with $\theta^{egsa} = (-87.00°, 128.00°)$. In this case the exit point method failed. Figure 5.2

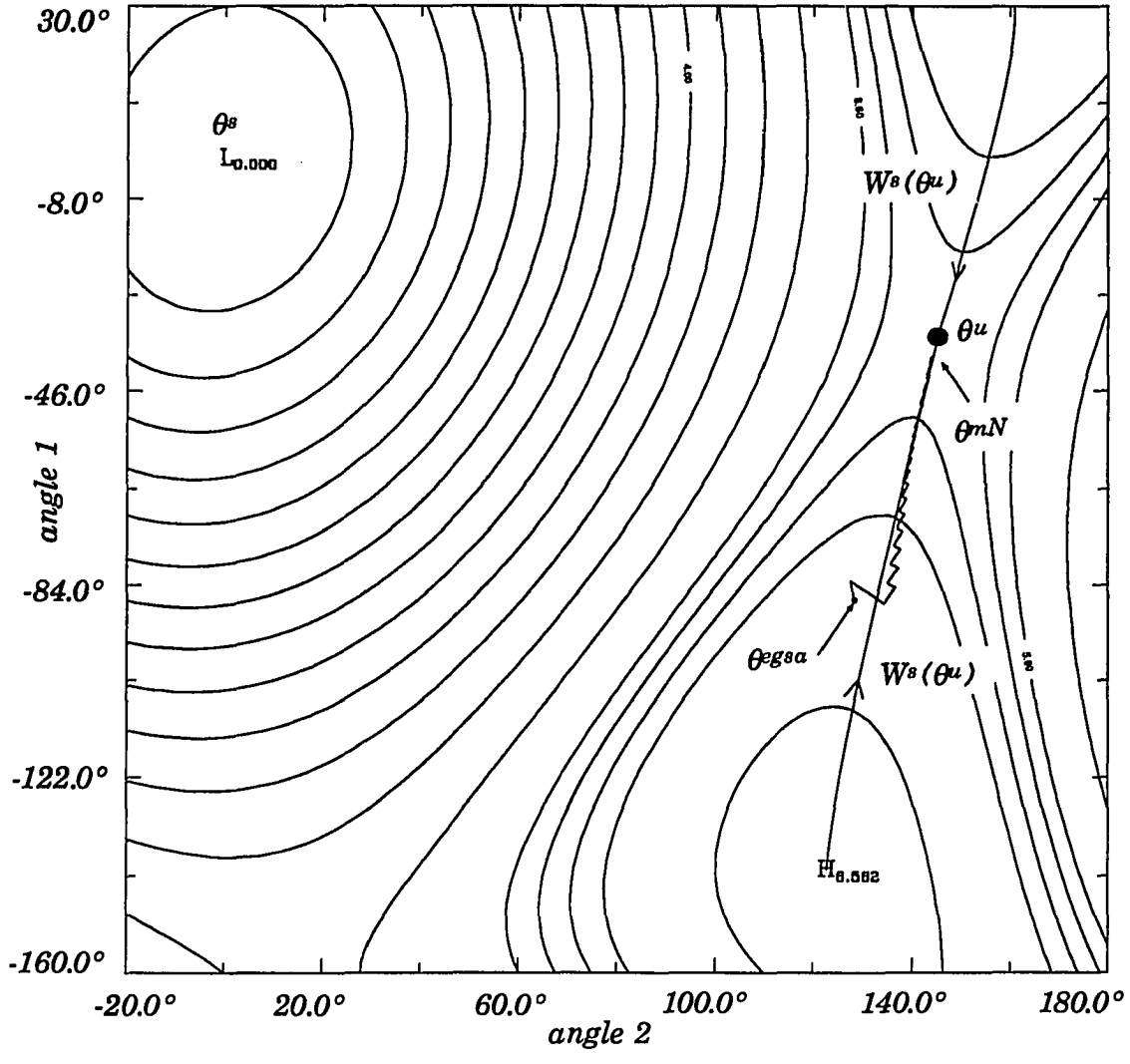

Figure 5.2 Illustration of shadowing the stable manifold for example 1

illustrates the numerical application of the shadowing method to this particular case. Figure 5.3 is similar to Figure 5.2 but the part of the figure where the points produced from the shadowing is enlarged. The numerical trajectory $N(\phi_{gs}(\theta^{m(i-1)},t_i))$ is shown as well as the part of the ray from θ^{ri} to θ^{mi} for all $i \in [1, ..., N]$. The following is a list of parameters used in this case. The time $t_i = 0.1$ seconds for all $i \in [1, ..., N]$. The parameter $\eta = 0.05$ and the parameter $\beta = 0.1$. With these parameters the application of the shadowing method will produce a sequence of 29 points $\{\theta^{mi}\}_{i=0}^{28}$. The first point $\theta^{m0} = \theta^{egs\alpha}$ was input to the shadowing method and the last 28 points where actually produced through the method. Hence, $N = 28$. Note that the values for the parameters such as t_i and β are chosen on heuristic basis.

The shadowing method does work in this case where as step (ii) of the exit point method failed. It seems from Figure 5.3 that the sequence seems to shadow the stable manifold and that the sequence seems to be converging to the controlling UEP θ^u. The location of the controlling UEP in this case is θ^u = *(-34.89°, 145.11°)* and the point θ^{m28} = *(-39.27°, 143.96°)* and from the location θ^{m28} is indeed relatively close to θ^u. Application of a nonlinear algebraic solver did indeed produce the equilibrium point θ^u.

Example 2

There was also another example given in Section 4.8 where a minimum gradient point was detected but the application of the nonlinear algebraic solver produced an equilibrium point which was not θ^u. The shadowing method was applied to the situation and Figure 5.4 illustrates the results. The parameters used in this case are the same as those used in example 1 of this section. The value of N in this example is 36. The location of $\theta^{egs\alpha}$ is *(-120.00°, 123.41°)*. The point θ^{m36} is located at *(-39.56°, 143.86°)* and θ^u at *(-34.89°, 145.11°)* and these two points are relatively close to each other. Where the application of the existing exit point method fails to produce θ^u in this example the application of the shadowing method which is substituted for step (ii) produces θ^u.

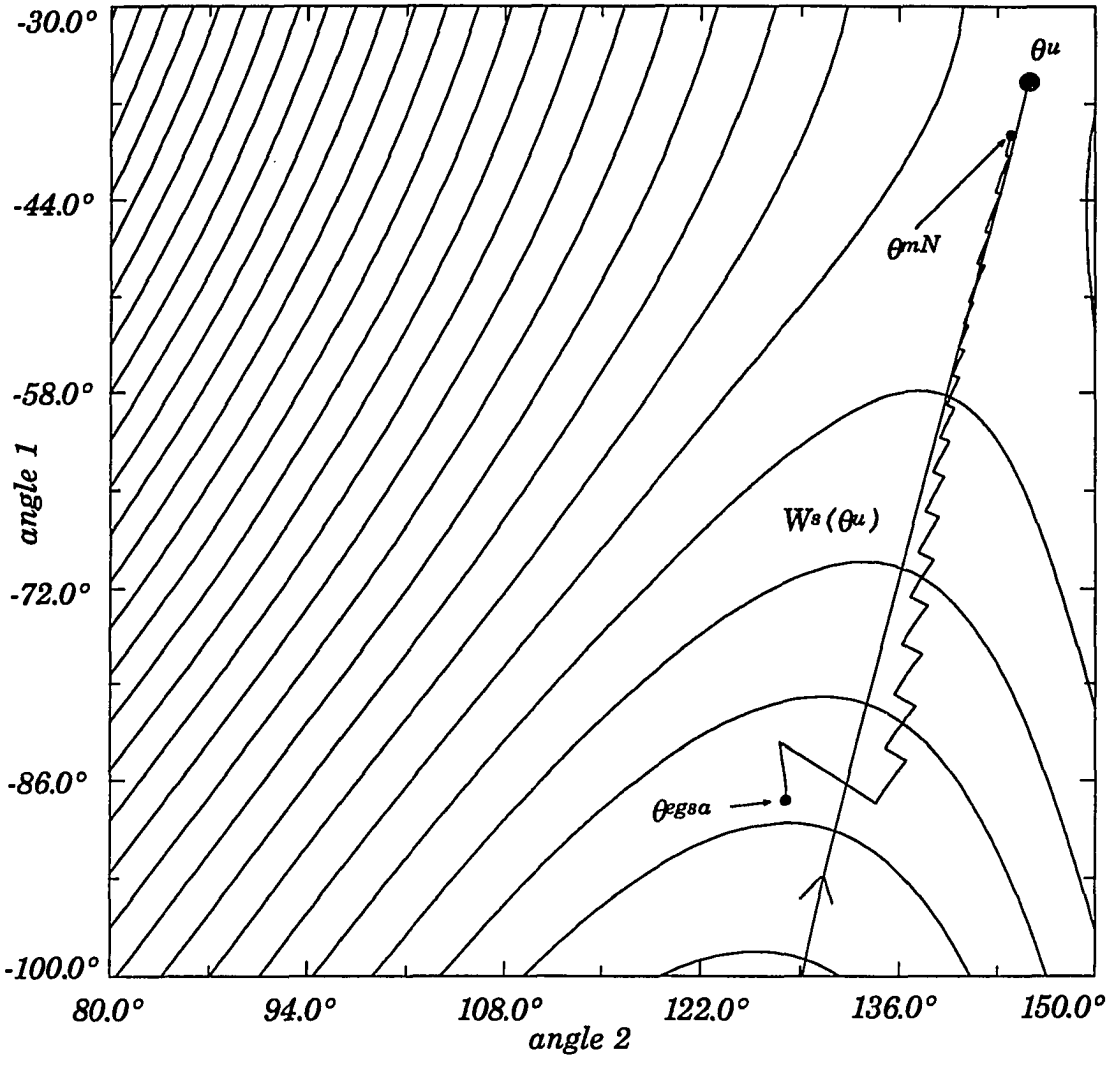

Figure 5.3 Close up of the shadowing method for example 1

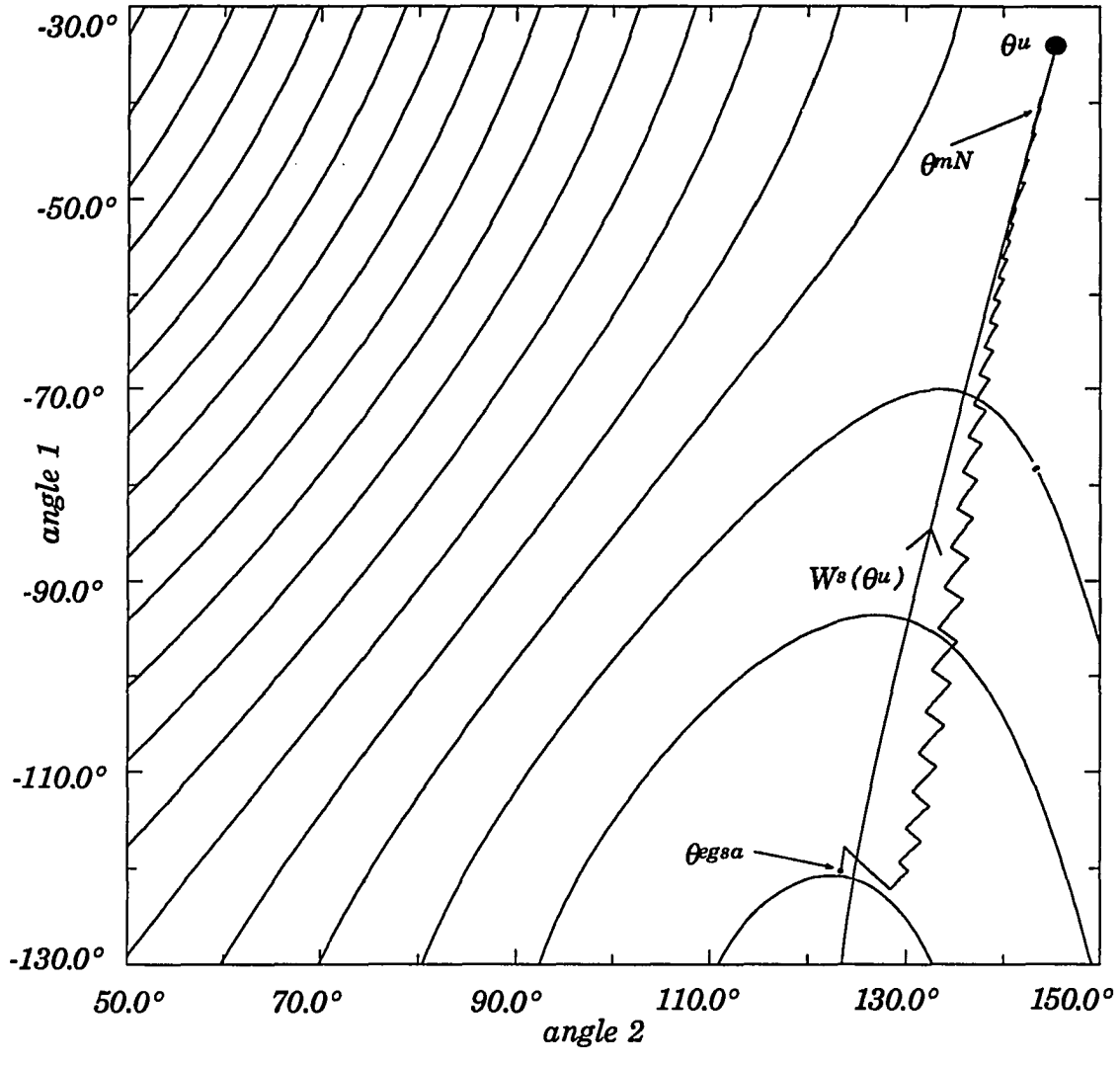

Figure 5.4 Illustration of the shadowing method for example 2

5.3 Analytical Foundation for the Shadowing Method

The contents of Section 5.1 was a presentation of the three step cycle of the shadowing method. The application of the method produced a finite sequence with the last point in the sequence relatively close in distance to the controlling UEP θ^u. Two examples were presented in the previous section. These examples did provide visual proof that the shadowing method did indeed work as intended. However, these are only two examples and the dimension associated is relatively small. Therefore, a mathematical analysis of this method is needed and this is the theme of this section.

The contents of this section is a presentation of an analytical foundation for the shadowing method when applied to the unloaded gradient system model from Section 3.2, equation (3.11). The main result of this section is that given the point θ^{m0}, and under certain assumptions and conditions, an infinite sequence $\{t_i\}_{i=1}^{\infty}$ can be found such that by using these t_i's in the solution of the gradient system the resulting infinite sequence $\{\theta^{mi}\}_{i=0}^{\infty}$ converges to θ^u.

The following is an analogy to the outline of the scheme used to show that the infinite sequence $\{\theta^{mi}\}_{i=0}^{\infty}$ converges to θ^u. Suppose there is an open interval on the real line $A = (a, b)$ and a function F such that the $inf(F(A)) = a$. *inf* refers to the infimum of a set. Suppose there exist an algorithm such that given an initial condition $c^0 \in (a, b)$ the application of this algorithm produces a sequence of points $\{c^i\}_{i=0}^{\infty} \subset (a, b)$ such that $F(c^{(i+1)}) < F(c^i)$. Also, suppose that the sequence $\{c^i\}_{i=0}^{\infty}$ does not converge to any point $c \in (a, b)$ then it must converge to the point a.

The outline of the above analogy is basically what will be employed to give analytical foundation to the shadowing method. The interval A is substituted for a $(n\text{-}1)\text{-}1$ dimensional manifold M^{GW}. The function F is substituted for by the function V_{PE}. The time sequence $\{t_i\}_{i=1}^{\infty}$ is found such that through the solution of the gradient system $V_{PE}(\theta^{m(i+1)}) < V_{PE}(\theta^{mi})$. The point a represents the controlling UEP θ^u and this controlling UEP is such that $V_{PE}(\theta^u) = inf(V_{PE}(M^{GW}))$.

Two points need to be made concerning the stability region/stability boundary of the unloaded gradient system. The first is given in Proposition 5.1 which follows from Assumption 3.2.7 of Section 3.2 from Chapter 4. The second is an assumption that needs to be made and is done so in Assumption 5.2.

Proposition 5.1

As noted in Section 3.2, θ^s is the SEP of the gradient system (3.11) and $\partial A(\theta^s)$ is the corresponding stability boundary. Take any $\theta^r \in R^{(n-1)}$ and denote the set $S_{ray}(\theta^r)$ as $S_{ray}(\theta^r) = \{ \theta : \theta = (\theta^r - \theta^s)\, \alpha + \theta^s, \alpha \geq 0 \}$ which is an affine ray emanating from θ^s . Then there exist a $\alpha^* > 0$ such that $((\theta^r - \theta^s)\, \alpha^* + \theta^s) \in \partial A(\theta^s)$. In other words, the ray formed by θ^r intersects the stability boundary of the unloaded gradient system. As noted earlier, the unloaded gradient system is the gradient system with $P_i = 0$, $i = 1, \ldots, n-1$.

Proof:

It was assumed in Assumption 3.2.7 that the stability region $A(\theta^s)$ of the unloaded gradient system is bounded. Since the stability region is open there exist a $\alpha^s > 0$ such that $S_{ray}(\theta^r) \in A(\theta^s)$ for $0 \leq \alpha < \alpha^s$. Suppose that there does not exist a $\alpha^* > 0$ such that $((\theta^r - \theta^s)\, \alpha^* + \theta^s) \in \partial A(\theta^s)$. Then $S_{ray}(\theta^r) \in A(\theta^s)$ for $\alpha > 0$. This implies that $A(\theta^s)$ is unbounded which is a contradiction. Hence, the ray formed by θ^r does indeed intersect the stability boundary of the unloaded gradient system.

■

Assumption 5.2

The intersection of the ray $S_{ray}(\theta^r)$ as explained in Proposition 5.1 and the stability boundary $\partial A(\theta^s)$ consists of a singleton set (i.e., a set containing only one element).

The Assumption 3.2.7 and Assumption 5.1 are confirmed by observing Figure 4.4 where the stability region and stability boundary of the unloaded gradient system based on the unloaded 3-machine system are shown.

Let θ^u be the controlling UEP. The definition of the controlling UEP as used in this dissertation work was given in Definition 3.1.6 of Section 3.1.2 from Chapter 3. The definition will be repeated here. The controlling UEP θ^u is the equilibrium point which anchors the stable manifold that is intersected by the disturbed trajectory. This stable manifold is part of the stability boundary of the swing system. In other words, $\phi^d(\theta^{s1},0,t) \cap W^s(\theta^u,0) = \varnothing$ for some $t > 0$.

The equilibrium type of UEP θ^u is relevant with respect to the shadowing method. It will be assumed in Assumption 5.3 that the controlling UEP θ^u is type-*1*. This assumption itself has foundation which is explained as follows.

Denote $B^o(\varepsilon,\theta,0) \subset R^{2(n-1)}$ as the open ball with radius $\varepsilon > 0$ and centered at the point $(\theta,0)$. It was assumed in Theorem 3.1.8 of Section 3.1.2 from Chapter 3 that the pre-disturbance system SEP θ^{s1} is relatively close to the post-disturbance SEP θ^s. Let ε be such that $(\theta^{s1},0) \in B^o(\varepsilon,\theta,0)$. It seems reasonable to argue that for any $(\theta^*,0) \in B^o(\varepsilon,\theta,0)$, $\phi^d(\theta^*,0,t) \cap \partial A(\theta^s,0) \neq \varnothing$ for some $t > 0$. Denote $S^* \subset \partial A(\theta^s,0)$ to be the set such that $\phi^d(B^o(\varepsilon,\theta,0),t) \cap S^* \neq \varnothing$ for $t > 0$. Suppose that there are points $(\theta^*,0) \in B^o(\varepsilon,\theta,0)$ such that $\phi^d(\theta^*,0,t) \cap W^s(\theta^\alpha,0) \neq \varnothing$ for some $t > 0$ where $\theta^\alpha \in \partial A(\theta^s,0)$ is type-k, $1 < k < (n-1)-1$. Note that $W^s(\theta^\alpha,0) \subset \partial A(\theta^s,0)$. It was shown in example 3.3.17.2 of [43] that the stable manifold $W^s(\theta^\alpha,0)$, which is of dimension $(n-1)-k$, has a Lebesque measure of zero in the $(n-1)-1$ dimensional $\partial A(\theta^s,0)$. The Lebesque measure can be thought of as a measure of volume. In other words, the $(n-1)-k$ dimensional stable manifold $W^s(\theta^\alpha,0)$ does not take up any volume in the $(n-1)-1$ dimensional $\partial A(\theta^s,0)$. The trajectory $\phi^d(\theta,0,t)$ can be thought of as a mapping from $B^o(\varepsilon,\theta,0)$ to S^* given appropriate $t > 0$. The appropriate $t > 0$ is such that $\phi^d(\theta^*,0,t) \cap S^* \neq \varnothing$ with $(\theta^*,0) \in B^o(\varepsilon,\theta,0)$. The inverse of the mapping from S^* to $B^o(\varepsilon,\theta,0)$ would have the following form, $\phi^d(\theta,\varpi,-t)$ with $t > 0$ which appropriate. This mapping is a diffeomorphism [43] due to the fact that $\phi^d(\theta,\varpi,t)$ is continuously differentiable and is unique with respect to (θ,ϖ)

and t. It is shown in example 3.3.17.1 of [43] that since $W^s(\theta^\alpha,0)$ has zero measure in $\partial A(\theta^s,0)$ the set $S^{**} \subset B^o(\varepsilon,\theta,0)$ defined by $S^{**} = \{ \phi^d(\theta,\varpi,-t), (\theta,\varpi) \in S^* \cap W^s(\theta^\alpha,0)$ with appropriate $t > 0\}$ has a Lebesque measure of zero in $B^o(\varepsilon,\theta,0)$. In other words, the set S^{**} takes up no volume in the set $B^o(\varepsilon,\theta,0)$. With this in mind it can be said that *almost nowhere* in the set $B^o(\varepsilon,\theta,0)$ are initial points $(\theta,0)$ such that $\phi^d(\theta,0,t)$ intersects a stable manifold of dimension $(n\text{-}1)\text{-}k$, $1 < k < (n\text{-}1)$, $t > 0$. Therefore, it can be said that the point $(\theta^{s1},0)$ for all practical purposes is not in the set S^{**}. Hence, $(\theta^{s1},0)$ is such that $\phi^d(\theta^{s1},0,t)$ intersects a stable manifold of dimension $(n\text{-}1)\text{-}1$, $t > 0$. With this in mind the following assumption is made.

Assumption 5.3

Assume that the controlling UEP θ^u is type-*1*.

Let $S^e(\theta^u) = \{ \theta : V_{PE}(\theta) > V_{PE}(\theta^u) \} \subset R^{(n-1)}$, where V_{PE} is defined by equation (3.5c). Denote the set $S^{high}(\theta^u) \subset R^{(n-1)}$as $S^{high}(\theta^u) = \{ \theta : \theta \in S^e(\theta^u)$ and there exist a continuous path that connects θ with θ^u such that every point on the path is in the set $S^e(\theta^u) \}$. Denote $\partial S^{high}(\theta^u)$ as the boundary of the set $S^{high}(\theta^u)$. The set $S^{high}(\theta^u)$ is an open subset of $R^{(n-1)}$ and hence a $(n\text{-}1)\text{-}1$ dimensional manifold [44, Chapter 11, Theorem 2.9].

Note that $W^s(\theta^u)\backslash\{\theta^u\} \subset S^{high}(\theta^u)$ and this is so because as shown in Theorem 3.2.1 of Section 3.2, V_{PE} decreases along the trajectories in $W^s(\theta^u)$.

The next five propositions and assumptions along with general remarks are given so that a (n-1)-1 dimensional manifold M^G can be defined.

Proposition 5.4

Given $\theta^W \in S^{high}(\theta^u)$, form the ray $S_{ray}(\theta^W)$ and note that $\alpha = 1$ on the ray at the point θ^W. There exist a α^a, $0 < \alpha^a < 1$ and $\alpha^b > 1$ such that $S_{ray}(\theta^W) \cap \partial S^{high}(\theta^u) \neq \varnothing$ at $\alpha = \alpha^a$ and at $\alpha = \alpha^b$.

Proof:

From the definition of the set $S^{high}(\theta^u)$ the point $\theta^W \in S^{high}(\theta^u)$ has a higher energy value than the point θ^u (i.e., $V_{PE}(\theta^W) > V_{PE}(\theta^u)$). Also, note that since $\theta^u \in \partial A(\theta^s)$ and V_{PE} decreases along the trajectories of the gradient system, $V_{PE}(\theta^u) > V_{PE}(\theta^s)$. Therefore, $V_{PE}(\theta^W) > V_{PE}(\theta^s)$. At the point $\theta^W \in S_{ray}(\theta^W)$ the value of α is *1*. Consider the connected, compact interval *[0, 1]* and note that from equation (5.1) $V_{PE} = 0$ at $\alpha = 0$ on the ray and $V_{PE} = V_{PE}(\theta^W)$ at $\alpha = 1$ on the ray. From the Intermediate Value Theorem and the fact that V_{PE} (5.1) is continuous on the ray there exist a $\alpha^a \in [0, 1]$ such that $V_{PE} = V_{PE}(\theta^u)$ at $\alpha = \alpha^a$. Because of the value of V_{PE} at $\alpha = \alpha^a$, α^a must be such that $\alpha^a \in (0, 1)$. Also, from the preceding argument there exist a $\alpha^d \in [0, \alpha^a]$ with $0 < V_{PE}((\theta^W - \theta^s)\,\alpha^d + \theta^s) < V_{PE}((\theta^W - \theta^s)\,\alpha^a + \theta^s)$. Because of the values of V_{PE} at $\alpha = 0$ and V_{PE} at $\alpha = \alpha^a$, $\alpha^d \in (0, \alpha^a)$.

As shown in Section 5.1 the function V_{PE} (5.1) is an almost periodic function of α on the ray. Let $\gamma = V_{PE}((\theta^W - \theta^s)\,\alpha^a + \theta^s) - V_{PE}((\theta^W - \theta^s)\,\alpha^d + \theta^s) > 0$. Set χ such that $0 < \chi < \gamma$. From the definition of an almost periodic function as given in Section 5.1 there exist a scalar $\iota(\chi) > 0$ such that for any interval $I \subset R^+$ of length $\iota(\chi)$ there is a $\alpha^I \in I$ with

$$\left| V_{PE}((\theta^W - \theta^s)\,\alpha^d + \theta^s) - V_{PE}((\theta^W - \theta^s)\,(\alpha^d + \alpha^I) + \theta^s) \right| \leq \chi < \gamma$$

Take the interval I such that $\alpha > 1$, $\forall\, \alpha \in I$. Now, it is seen that $\alpha^d + \alpha^I > 1$ and $V_{PE}((\theta^W - \theta^s)\,(\alpha^d + \alpha^I) + \theta^s) < V_{PE}((\theta^W - \theta^s)\,\alpha^a + \theta^s)$. Apply the Intermediate Value Theorem once again. It is known that $\alpha^d + \alpha^I > 1$ and that $V_{PE}((\theta^W - \theta^s)\,(\alpha^d + \alpha^I) + \theta^s) < V_{PE}((\theta^W - \theta^s)\,\alpha^a + \theta^s)$. There exist a $\alpha^b \in [1, \alpha^d + \alpha^I]$, where $[1, \alpha^d + \alpha^I]$ is a connected, compact interval, such that $V_{PE} = V_{PE}(\theta^u)$ at $\alpha = \alpha^b$. Because of the values of V_{PE} at $\alpha = 1$, and V_{PE} at $\alpha = \alpha^d + \alpha^I$, $\alpha^b \in (1, \alpha^d + \alpha^I)$. ■

Given $\theta^W \in S^{high}(\theta^u)$, start at a value of $\alpha = 1$, decrease α to $\alpha = \alpha^{eau}$ where $V_{PE}((\theta^W - \theta^s)\,\alpha^{eau} + \theta^s) = V_{PE}(\theta^u)$. Start at a value of $\alpha = 1$, increase α

to $\alpha = \alpha^{ebu}$ where $V_{PE}((\theta^W - \theta^s)\ \alpha^{ebu} + \theta^s) = V_{PE}(\theta^u)$. From Proposition 5.3 the two values α^{eau} and α^{ebu} exist. define the corresponding open interval $I^{\alpha ou} = (\alpha^{eau}, \alpha^{ebu})$, the compact interval $I^{\alpha cu} = [\alpha^{eau}, \alpha^{ebu}]$ and the set $S^I(\theta^W) = \{\ \theta : \theta \in S_{ray}(\theta^W)$ for $\alpha \in I^{\alpha ou}\}$. Note that $S^I(\theta^W) \subset S^{high}(\theta^u) \cap S_{ray}(\theta^W)$.

Proposition 5.5

Let $\theta^W \in S^{high}(\theta^u)$. There exist a $\alpha^m \in I^{\alpha ou}$, where $I^{\alpha ou}$ is defined above, such that V_{PE} (5.1) attains a local maximum along the ray $S_{ray}(\theta^W)$ at $\alpha = \alpha^m$.

Proof:

Consider the compact interval $I^{\alpha cu}$ as defined above. Because V_{PE} is a continuous function of α on the ray the Extreme-Value Theorem implies that there exist a $\alpha^* \in I^{\alpha cu}$ such that $V_{PE}((\theta^W - \theta^s)\ \alpha^* + \theta^s) \geq V_{PE}((\theta^W - \theta^s)\ \alpha + \theta^s)$ for $\alpha \in I^{\alpha cu}$. Since V_{PE} at $\alpha = 1$ is greater than both V_{PE} at $\alpha = \alpha^{eau}$ and V_{PE} at $\alpha = \alpha^{ebu}$, this implies that $\alpha^m \in I^{\alpha ou}$. From equation (5.2) it is seen that the equation for $dV_{PE}/d\alpha$ along the ray is

$$\frac{dV_{PE}}{d\alpha} = \frac{\partial V_{PE}}{\partial \theta}\frac{d\theta}{d\alpha} = -M^{\theta}\, g((\theta^W - \theta^s)\alpha + \theta^s) \cdot (\theta^W - \theta^s) \qquad (5.3)$$

The vector function $g((\theta^W - \theta^s)\ \alpha + \theta^s)$ is given in Appendix A, Section A.3 and is repeated here in scalar form as

$$g_i((\theta^W - \theta^s)\ \alpha + \theta^s) = -\sum_{\substack{j=1 \\ j \neq i}}^{n-1} C_{ij} \sin\left(\Omega_{ij}\,\alpha + \theta_i^s - \theta_j^s\right)$$

$$- C_{in} \sin\left(\Delta_i\,\alpha + \theta_i^s + m^s\right)$$

where Ω_{ij}, Δ_i and m^s are defined in Appendix A, Section A.3. It is seen that

$$- M^{\theta} g((\theta^{W} - \theta^{s})\alpha^{m} + \theta^{s}) \cdot (\theta^{W} - \theta^{s}) = 0 \qquad (5.4)$$

Since equation (5.4) is composed of sine terms, the root α^m of equation (5.4) is isolated and hence, V_{PE} at $\alpha = \alpha^m$ is a local maximum along the ray. ■

Assumption 5.6

Let $\theta^W \in S^{high}(\theta^u)$. Given the open interval $I^{\alpha ou}$ as defined above assume the following. There exist only one $\alpha^m \in I^{\alpha ou}$ such that $-M^{\theta} g((\theta^W - \theta^s)\ \alpha^m + \theta^s) \cdot (\theta^W - \theta^s) = 0$. In other words, it is assumed that there is only one maximum of V_{PE} on the ray $S_{ray}(\theta^W)$ when V_{PE} is evaluated in the interval $I^{\alpha ou}$.

From Proposition 5.5 it is seen that if $\theta^W \in S^{high}(\theta^u)$ there exist a $\alpha^m \in I^{\alpha ou}$ such that there is a local maximum of V_{PE} on the ray $S_{ray}(\theta^W)$ at α^m, where $I^{\alpha ou}$ is defined above and by Assumption 5.6 this maximum is the only one occurring on the ray $S_{ray}(\theta^W)$ in $S^{high}(\theta^u) \cap S_{ray}(\theta^W)$. Hence, α^m satisfies $-M^{\theta} g((\theta^W - \theta^s)\ \alpha^m + \theta^s) \cdot (\theta^W - \theta^s) = 0$. Let $\theta^m = ((\theta^W - \theta^s)\ \alpha^m + \theta^s)$ and note that $\theta^m \in S^{high}(\theta^u)$. The term $(\theta^W - \theta^s)$ only denotes the direction of the ray and $(\theta^m - \theta^s)$ denotes the same direction, hence, $-M^{\theta} g(\theta^m) \cdot (\theta^m - \theta^s) = 0$.

Denote the function $G(\theta)$: $S^{high}(\theta^u) \rightarrow R$ as $G(\theta) = -M^{\theta} g(\theta) \cdot (\theta - \theta^s)$. Denote the set $S^G(\theta^u) = \{\ \theta : \theta \in S^{high}(\theta^u),\ G(\theta) = 0\ \}$. It is seen from Proposition 5.5 that the set $S^G(\theta^u)$ is non-empty. The set $S^G(\theta^u)$ can also be denoted by $G^{-1}(0)$.

Proposition 5.7

The rank of the mapping $G(\theta)$: $S^{high}(\theta^u) \rightarrow R$ is 1, $\forall\ \theta \in S^G(\theta^u)$.

Proof:

Let $\theta \in S^G(\theta^u)$ and change the local coordinate system so that one of the new coordinate axis is in alignment with the ray $S_{ray}(\theta)$. Since $\theta \in S^G(\theta^u)$ there is a local maximum of V_{PE} at the point θ. Since this maximum is local or isolated this implies that the partial of $G(\theta)$ along the coordinate axis, which is in alignment with the ray, is not zero. ■

Proposition 5.8

The set $S^G(\theta^u)$ is a closed, regular *(n-1)-1* dimensional submanifold denoted by M^G.

Proof:

Given the result of Proposition 5.7 apply Theorem 5.8 and Collary 5.9 from [45, p. 79-80]. ■

Proposition 5.9

Denote the nonempty set $S^{GW} = S_{ray}(W^s(\theta^u)) \cap M^G$; the set S^{GW} is a regular *(n-1)-1* dimensional submanifold denoted by M^{GW}.

Proof:

Take any point $\theta \in W^s(\theta^u)$, then from Proposition 5.5 and Assumption 5.6 $S_{ray}(\theta) \cap M^G \neq \varnothing$. The function $S_{ray}(\theta)$: $W^s(\theta^u) \rightarrow M^{GW} \subset M^G$ can be considered a diffeomorphism with the obvious inverse from M^{GW} to $W^s(\theta^u)$. Apply Corollary 1.5 from [46] which states that $S_{ray}(W^s(\theta^u)) \cap M^G$ is a regular submanifold of dimension $m \leq (n-1)-1$. The same result applies to the inverse so that $S_{ray}(M^{GW}) \cap W^s(\theta^u)$ is a regular submanifold of dimension $(n-1)-1 \leq m$. It follows that $m = (n-1)-1$. ■

Assumption 5.10

Assume that $V_{PE}((\theta^u - \theta^s)\ \alpha + \theta^s) < V_{PE}(\theta^u)\ \forall\ \alpha \in [0\ ,\ 1)$.

Proposition 5.11

$\theta^u = \partial S^{high}(\theta^u) \cap \partial M^{GW}$.

Proof:

It is clear that $\theta^u \in \partial S^{high}(\theta^u)$. It is clear from Assumption 5.10 that there is a maximum of V_{PE} on the ray $S_{ray}(\theta^u)$ at the point θ^u. Take a sequence of points $\{\theta^{aj}\}_{j=1}^{\infty} \subset W^s(\theta^u)$ such that $\theta^{aj} \to \theta^u$ as $j \to \infty$. It has been shown in Proposition 5.5 and Assumption 5.6 that there is an unique maximum on the ray $S_{ray}(\theta^{aj})$ in the submanifold $M^{GW} \subset S^{high}(\theta^u)$. Let $\{\theta^{bj}\}_{j=1}^{\infty} \subset M^{GW}$ be the corresponding sequence of maximum points on the rays defined by θ^{aj}. Since V_{PE} is continuous it follows that $\theta^{bj} \to \theta^{s1}$ as $j \to \infty$. This gives the result that $\theta^u \in \partial M^{GW}$. Hence, $\theta^u \subset \partial S^{high}(\theta^u) \cap \partial M^{GW}$. It can be seen that points in ∂M^{GW} directly correlate to points in $\partial W^s(\theta^u)$. Now show that θ^u is the only point in $\partial S^{high}(\theta^u) \cap \partial M^{GW}$. It is seen that for all $\theta \in \partial W^s(\theta^u) \backslash \{\theta^u\}$, $V_{PE}(\theta) > V_{PE}(\theta^u)$. It is clear that $S_{ray}(\theta) \cap M^G \neq \varnothing$. This implies that $(S_{ray}(\theta) \cap \partial M^{GW}) \in M^G$. It is clear that $\partial S^{high}(\theta^u) \cap M^G = \varnothing$. Therefore, this implies that $\partial S^{high}(\theta^u) \cap \partial M^{GW} = \varnothing$ for all $\theta \in \partial W^s(\theta^u) \backslash \{\theta^u\}$. Hence, $\theta^u = \partial S^{high}(\theta^u) \cap \partial M^{GW}$. ■

Let $\theta^{m(i-1)} \in M^{GW}$. The point $\theta^{m(i-1)}$ should be thought of as an element from the sequence $\{\theta^{mi}\}_{i=0}^{\infty}$ as defined in Section 5.1 which results from the application of the shadowing method. At the point $\theta^{m(i-1)}$ there is a corresponding equipotential surface or as sometimes referred to a *level set*. This level set is denoted by $V_{PE}^{-1}(V_{PE}(\theta^{m(i-1)}))$. Note that a critical point of V_{PE} is equivalent to an equilibrium point of the gradient system (3.11). If $\theta^{m(i-1)}$ is not a critical point of V_{PE} then $\partial V_{PE}(\theta^{m(i-1)}) / \partial \theta_i \neq 0$ for at least some $i \in [1, ..., n-1]$ and if this is so the rank of the mapping V_{PE}: $R^{(n-1)} \to R$ is 1 at the point $\theta^{m(i-1)}$.

Proposition 5.12

The level set $V_{PE}^{-1}(V_{PE}(\theta^{m(i-1)}))\backslash\{$ critical points of V_{PE} in $V_{PE}^{-1}(V_{PE}(\theta^{m(i-1)}))\}$ is a closed, regular $(n-1)-1$ dimensional submanifold denoted by $M^V(\theta^{m(i-1)})$.

Proof:

This is shown in Example 5 from [37, p. 155]. The actual proof is Theorem 5.8 from [45, p. 79-80]. ■

Based at the point $\theta^{m(i-1)} \in M^{GW}$ is the negative gradient vector $-\nabla V_{PE}(\theta^{m(i-1)}) = z(\theta^{m(i-1)})$. This vector is normal to the $(n-1)-1$ dimensional submanifold $M^V(\theta^{m(i-1)})$ at the point $\theta^{m(i-1)}$.

The vector $z(\theta^{m(i-1)})$, which is based at the point $\theta^{m(i-1)}$, points in the direction of decreasing V_{PE} since it is the negative gradient vector. The ray $S_{ray}(\theta^{m(i-1)})$ and the vector $z(\theta^{m(i-1)})$, which are orthogonal to each other, span a two-dimensional plane $T_2 = span\{S_{ray}(\theta^{m(i-1)}), z(\theta^{m(i-1)})\}$. Let $D_\varepsilon(\theta^{m(i-1)}) \subset T_2$ be an open disk of radius $\varepsilon > 0$ centered at the point $\theta^{m(i-1)}$. Let ε be such that $\theta^s \notin D_\varepsilon(\theta^{m(i-1)})$ then it can be seen that since $D_\varepsilon(\theta^{m(i-1)}) \subset T_2$ the ray $S_{ray}(\theta^{m(i-1)})$ separates the disk into two disjoint sets. Denote these two sets as $S^{D\varepsilon L}(\theta^{t1})$ and $S^{D\varepsilon H}(\theta^{m(i-1)})$ and let $S^{D\varepsilon L}(\theta^{m(i-1)}) \cap z(\theta^{m(i-1)}) \neq \varnothing$ and $S^{D\varepsilon H}(\theta^{m(i-1)}) \cap z(\theta^{m(i-1)}) = \varnothing$.

Assumption 5.13

Assume there exist a sufficiently small ε with $\theta^s \notin D_\varepsilon(\theta^{m(i-1)})$ such that $V_{PE}(\theta) < V_{PE}(\theta^{m(i-1)})$, $\forall\, \theta \in S^{D\varepsilon L}(\theta^{m(i-1)})$ and $S^{D\varepsilon L}(\theta^{m(i-1)}) \subset S^{high}(\theta^{t1})$.

Let $\theta_\rho = (z(\theta^{m(i-1)})\, \rho + \theta^{m(i-1)})$. Take $\xi^o > 0$ so that $\theta_\rho \in S^{D\varepsilon L}(\theta^{m(i-1)})$, $\forall\, \rho \in (0, \xi^o)$. This $\xi^o > 0$ does indeed exist which follows directly from Assumption 5.13.

Proposition 5.14

Take a sequence of points $\{\theta^{sj}\}_{j=1}^{\infty} \subset \{\theta : \theta = \theta_\rho, \rho \in (0, \xi^o)\}$ such that $\theta^{sj} \rightarrow \theta^{m(i-1)}$ as $j \rightarrow \infty$, with $d(\theta^{sj},\theta^{m(i-1)}) > d(\theta^{s(j+1)},\theta^{m(i-1)})$, where $d(\cdot,\cdot)$ is the 2-norm. There exist an integer $k > 0$ so that for $j > k$, $S_{ray}(\theta^{sj}) \cap S^{D\varepsilon L}(\theta^{m(i-1)}) \cap M^G \neq \varnothing$.

Proof:
It follows from Proposition 5.5 that $S_{ray}(\theta^{sj}) \cap M^G \neq \varnothing$. For every θ^{sj} let θ^{gj} be the corresponding point in M^G (i.e., $\theta^{gj} \in M^G$). From Assumption 5.6 this point θ^{gj} is uniquely determined. It is seen as $j \rightarrow \infty$, $\theta^{gj} \rightarrow \theta^{m(i-1)}$ since $\theta^{m(i-1)} \in M^G$ and M^G is a regular manifold. In other words, $d(\theta^{gj},\theta^{m(i-1)}) \rightarrow 0$ as $j \rightarrow \infty$. Hence, there exist an integer $L > 0$ such that $d(\theta^{gj},\theta^{m(i-1)}) < \varepsilon$, $\forall\ j > L$. Therefore, for $j > L$, $\theta^{gj} \in S^{D\varepsilon L}(\theta^{m(i-1)})$, where $S^{D\varepsilon L}(\theta^{m(i-1)})$ is denoted in Assumption 5.13, so k can be taken as $k > L$. ■

Proposition 5.15

If the solution of the gradient system $\phi_{gs}(\theta^{m(i-1)},t_i)$ is approximated by an one-step Euler method then the solution will have the form $\theta^{ri} = \theta^{m(i-1)} + z(\theta^{m(i-1)})\, t_i$. Let $\theta^{mi} = S_{ray}(\theta^{ri}) \cap M^G$. Given $\theta^{m(i-1)} \in M^G$ and $\theta^{m(i-1)} \notin H$ there exist a $t_{ie} > 0$ such that for $t_i \in (0,t_{ie})$, $V_{PE}(\theta^{mi}) < V_{PE}(\theta^{m(i-1)})$.

Proof:
It follows from Proposition 5.14 that there exist a $\xi^e \in (0,\xi^o)$ such that $S_{ray}(\theta_\rho) \cap S^{D\varepsilon L}(\theta^{m(i-1)}) \cap M^G \neq \varnothing$, $\forall\ \rho \in (0, \xi^o)$. The Euler solution would give exactly the same point θ_ρ if $t_i = \rho$. Therefore, let $t_{ie} = \xi^e$. ■

Due to the assumptions and propositions given in Chapter 3 pertaining to the stability boundary of the gradient system and the assumptions and propositions given in this section the following result is seen to be true. Let $\theta^W \in R^{(n-1)} \backslash \{\theta^s\}$. As noted in Proposition 5.1 $S_{ray}(\theta^W) \cap \partial A(\theta^s) \neq \varnothing$. It was also

assumed that this intersection consisted of a singleton set. Suppose $S_{ray}(\theta^W) \cap W^s(\theta^u) \neq \varnothing$ and $S_{ray}(\theta^W) \cap \theta^u \neq \varnothing$. Since it was assumed in Assumption 5.3 that θ^u is type-*1*, $W^s(\theta^u)$ has dimension *(n-1)-1* which is the same dimension as the stability boundary. Take any vector $v(\theta^W)$ which is based at the point θ^W and is orthogonal to $S_{ray}(\theta^W)$. Take a sequence of points $\{\theta^{sj}\}_{j=1}^{\infty}$ that converges to θ^W as $j \rightarrow \infty$ such that $d(\theta^{sj},\theta^W) > d(\theta^{s(j+1)},\theta^W)$. It follows that there exist an integer $L > 0$ such that $\forall j > L$ $S_{ray}(\theta^{sj}) \cap W^s(\theta^u) \neq \varnothing$. This further implies that there exist a $\mu^0(\theta^W) > 0$ and an interval $I(\theta^W)$ defined by $I(\theta^W) = \{ \theta : \theta = \theta^W + v(\theta^W)\, \mu\, ,\, \mu \in (0,\mu^0(\theta^W)) \}$ such that $S_{ray}(I(\theta^W)) \cap W^s(\theta^u) \neq \varnothing$.

Since θ^u was taken to be the type-*1* controlling UEP, $Ang(\phi^d(\theta^{s1},0,t)) \cap W^s(\theta^u) \neq \varnothing$ for some $t > 0$. It was explained on a heuristic basis why the approximate exit point, $\theta^{egsa} \in Ang(\phi^d(\theta^{s1},0,t))$, is relatively close to $W^s(\theta^u)$.and this was due to the shape of the equipotential contours of V_{PE} around $W^s(\theta^u)$. The same argument can be applied to the ray concept. The mechanism for detecting the point θ^{m0} was presented in Section 5.1 It seems reasonable then, to argue that $S_{ray}(\theta^{m0}) \cap W^s(\theta^u) \neq \varnothing$.

Proposition 5.16

Given $\theta^{m0} \in M^{GW}$ with $\theta^{m0} \notin H$, then there exist a sequence of non-empty intervals $\{ (0, \Gamma_i) \}_{i=1}^{\infty}$ such that by utilizing the Euler method for the solution of the gradient system with $t_i \in (0, \Gamma_i)$ the resulting sequence $\{\theta^{mi}\}_{i=0}^{\infty}$ converges to θ^u.

Proof:

It has been shown in Proposition 5.12 that given $\theta^{m(i-1)} \in M^G$ and $\theta^{m(i-1)} \notin H$ there is a corresponding interval $(0,t_{ie})$ such that $V_{PE}(\theta^{mi}) < V_{PE}(\theta^{m(i-1)})$, where $\theta^{mi} = S_{ray}(\theta^{m(i-1)} + z(\theta^{m(i-1)})\, t_i) \cap M^G$ for $t_i \in (0,t_{ie})$. Therefore, pick $(0, \Gamma_i) \subset (0,t_{ie})$ such that for $\forall\, t_i \in (0, \Gamma_i)$, $(\theta^{m(i-1)} + z(\theta^{m(i-1)})\, t_i) \in I(\theta^{m(i-1)})$ and $\theta^{mi} \notin H$. Therefore, for each i, V_{PE} is decreasing along the sequence $\{\theta^{mi}\}_{i=0}^{\infty}$ and $\{\theta^{mi}\}_{i=0}^{\infty} \subset M^{GW}$. However, $\{\theta^{mi}\}_{i=0}^{\infty} \subset S^{high}(\theta^u)$ so that $V_{PE}(\theta^{mi}) > V_{PE}(\theta^u)$ for all i.

Suppose that for every possible sequence $\{t_i\}_{i=1}^{\infty}$ with $t_i \in (0, \Gamma_i)$ that the resulting sequence $\{\theta^{mi}\}_{i=0}^{\infty}$ converges to some point $\theta^c \in M^{GW}$. If $\{\theta^{mi}\}_{i=0}^{\infty} \to \theta^c \in M^G$ then $d(\theta^{m(i-1)}, \theta^{mi}) \to 0$ as $i \to \infty$ or $\mu^0(\theta^{m(i-1)}) \to 0$ as $i \to \infty$. If $d(\theta^{m(i-1)}, \theta^{mi}) \to 0$ as $i \to \infty$, this implies that $t_{ie} \to 0$ and further implies that the ε-disk as used in Assumption 5.10 shrink to a zero radius. This shows a contradiction against Assumption 5.10 since for any $\theta^{m(i-1)} \in M^G$ the disk has a non-zero radius. The same argument applies for $\mu^0(\theta^{m(i-1)}) \to 0$ as $i \to \infty$ which shows a contradiction since $\mu^0(\theta^c) > 0$. Therefore, the sequence $\{\theta^{mi}\}_{i=0}^{\infty} \subset M^{GW}$ must converge to some point on $\partial S^{high}(\theta^u)$. It has been shown in Proposition 5.11 that θ^u is this point. ■

The main result of this section was Proposition 5.16. Therefore, it can be theoretically stated that by applying the shadowing method with employing the Euler integration method for the numerical solution of the associated gradient system and with the appropriate elements of the sequence $\{t_i\}_{i=1}^{\infty}$ for the Euler method the resulting sequence $\{\theta^{mi}\}_{i=0}^{\infty}$ converges to θ^u and $S_{ray}(\theta^{mi}) \cap W^s(\theta^u) \neq \varnothing$. Again from previous discussion it may be argued that θ^{mi} is relatively close to $W^s(\theta^u)$. This idea is reflected in Figures 5.2, 5.3 and 5.4 where the points from the resulting finite sequence $\{\theta^{mi}\}_{i=0}^{N}$ seems relatively close to $W^s(\theta^u)$ and θ^{mN} is relatively close to the controlling UEP θ^u.

5.4 Concluding Remarks on the Shadowing Method

The first three sections of this chapter contained the algorithm of the shadowing method, two examples that numerically illustrated the shadowing method and an analytical foundation for the method.

In this section three remarks are put forth that pertain to the shadowing method. The three remarks are focused on: 1) the infinite

sequence $\{t_i\}_{i=1}^{\infty}$ and the Euler method, 2) the time value t_i that is used and 3) the usefulness of the sequence $\{\theta^{mi}\}_{i=0}^{N}$.

Remark 1. The infinite sequence $\{t_i\}_{i=1}^{\infty}$ and the Euler method,

Suppose that the Euler method is employed to numerically approximate $\phi_{gs}(\theta,t)$ in the shadowing method algorithm when applied to the unloaded gradient system model. Then, by Proposition 5.16 there exist an infinite sequence of time steps $\{t_i\}_{i=1}^{\infty}$ such that the resulting sequence $\{\theta^{mi}\}_{i=0}^{\infty}$ converges to the controlling UEP θ^u. Two points need to be made about the infinite sequence of time steps . First, it was shown how to construct this sequence in the proof of Proposition 5.16 and this consisted of t_i satisfying two constraints. Hence, additional computation is needed to provide verification of these constraints. Secondly, it is impossible to perform the algorithm of the shadowing method when an infinite sequence is involved.

It must be remembered that the practical purpose of applying the shadowing method is to produce a point θ^{mN} that is relatively close to the controlling UEP θ^u. Then, when the nonlinear algebraic solver is applied there is no doubt that the point θ^{mN} is in the domain of convergence of θ^u and that θ^u will be produced. Hence, if the three step cycle is numerically processed a relatively large number of times with acceptable t_i's the last point in the sequence should be relatively close to θ^u.

This idea is reflected in the two examples given in Section 5.2. The relatively large number of three step cycles were 28 and 36 for example 1 and example 2 respectively. The main result also supports the idea of the stopping criterion for the three step cycle process. This stopping criterion is based on the 1-norm of the vector z being smaller than a given value β. It can be seen that as the infinite sequence $\{\theta^{mi}\}_{i=0}^{\infty}$ converges to θ^u the 1-norm of the vector z must go to zero.

In the numerical algorithm describing the three step cycle of the exit point method the true solution $\phi_{gs}(\theta,t)$ of the gradient system was implemented. In the actual numerical scheme this solution needs to be

approximated numerically. The numerical scheme that was assumed in the mathematical foundation of the shadowing method was the Euler method. The Euler method was picked for the convenience of proving Proposition 5.15 and the claim made in Proposition 5.16 is not that by only applying the Euler method will the sequence converge to the controlling UEP. It is, however, strongly believed that the same conclusion of Proposition 5.16 can be proved if the true solution of the gradient system, namely $\phi_{gs}(\theta,t)$, is used and this will be attempted.

The numerical ordinary differential equation (ODE) solver method used in the shadowing method when applied to example 1 and example 2 was the 4^{th} order Runge-Kutta method and not the Euler method. This is simply because the 4^{th} order Runge-Kutta method numerically approximates the true solution better than the Euler method.

Remark 2. The time value t_i that is used,

Since construction of an infinite sequence of time steps is impossible a finite one is constructed. It was noted earlier that if the Euler method is used it would be computationally cumbersome to verify if t_i is satisfactory. Since the Euler method may not be employed the verification process of the time step may not be applicable. Therefore, the t_i need to be chosen on a heuristic basis.

Suppose that Proposition 5.16 has been shown to hold true when the actual solution of the gradient system is used in the shadowing algorithm. What is needed to make the shadowing technique most effective is if these t_i's can be chosen optimally. Or in other words, determine an *optimal finite sequence* $\{t_i\}_{i=1}^{N}$ such that the amount of computation time is minimal with the objective being that θ^{mN} is in the domain of convergence of θ^{u}. At the time of writing this dissertation there is no known scheme that will produce this finite time sequence and thus, this a future research project.

In both example 1 and example 2 from Section 5.2 $t_i = 0.1$ was chosen and this was kept constant for all t_i in the finite sequence $\{t_i\}_{i=1}^{N}$. It might seem as the points of $\{\theta^{mi}\}_{i=0}^{N}$ get relatively closer to θ^{u} the corresponding t_i must be chosen smaller and smaller. This need not be the case since near

the UEP the length of the vector $z(\theta^{m(i-1)})$ becomes smaller and smaller. Hence, $z(\theta^{m(i-1)})\, t_i$ becomes smaller and smaller and this is the basic mechanism that advances the sequence.

Remark 3. The usefulness of the sequence $\{\theta^{mi}\}_{i=0}^{N}$,

The method that is described in this chapter is referred to as shadowing the stable manifold. Upon the numerical application the method produces a sequence of points $\{\theta^{mi}\}_{i=0}^{N} \subset M^{GW}$. As explained in Section 5.1 it is called shadowing the stable manifold because it is thought that the points θ^{mi} are relatively close to $W^s(\theta^u)$. This closeness depends on the shape of the equipotential energy surface around $W^s(\theta^u)$. From the numerical examples such as the ones given in this chapter it does seems as if the points in the set M^{GW} are relatively close to the points in the set $W^s(\theta^u)$.

However, the implication that every point in $\{\theta^{mi}\}_{i=0}^{N}$ may be close to $W^s(\theta^u)$ was not the focus of this chapter. The focus was on the prediction that the last point in $\{\theta^{mi}\}_{i=0}^{N}$, θ^{mN} might be relatively close to θ^u. In fact $\{\theta^{mi}\}_{i=0}^{\infty}$ converges to θ^u if the t_i's are chosen appropriately. If, however, it is such that points in $W^s(\theta^u)$ are relatively close to points in M^{GW} then the sequence $\{\theta^{mi}\}_{i=0}^{N}$ may be used in some fashion to determine how the stability boundary in terms of the stable manifold $W^s(\theta^u)$ might change as system parameters such as C_{ij} change.

6. INCLUSION OF TRANSFER CONDUCTANCES INTO THE POWER SYSTEM MODEL

The swing system that was presented in Chapter 3 and the associated gradient system that was presented in Chapters 3, 4 and 5 were based on a lossless power system model. That is, a system when reduced to the internal generator buses had no transfer conductances present in the resulting Y_{BUS} matrix. This reduced system is realized when the system has no line resistance and no real load. The swing system model, however, cannot be considered Hamiltonian [34] since energy is dissipated because of the presence of non-zero uniform damping.

The assumption that transfer conductances can be neglected is unrealistic [12] and hence, it is considered that the swing system model does not realistically model the dynamic behavior in a real power system. The reason that the transfer conductances were neglected is to make possible a rigorous mathematical analysis of the swing system and gradient system. A property that was shown to hold for both the swing and gradient system was that the stability boundary was equal to the union of the stable manifolds of unstable equilibrium on the stability boundary. This property was shown to hold due to the existence of a valid energy function as shown in Chapter 3. However, the existence of such a energy function when real load and line resistance are included in the system is still unclear at the present time.

The contents of this chapter is an explanation of what happens to the properties of the swing system and gradient system when transfer conductances are present in the system.

Section 6.1 The effect of the inclusion of transfer conductances on the structure of the stability boundary of the gradient system is analyzed. The effect of the inclusion of transfer conductances on the structure of the stability boundary of the swing system model from Chapter 3 is analyzed.

Finally, the effect of the inclusion of transfer conductances on the connection between the gradient system and the swing system is analyzed.

Section 6.2 Transfer conductances are introduced into the unloaded 3-machine system. Static bifurcation is observed and this phenomenon is briefly analyzed. Finally, the stability boundary of the lossy gradient system for the 3-machine is examined through vector field plots.

6.1 Persistence of Properties with the Inclusion of Transfer Conductances

6.1.1 The Lossy Gradient System

In this section it is shown that for the function V_{PE} (2.11b), $\dot{V}_{PE} < 0$ along the asymptotically stable trajectories with respect to θ^s of the lossy gradient system. The trajectory needs to start within the stability region $A(\theta^s)$ because V_{PE} is path dependent and is evaluated with respect to the asymptotically stable equilibrium point θ^s. This result seems somewhat trivial but it points out the following fact. The function V_{PE} (2.11b) cannot be used to show that $\dot{V}_{PE} < 0$ along a trajectory in $\partial A(\theta^s)$ which is the idea that is employed in showing that the stability boundary is equal to the union of the stable manifolds of unstable equilibrium on the stability boundary.

The associated gradient system, which is derived from the swing system, was defined in Section 3.2 and is repeated here in vector-matrix form as

$$\dot{\theta} = - \nabla V_{PE} = \frac{- \partial V_{PE}}{\partial \theta} = z = M^{\theta} g$$

The derivative $\partial V_{PE} / \partial \theta$ was given in Appendix A, Section A.2. As noted in Section 3.1.1 the function V_{PE} (3.5c) is equivalent to the V_{PE} function

given by equation 2.12 with $D_{ij} = 0$ (i.e., neglecting transfer conductances in the reduced Y_{BUS} matrix). Also, the function g_i (3.2) is equivalent to f_i, (2.8), when $D_{ij} = 0$. With $D_{ij} = 0$ the derivation of V_{PE} as shown in Section 2.2 becomes

$$V_{PE}(\theta) = - \int_{\tau=0}^{\tau=t} \left[\left[M^{\theta} g(\Theta(\tau)) \right] \cdot \frac{d\Theta(\tau)}{d\tau} \right] d\tau$$

where $\Theta(\tau)$ is some path parameterized by τ, $0 \leq \tau \leq t$, with $\Theta(0) = \theta^s$ and $\Theta(t) = \theta$. Note that because the system is lossless the above integral is path independent and this follows from a similar discussion as given in Section 2.2. This integral can be evaluated and a closed form expression for V_{PE} results and this is equation (3.5c).

When transfer conductances are present the gradient system will be denoted as the *lossy gradient system* and will be defined as follows with the new variable w introduced

$$\dot{\theta} = M^{\theta} f = w \tag{6.1}$$

It was shown in Section 3.2 that the equilibrium points of the gradient system are hyperbolic. Since there are transfer conductances present, the vector field w (6.1) is not the gradient of any scalar function, therefore, it will be assumed that the equilibrium points of the lossy gradient system are hyperbolic. As first assumed in Section 3.2 the stable and unstable manifolds are assumed to intersect transversally. Again, it will be assumed that θ^s is an asymptotically stable equilibrium point for the lossy gradient system (6.1). Since θ^s is asymptotically stable there exist a stability region $A(\theta^s) \subset R^{(n-1)}$ which will be assumed not dense in $R^{(n-1)}$. With this assumption there exist a stability boundary for $A(\theta^s)$ denoted by $\partial A(\theta^s)$. Again, $\phi_{gs}(\theta,t)$ will be denoted as the solution to (6.1).

In order to show that $\dot{V}_{PE} < 0$ along the asymptotically stable trajectories with respect to θ^s of the lossy gradient system the following is put forth. Let $\theta \in A(\theta^s)$, then $\phi_{gs}(\theta,t) \rightarrow \theta^s$ as $t \rightarrow \infty$. Let $\Theta(\tau)$, parameterized by τ,

be the path taken by $\phi_{gs}(\theta,t)$ as $t \rightarrow \infty$ but oriented in the opposite direction. Define $V_{PE}(\theta)$ as

$$V_{PE}(\theta) = - \int_{\tau=0}^{\tau=T} \left[w(\Theta(\tau)) \cdot \frac{d\Theta(\tau)}{d\tau} \right] d\tau \tag{6.2}$$

where $0 \leq \tau \leq T$, $\Theta(0) = \theta^s$ and $\Theta(T) = \theta$. It is thus seen from the integral (6.2) that $V_{PE}(\theta^s) = 0$. Since the path taken by $\Theta(\tau)$ is oriented in the opposite direction as $\phi_{gs}(\theta,t)$ it follows that $d\Theta(\tau)/d\tau = - w(\Theta(\tau))$. The integral (6.2) now becomes

$$V_{PE}(\theta) = \int_{\tau=0}^{\tau=T} \left[w(\Theta(\tau)) \cdot w(\Theta(\tau)) \right] d\tau \tag{6.3}$$

For the integrand in the integral (6.3), $w(\Theta(\tau)) \cdot w(\Theta(\tau)) > 0$ for $\Theta(\tau) \notin H$. The set H was defined in Section 3.2 as the set of all equilibrium points for the lossless gradient system. Here the set H will be denoted as the set of all equilibrium points for the lossy gradient system. Since $\theta \in A(\theta^s)$ for integral (6.2) and integral (6.3) and $\phi_{gs}(\theta,t) \in A(\theta^s)$ $\forall\, 0 \leq t < \infty$, $w(\Theta(\tau)) \cdot w(\Theta(\tau)) > 0$ for $0 < \tau \leq T$. This implies that $V_{PE}(\theta) > 0$ for $\theta \in A(\theta^s) \backslash \{\theta^s\}$.

The function $V_{PE}(\theta)$ with $\theta \in A(\theta^s)$ can also be formulated in another manner. The path $\Theta(\tau)$ can be taken as $\phi_{gs}(\theta,t)$, $t \rightarrow \infty$, and oriented in the same direction as $\phi_{gs}(\theta,t)$ with $\Theta(0) = \phi_{gs}(\theta,0)$ and $\Theta(\infty) = \theta^s$. The integral now takes the form

$$V_{PE}(\theta) = \lim_{T \rightarrow \infty} \int_{\tau=0}^{\tau=T} \left[w(\Theta(\tau)) \cdot \frac{d\Theta(\tau)}{d\tau} \right] d\tau \tag{6.4}$$

Since $\Theta(\tau)$ is oriented in the same direction as $\phi_{gs}(\theta,t)$, $d\Theta(\tau)/d\tau = w(\Theta(\tau))$ and the integral (6.4) can be written as

$$V_{PE}(\theta) = \lim_{T \to \infty} \int_{\tau=0}^{\tau=T} \left[w(\Theta(\tau)) \cdot w(\Theta(\tau)) \right] d\tau \qquad (6.5)$$

It can be seen that as $T \to \infty$, $w(\Theta(T)) \to 0$, . However, this does not imply that the integral (6.5) exist, therefore, it will be assumed that it does. Again for the integrand of integral (6.5), $w(\Theta(\tau)) \cdot w(\Theta(\tau)) > 0$ for $0 \leq \tau < \infty$, so that $V_{PE}(\theta) > 0$ for $\theta \in A(\theta^s) \backslash \{\theta^s\}$.

Given $V_{PE}(\theta)$ (6.5) for $\theta \in A(\theta^s)$ it will be shown below that $\dot{V}_{PE} < 0$ for $\theta \in A(\theta^s)$. Let $q(\Theta(\tau)) = w(\Theta(\tau)) \cdot w(\Theta(\tau)) > 0$ for $\Theta(\tau) \in A(\theta^s) \backslash \{\theta^s\}$. The time derivative of $V_{PE}(\theta)$ is defined as

$$\frac{V_{PE}(\theta(t))}{dt} = \lim_{h \to 0} \frac{1}{h} \left[V_{PE}(\theta(t+h)) - V_{PE}(\theta(t)) \right]$$

This can be formulated as

$$\dot{V}_{PE} = \lim_{h \to 0} \frac{1}{h} \left[\lim_{T \to \infty} \int_{\tau=h}^{\tau=T} q(\Theta(\tau))\, d\tau - \lim_{T \to \infty} \int_{\tau=0}^{\tau=T} q(\Theta(\tau))\, d\tau \right]$$

$$\dot{V}_{PE} = \lim_{h \to 0} \frac{1}{h} \left[- \int_{\tau=0}^{\tau=h} q(\Theta(\tau))\, d\tau \right]$$

From the Mean Value Theorem for Integrals it is seen that

$$\int_{\tau=0}^{\tau=h} q(\Theta(\tau))\, d\tau = q(\Theta(\xi))\, h \quad \text{for } 0 \leq \xi \leq h$$

Therefore, in the limit as $h \to 0$, $\dot{V}_{PE} = - q(\theta) < 0$.

In order to show that the stability boundary is equal to the union of the stable manifolds of unstable equilibrium points on the stability boundary there were three conditions that needed to be satisfied [47, Section 4]. The first two are hyperbolic equilibrium points on the stability boundary and

transversality at the intersections of stable and unstable manifolds. The third is that trajectories in the stability boundary converge to an equilibrium point in the stability boundary. This third condition was shown to be true for the lossless gradient system as shown in Section 3.2 by utilization of the function V_{PE} (3.5c). The V_{PE} from equation (6.5) is shown to decrease along asymptotically stable trajectories with respect to θ^s of the lossy gradient system. However, this V_{PE} function (6.5) cannot be utilized to show that trajectories in the stability boundary converge to an equilibrium point in the stability boundary. This is due to the fact that V_{PE} (6.5) is path dependent. Therefore, it is unclear if the stability boundary is equal to the union of the stable manifolds of unstable equilibrium points on the stability boundary. Hence, it must be assumed that trajectories in the stability boundary converge to an equilibrium point in the stability boundary in order to show that the stability boundary of the lossy gradient system is equal to the union of the stable manifolds of unstable equilibrium on the stability boundary.

Another interesting point can be made. The vector field of the lossless gradient system was defined by the negative gradient of the function V_{PE} (3.5c). However, for the lossy gradient system the vector field given by (6.1) is not the negative gradient of the V_{PE} (6.5) as shown below. Let C_1 be the path taken by $\phi_{gs}(\theta,t)$, $t \rightarrow \infty$. The integral (6.5) can be formulated into a line integral along the path C_1.

$$V_{PE}(\theta) = \int_{\theta\ C_1}^{\theta^s} w(\Theta) \cdot d\Theta \tag{6.6}$$

The negative gradient of V_{PE} will take the form $-\partial V_{PE} / \partial \theta_i$, $i = 1, \ldots, n-1$. From the definition of the derivative

$$\frac{\partial V_{PE}(\theta)}{\partial \theta_i} = \lim_{h \rightarrow 0} \frac{V_{PE}(\theta + h\, a_i) - V_{PE}(\theta)}{h}$$

where a_i is an unit vector in the same direction as the coordinate axis corresponding to θ_i. Let C_2 be the path defined by $\phi_{gs}(\theta + h\, a_i, t)$, $t \rightarrow \infty$ where

h is small so that $(\theta + h\ a_i) \in A(\theta^s)$. The partial derivative $\partial V_{PE} / \partial \theta_i$ now becomes

$$\frac{\partial V_{PE}(\theta)}{\partial \theta_i} = \lim_{h \to 0} \frac{1}{h} \left[\int_{(\theta + h\ a_i)\ C_2}^{\theta^s} w(\Theta) \cdot d\Theta - \int_{\theta\ C_1}^{\theta^s} w(\Theta) \cdot d\Theta \right]$$

$$= - \lim_{h \to 0} \frac{1}{h} \left[\int_{\theta^s\ -C_2}^{(\theta + h\ a_i)} w(\Theta) \cdot d\Theta + \int_{\theta\ C_1}^{\theta^s} w(\Theta) \cdot d\Theta \right]$$

$$= - \lim_{h \to 0} \frac{1}{h} \left[\int_{\theta\ -C_2 + C_1}^{(\theta + h\ a_i)} w(\Theta) \cdot d\Theta \right] \qquad (6.7)$$

Suppose this integral (6.7) was path independent. Then the integral (6.6) in the limit would be [48, Section 16.3]

$$\frac{\partial V_{PE}(\theta)}{\partial \theta_i} = - \lim_{h \to 0} \frac{1}{h} \left[\int_{\theta\ C_3}^{(\theta + h\ a_i)} w(\Theta) \cdot d\Theta \right] = - w_i(\theta)$$

where C_3 is some arbitrary smooth path connecting $(\theta + h\ a_i)$ and θ. However, since the path is $-C_2 + C_1$ and the integral is path dependent, it can be stated that in general

$$\frac{\partial V_{PE}(\theta)}{\partial \theta_i} \neq - w_i(\theta)$$

Therefore, the lossy gradient system cannot be formed by the negative gradient of V_{PE} (6.2).

6.1.2 The Realistic Power System Model

The differential equations of the classical model in the COI reference frame are given by equation (2.6) and are repeated here in vector-matrix form.

$$\begin{aligned} \dot{\varpi} &= M^{-1} f \\ \dot{\theta} &= \varpi \end{aligned} \tag{6.8}$$

Similar to what was stated in Section 6.1, in order to claim that the stability boundary of the classical system is equal to the union of the stable manifolds of unstable equilibrium on the stability boundary three conditions needed to be satisfied. The first condition is that equilibrium points on the stability boundary need to be hyperbolic. The Jacobian matrix for equation (6.8) (e.g. refer to Section 3.1 for the Jacobian for the swing system) will generally have zero real-part eigenvalues because the *(n-1)* by *(n-1)* matrix $M^{-1} D_\theta f$ will generally have all negative real eigenvalues. Therefore, in order that hyperbolic equilibrium points result non-zero uniform damping is added to the system (6.8). The derivation of the differential equations in COI with uniform damping follows directly from the discussion in Appendix A, Section A.1. The uniform damping is such that $D_i / M_i = c > 0 \ \forall \ i \in [1, ..., n]$. The differential equations in vector-matrix form become

$$\begin{aligned} \dot{\varpi} &= M^{-1} f - c\, \varpi \\ \dot{\theta} &= \varpi \end{aligned} \tag{6.9}$$

It is assumed that $(\theta^s,0)$ is an asymptotically stable equilibrium point which results in a stability region $A(\theta^s,0)$ and corresponding stability boundary $\partial A(\theta^s,0)$. The assumption of transversal intersection of the stable and unstable manifolds also needs to be assumed. The third condition again is that trajectories in the stability boundary of (6.9) converge to an equilibrium point in the stability boundary.

The third condition was shown to be true for the swing system in Section 3.1 due to the existence of the function V_{PE} (3.5a). It was shown in [49] that there does not exist in general an energy function of Lyapunov-like function that can be utilized in showing that trajectories in the stability boundary $\partial A(\theta^s,0)$ of (6.9) converge to an equilibrium point in the stability boundary. In the absence of any analytical justification pertaining to the convergence of trajectories in the stability boundary it must be assumed so. However, there are known cases where the assumption that trajectories in the stability boundary converge to an equilibrium point in the stability boundary are shown to be invalid for a system of the form (6.9). In references [49] , [50] and [51] it is shown that oscillatory solution of a system of the form (6.9) exist thus showing that trajectories do not converge to an equilibrium point.

6.1.3 The Connection Between the Realistic and Lossy Gradient Systems

It is clear that θ is an equilibrium point of the lossy gradient system if and only if $(\theta,0)$ is an equilibrium point of the classical system. The main result from Section 3.3 is that θ is an equilibrium point on the stability boundary of the gradient system if and only if $(\theta,0)$ is an equilibrium point on the stability boundary of the swing system. It is unclear, however, if this property persists under the inclusion of transfer conductances into the reduced Y_{bus} matrix. It is unclear because Theorem 5.2 from [21], which is one of the theorems needed for the result of Theorem 3.3.5 in Section 3.3, cannot be applied. In a part of Theorem 5.2 an energy function is defined in which the integral $U(x) = \int^x f(y) \cdot dy$ is used. When there are no transfer conductances $\partial U(x)/\partial x = f(x)$ and this is the result needed in the theorem but, since transfer conductances are present it can be stated that in general $\partial U(x)/\partial x \neq f(x)$. Hence, this part of the proof does not seem to hold but, there can be no claim made that the overall result of Theorem 5.2 in [21] is invalid.

As pointed out in Subsections 6.1.1 and 6.1.2, it has not been proved that when transfer conductances are present in the system the stability boundary of the system is equal to the union of the stable manifolds of

unstable equilibrium on the stability boundary. In fact, in Subsection 6.1.2 a counter-example was shown to exist. Suppose that when transfer conductances are present in the system the stability boundaries of the classical and lossy gradient systems are equal to the union of the stable manifolds of unstable equilibrium on the respective stability boundaries. It is also unclear in this situation whether or not Theorem 3.3.5 from Section 3.3 still holds. This theorem states that an equilibrium point θ is on the stability boundary of the gradient system if and only if $(\theta,0)$ is on the stability boundary of the swing system.

In conclusion to this section, it must be stated that when transfer conductances are added a rigorous mathematical analysis of the resulting lossy gradient system and classical system is incomplete and many unanswered questions still remain. In light of this situation numerical data which resulted from an analysis on the 3 machine system will presented in the next section in order that some heuristic insight into the above mentioned problems be obtained.

6.2 Analysis of the Stability Boundary of the Lossy Gradient System

The main result of Sections 6.1.1 and 6.1.2 was that when transfer conductances are included in to the reduced Y_{bus} matrix it is uncertain if both equations (6.10) and (6.11) given below hold.

$$\partial A(\theta^s) = \bigcup_{(\theta^i) \in HB} W^s(\theta^i) \tag{6.10}$$

$$\partial A(\theta^s,0) = \bigcup_{(\theta^i,0) \in EB} W^s(\theta^i,0) \tag{6.11}$$

The concept of the energy margin as defined in Section 3.1.3 was based on the idea that is shown by equation (6.11). In order to stay with this idea of

energy margin in a realistic power system it will be assumed that equation (6.11) is indeed true.

The validity of equation (6.10) when transfer conductances are included into the system has a definite connection to the shadowing method which was described in Section 5.1. The shadowing method is used to shadow the stable manifold $W^s(\theta^u)$ where θ^u is the given controlling UEP. The definition of the controlling UEP as used in this dissertation work is given in Definition 3.1.6 from Section 3.1.2. The purpose of the application of the shadowing method is to derive a point which is relatively close to θ^u. This technique was based on the lossless gradient system and was given analytical foundation for the unloaded gradient system model. Therefore, in order that the shadowing method be applicable in the system with transfer conductances it will be assumed that equation (6.10) is true. It will also be assumed that Theorem 3.3.5 from Section 3.3 holds true. This theorem states that an equilibrium point θ is on the stability boundary of the gradient system if and only if $(\theta,0)$ is on the stability boundary of the swing system.

Since the lossy gradient system (6.1) is 2-dimensional for the 3-machine system, the stability boundary can be numerically observed through a vector field plot of (6.1). The 3-machine system was given in Appendix B, Section B.3 which will now be referred to as the loaded 3-machine system. As transfer conductances are introduced into the system the stability boundary of the unloaded gradient system as shown in Figure 4.4 will change. The objective is to see if the union of the stable manifolds of the lossy gradient system still represent its stability boundary. In other words, address the validity of (6.10) when transfer conductances are present. In the following subsection (6.2.1) transfer conductances are introduced into the unloaded 3-machine system. It is seen that as the transfer conductances are introduced static bifurcation of equilibrium points occur and this is presented in Subsection 6.2.2. Finally, in Subsection 6.2.3 the vector field plots are given and examined.

6.2.1 Introduction of Transfer Conductances into the Unloaded 3-machine System

For the purpose of introducing transfer conductances into the unloaded 3-machine system a new system will be needed which is a modified version of the loaded 3-machine system. The modification is that all line resistance is neglected. The solution data for this modified 3-machine system is given in Table 6.1. Note that in the 3-machine system buses *1* and *2* are *PV* buses, bus *3* is the *swing bus* and buses *4*, *5* and *7* are *PQ* buses.

Table 6.1 Power flow solution data for the modified 3-machine system

Bus number	Voltage magnitude (pu)	Voltage angle (degrees)	Real power load (pu)	Reactive power load (pu)	Real power generation (pu)	Reactive power generation (pu)
1	*1.025*	*4.873*	*0.00*	*0.00*	*0.85*	*-0.08*
2	*1.025*	*9.483*	*0.00*	*0.00*	*1.63*	*0.19*
3	*1.040*	*0.000*	*0.00*	*0.00*	*0.67*	*0.16*
4	*1.011*	*-3.853*	*1.25*	*0.50*	*0.00*	*0.00*
5	*1.018*	*0.872*	*1.00*	*0.35*	*0.00*	*0.00*
6	*1.032*	*-2.060*	*0.00*	*0.00*	*0.00*	*0.00*
7	*1.028*	*-3.482*	*0.90*	*0.30*	*0.00*	*0.00*
8	*1.031*	*2.171*	*0.00*	*0.00*	*0.00*	*0.00*
9	*1.022*	*3.902*	*0.00*	*0.00*	*0.00*	*0.00*

All per-unit values based on a system base of *100 MW*

Transfer conductances are introduced into the unloaded 3-machine system in the following manner. The unloaded 3-machine system is transformed into the modified version of the loaded 3-machine system by linearly varying the input data values to the power flow equations. The linear transformation takes the following form

$$\Gamma^{in} = (\Gamma^{mv} - \Gamma^{un})\,\lambda + \Gamma^{un} \quad 0 \le \lambda \le 1 \tag{6.12}$$

The variable Γ in (6.12) represents the following different inputs to the power flow formulation: the terminal bus voltage magnitude and real power injection for the *PV* buses *1* and *2*, the real power load and reactive power load for the *PQ* buses *4*, *5* and *7* and the terminal bus voltage magnitude on the *swing bus*, bus *3*. The super-scripts on the variable Γ represent the *in*-intermediate values, *mv*-modified version and *un*-unloaded. At a specific value of λ, $0 \leq \lambda \leq 1$, the intermediate values are calculated and with these as inputs for the power flow equations a solution is computed. For example, with $\lambda = 0.5$ the intermediate value of the terminal bus voltage magnitude at bus *1* is *1.04 = (1.025 - 1.055) 0.5 + 1.055 pu*. The value of 1.025 was taken from Table 6.1 and the value of 1.055 was taken from Table B.7 from Appendix B, Section B.3.

To show how the stability boundary of the lossy gradient system changes as the system is transformed from the unloaded system to the modified system, the variable λ will take on the values of $\lambda \in$ *[0.0, 0.02, 0.04, ..., 0.98, 1.0]*. For each of these values of λ a power solution is determined. All constant power loads are converted, based on the solved bus voltage, into constant admittance loads. The transient reactances are included and the system is reduced to the internal bus of each machine. Finally, the internal bus voltage magnitude and angle are calculated. These internal bus voltage angles correspond to the SEP of the gradient system (6.1). The reduced Y_{bus} has the form $G + jB$, where G and B have corresponding elements G_{ij} and B_{ij}. The variables $C_{ij} = E_i E_j B_{ij}$ and $D_{ij} = E_i E_j G_{ij}$ are computed with E_i being the internal bus voltage magnitude for machine i.

The equations of the lossy gradient system are given by equation (6.1) and are repeated here

$$\dot{\theta} = M^{\theta} f = w \tag{6.13}$$

The vector function f is given in equation (2.7) from Section 2.1. Since the loading in the system is dependent on the parameter λ, the variables P_{mi}, C_{ij} and D_{ij} are functions of λ. The function f_i is then given as

$$f_i = P_{mi}(\lambda) - D_{ii}(\lambda) - \sum_{\substack{j=1 \\ j \neq i}}^{n-1} \left[C_{ij}(\lambda) \sin\left(\theta_i - \theta_j\right) + D_{ij}(\lambda) \cos\left(\theta_i - \theta_j\right) \right]$$

$$- C_{in}(\lambda) \sin\left(\theta_i + \frac{1}{M_n}\left(M_1\theta_1 + M_2\theta_2 + \cdots + M_{n-1}\theta_{n-1}\right)\right)$$

$$- D_{in}(\lambda) \cos\left(\theta_i + \frac{1}{M_n}\left(M_1\theta_1 + M_2\theta_2 + \cdots + M_{n-1}\theta_{n-1}\right)\right)$$

$$- \frac{M_i}{M_T} \sum_{k=1}^{n} D_{mk}(\lambda) + 2\frac{M_i}{M_T} \sum_{k=1}^{n-1} \sum_{j=k+1}^{n-1} D_{kj}(\lambda) \cos\left(\theta_k - \theta_j\right)$$

$$+ 2\frac{M_i}{M_T} \sum_{k=1}^{n-1} D_{kn}(\lambda) \cos\left(\theta_k + \frac{1}{M_n}\left(M_1\theta_1 + M_2\theta_2 + \cdots + M_{n-1}\theta_{n-1}\right)\right) \quad (6.14)$$

and the positive definite matrix M^{θ} is defined as

$$M_{ij}^{\theta} = \begin{cases} \left(1 + \frac{M_i}{M_n}\right) & \text{if } i = j \\ \frac{M_i}{M_n} & \text{if } i \neq j \end{cases}$$

As λ is varied from 0 to 1 the resulting terms $P_{mi}(\lambda)$, $C_{ij}(\lambda)$ and $D_{ij}(\lambda)$ are seen to be smooth functions of λ as shown in the plots of Figures 6.1, 6.2, and 6.3.

6.2.2 Static Bifurcation in the Lossy Gradient System and Classical System

Before any vector field plots of (6.13) are given a diagram of how the equilibrium points of (6.12) move in the state space as λ is varied is given. When $\lambda = 0$, the lossy gradient system is equivalent to the unloaded gradient system (i.e., $P_{mi}(0) = 0$ and $D_{ij}(0) = 0$ which can also be seen in Figures 6.2 and

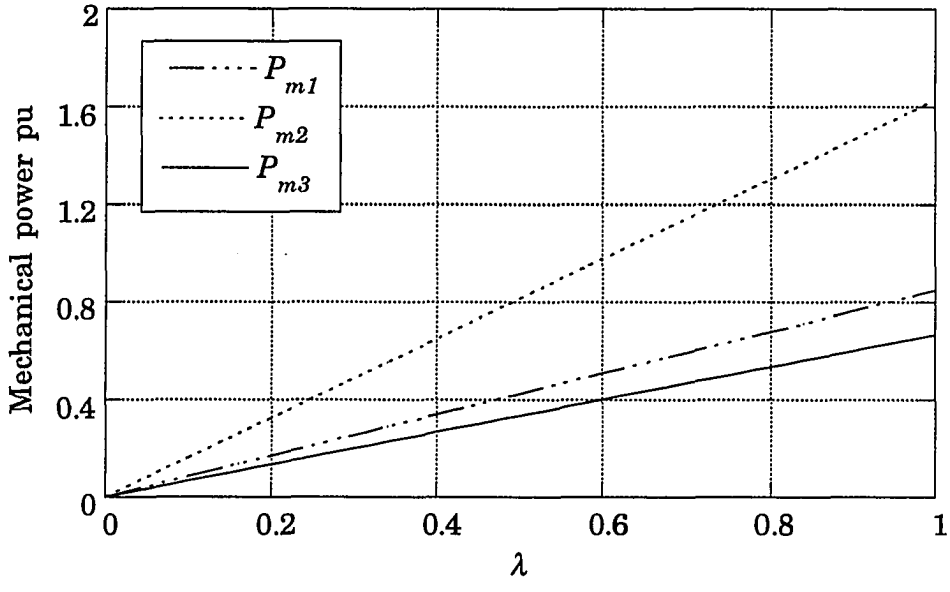

Figure 6.1 Mechanical power versus the parameter λ

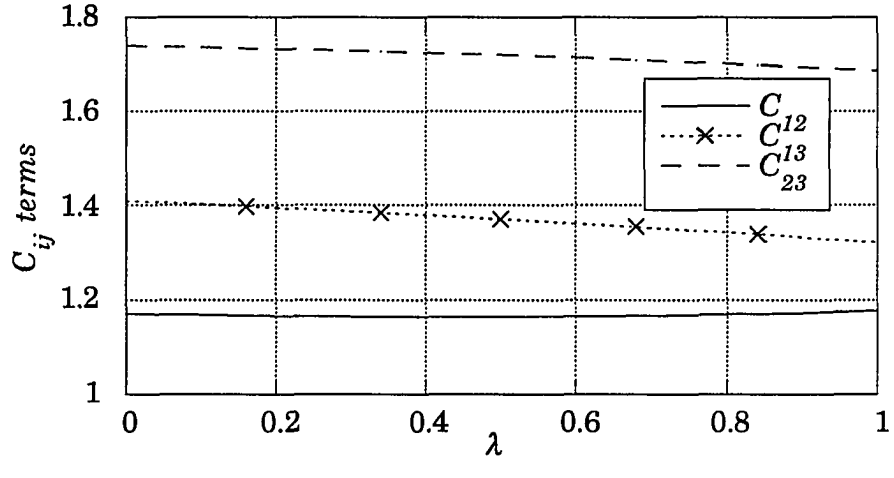

Figure 6.2 The C_{ij} terms versus the parameter λ

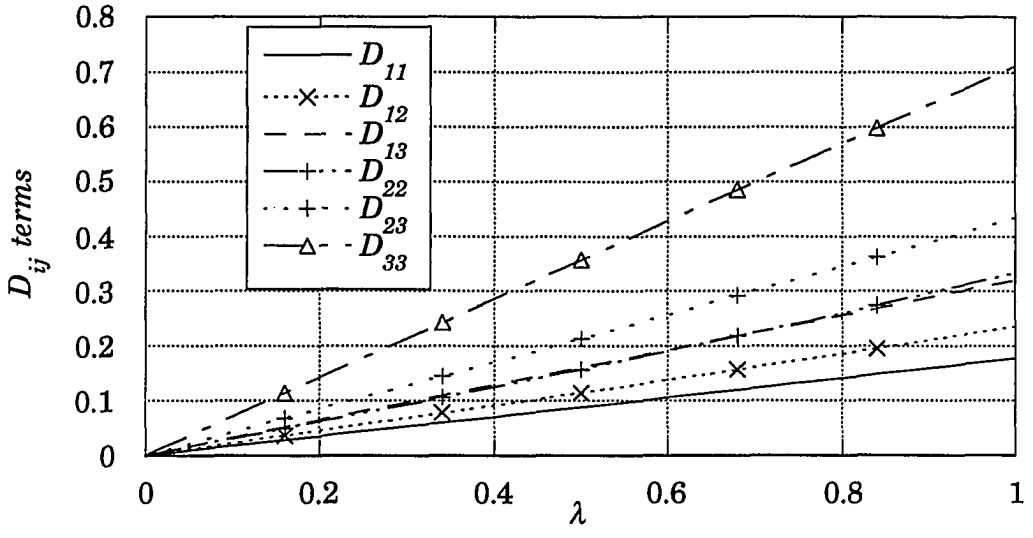

Figure 6.3 The D_{ij} terms versus the parameter λ

6.3). At this value of λ the equilibrium points of interest are shown in Figure 4.4. These equilibrium points are the twelve equilibrium points on the stability boundary and the SEP. These equilibrium points were first given in Table 4.1 and are repeated here in Table 6.2 so they can be numbered. As λ is increased to a value of *0.01* the new equilibrium points are solved for by using the equilibrium points at $\lambda = 0$ as initial guesses. This process is then continued as λ is increased. Figure 6.4 is a diagram that illustrates the movement of the thirteen equilibrium points in the state space. The numbers correspond to the equilibrium points given in Table 6.2. The SEP is taken as number *13*. Figure 6.4 can actually be described as a *bifurcation diagram* [34] projected onto the state space. The paths shown are the paths taken by the equilibrium points when λ is increased. The arrows show the direction along the path in which the equilibrium move as λ is increased. Similar diagrams have been constructed in [52] and [53], however, the COI reference frame is not employed in these two references. Reference [54] is a survey report of bifurcation and chaos in power systems.

Table 6.2 Equilibrium points on the stability boundary of the unloaded gradient system

Equilibrium points (θ_1, θ_2)			
Equilibrium number	Sources	Equilibrium number	Saddles
1	*(139.92°, -122.68°)*	*7*	*(163.58°, -16.42°)*
2	*(187.23°, 89.83°)*	*8*	*(128.69°, 128.69°)*
3	*(70.14°, 167.55°)*	*9*	*(-34.89°, 145.11°)*
4	*(-139.92°, 122.68°)*	*10*	*(-163.58°, 16.42°)*
5	*(-187.23°, -89.83°)*	*11*	*(-128.69°, -128.69°)*
6	*(-70.14°, -167.55°)*	*12*	*(34.89°, -145.11°)*

It can be observed in the bifurcation diagram of Figure 6.4 that *static bifurcation* [54, Section 2] occurs. Generally speaking, static bifurcation is defined by a change in the number of equilibrium points of the system as a parameter of the system is varied. Figure 4.3 from Section 4.3.2 is repeated in Figure 6.5 with the thirteen equilibrium points denoted. Also, shown and numbered in Figure 6.5 are four other equilibrium points which are of interest and are denoted as *14*, *15* ,*16* and *17*. In Figure 6.5 unstable equilibrium points *14* and 15 are on the stability boundary of the neighboring stable equilibrium point *16*. Note that the relative position of unstable equilibrium point *14* with respect to neighboring stable equilibrium point *16* is equivalent to the relative position of unstable equilibrium point *9* with respect to stable equilibrium point *13* and this is due to the symmetry in the system (6.13). In fact, equilibrium points *14* and *9* have been named *identical points* [39]. In the lossless case, V_{PE} has the same value when evaluated at identical points. For λ between *0* and approximately *0.60* all thirteen equilibrium points of interest are seen to persist. As λ is increased through the value of approximately *0.60* static bifurcation occurs. The three pair of

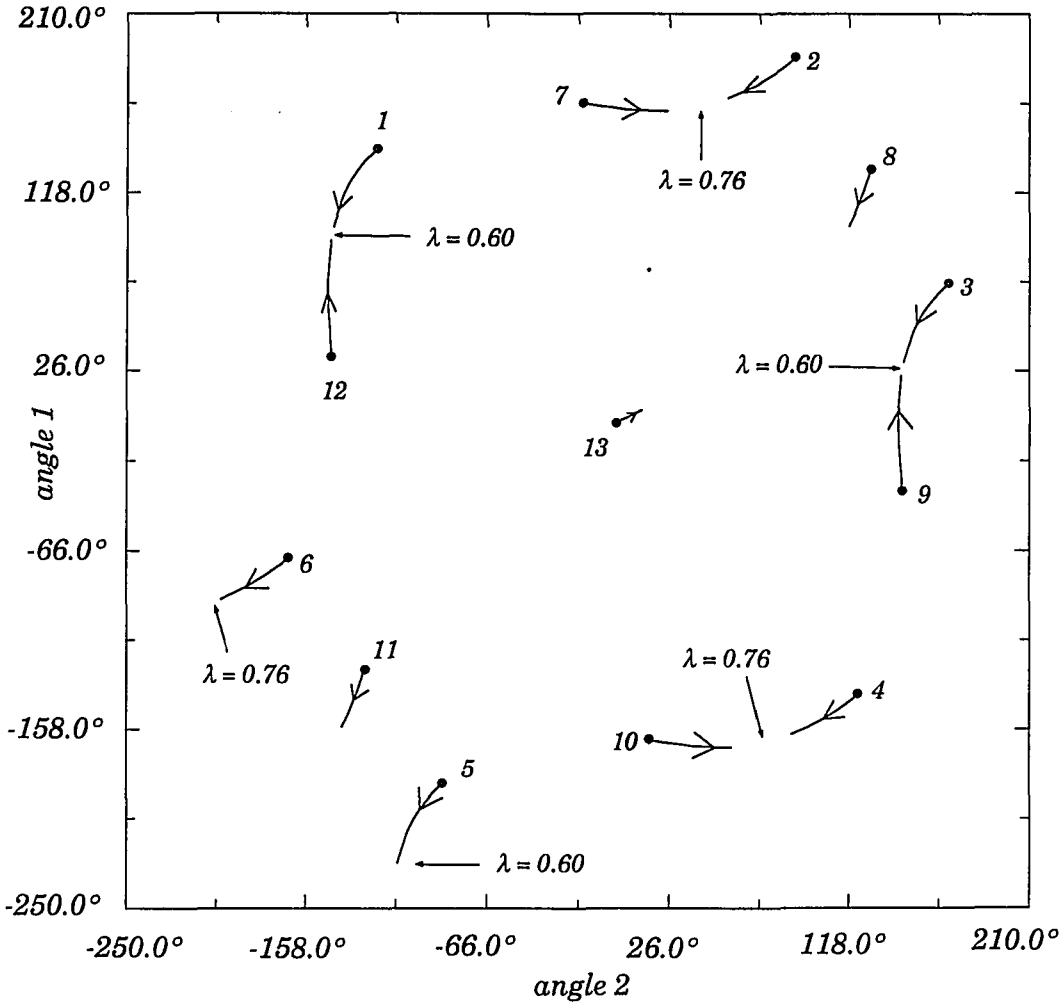

Figure 6.4 Bifurcation diagram projected onto the state space

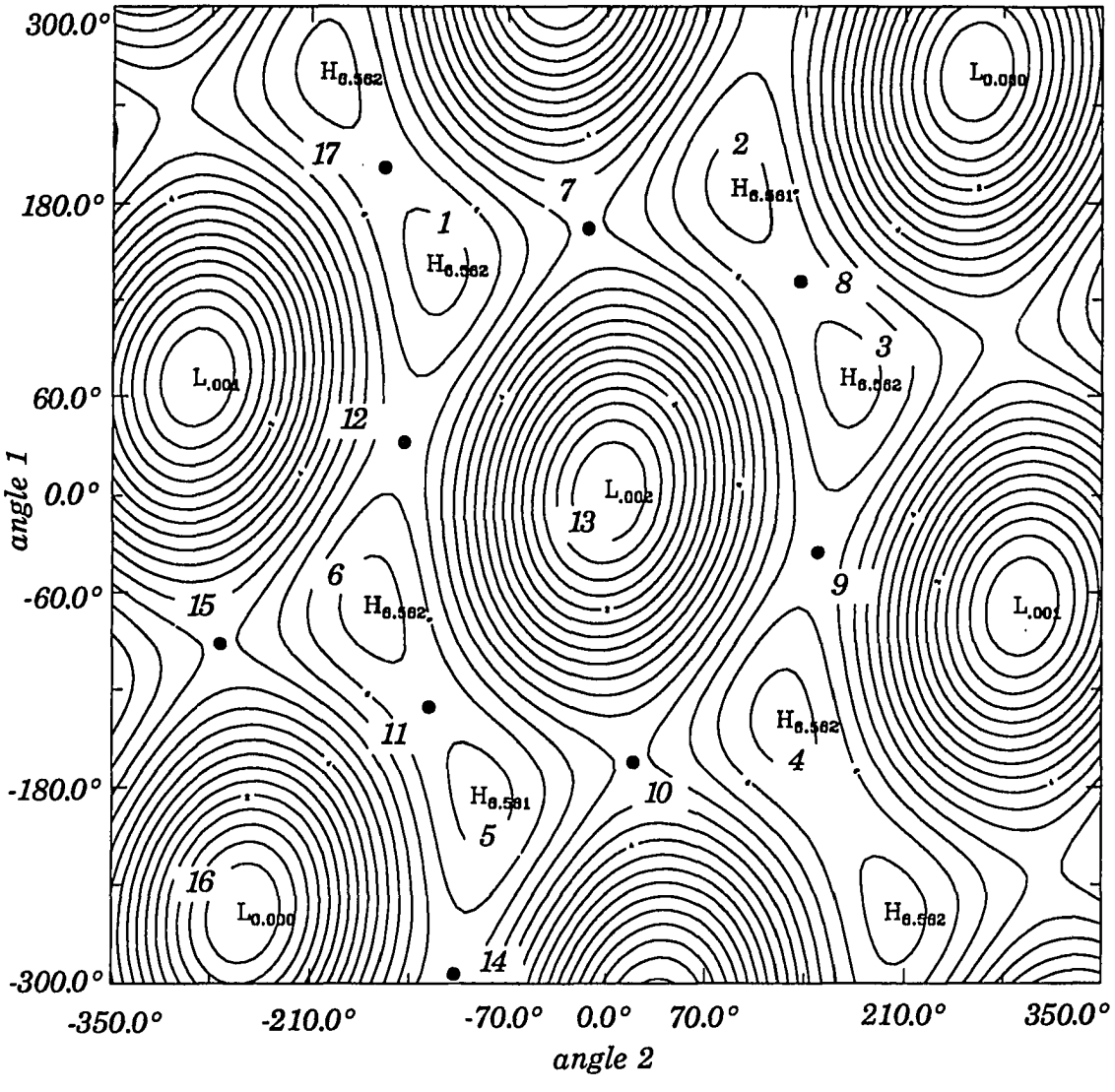

Figure 6.5 Numbering equilibrium points

unstable equilibrium points (*1* and *12*), (*3* and *9*) and (*5* and 14 as shown in Figure 6.5) coalesce and any further increase in the parameter λ these equilibrium points disappear. In each pair of these equilibrium points there is a saddle point and a source point. Note that the stability of the equilibrium points is with respect to the lossy gradient system (6.13). In Figure 6.4 the corresponding paths do not exactly touch due to the discrete set of values from which λ is taken.

At a value of $\lambda \approx 0.76$ another three pair of equilibrium points, (*7* and *2*), (*10* and *4*) and (*6* and *15* as is shown in Figure 6.5) coalesce and any further increase in the parameter λ these equilibrium points disappear. Again the pairs appear as a saddle point and a source point. As the parameter is further increased to a value of just beyond *0.76* there are only three equilibrium points out of the original thirteen of interest still present and these three persist as λ is increased to 1. These three are the SEP and two saddles, equilibrium points *13*, *8* and *11*, respectively. Note that if the SEP was non-existent after the parameter is increased beyond a certain value, all analysis of this type would have to stop because the construction of the parameters in (6.13) are evaluated around this SEP.

The static bifurcation that is shown in Figure 6.4 seems to resemble a *saddle-node bifurcation* [33] [34] and [54] . This may be so because with respect to the dynamics of the lossy gradient system (6.13) a saddle point and an unstable node coalesce and then cease to exist for any further increase in the parameter value. However, it is not clear that this can be deemed saddle-node bifurcation since certain conditions need to be satisfied in order that a strict claim be made on this type of bifurcation [34, Section 3.1.A], [33, Theorem 3.4.1, Section 3.4] and [54, Theorem 1, Section 4.2].

Since equilibrium points of the lossy gradient system (6.13) correspond to equilibrium points of the classical system (6.9) this static bifurcation occurs in the classical system as well. A saddle point (type-*1*) and a source point (type-*2*) pair coalesce with respect to lossy gradient system. It was shown in Theorem 3.3.3 from Section 3.3.3 that if θ was a type-k equilibrium point on the stability of the gradient system then $(\theta,0)$ was a type-k equilibrium point on the stability of the swing system. Suppose that this theorem is true when transfer conductances are added in the system.

Hence, with respect to the classical system this pair consists of a type-*1* equilibrium point and a type-*2* equilibrium point both which are saddles. This correlates to Theorem 1 from [58, Section 4.2]. This theorem provides conditions that need to be satisfied in order that saddle-node bifurcation can occur. As shown in this theorem, if indeed saddle-node bifurcation occurs and two equilibrium coalesce and one of the equilibrium points has a k-dimensional stable manifold (i.e., type-$(n-1)$-k) the other will have a $(k+1)$-dimensional stable manifold (i.e., type-$(n-1)$-k-1). This corresponds directly with a pair of type-*1* and a type-*2* equilibrium points from the classical system that coalesce and then disappear.

Finally, out of the thirteen equilibrium points of interest only three are still present at a parameter value of *1.0*. Equilibrium points *1, 2, 3, 4, 5, 6, 7, 9, 10* and *12* all disappear. One of the conditions that needs to met for a static bifurcation to occur is that the corresponding Jacobian must be singular. This is also equivalent to the Jacobian having a zero eigenvalue or a zero determinant.

The Jacobian J_{lgs} for the lossy gradient system (6.13) has the form of the following $(n-1) \times (n-1)$ matrix.

$$J_{lgs} = M^{\theta} D_{\theta} f$$

where $D_{\theta} f = \partial f_i / \partial \theta_j$ for $i = 1, \ldots, n-1$ and $j = 1, \ldots, n-1$. The Jacobian J_{cs} for the classical system (6.9) has a form similar to the Jacobian of the swing system as given in Section 3.1.3. The $2(n-1) \times 2(n-1)$ matrix for J_{cs} has the following form

$$J_{cs} = \begin{bmatrix} 0 & I \\ M^{-1} D_{\theta} f & -c\, I \end{bmatrix}$$

The scalar value $c > 0$ is the uniform damping coefficient which is the ratio of D_i / M_i for all i of the system and will be taken as $c = 0.1$. Note that in the COI formulation

$$\theta_n = -\frac{1}{M_n}\left(M_1\theta_1 + M_2\theta_2 + \cdots + M_{n-1}\theta_{n-1}\right)$$

With θ_n explicitly shown the $(n-1) \times (n-1)$ matrix $D_\theta f$ can be defined as

$$\frac{\partial f_i}{\partial \theta_i} = \sum_{\substack{j=1 \\ j \neq i}}^{n} \left[-C_{ij}(\lambda)\cos\left(\theta_i - \theta_j\right)\right] - C_{in}(\lambda)\frac{M_i}{M_n}\cos\left(\theta_i - \theta_n\right)$$

$$+\left(1 - \frac{2M_i}{M_T}\right)\left[\sum_{\substack{j=1 \\ j \neq i}}^{n} D_{ij}(\lambda)\sin\left(\theta_i - \theta_j\right) + \frac{M_i}{M_n}D_{in}(\lambda)\sin\left(\theta_i - \theta_n\right)\right]$$

and for $i \neq q$

$$\frac{\partial f_i}{\partial \theta_q} = -\frac{2M_i}{M_T}\left[\sum_{\substack{j=1 \\ j \neq q}}^{n} D_{qj}(\lambda)\sin\left(\theta_q - \theta_j\right) + \frac{M_q}{M_n}D_{qn}(\lambda)\sin\left(\theta_q - \theta_n\right)\right]$$

$$+\frac{M_q}{M_n}\left[D_{in}(\lambda)\sin\left(\theta_i - \theta_n\right) - C_{in}(\lambda)\cos\left(\theta_i - \theta_n\right)\right]$$

$$+ C_{iq}(\lambda)\cos\left(\theta_i - \theta_q\right) - D_{iq}(\lambda)\sin\left(\theta_i - \theta_q\right)$$

Tables 6.3, 6.4, 6.5 and 6.6 present the determinant and the two eigenvalues of J_{lgs} and the four eigenvalues of J_{cs} for the different equilibrium points as λ is varied .

One interesting observation can be made and is taken advantage of in presenting the eigenvalue data. Due to the symmetry in the system (6.13) [39] the following sets of equilibrium points have the same eigenvalues when both J_{cs} and J_{lgs} are evaluated at these equilibrium points.

set-1	*(1, 3, 5)*	*set-2*	*(9, 12, 14)*
set-3	*(2, 4, 6)*	*set-4*	*(7, 10, 15)*

Table 6.3 Eigenvalue data for equilibrium points *1*, *3* and *5*

λ	*det*	e_{l1}	e_{l2}	e_{c1}	e_{c2}	e_{c3}	e_{c4}
0.00	2.64	1.11	2.38	8.07	-8.17	7.21	-7.31
0.02	2.62	1.09	2.40	7.98	-8.08	7.25	-7.35
0.04	2.59	1.07	2.42	7.90	-8.00	7.29	-7.39
0.06	2.57	1.05	2.45	7.81	-7.91	7.34	-7.44
0.08	2.54	1.03	2.47	7.72	-7.82	-7.48	7.38
0.10	2.51	1.01	2.49	7.62	-7.72	7.44	-7.54
0.12	2.48	0.98	2.52	-7.60	-7.60	7.50	7.50
0.14	2.45	0.96	2.54	-7.58	-7.58	7.48	7.48
0.16	2.41	0.94	2.56	-7.55	-7.55	7.45	7.45
0.18	2.38	0.92	2.58	7.31	-7.41	7.55	-7.65
0.20	2.34	0.90	2.61	7.20	-7.30	7.60	-7.70
0.22	2.30	0.88	2.63	7.10	-7.20	7.64	-7.74
0.24	2.26	0.85	2.65	6.99	-7.09	7.69	-7.79
0.26	2.22	0.83	2.67	6.88	-6.98	7.73	-7.83
0.28	2.17	0.81	2.69	6.77	-6.87	7.78	-7.88
0.30	2.12	0.78	2.72	6.66	-6.76	7.82	-7.92
0.32	2.07	0.76	2.74	6.54	-6.64	7.87	-7.97
0.34	2.02	0.73	2.77	6.42	-6.52	7.92	-8.02
0.36	1.96	0.70	2.79	6.28	-6.38	7.97	-8.07
0.38	1.90	0.68	2.81	6.15	-6.25	8.02	-8.12
0.40	1.84	0.65	2.84	6.00	-6.10	8.08	-8.18
0.42	1.77	0.62	2.87	5.84	-5.94	8.13	-8.23
0.44	1.69	0.58	2.90	5.67	-5.77	8.19	-8.29
0.46	1.61	0.55	2.93	5.48	-5.58	8.26	-8.36
0.48	1.51	0.51	2.96	5.28	-5.38	8.33	-8.43
0.50	1.41	0.47	2.99	5.04	-5.14	8.40	-8.50
0.52	1.29	0.43	3.03	4.78	-4.88	8.49	-8.59
0.54	1.15	0.37	3.08	4.45	-4.55	8.58	-8.68
0.56	0.98	0.31	3.13	4.04	-4.14	8.70	-8.80
0.58	0.74	0.23	3.20	3.45	-3.55	8.84	-8.94
0.60	0.29	0.09	3.32	2.09	-2.19	9.10	-9.20

det - determinant of the Jacobian of the lossy gradient system

e_{li} - i^{th} eigenvalue of the lossy gradient system

e_{ci} - i^{th} eigenvalue of the classical system

Table 6.4 Eigenvalue data for equilibrium points *9*, *12* and *14*

λ	det	e_{l1}	e_{l2}	e_{c1}	e_{c2}	e_{c34}
0.00	-4.04	-0.95	4.24	10.82	-10.92	-0.05 ± j6.70
0.02	-4.03	-0.95	4.23	10.82	-10.92	-0.05 ± j6.70
0.04	-4.02	-0.95	4.23	10.81	-10.91	-0.05 ± j6.69
0.06	-3.99	-0.94	4.23	10.81	-10.91	-0.05 ± j6.67
0.08	-3.97	-0.94	4.22	10.80	-10.90	-0.05 ± j6.66
0.10	-3.94	-0.93	4.22	10.79	-10.89	-0.05 ± j6.63
0.12	-3.90	-0.93	4.21	10.78	-10.88	-0.05 ± j6.61
0.14	-3.86	-0.92	4.20	10.77	-10.87	-0.05 ± j6.58
0.16	-3.81	-0.91	4.19	10.75	-10.85	-0.05 ± j6.55
0.18	-3.75	-0.90	4.18	10.73	-10.83	-0.05 ± j6.51
0.20	-3.69	-0.89	4.17	10.71	-10.81	-0.05 ± j6.47
0.22	-3.63	-0.87	4.16	10.69	-10.79	-0.05 ± j6.43
0.24	-3.55	-0.86	4.15	10.67	-10.77	-0.05 ± j6.37
0.26	-3.48	-0.84	4.13	10.65	-10.75	-0.05 ± j6.32
0.28	-3.39	-0.82	4.12	10.62	-10.72	-0.05 ± j6.26
0.30	-3.30	-0.80	4.10	10.59	-10.69	-0.05 ± j6.19
0.32	-3.20	-0.78	4.08	10.56	-10.66	-0.05 ± j6.11
0.34	-3.09	-0.76	4.06	10.52	-10.62	-0.05 ± j6.03
0.36	-2.98	-0.74	4.04	10.49	-10.59	-0.05 ± j5.94
0.38	-2.86	-0.71	4.02	10.45	-10.55	-0.05 ± j5.84
0.40	-2.73	-0.68	3.99	10.40	-10.50	-0.05 ± j5.73
0.42	-2.59	-0.65	3.97	10.35	-10.45	-0.05 ± j5.61
0.44	-2.44	-0.62	3.94	10.30	-10.40	-0.05 ± j5.47
0.46	-2.28	-0.58	3.90	10.24	-10.34	-0.05 ± j5.32
0.48	-2.10	-0.54	3.87	10.18	-10.28	-0.05 ± j5.14
0.50	-1.91	-0.50	3.83	10.11	-10.21	-0.05 ± j4.94
0.52	-1.70	-0.45	3.79	10.02	-10.12	-0.05 ± j4.70
0.54	-1.47	-0.39	3.74	9.93	-10.03	-0.05 ± j4.40
0.56	-1.20	-0.32	3.68	9.82	-9.92	-0.05 ± 4.02
0.58	-0.86	-0.24	3.60	9.67	-9.77	-0.05 ± j3.45
0.60	-0.30	-0.09	3.47	9.41	-9.51	-0.05 ± j2.09

det - determinant of the Jacobian of the lossy gradient system
e_{li} - i^{th} eigenvalue of the lossy gradient system
e_{ci} - i^{th} eigenvalue of the classical system

Table 6.5 Eigenvalue data for equilibrium points *2*, *4* and *6*

λ	det	e_{l1}	e_{l2}	e_{c1}	e_{c2}	e_{c3}	e_{c4}
0.00	2.64	1.11	2.38	8.07	-8.17	7.21	-7.31
0.02	2.65	1.13	2.35	8.14	-8.24	-7.26	7.16
0.04	2.67	1.15	2.33	8.21	-8.31	7.12	-7.22
0.06	2.68	1.17	2.30	8.28	-8.38	7.07	-7.17
0.08	2.69	1.18	2.27	8.35	-8.45	7.03	-7.13
0.10	2.70	1.20	2.25	8.42	-8.52	6.98	-7.08
0.12	2.71	1.22	2.22	8.49	-8.59	6.93	-7.03
0.14	2.71	1.24	2.19	8.56	-8.66	6.89	-6.99
0.16	2.72	1.26	2.16	8.63	-8.73	6.84	-6.94
0.18	2.72	1.28	2.13	8.70	-8.80	6.79	-6.89
0.20	2.72	1.29	2.10	8.77	-8.87	6.73	-6.83
0.22	2.72	1.31	2.07	8.84	-8.94	6.68	-6.78
0.24	2.72	1.33	2.04	8.91	-9.01	6.62	-6.72
0.26	2.71	1.35	2.01	8.98	-9.08	6.57	-6.67
0.28	2.71	1.37	1.98	9.05	-9.15	6.51	-6.61
0.30	2.70	1.38	1.95	9.12	-9.22	6.45	-6.55
0.32	2.69	1.40	1.92	9.19	-9.29	-6.48	6.38
0.34	2.67	1.42	1.89	9.26	-9.36	6.32	-6.42
0.36	2.65	1.43	1.86	9.33	-9.43	6.25	-6.35
0.38	2.63	1.44	1.83	9.40	-9.50	6.18	-6.28
0.40	2.61	1.80	1.45	9.47	-9.57	6.10	-6.20
0.42	2.59	1.78	1.45	9.54	-9.64	6.03	-6.13
0.44	2.56	1.76	1.45	9.62	-9.72	5.94	-6.04
0.46	2.52	1.75	1.44	9.69	-9.79	5.86	-5.96
0.48	2.48	1.75	1.42	9.77	-9.87	5.77	-5.87
0.50	2.44	1.76	1.39	9.85	-9.95	5.67	-5.77
0.52	2.39	1.77	1.36	9.93	-10.03	5.57	-5.67
0.54	2.34	1.78	1.31	10.01	-10.11	5.47	-5.57
0.56	2.28	1.80	1.27	10.09	-10.19	5.35	-5.45
0.58	2.22	1.83	1.21	10.18	-10.28	5.23	-5.33
0.60	2.14	1.85	1.16	10.27	-10.37	5.09	-5.19
0.62	2.06	1.88	1.09	10.36	-10.46	4.94	-5.04
0.64	1.96	1.91	1.02	10.46	-10.56	4.78	-4.88
0.66	1.85	1.95	0.95	10.56	-10.66	4.60	-4.70
0.68	1.72	1.99	0.87	10.67	-10.77	4.39	-4.49
0.70	1.57	2.03	0.77	10.79	-10.89	4.14	-4.24
0.72	1.39	2.08	0.67	10.93	-11.03	3.84	-3.94
0.74	1.15	2.14	0.54	11.08	-11.18	3.44	-3.54
0.76	0.80	2.21	0.36	11.29	-11.39	2.82	-2.92

det - determinant of the Jacobian of the lossy gradient system

e_{li} - i^{th} eigenvalue of the lossy gradient system

e_{ci} - i^{th} eigenvalue of the classical system

Table 6.6 Eigenvalue data for equilibrium points *7*, *10* and *15*

λ	det	e_{l1}	e_{l2}	e_{c1}	e_{c2}	e_{c34}
0.00	-5.55	3.16	-1.76	13.44	-13.54	-0.05 ± j6.33
0.02	-5.54	3.16	-1.76	13.44	-13.54	-0.05 ± j6.33
0.04	-5.53	3.15	-1.75	13.43	-13.53	-0.05 ± j6.32
0.06	-5.51	3.15	-1.75	13.42	-13.52	-0.05 ± j6.32
0.08	-5.49	3.14	-1.75	13.41	-13.51	-0.05 ± j6.31
0.10	-5.47	3.14	-1.74	13.41	-13.51	-0.05 ± j6.30
0.12	-5.44	3.14	-1.73	13.40	-13.50	-0.05 ± j6.29
0.14	-5.40	3.13	-1.73	13.38	-13.48	-0.05 ± j6.27
0.16	-5.36	3.12	-1.72	13.37	-13.47	-0.05 ± j6.25
0.18	-5.32	3.12	-1.71	13.36	-13.46	-0.05 ± j6.24
0.20	-5.27	3.11	-1.69	13.35	-13.45	-0.05 ± j6.21
0.22	-5.22	3.10	-1.68	13.33	-13.43	-0.05 ± j6.19
0.24	-5.16	3.10	-1.67	13.31	-13.41	-0.05 ± j6.16
0.26	-5.10	3.09	-1.65	13.30	-13.40	-0.05 ± j6.13
0.28	-5.03	3.08	-1.63	13.28	-13.38	-0.05 ± j6.10
0.30	-4.96	3.07	-1.61	13.26	-13.36	-0.05 ± j6.07
0.32	-4.88	3.06	-1.59	13.24	-13.34	-0.05 ± j6.03
0.34	-4.80	3.05	-1.57	13.22	-13.32	-0.05 ± j5.99
0.36	-4.71	3.04	-1.55	13.19	-13.29	-0.05 ± j5.94
0.38	-4.62	3.03	-1.52	13.17	-13.27	-0.05 ± j5.89
0.40	-4.52	3.02	-1.50	13.14	-13.24	-0.05 ± j5.84
0.42	-4.42	3.00	-1.47	13.12	-13.22	-0.05 ± j5.79
0.44	-4.31	2.99	-1.44	13.09	-13.19	-0.05 ± j5.73
0.46	-4.19	2.98	-1.41	13.06	-13.16	-0.05 ± j5.66
0.48	-4.06	2.96	-1.37	13.02	-13.12	-0.05 ± j5.59
0.50	-3.93	2.95	-1.34	12.99	-13.09	-0.05 ± j5.51
0.52	-3.79	2.93	-1.30	12.95	-13.05	-0.05 ± j5.43
0.54	-3.65	2.91	-1.25	12.91	-13.01	-0.05 ± j5.34
0.56	-3.49	2.89	-1.21	12.87	-12.97	-0.05 ± j5.24
0.58	-3.33	2.87	-1.16	12.82	-12.92	-0.05 ± j5.14
0.60	-3.15	2.85	-1.11	12.77	-12.87	-0.05 ± j5.02
0.62	-2.96	2.82	-1.05	12.72	-12.82	-0.05 ± j4.89
0.64	-2.76	2.80	-0.99	12.66	-12.76	-0.05 ± j4.74
0.66	-2.54	2.77	-0.92	12.60	-12.70	-0.05 ± j4.57
0.68	-2.31	2.74	-0.84	12.53	-12.63	-0.05 ± j4.38
0.70	-2.04	2.70	-0.76	12.44	-12.54	-0.05 ± j4.15
0.72	-1.74	2.66	-0.66	12.35	-12.45	-0.05 ± j3.86
0.74	-1.39	2.60	-0.53	12.23	-12.33	-0.05 ± j3.48
0.76	-0.92	2.53	-0.36	12.06	-12.16	-0.05 ± j2.88

det - determinant of the Jacobian of the lossy gradient system
e_{li} - i^{th} eigenvalue of the lossy gradient system
e_{ci} - i^{th} eigenvalue of the classical system

At a parameter value of $\lambda \approx 0.60$ equilibrium points from *set-1* coalesce with equilibrium points from *set-2* and at a parameter value of $\lambda \approx 0.76$ equilibrium points from *set-3* coalesce with equilibrium points from *set-4*. This symmetry can be observed in Figure 6.4 for these four sets. The eigenvalues for the sets *set-1*, *set-2*, *set-3* and *set-4* are given in Tables 6.3, 6.4, 6.5 and 6.6, respectively.

It can be observed in these tables that the determinant does indeed get relatively close to zero and actually becomes zero but this cannot be observed because of the discrete set of values from which λ is taken. It can also be observed that for type-*1* equilibrium points of the classical system there are complex eigenvalues for which the real part is the negative one-half of the uniform damping constant.

6.2.3 Vector Field Plots of the Lossy Gradient System

As noted earlier, when the parameter λ has a value of *1* there are only three equilibrium points of interest still remaining. These are the SEP (no. *13*) and two saddle points (no. *8* and no. *11*). Equilibrium points *8* and *11* are still type-*1* with respect to the classical system. Vector plots of the lossy gradient system (6.13) will not be given for values of λ between *0* and *1*. The stability boundary of the lossy gradient system at a value of $\lambda = 0$ has already been shown in Figure 4.4 from Section 4.3.2. Figures 6.6, 6.7, 6.8 and 6.9 are vector field plots of the lossy gradient system for a value of $\lambda = 1$ with the corresponding stable manifolds. Instead of one figure for the vector field plot, four are given so that the resolution is better. An observation of the axis in each figure will show where each plot fits into the full vector field plot.

Figure 6.6 represents quadrant 1 of the state-space. It follows that Figures 6.7, 6.8 and 6.9 represent quadrants 2, 3 and 4 respectively. It was shown in Figure 6.4 that out of the equilibrium points of interest only three remain when $\lambda = 1$. These are equilibrium points *8*, *11* and *13* and denote these equilibrium points as θ^8, θ^{11} and θ^{13}, respectively. The SEP is equilibrium point $\theta^{13} = \theta^s$ and is shown in Figure 6.6 and has coordinates $(6.74°, 13.70°)$. Note that the coordinates are given in (θ_1, θ_2) format.

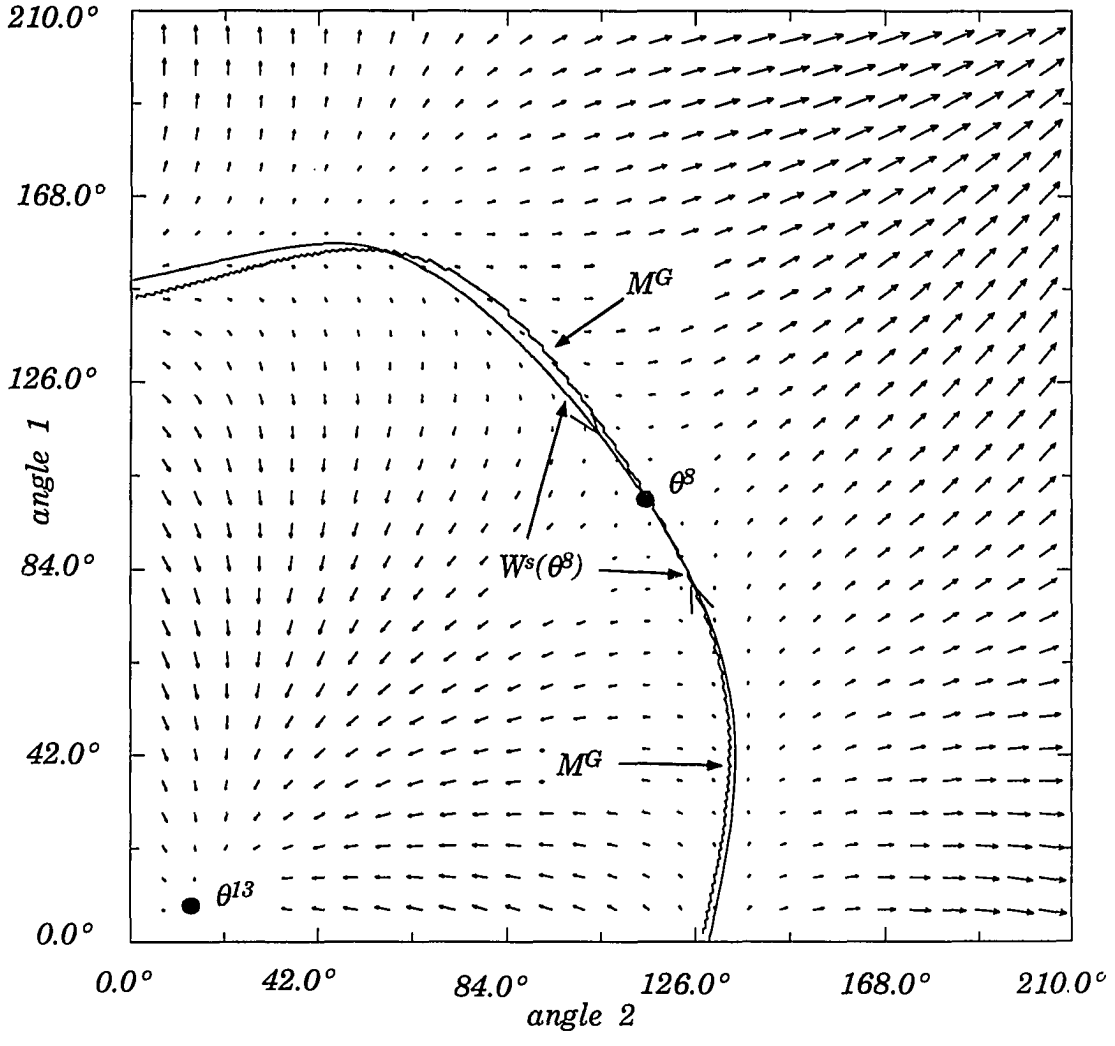

Figure 6.6 Vector field plot for quadrant 1

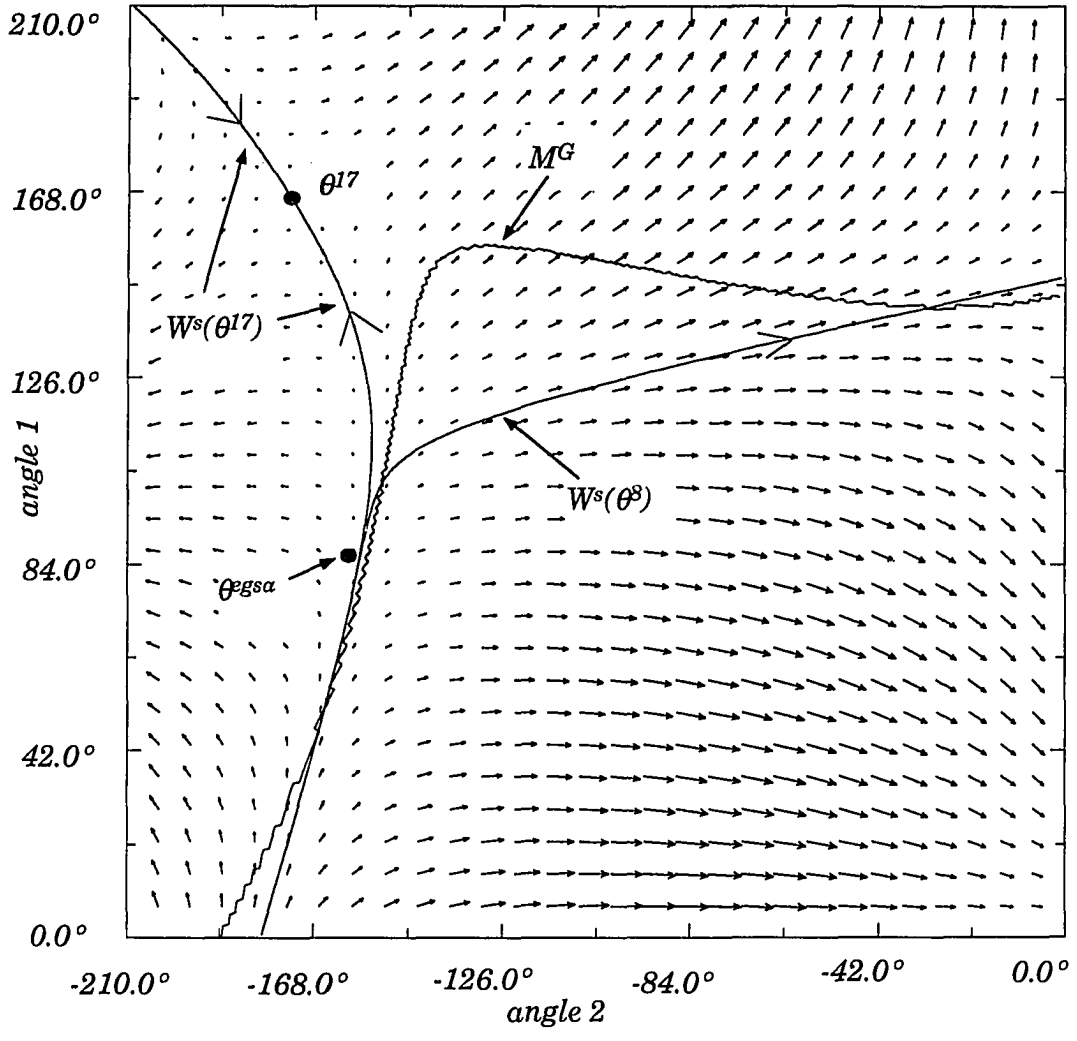

Figure 6.7 Vector field plot for quadrant 2

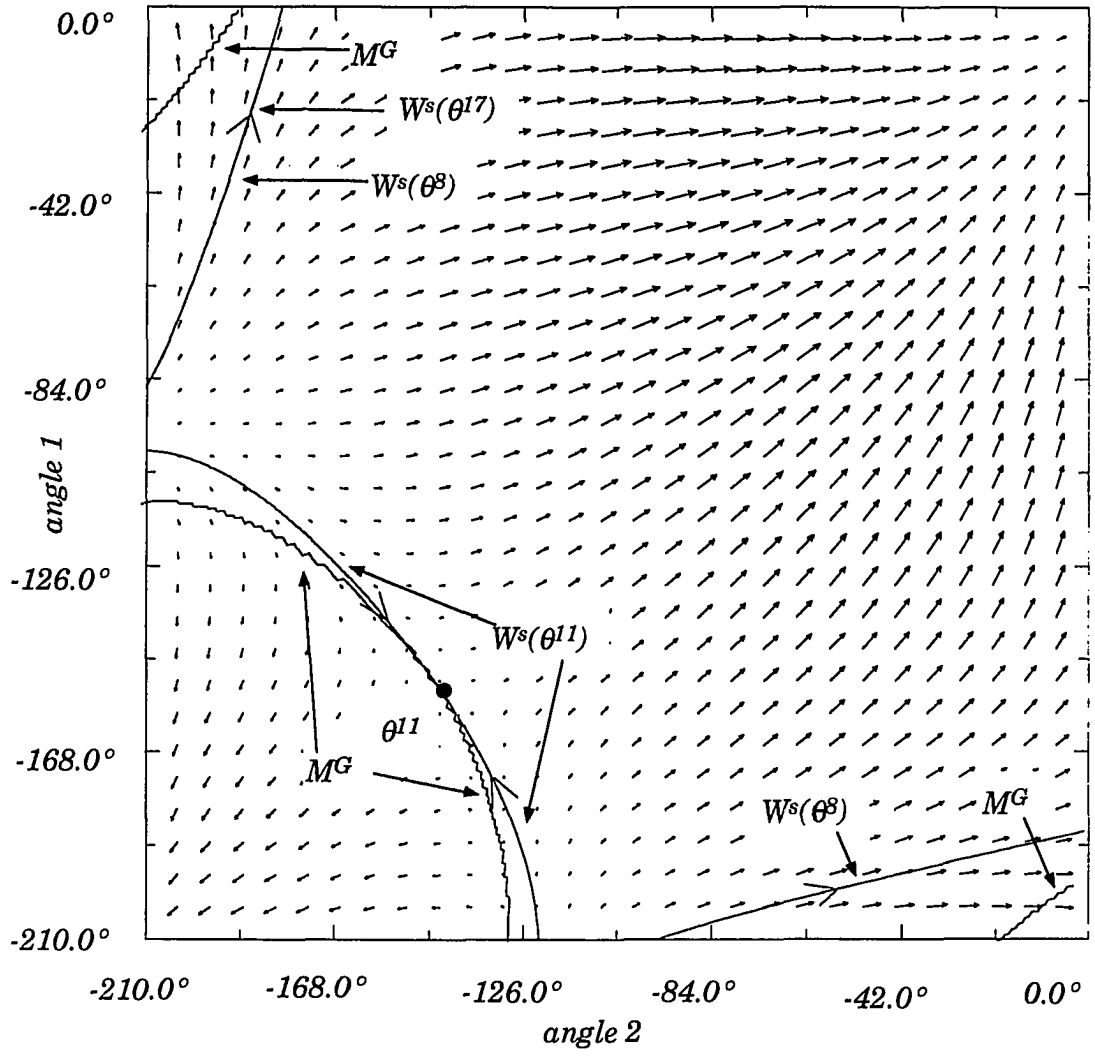

Figure 6.8 Vector field plot for quadrant 3

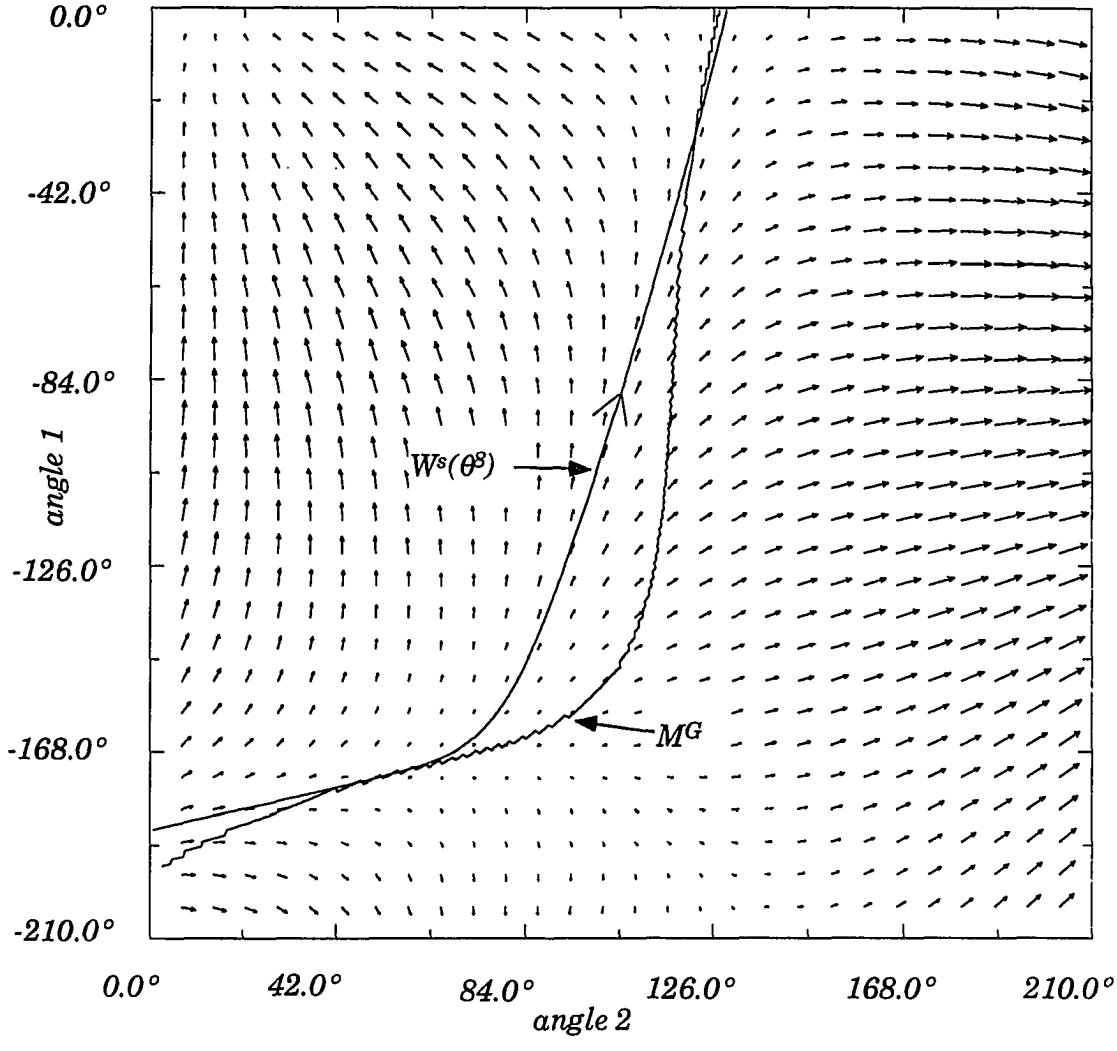

Figure 6.9 Vector field plot for quadrant 4

Equilibrium point θ^8, which is located at *(97.94°, 116.29°)* is also shown in Figure 6.6. In Figure 6.7 equilibrium point θ^{17} is shown and is located at coordinates *(167.73°, -173.93°)*. This equilibrium point was originally shown in Figure 6.5. In Figure 6.8 equilibrium point θ^{11} is shown with coordinates *(159.43°, -141.10°)* and in Figure 6.9 there are no equilibrium points. It can be seen that the equilibrium points θ^8, θ^{11} and θ^{17} are all identical points. In fact at a value of $\lambda = 1$ there are only two kinds of equilibrium points left in the system. Stable equilibrium points such as equilibrium point θ^{13} and all of these equilibrium points are identical. The other kind is unstable equilibrium points such as equilibrium points θ^8, θ^{11} and θ^{17} which are type-*1* and are all identical.

The purpose of presenting these vector field plots is to show the stability boundary of the SEP $\theta^s = \theta^{13}$ and also to show the flow in this area around θ^s. The stable manifolds for the three type-*1* equilibrium points θ^8, θ^{11} and θ^{17} are seen in the figures. A closer look will reveal that the stable manifolds of θ^8 and θ^{11} are actually part of the stability boundary for θ^s and that the stability region is unbounded. It seems that the stable manifolds for θ^8 and θ^{17} come together in Figures 6.7 and 6.8, however, they are actually distinct trajectories and the reason follows from uniqueness of solutions of the gradient system. An even closer look will reveal that the dynamics of the system around each of the equilibrium points θ^8, θ^{11} and θ^{17} are the same. In fact, this observation is part of the definition of identical point. Note that the stable manifolds of the equilibrium points θ^8, θ^{11} and θ^{17} all lie in the same position with respect to their corresponding equilibrium points (i.e., the stable manifolds slope from the lower right to the upper left).

In the three step cycle of the shadowing method as shown in Section 5.1 of Chapter 5 the third step of the cycle consists of finding a maximum of V_{PE} along a ray. This was found by equating $M^\theta g(\theta) \cdot (\theta - \theta^s) = 0$. However, the lossy gradient system cannot be formed by taking the negative gradient of a scalar function as shown in Subsection 6.1.1. Hence, the third step would consist of evaluating $M^\theta f(\theta) \cdot (\theta - \theta^s) = 0$. In other words, when the vector $M^\theta f(\theta)$ is orthogonal to the vector $(\theta - \theta^s)$. As noted in Section 5.3 the manifold M^G is denoted by the set of points for which $M^\theta g(\theta) \cdot (\theta - \theta^s) = 0$ and for which $\theta \in S_{high}(\theta^u)$. The set $S_{high}(\theta^u)$ is not well defined in the lossy case since

there does not exist a well defined V_{PE} function. However, the manifold M^{GW} may be redefined in the following way. The manifold M^{GW} is the set of all points θ such that $M^{\theta}f(\theta) \cdot (\theta - \theta^s) = 0$, $S_{ray}(\theta) \cap W^s(\theta^u) \neq \varnothing$ and the point θ is relatively close to $W^s(\theta^u)$. This definition is not as precise as the one for the lossless case since the phrase relatively close is ambiguous. The manifold M^G for the two corresponding equilibrium points θ^8 and θ^{11} is shown in Figures 6.6, 6.7, 6.8 and 6.9. In fact, for all points on M^G as shown in these figures the corresponding ray intersects a stable manifold so that the manifold M^G is actually M^{GW}.

It is observed in these four figures that the manifold M^G is relatively close to $W^s(\theta^u)$ for $\theta^8 = \theta^u$ and $\theta^{11} = \theta^u$. The reason is the following. It is seen that the vector $M^{\theta}f(\theta) = w(\theta)$ from the vector field plots seem to continually point away from the stable manifold. For example, take any point θ in the plane constructed by the four figures with $\theta \neq \theta^s$. Form the ray $S_{ray}(\theta)$; it can be seen that by observing vectors in the vicinity of the stable manifold it is reasonable to say that there is a point $\theta^m \in S_{ray}(\theta)$ such that $M^{\theta}f(\theta^m) \cdot (\theta^m - \theta^s) = 0$ and this point θ^m is relatively close to one of the stable manifolds shown in these figures.

In Section 4.8 two problems corresponding to the exit point method were presented. Problem 2 was that the resultant equilibrium point was not the controlling UEP θ^u but instead a low point (i.e., a stable equilibrium point) or another unstable equilibrium point on the stability boundary. Suppose that the exit point method was applied to the lossy system depicted by Figures 6.6, 6.7, 6.8 and 6.9 and that the approximate exit point was detected at the point θ^{egsa} as shown in Figure 6.7. Taking this point as an initial point the flow of the system will pass relatively close to θ^{17}. If there is a minimum gradient point detected in the vicinity of θ^{17} the it seems reasonable to conclude that the resultant equilibrium point would in fact be θ^{17}. In this situation it is θ^8 that is the controlling UEP. Theoretically the exit point method failed in this situation and this failure correlates to problem 2 from Section 4.8, but in this situation the resultant equilibrium point is not even on the stability boundary. If the shadowing method is applied to this same situation it can be observed that the resultant equilibrium would be θ^8.

Therefore, with transfer conductances included, at least for this example, the stable manifolds $W^s(\theta^8)$ and $W^s(\theta^{11})$ are part of the stability boundary and it seems that the shadowing technique would work satisfactorily when applied.

7. APPLICATION OF THE SHADOWING METHOD TO REALISTIC POWER SYSTEMS FOR TRANSIENT STABILITY ASSESSMENT

As described in Section 1 of Chapter 5 the shadowing method is a technique from which a finite sequence of points is produced upon the application to a power system model. The last point in the sequence should be relatively close to the controlling UEP θ^u. This method was applied to the unloaded 3-machine system, which is an unrealistic system, and the results where given in Section 5.2 of Chapter 5. In order for this method to be part of a practical tool for transient stability assessment it must be able to be applied to large-scale realistic power system models.

In this Chapter results will be given from the application of the shadowing method to two large-scale power systems. These power systems are the IEEE 50-generator, 145 bus Ontario Hydro system [56] and the 161-generator, 903 bus Northern States Power system [57]. The machine data and real power generation for each system is given in Appendix C.

7.1 Outline of Numerical Algorithm

The steps taken for transient stability assessment using the TEF method with the shadowing method incorporated are the following.

Step 1

Apply step (i) from Algorithm-EP which consists of detecting the exit point of the gradient system. Algorithm-EP was given in Section 4.6 of Chapter 4. However, since this shadowing technique is being applied to realistic power systems with transfer conductances the lossy gradient system (6.13) will need to be substituted for the gradient system. The point θ^{m0} is detected along the projection of the disturbed trajectory and is detected when

$$-\left[M^{\theta} f(\theta^{m0})\right] \cdot (\theta^{m0} - \theta^{s}) = 0 \tag{7.1}$$

The point θ^{m0} that is detected should be relatively close to the approximate exit point. It must be made clear that the vector function f from equation (2.8) represents the dynamics of the post-disturbance system. The disturbed system will have the form

$$\begin{aligned} \dot{\varpi} &= M^{-1} f^{d} \\ \dot{\theta} &= \varpi \end{aligned} \tag{7.2}$$

with the pre-disturbance point $(\theta^{s1}, 0)$ as the initial condition. In the disturbed system equations (7.2) damping is neglected [30]. The vector function f^d has the same equation form as f. In most cases such as a three phase fault the vector function f^d is simply f with the terms C_{ij} and D_{ij} modified.

Step 2

Next, apply the shadowing technique as described in Section 5.2 of Chapter 5. The vector function $z = M^{\theta} g$ will be replaced by $M^{\theta} f$. The values of η and β need to be picked heuristically as discussed in Section 5.2. A sequence of points $\{\theta^{mi}\}_{i=0}^{N}$ with θ^{m0} initially given will be produced. Use the point θ^{mN} as an initial guess and solve the nonlinear algebraic vector function f to zero to determine the controlling UEP θ^{u}. Note that the first step in each cycle of the shadowing method is to solve the differential equations of the lossy gradient system. It was first observed in [57] that when the power system is large these differential equations seem to be stiff [58]. To overcome this obstacle a variable step-size ordinary differential equations solver called LSODE [59], [60] is employed.

Step 3

Once the controlling UEP is known apply the concept of the energy margin as given in Section 2.3 of Chapter 2. This application will consist of

evaluating the equation (2.16) for ΔV which is the energy margin. However, there is normally the consideration of the *corrected kinetic energy* which is explained in [27].

It is thought that when a disturbance occurs the generators are split into two groups which are the critical group of machines and the rest of the machines in the system. Let S^{cr} be the set of generator numbers for which the generator is in the critical group. Let S^{rs} be the set of generator numbers that are in the rest of the system.

The term

$$\frac{1}{2}\sum_{i=1}^{n} M_i \left(\varpi_i^{cl}\right)^2$$

which appears in equation (2.16) and is the kinetic energy term will be substituted for with the corrected kinetic energy term shown below

$$\frac{1}{2} M_{eq} \left(\varpi_{eq}^{cl}\right)^2$$

Where

$$M_{cr} = \sum_{i \in S^{cr}} M_i \quad \text{and} \quad M_{rs} = \sum_{i \in S^{rs}} M_i$$

$$M_{eq} = \frac{M_{cr}\, M_{rs}}{M_{cr} + M_{rs}}$$

$$\varpi_{cr} = \frac{\sum_{i \in S^{cr}} M_i\, \varpi_i}{M_{cr}} \quad \text{and} \quad \varpi_{rs} = \frac{\sum_{i \in S^{rs}} M_i\, \varpi_i}{M_{rs}}$$

$$\varpi_{eq} = \varpi_{cr} - \varpi_{rs}$$

7.2 Numerical Results

In total, there will be nine cases analyzed and the results from the analysis will be presented in this section. For each case a disturbance will be modeled in the system in the form of a three-phase fault on a major transmission line near a bus. The post-disturbance system will be identical to the pre-disturbance system except that the transmission line will be cleared. Using these two models the steps given in Section 7.1 will be applied. For each case the resulting relevant numerical results that will be presented are as follows.

Since this dissertation work focused on the shadowing method the most important result is the finite sequence $\{\theta^{mi}\}_{i=0}^{N}$ which is produced. It was pointed out that if N is taken large enough then the point θ^{mN} should be relatively close to θ^{u}. If the point $\theta^{m(N+1)}$ is taken as θ^{u} , and $\{\theta^{mi}\}_{i=0}^{N+1}$ is plotted versus i there should not be seen any distinguishable discontinuity and it should seem as if $\{\theta^{mi}\}_{i=0}^{N}$ converges to θ^{u}. This convergence was discussed in detail in Section 5.3 of Chapter 5. Since the power system has a large number of machines the vector θ^{mi} will be large and it will be cumbersome to present it for $0 \le i \le N+1$. Therefore, only certain states or machines in θ^{mi} will be presented. Denote θ_j^{mi} as the j^{th} state or machine in the vector θ^{mi} where i, again, is the i^{th} cycle of the shadowing method. As noted above the data for the sequence could be plotted as θ_j^{mi} versus i. However, the convergence of $\{\theta^{mi}\}_{i=0}^{N} \rightarrow \theta^{u}$ can be seen more easily if the plot is of θ_j^{mi} versus θ_k^{mi} for $0 \le i \le N+1$, where θ_k^{mi}, $k \ne j$, is some other state in θ^{mi}.

A plot of the 1-norm of the vector $M^{\theta} f(\theta^{mi}) = w(\theta^{mi})$ versus i for $0 \le i \le N$ will also be presented. The 1-norm of $M^{\theta} f(\theta^{mi}) = w(\theta^{mi})$ was first discussed in Section 5.1 of Chapter 5. The matrix M^{θ} is positive definite and hence, at the UEP θ^{u} the 1-norm of $M^{\theta} f(\theta^{u})$ is zero. If the 1-norm of $M^{\theta} f(\theta^{mi}) = w(\theta^{mi}) \rightarrow 0$, this indicates the convergence of $\{\theta^{mi}\}_{i=0}^{N}$ to an equilibrium point.

The last point in the sequence θ^{mN} and the UEP θ^{u} along with its type will be presented. Transient stability assessment results from the

application of the TEF method will be presented and compared to results from the application of time simulation. The Extended Transient Mid-term Stability Package (ETMSP V3.0) [61] will be used for time simulation purposes.

7.2.1 50-generator System Results

In this subsection there will be result presented from the analysis of seven cases with regard to the 50-generator system. In five of these cases the 50-generator system is modified with respect to the generation at the Bruce generating station. There are two generators at the Bruce generation station and in this dissertation they will be referred to as Bruce-1 and Bruce-2 with generator numbers 9 and 25, respectively. Bruce-1 (9) and Bruce-2 (25) are connected to the power flow buses 93 and 110, respectively. In the IEEE 50-generator system the real power generation at each of these two Bruce generators is *700 MW*. In these five cases the generation is changed at both the Bruce generators. The seven cases are listed in Table 7.1 with three-phase fault location, line dropped to clear the fault and generation at the two Bruce generators is shown.

Table 7.1 Case description for the 50-generator system

Case number	Fault location	Line cleared	Bruce-1 (MW)	Bruce-2 (MW)	Faulted Bus Description
1	66	66 - 69	700	700	Bus 66 is a *100 kV* bus connected to bus 7 through a fixed tap transformer
2	1	1 - 6	1300	1300	Bus 1 is the *500 kV* Bruce bus
3	7	7 - 6	700	700	Bus 7 is the *500 kV* Nanticoke bus
4	7	7 - 6	900	900	Bus 7 is the *500 kV* Nanticoke bus
5	7	7 - 6	1100	1100	Bus 7 is the *500 kV* Nanticoke bus
6	7	7 - 6	1300	1300	Bus 7 is the *500 kV* Nanticoke bus
7	7	7 - 6	1500	1500	Bus 7 is the *500 kV* Nanticoke bus

The exit point method, which was described in Section 4.6 of Chapter 4, failed when applied to each of these seven cases. Table 7.2 gives relevant information on the nature of the failure. As noted earlier, the LSODE routine is a variable step-size solver and given a certain time step it will internally solve the ODEs at intermediate time steps and will end at a time equal to or less than the original time step given. The step size given in all seven cases was *0.005* seconds. The LSODE uses a method based on *backward differential formulas* [60]. At each internal step the order of the method for the approximate solution may change and the average order of the solution method is also shown in Table 7.2

Table 7.2 Results from the application of the exit point method to the seven cases

Case number	Average order of the method	Description of the Failure
1	4	Minimum gradient point found; problem with convergence
2	5	Minimum gradient point found; convergence was to the SEP
3	4	Minimum gradient point found; convergence was to the SEP
4	4	Minimum gradient point found; convergence was to the SEP
5	5	Lossy gradient system trajectory converged to the SEP
6	4	Lossy gradient system trajectory converged to the SEP
7	5	Lossy gradient system trajectory converged to the SEP

When the shadowing method is applied to these seven cases the parameters that were described in Section 5.2 of Chapter 5 are taken as $\eta = 0.01$ and $\beta = 2.0$ for each case. The time step given for each cycle (i.e., t_i as shown in Section 5.2 of Chapter 5) is *0.05* seconds. It has been generally observed and holds so for these cases that the LSODE solver will solve the ODEs at three intermediate steps with the resultant time less than the original time step given or in this case less than *0.05* seconds. Therefore, the LSODE solver will not necessarily integrate up to the time of *0.05* seconds.

Table 7.3 shows the number of cycles needed to meet the tolerance of the 1-norm of $M^{\theta} f(\theta^{mi}) = w(\theta^{mi})$ to be less than $\beta = 2.0$ for each of the seven cases. This value of β was chosen so that the point θ^{mN} is relatively close to θ^{u}. Figures 7.1 and 7.2 show the plot of the 1-norm of $w(\theta^{mi})$ versus the number of cycles for each of the cases 1 through 7. Because cases 3, 4, 5, 6 and 7 are similar since the fault location and line cleared are identical there respective plots are all shown in Figure 7.2. These seven plots clearly show the convergence of $\{\theta^{mi}\}_{i=0}^{N}$ to some equilibrium point.

Table 7.3 Number of cycles for each case for the 50-generator system

Case number	Number of cycles
1	62
2	48
3	48
4	63
5	61
6	55
7	57

Tables 7.4, 7.5 and 7.6 hold the following information for each case. The internal generator number and the power flow bus number to which it is connected is given. The vector angle θ^{mN} is shown. This vector point θ^{mN} is the last point in the sequence which is produced by the application of the shadowing method. Finally, the controlling UEP is shown. The vector angle θ^{mN} and θ^{u} are positioned side by side for comparison of corresponding angles. It can be seen since β was chosen relatively small the corresponding angles in these two angle vectors are relatively close to each other. In all seven cases the resultant UEP was a type-*1* equilibrium point.

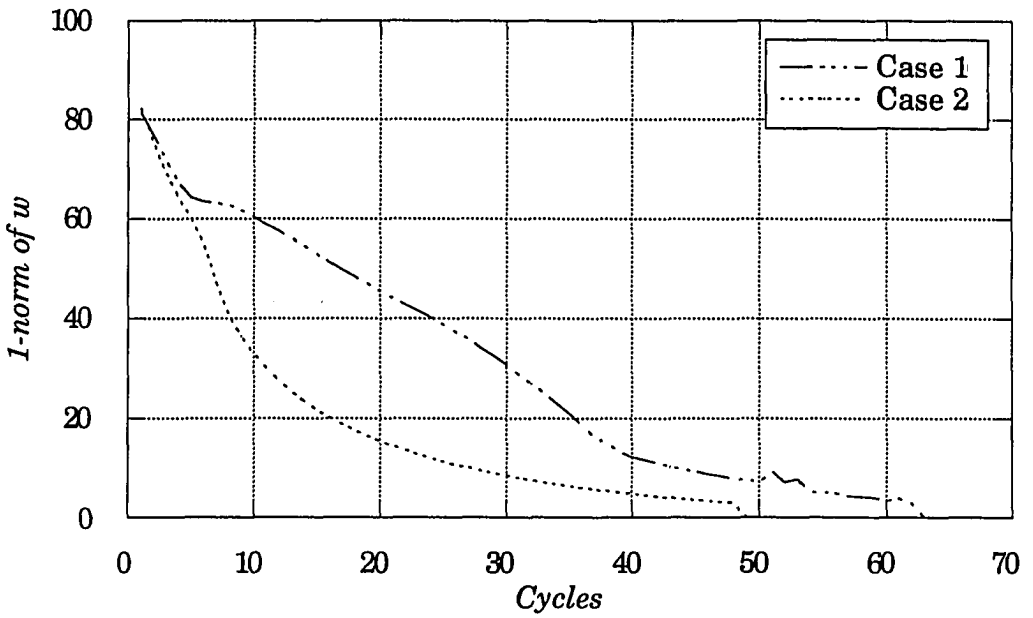

Figure 7.1 1-norm of w versus the number of cycles for Cases 1 and 2

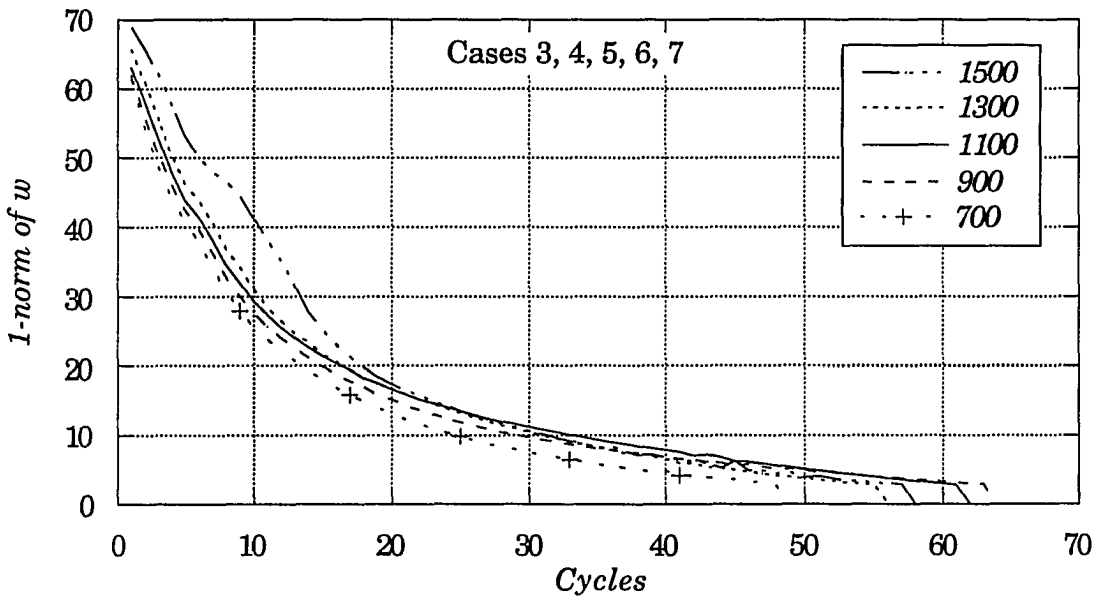

Figure 7.2 1-norm of w versus the number of cycles for Cases 3, 4, 5, 6 and 7

Table 7.4 UEP data for Case 1, Case 2 and Case 3

Gen. num.	Bus num.	Case 1 θ^{mN} (degrees)	Case 1 UEP (degrees)	Case 2 θ^{mN} (degrees)	Case 2 UEP (degrees)	Case 3 θ^{mN} (degrees)	Case 3 UEP (degrees)
1	60	72.21	86.18	79.08	100.27	43.41	54.84
2	67	132.29	131.37	118.82	121.21	84.69	86.80
3	79	112.49	115.49	119.95	127.41	73.40	79.89
4	80	108.72	115.89	116.50	127.61	70.37	80.35
5	82	119.07	130.56	108.34	120.31	64.13	76.34
6	89	146.87	144.44	155.49	155.66	106.61	109.14
7	90	72.22	107.18	86.42	121.22	50.72	73.76
8	91	129.11	132.18	121.96	127.18	76.29	82.90
9	93	129.35	127.74	161.89	162.39	87.59	89.93
10	94	84.90	96.07	92.20	110.32	55.00	64.44
11	95	75.76	90.64	81.18	105.31	56.30	65.90
12	96	130.53	130.73	133.84	135.34	84.24	90.73
13	97	135.83	134.89	123.40	126.69	90.25	93.01
14	98	152.06	149.19	160.79	160.43	112.44	114.74
15	99	137.79	135.40	161.03	160.39	96.70	98.70
16	100	137.89	134.73	145.80	145.40	96.09	98.82
17	101	131.79	129.96	137.29	138.07	92.12	94.25
18	102	56.32	56.34	54.99	55.17	44.55	44.85
19	103	134.45	131.11	142.22	141.73	91.87	94.95
20	104	155.31	153.58	158.55	159.69	183.28	185.43
21	105	139.76	138.37	145.10	146.18	99.37	101.88
22	106	140.06	138.61	145.26	146.28	99.53	101.95
23	108	129.83	130.60	103.49	106.77	61.01	63.60
24	109	110.96	118.06	99.18	107.83	54.47	63.37
25	110	129.34	127.67	162.92	163.35	88.27	90.58
26	111	150.47	148.76	149.30	150.67	154.88	157.41
27	112	131.23	129.41	136.71	137.49	91.51	93.63
28	115	-3.23	-3.06	-3.44	-3.55	-2.88	-2.99
29	116	5.96	6.14	5.73	5.65	3.25	3.23
30	117	16.71	16.89	16.23	16.19	11.00	11.07
31	118	9.22	9.38	9.07	9.01	5.35	5.38
32	119	-39.92	-40.62	-28.82	-28.82	-36.12	-35.72
33	121	120.09	121.49	75.93	79.73	36.93	39.01
34	122	122.57	122.25	95.94	99.01	61.31	63.18
35	124	123.65	122.90	107.27	109.84	72.05	74.14
36	128	-8.76	-9.76	1.93	2.41	-11.00	-10.31
37	130	-33.35	-33.76	-25.75	-25.77	-31.00	-30.75
38	131	-9.30	-9.46	-5.01	-5.04	-8.36	-8.23
39	132	27.53	27.51	27.51	27.85	19.38	19.81
40	134	-10.66	-10.59	-12.67	-12.93	-6.65	-6.95
41	135	27.90	28.58	27.31	27.71	31.17	31.31
42	137	-99.03	-98.72	-99.09	-99.79	-86.83	-87.62
43	140	-37.42	-37.34	-40.21	-40.70	-30.41	-31.06
44	142	1.98	2.03	3.28	3.19	2.71	2.68
45	143	10.22	10.31	10.89	10.85	8.27	8.32
46	144	2.51	2.47	4.82	4.72	4.04	4.03
47	145	11.09	11.19	4.35	4.05	15.75	15.33
48	136	2.56	2.90	1.61	1.57	6.49	6.30
49	141	-4.09	-3.94	-4.42	-4.56	-1.92	-2.09
50	139	-16.51	-16.45	-19.98	-20.40	-11.07	-11.67

Table 7.5 UEP data for Case 4, Case 5 and Case 6

Gen. num.	Bus num.	Case 4		Case 5		Case 6	
		θ^{mN} (degrees)	UEP (degrees)	θ^{mN} (degrees)	UEP (degrees)	θ^{mN} (degrees)	UEP (degrees)
1	60	59.63	75.96	64.03	80.93	62.37	79.23
2	67	106.08	110.81	111.74	114.00	107.70	109.57
3	79	95.67	104.79	102.13	109.62	100.03	107.48
4	80	91.75	105.06	97.33	109.82	94.66	107.59
5	82	88.39	101.19	94.30	105.46	91.16	102.39
6	89	131.35	135.20	138.12	139.38	135.63	136.81
7	90	63.71	96.73	66.64	101.82	65.28	99.97
8	91	100.81	108.10	107.35	112.34	104.44	109.39
9	93	118.08	122.12	131.11	132.69	134.78	136.18
10	94	71.59	85.77	76.48	90.77	74.96	89.07
11	95	66.93	81.91	69.96	86.26	68.95	84.95
12	96	109.53	116.37	116.02	120.49	112.94	117.73
13	97	112.16	116.93	117.71	119.95	113.67	115.51
14	98	137.23	140.74	143.87	144.75	141.20	142.01
15	99	124.01	127.58	133.88	134.82	134.41	135.14
16	100	121.15	124.87	128.17	129.23	125.79	126.79
17	101	116.13	119.95	122.64	123.98	120.01	121.20
18	102	49.92	50.42	52.15	52.29	52.59	52.74
19	103	117.16	120.99	124.28	125.43	121.96	123.08
20	104	189.90	191.88	183.13	184.39	173.21	174.81
21	105	123.40	127.53	129.78	131.49	127.13	128.70
22	106	123.55	127.60	129.96	131.59	127.32	128.81
23	108	82.42	87.56	89.27	92.05	86.53	88.85
24	109	78.65	88.27	85.07	92.77	82.23	89.93
25	110	119.18	123.20	132.64	134.19	136.74	138.10
26	111	166.70	169.57	163.02	164.56	154.35	156.05
27	112	115.52	119.33	122.04	123.39	119.43	120.62
28	115	-3.42	-3.67	-3.29	-3.42	-2.75	-2.86
29	116	4.22	4.10	5.00	4.89	5.75	5.67
30	117	13.37	13.39	14.70	14.63	15.58	15.54
31	118	6.98	6.94	8.00	7.92	8.79	8.73
32	119	-32.14	-31.61	-30.53	-30.34	-29.93	-29.74
33	121	56.28	61.34	62.95	65.75	60.00	62.21
34	122	80.72	85.59	86.82	89.31	83.28	85.20
35	124	93.28	98.11	99.30	101.65	95.52	97.44
36	128	-4.25	-3.03	-1.61	-1.05	-1.29	-0.80
37	130	-28.27	-27.95	-26.99	-26.90	-26.34	-26.24
38	131	-6.70	-6.56	-5.80	-5.77	-5.19	-5.16
39	132	23.90	24.68	25.54	25.88	25.57	25.86
40	134	-9.64	-10.16	-10.83	-11.11	-11.09	-11.35
41	135	28.78	28.81	28.18	28.52	28.57	28.94
42	137	-94.27	-95.77	-95.97	-96.68	-94.61	-95.26
43	140	-35.66	-36.65	-37.44	-37.98	-37.43	-37.95
44	142	2.84	2.74	3.19	3.11	3.71	3.65
45	143	9.51	9.52	10.25	10.21	10.82	10.80
46	144	4.30	4.22	4.69	4.62	5.22	5.16
47	145	10.75	10.10	7.96	7.62	6.26	5.93
48	136	3.66	3.27	2.89	2.81	3.24	3.19
49	141	-3.41	-3.74	-3.70	-3.86	-3.33	-3.47
50	139	-15.52	-16.39	-17.34	-17.83	-17.78	-18.25

Table 7.6 UEP data for Case 7

Generator number	Power flow bus	Case 7	
		θ^{mN} (degrees)	UEP (degrees)
1	60	57.91	74.01
2	67	99.75	101.86
3	79	93.77	101.54
4	80	87.90	101.56
5	82	84.08	95.85
6	89	128.65	130.46
7	90	62.52	94.37
8	91	97.13	102.90
9	93	133.77	135.65
10	94	70.44	83.82
11	95	66.15	80.74
12	96	105.10	111.33
13	97	105.56	107.80
14	98	134.01	135.49
15	99	130.40	131.61
16	100	118.84	120.62
17	101	113.06	114.74
18	102	52.04	52.38
19	103	115.01	117.03
20	104	160.62	162.82
21	105	120.15	122.24
22	106	120.35	122.35
23	108	79.96	82.47
24	109	75.35	83.70
25	110	136.12	137.97
26	111	142.57	144.81
27	112	112.67	114.34
28	115	-2.08	-2.17
29	116	6.37	6.35
30	117	16.05	16.11
31	118	9.32	9.34
32	119	-29.85	-29.55
33	121	53.65	55.88
34	122	76.26	78.24
35	124	87.93	90.05
36	128	-1.95	-1.35
37	130	-25.99	-25.81
38	131	-4.73	-4.65
39	132	24.87	25.25
40	134	-10.92	-11.23
41	135	29.46	29.76
42	137	-91.84	-92.64
43	140	-36.51	-37.15
44	142	4.29	4.25
45	143	11.24	11.27
46	144	5.80	5.76
47	145	4.96	4.56
48	136	4.13	4.01
49	141	-2.67	-2.82
50	139	-17.57	-18.14

In order to show two states in the sequence $\{\theta^{mi}\}_{i=0}^{N}$ Figures 7.3, 7.4 and 7.5 are shown for cases 1 through 7. For each case in the corresponding figure the states versus is plotted for $0 \leq i \leq N+1$, with $\theta^{m(N+1)} = \theta^{u}$. The numbers 20 and 25 are the generator numbers for which 20 corresponds to a machine connected to the Nanticoke bus (power flow bus number 104) and 25 corresponds to generator Bruce-2 (power flow bus number 110). Each plot starts at the exit point θ^{m0} and ends at the UEP $\theta^{m(N+1)}$. These plots along with the plots from Figures 7.1 and 7.2 clearly show the convergence of each of the seven sequences $\{\theta^{mi}\}_{i=0}^{N}$ to the respective θ^{u}. Again, since Cases 3, 4, 5, 6 and 7 have some similarities they are put in the same figure.

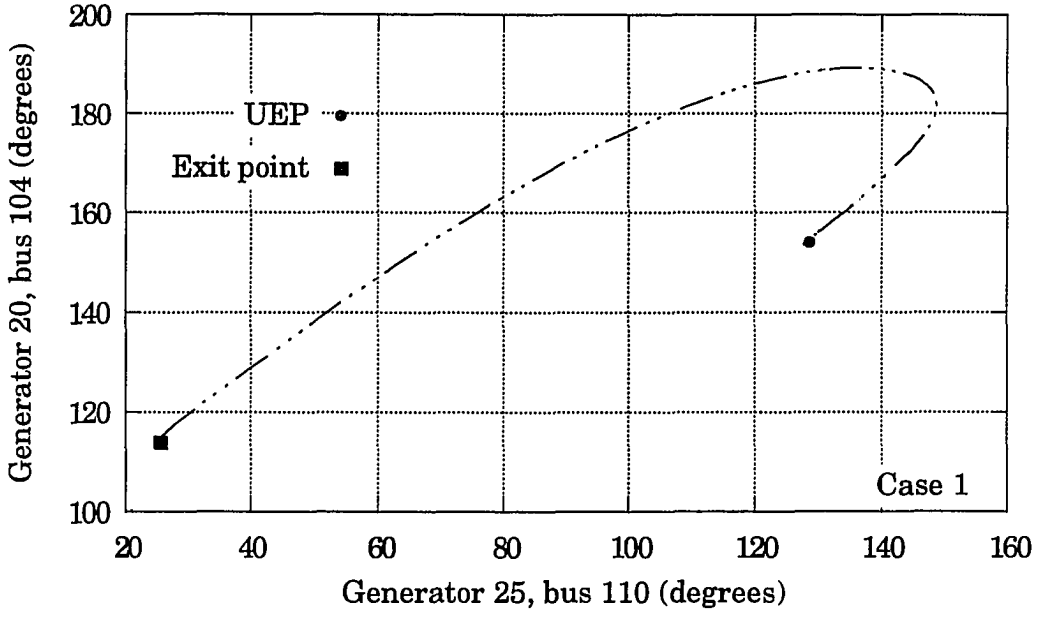

Figure 7.3 Illustration of shadowing for Case 1

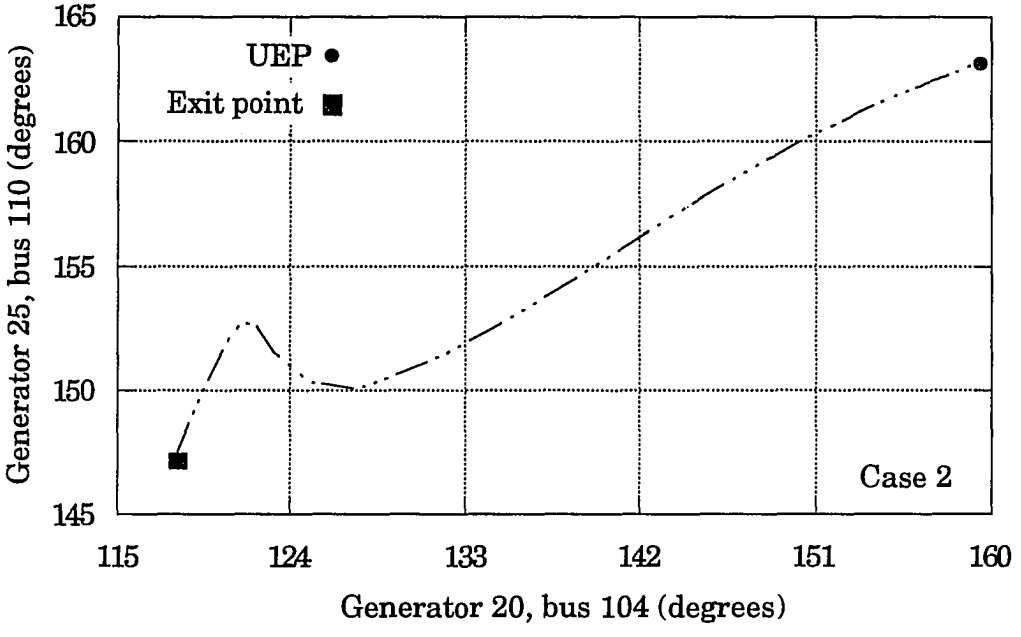

Figure 7.4 Illustration of shadowing for Case 2

Transient stability assessment results are shown in Table 7.7. Critical clearing times obtained from ETMSP are given. Results from the application of TEF method are given. They are the potential energy margin ΔV_{PE}, the corrected kinetic energy $V_{KE\text{-}corr}$, the normalized energy margin $\Delta V_n = (\Delta V_{PE} - V_{KE\text{-}corr})/V_{KE\text{-}corr}$ and a description of the criterion on which the corrected kinetic energy is evaluated is shown in Table 7.8. The potential energy margin ΔV_{PE} is taken from equation (2.16) from Chapter 2. The critical clearing times obtained from the application of the TEF method with the shadowing technique incorporated for these seven cases seem to match well with time simulation.

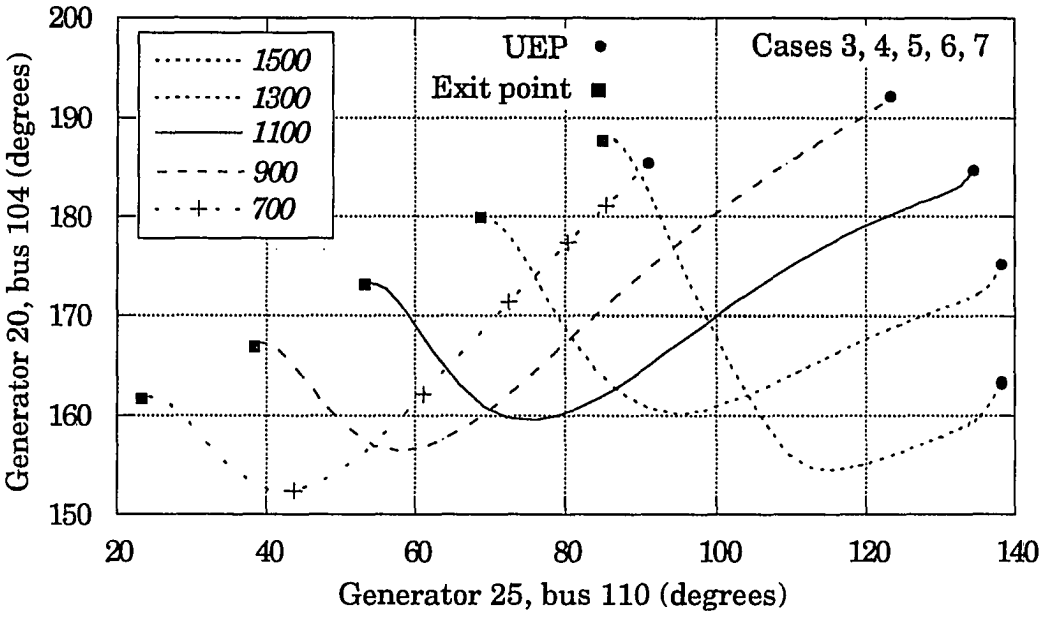

Figure 7.5 Illustration of shadowing for Cases 3, 4, 5, 6 and 7

Table 7.7 Transient stability assessment results for Cases 1 through 7

Case number	CCT ETMSP (seconds)	CCT TEF (seconds)	ΔV_{PE} (pu)	$V_{KE\text{-}corr}$ (pu)	ΔV_n (pu)
1	0.171	0.184	21.66	21.61	0.002
2	0.150	0.154	7.92	7.94	-0.003
3	0.115	0.111	6.92	6.88	0.005
4	0.115	0.127	5.76	8.80	-0.005
5	0.010	0.116	7.28	7.32	-0.005
6	0.080	0.082	4.70	4.70[a]	0.000
7	0.050	0.056	1.715	1.717	-0.001

CCT - critical clearing time
a - represents the total kinetic energy

Table 7.8 Criterion for the evaluation of the corrected kinetic energy for the 50-generator system

Case number	Criterion
1	Pick generator 20 and 26 to be in the critical group; they both have considerable relative speed at clearing since the fault is electrically close.
2	Pick generators that have an UEP angle above *130* degrees. All of these machines have about the same relative speed at clearing.
3	Same group and reason as used in Case 1.
4	Same group and reason as used in Case 1.
5	Same group and reason as used in Case 1.
6	The total kinetic energy was used
7	Same group and reason as used in Case 1.

7.2.2 161-generator System Results

In this subsection there are two cases (Cases 8 and 9) from the 161-generator system that are analyzed and these two cases are described in Table 7.9

The format for data presentation in this subsection follows similarly from the data presentation given in Subsection 7.2.1 for the 50-generator system .

Table 7.9 Case description for the 161-generator system

Case number	Fault location	Line cleared	Faulted Bus Description
8	1662	1662 - 1709	Bus 1662 is a *345 kV* bus
9	1655	1655 - 1739	Bus 1655 is a *345 kV* bus

When the shadowing method is applied to these two cases the parameters are taken as $\eta = 0.01$ and $\beta = 0.5$ for each case. The reason β is smaller for the 161-generator system than in the 50-generator case ($\beta = 2.0$) is because there are over 3 times as many machines. Hence, in order to have a relatively small difference in the corresponding angles in the angle vectors θ^{mN} and θ^{u} the value of β must be taken smaller. The time step given for each cycle is *0.05* seconds.

Table 7.10 shows the number of cycles needed to meet the tolerance of the 1-norm of $M^{\theta} f(\theta^{mi}) = w(\theta^{mi})$ to be less than $\beta = 0.5$ for each of the two cases. It can be seen that the number of cycles needed to meet the tolerance is much larger than those for the 50-generator system; again this is due to the fact that this is a larger system. Figure 7.6 contains the plot of the 1-norm of $w(\theta^{mi})$ versus the number of cycles for both Cases 8 and 9. These two plots clearly show the convergence of $\{\theta^{mi}\}_{i=0}^{N}$ to some equilibrium point.

Similar to Tables 7.4, 7.5 and 7.6, Table 7.11 holds the point θ^{mN} and the controlling UEP. Again, it can be noticed that these angles are relatively close to each other due to the relatively small value of β. The UEP was type-*1* in both cases.

Generators 38 (power flow bus 1680) and 39 (power flow bus 1681) are taken from the sequence $\{\theta^{mi}\}_{i=0}^{N}$ and plotted against one another in Figure 7.7 for Case 8 and in Figure 7.8 for Case 9. Generator 39 is a Sherco generator which is connected to the *345 kV* bus 1662 (faulted) through a fixed tap transformer. Generator 38 is a Monticello generator which is connected to the *345 kV* bus 1655 (faulted) through a fixed tap transformer. These plots along with the plots from Figure 7.5 clearly show the convergence of each of the two sequences $\{\theta^{mi}\}_{i=0}^{N}$ to the respective θ^{u}. The plots in Figures 7.7 and 7.8 appear to be slightly different than the plots in Figures 7.3, 7.4 and 7.5 since the plot seems to intersect itself. The reason is the following. If the points in the sequence $\{\theta^{mi}\}_{i=0}^{N}$ are connected then this will appear as a *1*-dimensional curve in $R^{(n-1)}$ space. What is actually shown in both Figures 7.7 and 7.8 is the projection of this *1*-dimensional curve into the plane spanned by the axes corresponding to machines 38 and 39. Therefore, it may appear as if this curve intersects itself but in $R^{(n-1)}$ space it is not. It is clear

Table 7.10 Number of cycles for each case for the 161-generator system

Case number	Number of cycles
8	218
9	293

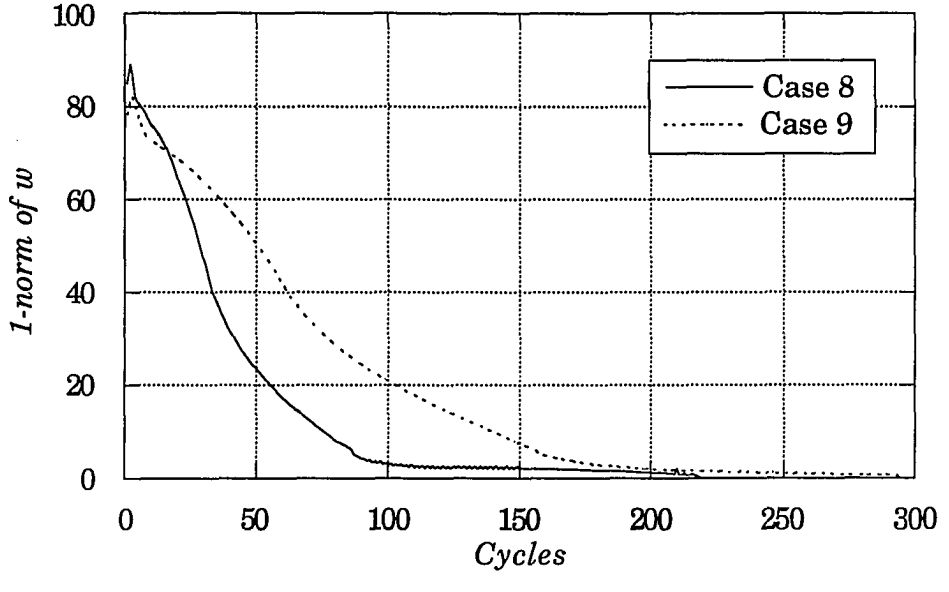

Figure 7.6 1-norm of w versus the number of cycles for Cases 8 and 9

Table 7.11 UEP data for Case 8 Case 9

Gen. num.	Bus num.	Case 8 θ^{mN} (degrees)	Case 8 UEP (degrees)		Case 9 θ^{mN} (degrees)	Case 9 UEP (degrees)
1	39	64.11	63.41		72.50	69.74
2	53	62.75	61.96		72.11	69.05
3	55	60.22	59.43		69.66	66.58
4	283	64.18	63.35		74.04	70.80
5	284	67.60	66.85		76.59	73.63
6	287	51.91	51.11		61.18	58.10
7	288	50.17	49.40		59.34	56.32
8	415	112.86	111.48		128.42	123.54
9	458	117.89	116.57		133.91	128.97
10	459	117.89	116.57		133.91	128.97
11	460	125.56	124.23		141.53	136.60
12	542	100.12	98.86		114.77	110.06
13	543	100.12	98.86		114.77	110.06
14	545	81.67	80.46		95.79	91.25
15	547	95.05	93.87		108.98	104.47
16	556	98.99	97.77		113.58	108.93
17	557	98.99	97.77		113.58	108.93
18	575	77.06	75.91		90.09	85.80
19	603	115.38	114.10		131.21	126.32
20	607	115.70	114.42		131.54	126.64
21	611	112.77	111.49		128.55	123.67
22	618	83.20	82.34		93.42	90.09
23	748	116.87	115.54	*kce*	133.20	128.21
24	749	120.62	119.28	*kce*	136.96	131.95
25	815	115.39	114.06	*kce*	131.82	126.81
26	845	112.19	110.82	*kce*	128.41	123.39
27	912	96.21	94.89	*kce*	113.51	108.26
28	1365	86.36	84.91	*kce*	108.19	102.04
29	1474	106.95	105.50	*kce*	128.69	122.65
30	1475	115.99	114.53	*kce*	137.70	131.67
31	1476	98.19	96.70	*kce*	119.98	113.84
32	1477	98.20	96.70	*kce*	119.98	113.85
33	1521	120.75	119.42	*kce*	137.03	132.05
34	1522	114.76	113.43	*kce*	131.05	126.07
35	1523	123.47	122.13	*kce*	139.74	134.75
36	1618	89.34	87.96	*kce*	108.53	102.44
37	1619	89.16	87.78	*kce*	108.34	102.25
38	1680	103.55	102.10	*kce*	129.84	123.45
39	1681	101.16	99.71	*kce*	126.13	119.76
40	1682	101.23	99.79	*kce*	126.21	119.84
41	1683	99.02	97.59	*kce*	123.93	117.59
42	1780	89.10	87.70	*kce*	110.75	104.52
43	1781	70.27	68.83	*kce*	89.40	83.33
44	1782	81.93	80.48	*kce*	101.54	95.37
45	1784	85.82	84.36	*kce*	105.60	99.39
46	1785	78.43	76.98	*kce*	99.28	93.08
47	1786	80.61	79.18	*kce*	101.56	95.36
48	1787	84.86	83.38	*kce*	106.43	100.11
49	1788	82.11	80.68	*kce*	103.54	97.31
50	1831	76.76	75.26	*kce*	97.61	91.43

Table 7.11 Continued

Gen. num.	Bus num.	Case 8 θ^{mN} (degrees)	Case 8 UEP (degrees)		Case 9 θ^{mN} (degrees)	Case 9 UEP (degrees)
51	2016	58.43	57.26	*kce*	72.40	67.67
52	2057	60.00	59.02	*kce*	72.66	68.56
53	2058	35.04	34.37		43.28	40.62
54	2085	40.21	39.78		45.33	43.66
55	2122	61.65	60.63	*kce*	75.19	70.84
56	2140	64.10	62.86	*kce*	80.46	75.24
57	2142	75.12	73.89	*kce*	91.99	86.67
58	2343	64.58	63.64		76.19	72.40
59	2446	51.10	50.42		59.61	56.85
60	2454	37.28	36.63		45.13	42.57
61	2591	57.98	57.22		67.17	64.16
62	2605	47.23	46.71		53.53	51.48
63	2710	39.41	38.96		44.90	43.13
64	2901	34.42	34.00		39.38	37.77
65	3001	154.47	154.09	*kce*	164.74	161.98
66	3002	154.77	154.40	*kce*	165.03	162.28
67	3003	155.22	154.67	*kce*	165.56	162.62
68	3004	156.05	155.50	*kce*	166.37	163.44
69	3005	156.53	155.97	*kce*	166.84	163.90
70	3006	157.15	156.57	*kce*	167.43	164.49
71	3010	166.95	166.37	*kce*	176.59	173.80
72	3030	145.44	144.84	*kce*	155.12	152.31
73	3032	142.60	142.02	*kce*	152.35	149.55
74	3588	197.86	196.55	*kce*	203.10	200.73
75	3590	208.28	207.44	*kce*	213.61	211.63
76	3591	175.33	174.31	*kce*	183.45	180.63
77	3595	195.04	194.01	*kce*	199.06	197.20
78	3596	198.82	197.50	*kce*	202.32	200.34
79	3598	214.34	212.05	*kce*	216.19	214.04
80	3600	184.38	183.55	*kce*	190.54	188.35
81	4015	48.01	47.63		52.67	51.16
82	4850	26.81	26.61		29.21	28.44
83	4852	19.18	18.97		21.63	20.85
84	4885	20.16	20.07		21.08	20.78
85	4888	8.64	8.57		9.26	9.05
86	4889	10.90	10.86		11.15	11.05
87	4890	9.56	9.42		11.27	10.72
88	4891	12.19	12.03		13.96	13.39
89	4892	10.33	10.15		12.46	11.78
90	4894	-12.22	-12.16		-13.33	-13.02
91	4903	24.88	24.68		27.15	26.42
92	4905	26.35	26.18		28.36	27.72
93	4949	30.50	30.30		32.88	32.12
94	4963	48.18	47.82		52.05	50.76
95	4964	23.06	22.83		25.69	24.86
96	4966	31.45	30.90		38.75	36.60
97	4970	24.77	24.62		26.55	25.97
98	4971	23.68	23.51		25.51	24.91
99	4972	22.29	22.19		23.38	23.03
100	4986	25.52	25.32		27.79	27.06

Table 7.11 Continued

Gen. num.	Bus num.	Case 8 θ^{mN} (degrees)	Case 8 UEP (degrees)	Case 9 θ^{mN} (degrees)	Case 9 UEP (degrees)
101	4987	24.92	24.73	27.07	26.38
102	4993	26.77	26.60	28.79	28.14
103	4994	38.00	37.70	41.79	40.64
104	5007	29.77	29.44	33.64	32.38
105	5870	-2.15	-2.14	-2.68	-2.55
106	5871	-11.18	-11.15	-11.98	-11.77
107	5872	3.59	3.55	3.78	3.69
108	5873	-8.06	-8.26	-6.35	-6.96
109	5874	14.16	14.01	15.70	15.17
110	5875	7.83	7.69	9.24	8.75
111	5876	9.23	8.99	11.71	10.88
112	5877	9.17	9.01	10.67	10.15
113	5878	-7.26	-7.26	-7.60	-7.53
114	5879	10.67	10.58	11.45	11.16
115	5880	12.86	12.75	13.87	13.51
116	5882	17.16	16.93	19.46	18.68
117	5883	13.44	13.29	14.97	14.45
118	5884	11.68	11.58	12.69	12.35
119	5888	14.27	14.05	16.55	15.79
120	5891	12.49	12.30	14.54	13.86
121	5892	14.93	14.83	15.97	15.61
122	5960	22.69	22.52	24.41	23.83
123	5961	7.82	7.51	11.37	10.21
124	5970	11.18	11.02	12.82	12.26
125	5971	24.09	23.98	25.04	24.71
126	5977	41.32	40.90	46.10	44.53
127	5981	25.72	25.56	27.31	26.76
128	5984	18.50	18.44	18.89	18.73
129	5985	12.78	12.75	12.76	12.73
130	5986	24.50	24.45	24.67	24.58
131	5987	19.48	19.55	18.31	18.64
132	5988	15.00	15.09	13.57	13.98
133	5989	-1.93	-1.86	-3.13	-2.79
134	6534	-6.88	-6.80	-7.60	-7.36
135	6536	-32.38	-32.16	-34.39	-33.71
136	6552	-20.29	-20.04	-22.40	-21.67
137	6609	-9.45	-8.32	-14.01	-11.92
138	6900	24.18	24.23	23.33	23.58
139	6935	7.10	7.13	6.74	6.84
140	6936	18.56	18.58	18.18	18.29
141	6937	13.02	13.02	13.01	13.00
142	6939	3.84	3.90	3.14	3.36
143	6940	13.27	13.32	12.41	12.66
144	6941	6.83	6.76	7.57	7.33
145	6942	3.02	3.05	2.77	2.85
146	6944	-34.97	-34.86	-36.24	-35.83
147	6945	13.61	13.70	12.32	12.71
148	6946	2.56	2.66	1.12	1.55
149	6947	-4.73	-4.65	-6.09	-5.69
150	6948	-27.17	-27.04	-28.96	-28.42

Table 7.11 Continued

Gen. num.	Bus num.	Case 8 θ^{mN} (degrees)	Case 8 UEP (degrees)	Case 9 θ^{mN} (degrees)	Case 9 UEP (degrees)
151	6949	-11.87	-11.76	-13.44	-12.96
152	6950	-8.44	-8.34	-9.85	-9.42
153	6951	-14.12	-14.01	-15.38	-14.98
154	6952	8.34	8.37	7.76	7.93
155	6953	-57.00	-56.77	-59.50	-58.69
156	6954	-62.37	-62.15	-64.60	-63.87
157	6955	-80.22	-80.00	-82.45	-81.72
158	6956	-42.16	-41.95	-44.18	-43.50
159	6502	-10.94	-10.68	-13.12	-12.36
160	6938	1.77	1.83	1.09	1.30
161	6943	-25.70	-25.58	-26.93	-26.52

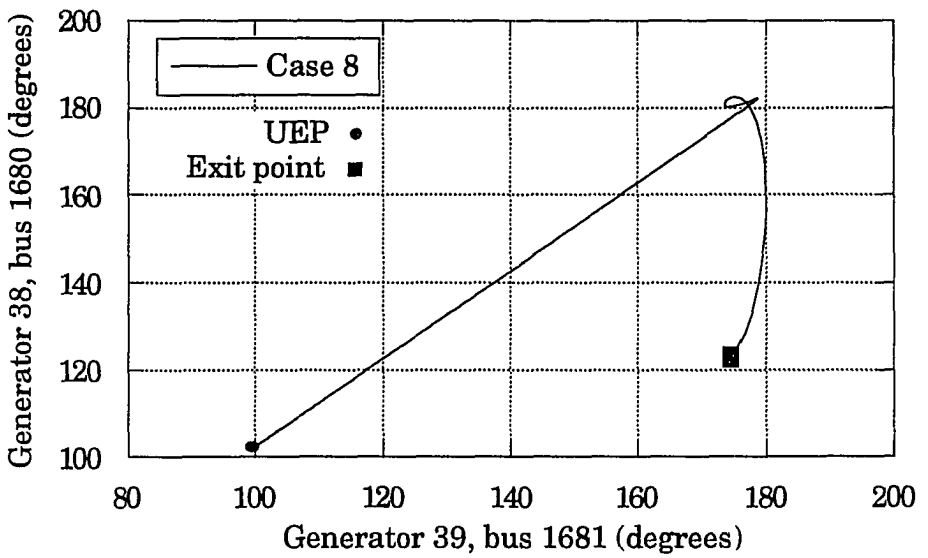

Figure 7.7 Illustration of shadowing for Case 8

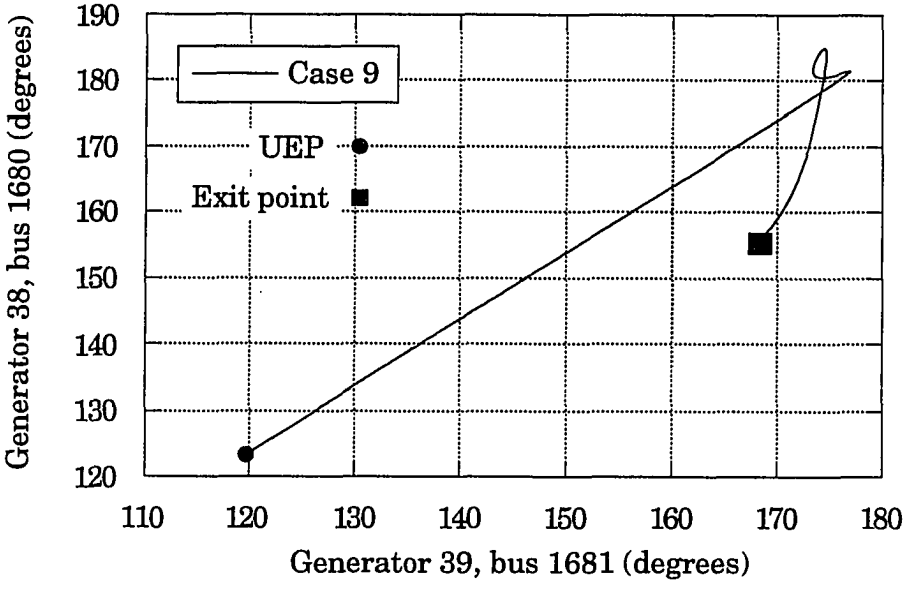

Figure 7.8 Illustration of shadowing for Case 9

that part of each graph in Figures 7.7 and 7.8 seem quite linear. However, there is no immediate reason why this is of any significance since this is again the projection onto a plane

Transient stability assessment results are shown in Table 7.11. In Case 8 the corrected kinetic energy was based on the machines that have a *kce* flag next to them in Table 7.11. These machines picked were based on two criteria. The machine had a relatively high clearing speed and the machine had a relatively large angle at the UEP. Therefore, based on the concept of the corrected kinetic energy the system must absorb this relatively large kinetic energy due to the relatively high clearing speeds. Since the system is being cleared near the critical clearing time the trajectory of the system should pass close to the UEP. Hence, the machines that have a relatively large angle at the UEP will generally swing near this UEP angle and thus pick up kinetic energy which then needs to be absorbed by the system. The critical clearing time is given in Table 7.12 and compares quite well with time simulation.

An analysis of Case 9 was performed in [57] in which a *modal transient energy function* was introduced. The UEP determined in [57] is identical to the UEP obtained by the shadowing method (this UEP is shown in Table 7.11). The transient stability assessment results from [57] for this case will be repeated in Table 7.12. In [57] the potential energy margin was replaced by a partial potential energy margin and the corrected kinetic energy was replaced by a partial kinetic energy margin. However, the results will be put under the heading of potential energy margin and corrected kinetic energy. The critical clearing time for Case 9 is given in Table 7.12 and compares quite well with time simulation.

Table 7.12 Transient stability assessment results for Case 8 and Case 9

Case number	CCT ETMSP (seconds)	CCT TEF (seconds)	ΔV_{PE} (pu)	$V_{KE\text{-}corr}$ (pu)	ΔV_n (pu)
8	0.111	0.107	4.25	4.23	0.005
9	0.1175	0.1178	9.43	9.34	0.055

CCT - Critical clearing time

7.3 Concluding Remarks

The results from the analysis of nine cases from two different large-scale power systems were given in this chapter. Seven of these cases involved the 50-generator system and two involved the 161-generator system. In all seven cases involving the 50-generator system the exit point method failed. On of the problems was an incomplete convergence to an equilibrium point. The other six were failures due do to the method converging to the SEP. This problem was first discussed in Chapter 4. This specific problem and others were the motivation for presenting the shadowing method. This method not only avoids these problems it actually is set-up to shadow the stable manifold of the controlling UEP which is thought to be part of the stability boundary of the lossy gradient system.

Transient stability assessment results that were produced from the application of the TEF method with the shadowing method incorporated for the given nine cases. The assessment results compared favorably with time simulation. However, the main result from this chapter and the focus of this dissertation is the fact that the sequence of points produced by the shadowing technique seemed to converge to the controlling UEP.

These two types of results given above should not be surprising at all for the following reasons.

- The use of the controlling UEP in the energy margin calculation was given mathematical foundation in Section 3.1.3 of Chapter 3. This was based on the fact that the stability boundary is composed solely of the corresponding stable manifolds.

- The connection between the swing system and the gradient system lies with the controlling UEP as shown in Section 3.3 of Chapter 3. The controlling UEP is on the stability boundary of both of these systems in the form of $(\theta^u,0)$ and θ^u.

- The shadowing method utilizes the stable manifold (part of the stability boundary) of the gradient system and it was rigorously shown in Section 5.2 of Chapter 5 that under reasonable circumstances the resultant sequence $\{\theta^{mi}\}_{i=0}^{N}$ produced by the application of the shadowing method converges to the controlling UEP.

- Doubts were raised in Chapter 6 on the validity that the stability boundary is composed solely of the corresponding stable manifolds when transfer conductances were introduced into the system. An example was given in the form of vector field plots that validated this conclusion and it was observed that the shadowing method would work satisfactorily.

- Results from this chapter validate all of these concepts and ideas.

In all nine cases the value of β, which is used as a stopping criteria, was chosen relatively small. This value was picked relatively small to show that the sequence does indeed converge to the controlling UEP. However, in a practical implementation of this method a relatively small value of would not be computationally feasible. It was first discussed in Remark 2 of Section 5.4 of Chapter 5 that an optimal sequence $\{t_i\}_{i=0}^{N}$ needs to be utilized with both t_i and N chosen correctly. This, however, is left for future work.

It can be noticed, however, from Figures 7.1, 7.2 and 7.6 of the 1-norm of $w(\theta^{mi})$ versus the number of cycles that the 1-norm of $w(\theta^{mi})$ seems to drop rapidly and then level off. It would seem reasonable that the application of the shadowing method could be stopped at the point when the 1-norm of $w(\theta^{mi})$ starts to level off and that the resulting initial guess would be in the domain of convergence of the controlling UEP.

8. CONCLUSIONS

The conclusions to this dissertation work are presented with respect to relevant chapters.

The swing system and the associated gradient system were presented in Chapter 3. The main idea presented in this chapter is that the stability boundary of the swing system, which was in the center of inertia reference frame, was composed solely of the corresponding stable manifolds. In order to do show this a valid energy function needs to exist. It was shown that there indeed exist a valid energy function in the COI reference frame. The notion that the stability boundary was composed solely of the corresponding stable manifolds led to the mathematical concept of the energy margin.

The exit point method was presented in Chapter 4. The heuristic foundation for this method was explained and examples given. It was pointed out that two basic problems can occur while applying the exit point method to detect the controlling UEP. These two problems were clearly shown in the two examples given in Chapter 4 and are listed below.

Problem 1 There may be no detection of the minimum gradient point since there is no analytical justification for the existence of this point.

Problem 2 The resultant equilibrium point may not be the controlling UEP. In fact it has been observed that this point can be an SEP, another equilibrium point on the stability boundary of the gradient system or even as shown in Subsection 6.2.3 an UEP which is not even on the stability boundary of the gradient system.

In Chapter 5 a new method, referred to as the shadowing method, was presented. It was shown that when this shadowing method was applied to

the examples from Chapter 4, for which the exit point method failed, the controlling UEP was correctly detected. A sound analytical foundation for this shadowing method was given. Under the reasonable assumption that the controlling UEP is type-*1* it was shown that an infinite sequence of time steps exist such that when the shadowing method is applied with the Euler integration scheme the resultant sequence that is produced converges to the controlling UEP. In the examples, however, a 4^{th} order Runge-Kutta was used to numerically solve the ODEs and this worked well. The Euler method was used in the proof for its convenience and future work will consists of including the more general solution of the gradient system in the analytical foundation.

It was discussed in Chapter 6 that when transfer conductances are introduced into the power system model the rigorous analytical foundation on which the swing and gradient system were based does not hold true. It was shown however, through an example that the stability boundary may still be composed solely of the corresponding stable manifolds and that if the shadowing method is applied it would work satisfactorily.

The results from the analysis of transient stability for two large-scale realistic power system models were presented in Chapter 7. In the seven of the nine cases in which the exit point method was applied failure occurred. When the shadowing technique was applied the controlling UEP was determined in all nine cases. In each case with the controlling UEP that was determined by the shadowing technique the transient stability assessment obtained from the TEF method compared satisfactorily with time simulation. In ever case analyzed it was shown that the finite sequence of points produced by the shadowing technique seemed to numerically converge to the controlling UEP.

BIBLIOGRAPHY

[1] *Annual Data Summary Report for the Regional Councils of NERC.* Princeton, New Jersey: North American Electric Reliability Council, 1985.

[2] *Proposed Terms and Definitions for Power System Stability*, by the Task Force on Terms and Definitions, System Dynamic Performance Subcommittee, Power System Engineering Committee PES. *IEEE Transactions on Power Apparatus and Systems*, Vol. PAS-101, No. 7 (July 1982): 1894-1898.

[3] LaSalle, J. and S. Lefschetz. *Stability by Liapunov's Direct Method with Applications*. Academic Press, New York, 1961.

[4] Kimbark, E. W. *Power System Stability. Vol. I.* John Wiley & Sons, Inc., New York, 1948.

[5] *Criteria of Stability of Electric Power Systems.* A report published by the all Union Institute of Scientific and Technological Information and the Academy of Sciences of the USSR Electric Technology and Electric Power Series, Moscow, USSR, 1971.

[6] Magnusson, P. C. "Transient Energy Method of Calculating Stability." *AIEE Transactions*, Vol. 66 (1947): 747-755.

[7] Aylett, P. D. "The Energy Integral Criterion of Transient Stability Limits of Power Systems." *Proceedings of the IEE*, Vol. 105 (Part C), (1958): 527-536.

[8] Tavora, C. J. and O. J. M. Smith. "Characterization of Equilibrium and Stability in Power Systems." *IEEE Transactions on Power Apparatus and Systems*, Vol. PAS-91, No. 3 (May 1972): 1127-1130.

[9] Gless, G. E. "Direct Method of Lyapunov Applied to Transient Power System Stability." *IEEE Transactions on Power Apparatus and Systems,* Vol. PAS-85, No. 2 (February 1966): 159-168.

[10] El-Abiad, A. H. and K. Nagappan. "Transient Stability Regions of Multimachine Power Systems." *IEEE Transactions on Power Apparatus and Systems,* Vol. PAS-85, No. 2 (February 1966): 169-179.

[11] Gupta, C. L. and A. H. El-Abiad. "Determination of the Closest Unstable Equilibrium State for Lyapunov Methods in Transient Stability Studies." *IEEE Transactions on Power Apparatus and Systems,* Vol. PAS-94, No. 5 (September 1976): 1699-1712.

[12] Sastry, V. R. "Validity of Neglecting Transfer Conductances in Transient Stability Studies." *Proceedings of the IEE*, Vol. 120 (Part C) (1973).

[13] Willems, J. L. "Direct Methods for Transient Stability Studies in Power System Analysis." *IEEE Transactions on Automatic Control*, Vol. AC-16, No. 4 (August 1971): 332-344.

[14] Uemura, K., J. Matsuki, I. Yamada, and T. Tsuji. "Approximation of an Energy Function in Transient Stability Analysis of Power Systems," *Electrical Engineering in Japan*, Vol. 92, No. 6, (November/December 1972): 96-100.

[15] Athay, T., V. Sherket, R. Podmore, S. Virmani and C. Puech. "Transient Energy Stability Analysis." *Proc. Conference on Systems Engineering for Power: Emergency Operating State Control*, Davos, Switzerland, 1979. U.S. Dept. of Energy Publication No. CONF-790904-PL, Section IV.

[16] Kakimoto, N., Y. Ohsawa, and M. Hayashi. "Transient Stability Analysis of Electric Power Systems via Lur'e Type Lyapunov Function." *Proceedings of IEE Japan*, Vol. 98 (May/June 1978): 63-78.

[17] Fouad, A. A. and S. E. Stanton. "Transient Stability Analysis of a Multimachine Power System. Part I: Investigation of System Trajectory; and Part II: Critical Transient Energy." *IEEE Transactions on Power Apparatus and Systems,* Vol. PAS-100, No. 8 (August 1981): 3408-3424.

[18] Fouad, A. A., K. C. Kruempel, K. R. C. Mamandur, S. E. Stanton, M. A. Pai, and V. Vittal. "Transient Stability Margin as a Tool for Dynamic Security Assessment." *EPRI Report EL-1755,* March, 1981.

[19] Fouad, A. A., V. Vittal, and T. Oh. "Critical Energy for Transient Stability Assessment of a Multimachine Power System." *IEEE Transactions on Power Apparatus and Systems,* Vol. PAS-103, No. 8 (1984): 2199-2206.

[20] Chiang, H. D., F. F. Wu, and P. P. Varaiya. "Foundations of Direct Methods for Power System Transient Stability Analysis." *IEEE Transactions on Circuits and Systems*, Vol. CAS-34, No. 2 (February 1987): 160-173.

[21] Chiang, H. D., F. F. Wu, and P. P. Varaiya. "Foundations of the Potential Energy Boundary Surface Method for Power System Transient Stability Analysis." *IEEE Transactions on Circuits and Systems*, Vol. CAS-35, No. 6 (June 1988): 712-728.

[22] Chiang, H. D., F. F. Wu, and P. P. Varaiya. "A BCU Method for Direct Analysis of Power System Transient Stability." *IEEE PS Winter Power Meeting, Paper 91SM423-4PWRS.*

[23] Vittal, V. "Power System Transient Stability Using the Critical Energy of Individual Machines." Ph.D. Dissertation, Iowa State University, Ames, Iowa, 1982.

[24] Michel, A. N., A. A. Fouad, and V. Vittal. "Power System Transient Stability Using Individual Machine Energy Functions." *IEEE Transactions on Power Apparatus and Systems,* Vol. PAS-30, No. 5 (May 1983): 266-276.

[25] Fouad, A. A. "Stability Theory - Criteria for Transient Stability." *Proceedings of the Engineering Foundation Conference on Systems Engineering for Power: Status and Prospects*, Henniker, New Hampshire, 1975.

[26] Ribbens-Pavella M. and F. J. Evans. "Direct Methods for Studying Dynamics of Large-scale Electric Power Systems - A Survey." *Automatica,* Vol. 21, No. 1 (1985): 1-21.

[27] Fouad, A. A., and V. Vittal. *Power System Transient Stability Analysis Using the Transient Energy Function Method.* Prentice Hall, Englewood Cliffs, New Jersey, 1991.

[28] Pai, M.A. *Energy Function Analysis for Power System Stability*. Kluwer Academic Publishers, Norwell, Massachusetts, 1989.

[29] Pai, M.A. *Power System Stability Analysis by the Direct Method of Lyapunov*. North-Holland Publishing, New York, 1981.

[30] Anderson, P. M., and A. A. Fouad. *Power System Control and Stability Vol. 1.* The Iowa State University Press, Ames, Iowa, 1977.

[31] Sastry, V. R. and P. G. Murthy, "Derivation of Completely Controllable and Completely Observable State Models for Multimachine Power System Stability Studies." *International Journal of Control*, Vol. 16 No. 4 (1972): 777-788.

[32] Hirsh, M. W. and S. Smale. *Differential Equations, Dynamical Systems, and Linear Algebra*. Academic Press Inc., San Diego, California, 1974.

[33] Guckenheimer, J. and P. Holmes. *Nonlinear Oscillations, Dynamical Systems, and Bifurcations of Vector Fields*. Springer-Verlag New York Inc., New York, 1983.

[34] Wiggins S. *Introduction to Applied Nonlinear Dynamical Systems, and Chaos*. Springer-Verlag New York Inc., New York, 1990.

[35] Zaborsky, J., G. Huang, B. Zheng and T. Leung. "On the Phase Portrait of a Class of Large Nonlinear Dynamic Systems such as the Power System." *IEEE Transactions on Automatic Control*, Vol. AC-33, No. 1 (January 1988): 4-15.

[36] Zaborsky, J., G. Huang and B. Zheng. "A Counterexample on a Theorem by Tsolas et. al. and an Independent Result by Zaborsky et. al." *IEEE Transactions on Automatic Control*, Vol. AC-33, No. 3 (March 1988): 316-317.

[37] Fleming, W. H. *Functions of Several Variables.* Springer-Verlag New York Inc., New York, 1977.

[38] Murdoch D. C. *Linear Algebra.* John Wiley and Sons Inc., New York, 1970.

[39] Berggren, B. and G. Andersson. "On the Nature of Unstable Equilibrium Points in Power Systems." *IEEE Transactions on Power Systems*, Vol. PS-8, No. 2 (May 1993): 738-745.

[40] Wolfram, S. *Mathematica: A System for Doing Mathematics by Computer*. Addison-Wesley Publishing Company Inc., Redwood City, California, 1991.

[41] Arrowsmith, D. K. and C. M. Place. *An Introduction to Dynamical Systems*. Cambridge University Press, Cambridge, England, 1991.

[42] Hale, J. K.. *Oscillations in Nonlinear Systems.* McGraw-Hill Book Company, Inc., New York, 1963.

[43] Berger, M and B. Gostiaux *Differential Geometry: Manifolds, Curves, and Surfaces.* Springer-Verlag New York Inc., New York, 1988.

[44] Smith K. T. *Primer of Modern Analysis.* Springer-Verlag New York Inc., New York, 1983.

[45] Boothby W. M. *An Introduction to Differentiable Manifolds and Riemannian Geometry.* Academic Press, Inc. San Diego, California, 1986.

[46] Kahn D. W. *Introduction to Global Analysis.* Academic Press, Inc. San Diego, California, 1980.

[47] Chiang, H. D., M. W. Hirsh and F. F. Wu. "Stability Regions of Nonlinear Autonomous Dynamical Systems." *IEEE Transactions on Circuits and Systems*, Vol. CAS-33, No. 1 (Jan. 1988): 16-27.

[48] Protter M. H., and C. B. Morrey. *A First Course in Real Analysis.* Springer-Verlag New York Inc., New York, 1977.

[49] Chiang, H. D. "Study of the Existence of Energy Functions for Power Systems with Losses." *IEEE Transactions on Circuits and Systems*, Vol. CAS-36, No. 11 (Nov. 1989): 1423-1429.

[50] Abed, E, H., and P. P. Varaiya. "Nonlinear Oscillations in Power System." *International Journal of Electric Power and Eenrgy Systems*, Vol. 6, (1984): 37-43.

[51] Alexander J. C. "Oscillatory Solutions of a Model of Nonlinear Swing Equations." *International Journal of Electric Power and Eenrgy Systems*, Vol. 8, (1986): 130-136.

[52] Tavora, C. J. and O. J. M. Smith. "Equilibrium Analysis of Power Ssytems." *IEEE Transactions on Power Apparatus and Systems*, Vol. PAS-91, No. 3 (May 1972): 1127-1130.

[53] Arapostathis, A., S. S. Sastry, and P. P. Varaiya, "Global Analysis of Swing Dynamics." *IEEE Transactions on Circuits and Systems*, Vol. CAS-29, No. 10 (Oct. 1982): 673-679.

[54] Varaiya, P. P., H. D. Chiang and F. F. Wu. "Bifurcation and Chaos in Power Systems: A Survey." *EPRI Report TR-100834,* August, 1992.

[55] Perko, L. *Differential Equations, and Dynamical Systems*. Springer-Verlag New York Inc., New York, 1991.

[56] Vittal, V. . "IEEE Test Committee Report: Transient Stability Test Systems for Direct Stability Methods." *IEEE Transactions on Power Systems*, Vol. PS-7, No. 1 (Feb. 1992): 37-44.

[57] Treinen, R. "Application of the Transient Energy Function Method to the Northern States Power System." Master's Thesis, Iowa State University, Ames, Iowa, 1991.

[58] Gear, C. W. *Numerical Intial Value Problems in Ordinary Differential Equations.* Prentice-Hall Inc., Englewood Cliffs, New Jersey, 1971.

[59] Hindmarsh, A. C. *LSODE/ODEPACK (1987).* Computing and Mathematics Research Div., 1-316 Lawrence Livermore National Laboratory, Livermore, California.

[60] Hindmarsh, A. C. "ODEPACK: a Systematized Collection of ODE Solvers." *Scientific Computing (Stepleman, R. S. Editor)*, North-Holland Publishing, Amsterdam, 1983, 55-64.

[61] Electric Power Research Institute. *Extended Transient Mid-Term Stability Package version 3.0, 1992.* EPRI Research Project 1208-9. Palo Alto, California.

[62] Strang G. *Linear Algebra and Its Applications.* Academic Press, Inc. New York, 1976.

[63] de Pillis J. *Linear Algebra.* Holt, Rinehart and Winston, Inc. New York, 1969.

[64] Chiang, H. D. and F. F. Wu. "Stability of Nonlinear Systems Described by a Second Order Vector Differential Equation." *IEEE Transactions on Circuits and Systems*, Vol. CAS-35, No. 6 (June 1988): 703-711.

[65] Winmmer, H. K. "Inertia Theorems for Matrices, Controllability, and Linear Vibrations." *Linear Algebra and Its Applications*, Vol. 8 (1974): 337-343.

[66] Berggren, B. "On the Analysis of Angle Stability in Power Systems by Utilization of the Transient Energy Function Method." Ph.D. Dissertation, Royal Institute of Technology, Stockholm, Sweden, 1992.

ACKNOWLEDGMENTS

I would like to thank my major professor Dr. V. Vittal for his support and supervision. I thank Dr. W Kliemann for his mathematical expertise and for the time he took to spend with me. I am also thankful to the other members of my committee: A. A. Fouad, J. D. McCalley and M. Khammash for there helpful comments.

I would also like to like to thank members of my family and other fellow graduate students such as Byongjun Lee and Vamsi Chadalavada for many hours of interesting conversation on power system topics.

This work was funded by the Electric Power Research Center at Iowa State University and I would like to thank the center director J. Lamont and everyone involved for there tireless effort in securing funds to support graduate students.

APPENDIX A

A.1 Derivation of the Swing System with Damping

In this section the derivation of the swing equations in the center of inertia reference frame is given. Equations similar to equations (2.1) are repeated here and note that damping is added and there are no transfer conductances.

$$M_i \dot{\omega}_i = P_i - P_{ei} - D_i \omega_i \qquad \text{(A.1.1)}$$

$$\dot{\delta}_i = \omega_i \qquad i = 1, 2, \ldots, n$$

where

$$P_i = P_{mi} - E_i^2 G_{ii}$$

$$P_{ei} = \sum_{\substack{j=1 \\ j \neq i}}^{n} C_{ij} \sin\left(\delta_i - \delta_j\right)$$

Note that everything in this section is defined in Chapter 2, however, there are a few differences as listed below.

D_i - damping constant, $D_i > 0$.
ω_i - machine rotor speed deviation from synchronous speed.

Uniform damping is assumed, so that for every machine in the system

$$\frac{D_i}{M_i} = c$$

where c is a constant.

Following the steps as shown in Chapter 2, equations (A.1.1) in the COI variables are

$$M_i \dot{\varpi}_i = P_i - P_{ei} - D_i \omega_i - \frac{M_i}{M_T} \sum_{j=1}^{n} (P_j - P_{ej} - D_j \omega_j) \qquad \text{(A.1.2a)}$$

$$\dot{\theta}_i = \varpi_i \qquad \text{(A.1.2b)}$$

Equation (A.1.2a) can be simplified.

$$\varpi_i = \omega_i - \omega_o \Rightarrow \omega_i = \varpi_i + \omega_o$$

$$M_i \dot{\varpi}_i = P_i - P_{ei} - D_i \varpi_i - D_i \omega_o$$

$$- \frac{M_i}{M_T} \sum_{j=1}^{n} (P_j - P_{ej}) + \frac{M_i}{M_T} \sum_{j=1}^{n} D_j \varpi_j + \frac{M_i}{M_T} \sum_{j=1}^{n} D_j \omega_o \qquad \text{(A.1.3)}$$

Three of the four terms in equation (A.1.3) associated with damping can be eliminated.

$$- D_i \omega_o = - M_i c \omega_o$$

$$\frac{M_i}{M_T} \sum_{j=1}^{n} D_j \varpi_j = c \frac{M_i}{M_T} \sum_{j=1}^{n} M_j \varpi_j$$

$$\frac{M_i}{M_T} \sum_{j=1}^{n} D_j \omega_o = \omega_o \frac{M_i}{M_T} \sum_{j=1}^{n} c M_j = \omega_o M_i c$$

Since

$$\sum_{j=1}^{n} M_j \, \varpi_j = 0$$

Equation (A.1.2a) can now be written as

$$M_i \, \dot{\varpi}_i = P_i - P_{ei} - D_i \, \varpi_i - \frac{M_i}{M_T} \sum_{j=1}^{n} (P_j - P_{ej})$$

This equation can be further simplified since $C_{ij} = C_{ji}$ and $sin(\theta_i - \theta_j) = - sin(\theta_j - \theta_i)$, then

$$\frac{M_i}{M_T} \sum_{j=1}^{n} P_{ej} = \frac{M_i}{M_T} \sum_{j=1}^{n} \sum_{\substack{k=1 \\ k \neq j}}^{n} C_{jk} \, sin\left(\theta_j - \theta_k\right) = 0$$

Also, since there are no transfer conductances, the total power injected in to the system must be zero.

$$\sum_{i=1}^{n} P_i = 0$$

Equation (A.1.2) can then be written as

$$M_i \, \dot{\varpi}_i = P_i - P_{ei} - D_i \, \varpi_i$$

$$\dot{\theta}_i = \varpi_i \qquad\qquad i = 1, 2, \ldots, n\text{-}1$$

A.2.1 Derivation of $\dot{V}$ for the Swing System

The following section shows the derivation of

$$\dot{V} = \sum_{k=1}^{n-1} \left[\frac{\partial V}{\partial \theta_k} \dot{\theta}_k + \frac{\partial V}{\partial \varpi_k} \dot{\varpi}_k \right] \tag{A.1}$$

The energy function from Chapter 3 is

$$\begin{aligned} V = & \frac{1}{2} \sum_{i=1}^{n-1} M_i \varpi_i^2 + \frac{1}{2} \frac{1}{M_n} \left(\varpi_1 M_1 + \cdots + \varpi_{n-1} M_{n-1} \right)^2 \\ & - \sum_{i=1}^{n-1} P_i \left(\theta_i - \theta_i^s \right) + \frac{P_n}{M_n} \left(\left(\theta_1 - \theta_1^s \right) M_1 + \cdots + \left(\theta_{n-1} - \theta_{n-1}^s \right) M_{n-1} \right) \\ & - \sum_{i=1}^{n-1} \sum_{j=i+1}^{n-1} C_{ij} \left(\cos \theta_{ij} - \cos \theta_{ij}^s \right) \\ & - \sum_{i=1}^{n-1} C_{in} \cos \left(\theta_i + \frac{1}{M_n} \left(\theta_1 M_1 + \cdots + \theta_{n-1} M_{n-1} \right) \right) \\ & + \sum_{i=1}^{n-1} C_{in} \cos \left(\theta_i^s + \frac{1}{M_n} \left(\theta_1^s M_1 + \cdots + \theta_{n-1}^s M_{n-1} \right) \right) \end{aligned} \tag{A.2}$$

The derivation of (A.1) will be put into three subsections,

<u>Subsection 1</u>

Derivation of

$$\frac{\partial V}{\partial \theta_k} \quad k \in [1, \cdots, n-1]$$

The terms associated with θ^s in equation (A.2) are constant so the derivation turns into

$$\frac{\partial V}{\partial \theta_k} = \frac{\partial}{\partial \theta_k}\left[- \sum_{i=1}^{n-1} P_i\, \theta_i + \frac{P_n}{M_n}\left(\theta_1 M_1 + \cdots + \theta_{n-1} M_{n-1}\right)\right]$$

$$+ \frac{\partial}{\partial \theta_k}\left[- \sum_{i=1}^{n-1} \sum_{j=i+1}^{n-1} C_{ij} \cos\, \theta_{ij}\right]$$

$$+ \frac{\partial}{\partial \theta_k}\left[- \sum_{i=1}^{n-1} C_{in} \cos\left(\theta_i + \frac{1}{M_n}\left(\theta_1 M_1 + \cdots + \theta_{n-1} M_{n-1}\right)\right)\right]$$

Term by term

$$\frac{\partial}{\partial \theta_k}\left[- \sum_{i=1}^{n-1} P_i\, \theta_i + \frac{P_n}{M_n}\left(\theta_1 M_1 + \cdots + \theta_{n-1} M_{n-1}\right)\right] = - P_k + \frac{M_k}{M_n} P_n$$

$$\frac{\partial}{\partial \theta_k}\left[- \sum_{i=1}^{n-1} C_{in} \cos\left(\theta_i + \frac{1}{M_n}\left(\theta_1 M_1 + \cdots + \theta_{n-1} M_{n-1}\right)\right)\right]$$

$$= \frac{\partial}{\partial \theta_k}\left[- \sum_{i=1}^{k-1} C_{in} \cos\left(\theta_i + \frac{1}{M_n}\left(\theta_1 M_1 + \cdots + \theta_{n-1} M_{n-1}\right)\right)\right]$$

$$+ \frac{\partial}{\partial \theta_k} C_{kn} \cos\left(\theta_k + \frac{1}{M_n}\left(\theta_1 M_1 + \cdots + \theta_{n-1} M_{n-1}\right)\right)$$

$$+ \frac{\partial}{\partial \theta_k}\left[- \sum_{i=k+1}^{n-1} C_{in} \cos\left(\theta_i + \frac{1}{M_n}\left(\theta_1 M_1 + \cdots + \theta_{n-1} M_{n-1}\right)\right)\right]$$

$$= \frac{M_k}{M_n} \sum_{i=1}^{k-1} C_{in} \sin\left(\theta_i + \frac{1}{M_n}\left(\theta_1 M_1 + \cdots + \theta_{n-1} M_{n-1}\right)\right)$$

$$+ \left(1 + \frac{M_k}{M_n}\right) C_{kn} \sin\left(\theta_k + \frac{1}{M_n}\left(\theta_1 M_1 + \cdots + \theta_{n-1} M_{n-1}\right)\right)$$

$$+\frac{M_k}{M_n}\sum_{i=k+1}^{n-1} C_{in}\sin\left(\theta_i+\frac{1}{M_n}\left(\theta_1M_1+\cdots+\theta_{n-1}M_{n-1}\right)\right)$$

$$=\frac{M_k}{M_n}\sum_{i=1}^{n-1} C_{in}\sin\left(\theta_i+\frac{1}{M_n}\left(\theta_1M_1+\cdots+\theta_{n-1}M_{n-1}\right)\right)$$

$$+C_{kn}\sin\left(\theta_k+\frac{1}{M_n}\left(\theta_1M_1+\cdots+\theta_{n-1}M_{n-1}\right)\right)$$

$$=-\frac{M_k}{M_n}\sum_{i=1}^{n-1} C_{ni}\sin\left(-\frac{1}{M_n}\left(\theta_1M_1+\cdots+\theta_{n-1}M_{n-1}\right)-\theta_i\right)$$

$$+C_{kn}\sin\left(\theta_k+\frac{1}{M_n}\left(\theta_1M_1+\cdots+\theta_{n-1}M_{n-1}\right)\right)$$

$$\frac{\partial}{\partial\theta_k}\left[-\sum_{i=1}^{n-1}\sum_{j=i+1}^{n-1} C_{ij}\cos\theta_{ij}\right]$$

$$=\frac{\partial}{\partial\theta_k}\left[-\sum_{i=1}^{k-1}\left[\sum_{j=i+1}^{k-1} C_{ij}\cos\left(\theta_i-\theta_j\right)+C_{ik}\cos\left(\theta_i-\theta_k\right)\right]\right]$$

$$+\frac{\partial}{\partial\theta_k}\left[-\sum_{i=1}^{k-1}\sum_{j=k+1}^{n-1} C_{ij}\cos\left(\theta_i-\theta_j\right)\right]$$

$$+\frac{\partial}{\partial\theta_k}\left[-\sum_{j=k+1}^{n-1} C_{kj}\cos\left(\theta_k-\theta_j\right)\right]$$

$$+\frac{\partial}{\partial\theta_k}\left[-\sum_{i=k+1}^{n-1}\sum_{j=i+1}^{n-1} C_{ij}\cos\left(\theta_i-\theta_j\right)\right]$$

The individual terms are

$$\frac{\partial}{\partial\theta_k}\left[-\sum_{i=1}^{k-1}\sum_{j=i+1}^{k-1} C_{ij}\cos\left(\theta_i-\theta_j\right)\right]=0$$

$$\frac{\partial}{\partial\theta_k}\left[-\sum_{i=1}^{k-1} C_{ik}\cos\left(\theta_i-\theta_k\right)\right]=-\sum_{i=1}^{k-1} C_{ik}\sin\left(\theta_i-\theta_k\right)$$

$$\frac{\partial}{\partial\theta_k}\left[-\sum_{i=1}^{k-1}\sum_{j=k+1}^{n-1} C_{ij}\cos\left(\theta_i-\theta_j\right)\right]=0$$

$$\frac{\partial}{\partial\theta_k}\left[-\sum_{j=k+1}^{n-1} C_{kj}\cos\left(\theta_k-\theta_j\right)\right]=\sum_{j=k+1}^{n-1} C_{kj}\sin\left(\theta_k-\theta_j\right)$$

$$\frac{\partial}{\partial\theta_k}\left[-\sum_{i=k+1}^{n-1}\sum_{j=i+1}^{n-1} C_{ij}\cos\left(\theta_i-\theta_j\right)\right]=0$$

Therefore,

$$\frac{\partial}{\partial\theta_k}\left[-\sum_{i=1}^{n-1}\sum_{j=i+1}^{n-1} C_{ij}\cos\,\theta_{ij}\right]$$

$$=-\sum_{i=1}^{k-1} C_{ik}\sin\left(\theta_i-\theta_k\right)+\sum_{j=k+1}^{n-1} C_{kj}\sin\left(\theta_k-\theta_j\right)$$

$$=\sum_{i=1}^{k-1} C_{ki}\sin\left(\theta_k-\theta_i\right)+\sum_{i=k+1}^{n-1} C_{ki}\sin\left(\theta_k-\theta_i\right)$$

$$=\sum_{\substack{i=1\\ i\neq k}}^{n-1} C_{ki}\sin\left(\theta_k-\theta_i\right)$$

Combining all terms

$$\frac{\partial V}{\partial \theta_k} = - P_k + \frac{M_k}{M_n} P_n$$

$$- \frac{M_k}{M_n} \sum_{i=1}^{n-1} C_{ni} \sin \left(- \frac{1}{M_n} \left(\theta_1 M_1 + \cdots + \theta_{n-1} M_{n-1} \right) - \theta_i \right)$$

$$+ C_{kn} \cos \left(\theta_k + \frac{1}{M_n} \left(\theta_1 M_1 + \cdots + \theta_{n-1} M_{n-1} \right) \right)$$

$$+ \sum_{\substack{i=1 \\ i \neq k}}^{n-1} C_{ki} \sin \left(\theta_k - \theta_i \right)$$

$$\frac{\partial V}{\partial \theta_k} = - P_k + \sum_{\substack{i=1 \\ i \pi k}}^{n} C_{ki} \sin \left(\theta_k - \theta_i \right)$$

$$+ \frac{M_k}{M_n} \left[P_n - \sum_{i=1}^{n-1} C_{ni} \sin \left(- \frac{1}{M_n} \left(\theta_1 M_1 + \cdots + \theta_{n-1} M_{n-1} \right) - \theta_i \right) \right]$$

g_i as defined in Section 3.1 can be used here and the above can be written as

$$\frac{\partial V}{\partial \theta_k} = - g_k + \frac{M_k}{M_n} g_n$$

However, g_n is defined by equation (3.7) so the above can be written as

$$\frac{\partial V}{\partial \theta_k} = - g_k - \frac{M_k}{M_n} (g_1 + \cdots + g_{n-1}) \qquad \text{(A.3)}$$

$$\frac{\partial V}{\partial \theta_k} = - \left(1 + \frac{M_k}{M_n} \right) g_k - \frac{M_k}{M_n} (g_1 + \cdots + g_{k-1} + g_{k+1} + \cdots + g_{n-1})$$

Subsection 2

Derivation of

$\frac{\partial V}{\partial \varpi_k}$ $k \in [1, \cdots, n\text{-}1]$

$$\frac{\partial}{\partial \varpi_k}\left[\frac{1}{2}\sum_{i=1}^{n-1} M_i\,\varpi_i^2 + \frac{1}{2}\frac{1}{M_n}\left(\varpi_1 M_1 + \cdots + \varpi_{n-1}M_{n-1}\right)^2\right]$$

$$= M_k\varpi_k + \frac{M_k}{M_n}\left(\varpi_1 M_1 + \cdots + \varpi_{n-1}M_{n-1}\right)$$

$$\frac{\partial V}{\partial \varpi_k} = M_k\varpi_k + \frac{M_k}{M_n}\left(\varpi_1 M_1 + \cdots + \varpi_{n-1}M_{n-1}\right) \qquad \text{(A.4)}$$

Subsection 3

Derivation of

$\dot{\varpi}_k$ $k \in [1, \cdots, n\text{-}1]$

$$\dot{\varpi}_k = \frac{h_k}{M_k} = \frac{g_k - D_k\,\varpi_k}{M_k} \qquad \text{(A.5)}$$

The total time derivative can now be written as

$$\dot{V} = \sum_{i=1}^{n-1}\left[-g_i - \frac{M_i}{M_n}\left(g_1 + \cdots + g_{n-1}\right)\right]\varpi_i$$

$$+ \sum_{i=1}^{n-1} \left[M_i \varpi_i + \frac{M_i}{M_n} \left(\varpi_1 M_1 + \cdots + \varpi_{n-1} M_{n-1} \right) \right] \frac{g_i - D_i \varpi_i}{M_i} \qquad \text{(A.6)}$$

Equation (A.6) can be put into a more convenient vector - matrix notation.

$$\dot{V} = \frac{\partial V}{\partial \theta} \cdot \dot{\theta} + \frac{\partial V}{\partial \varpi} \cdot \dot{\varpi}$$

$$\dot{V} = \left[- M^{\theta} g \right]^T \varpi + \left[M^{\varpi} \varpi \right]^T \left[M^{-1} h \right]$$

$$\dot{V} = \left[- M^{\theta} g \right]^T \varpi + \left[M^{\varpi} \varpi \right]^T M^{-1} \left[g - D \varpi \right]$$

where

$$M^{-1} = \begin{bmatrix} \frac{1}{M_1} & 0 & 0 \\ 0 & \ddots & 0 \\ 0 & 0 & \frac{1}{M_{n-1}} \end{bmatrix}$$

$$D = \begin{bmatrix} D_1 & 0 & 0 \\ 0 & \ddots & 0 \\ 0 & 0 & D_{n-1} \end{bmatrix}$$

$$\frac{\partial V}{\partial \theta} = \begin{bmatrix} \frac{\partial V}{\partial \theta_1} & \cdots & \frac{\partial V}{\partial \theta_{n-1}} \end{bmatrix}^T$$

$$\frac{\partial V}{\partial \theta} = - \begin{bmatrix} 1 + \frac{M_1}{M_n} & \cdots & \frac{M_1}{M_n} \\ \vdots & \ddots & \vdots \\ \frac{M_{n-1}}{M_n} & \cdots & 1 + \frac{M_{n-1}}{M_n} \end{bmatrix} \begin{bmatrix} g_1 \\ \vdots \\ g_{n-1} \end{bmatrix} = - M^{\theta} g \qquad \text{(A.7)}$$

The elements of M^{θ} can be defined as

$$M_{ij}^{\theta} = \begin{cases} \left(1 + \dfrac{M_i}{M_n}\right) & \text{if } i = j \\ \dfrac{M_i}{M_n} & \text{if } i \neq j \end{cases}$$

$$\frac{\partial V}{\partial \varpi} = \left[\frac{\partial V}{\partial \varpi_1} \cdots \frac{\partial V}{\partial \varpi_{n-1}}\right]^T$$

$$\frac{\partial V}{\partial \varpi} = \begin{bmatrix} M_1\left(1 + \dfrac{M_1}{M_n}\right) & \cdots & \dfrac{M_1 M_{n-1}}{M_n} \\ \vdots & \ddots & \vdots \\ \dfrac{M_{n-1} M_1}{M_n} & \cdots & M_{n-1}\left(1 + \dfrac{M_{n-1}}{M_n}\right) \end{bmatrix} \begin{bmatrix} \varpi_1 \\ \vdots \\ \varpi_{n-1} \end{bmatrix} = M^{\varpi}\,\varpi$$

The elements of M^{ϖ} can be defined as

$$M_{ij}^{\varpi} = \begin{cases} M_i\left(1 + \dfrac{M_i}{M_n}\right) & \text{if } i = j \\ \dfrac{M_i M_j}{M_n} & \text{if } i \neq j \end{cases}$$

The continuation of the derivation in vector-matrix form is

$$\dot{V} = \left[-M^{\theta} g\right]^T \varpi + \left[M^{\varpi}\varpi\right]^T \left[M^{-1} g\right] - \left[M^{\varpi}\varpi\right]^T \left[M^{-1} D\,\varpi\right]$$

$$\dot{V} = \left[-M^{\theta} g\right]^T \varpi + \left[M^{-1} g\right]^T \left[M^{\varpi}\varpi\right] - \left[M^{\varpi}\varpi\right]^T \left[M^{-1} D\,\varpi\right]$$

$$\dot{V} = g^T\left[-M^{\theta}\right]^T \varpi + g^T\left[M^{-1}\right]^T M^{\varpi}\varpi - \varpi^T\left[\left[M^{\varpi}\right]^T M^{-1} D\right]\varpi$$

$$\dot{V} = g^T\left[\left[-M^{\theta}\right]^T + \left[M^{-1}\right]^T M^{\varpi}\right]\varpi - \varpi^T\left[\left[M^{\varpi}\right]^T M^{-1} D\right]\varpi$$

Note that since M is diagonal

$$\left[M^{-1}\right]^T = M^{-1}$$

$$\dot{V} = g^T\left[\left[-M^{\theta}\right]^T + M^{-1}\,M^{\varpi}\right]\varpi - \varpi^T\left[\left[M^{\varpi}\right]^T M^{-1}\,D\right]\varpi$$

$$-\left[M^{\theta}\right]^T_{ij} = \begin{cases} -\left(1+\dfrac{M_i}{M_n}\right) & \text{if } i=j \\ -\dfrac{M_j}{M_n} & \text{if } i\neq j \end{cases}$$

$$\left[M^{-1}\,M^{\varpi}\right]_{ij} = \begin{cases} \dfrac{1}{M_i}M_i\left(1+\dfrac{M_i}{M_n}\right) = \left(1+\dfrac{M_i}{M_n}\right) & \text{if } i=j \\ \dfrac{1}{M_i}\dfrac{M_i\,M_j}{M_n} = \dfrac{M_j}{M_n} & \text{if } i\neq j \end{cases}$$

Therefore, if terms of these matrices are added

$$\left[\left[-M^{\theta}\right]^T + M^{-1}\,M^{\varpi}\right] = 0$$

The time derivative simplifies to

$$\dot{V} = -\varpi^T\left[\left[M^{\varpi}\right]^T M^{-1}\,D\right]\varpi \qquad \text{(A.8)}$$

Define

$$M^{\upsilon} = \left[\left[M^{\varpi}\right]^T M^{-1}\,D\right]$$

Equation (A.8) becomes

$$\dot{V} = -\varpi^T\,M^{\upsilon}\,\varpi \qquad \text{(A.9)}$$

The matrix M^{υ} has the following form

$$M^v = \begin{bmatrix} D_1\left(1+\frac{M_1}{M_n}\right) & \cdots & \frac{M_1 D_{n-1}}{M_n} \\ \vdots & \ddots & \vdots \\ \frac{M_{n-1} D_1}{M_n} & \cdots & D_{n-1}\left(1+\frac{M_{n-1}}{M_n}\right) \end{bmatrix} \quad \text{(A.10)}$$

The elements of M^v are

$$M^v_{ij} = \begin{cases} D_i\left(1+\frac{M_i}{M_n}\right) & \text{if } i=j \\ \frac{M_i D_j}{M_n} & \text{if } i \neq j \end{cases}$$

A.2.2 Derivation of the Negative Definiteness of $\dot{V}$ for the Swing System

It is shown in this section that

$$\dot{V} = -\, v^T M^v v < 0 \quad \forall v \neq 0 \quad \text{(A.11)}$$

This can be shown by showing that M^v is a positive definite matrix [62].

Property A.1.1

The matrix M^θ is positive definite.

Proof:

In order to show this it must be shown that

$$x^T M^\theta x > 0 \quad \forall x \neq 0$$

Define the matrix M^r to be

$$M^r = \begin{bmatrix} M_1 & \cdots & M_1 \\ \vdots & \ddots & \vdots \\ M_{n-1} & \cdots & M_{n-1} \end{bmatrix}$$

so that

$$M^{\theta} = I + \frac{1}{M_n} M^r$$

and then

$$x^T M^{\theta} x = x^T I x + \frac{1}{M_n} x^T M^r x$$

Clearly

$$x^T I x > 0 \quad \forall x \neq 0$$

It can be shown that

$$\frac{1}{M_n} x^T M^r x \geq 0 \quad \forall x \neq 0$$

All of the columns of the matrix M^r are identical. This shows that this matrix has rank of one and will have all zero eigenvalues except one. This one non zero eigenvalue λ_{n-1} is

$$\lambda_{n-1} = \sum_{i=1}^{n-1} M_i > 0$$

If λ_{n-1} is in fact an eigenvalue of M^r then $det(M^r - \lambda_{n-1} I) = 0$.

$$M^r - \lambda_{n-1} I = \begin{bmatrix} -M_2 & \cdots & -M_{n-1} & \cdots & M_1 \\ \vdots & & & \ddots & \vdots \\ M_{n-1} & & & \cdots & -M_1 \cdots -M_{n-2} \end{bmatrix}$$

The elements of $[M^r - \lambda_{n-1} I]$ are

$$\left[M^r - \lambda_{n-1} I\right]_{ij} = \begin{cases} -\sum_{\substack{k=1 \\ k \neq i}}^{n-1} M_k & \text{if } i = j \\ M_i & \text{if } i \neq j \end{cases}$$

It is easily seen that the first row of $[M^r - \lambda_{n-1} I]$ is equal to the negative summation of row *2* through row *n-1*. Hence, $[M^r - \lambda_{n-1} I]$ is singular which implies that $\det(M^r - \lambda_{n-1} I) = 0$. It is seen from this that M^r is positive semi-definite [62] since the first $n-2$ eigenvalues are zero and the $(n-1)^{th}$ eigenvalue is positive.

Since

$$\frac{1}{M_n} x^T M^r x \geq 0 \quad \forall x \neq 0 \text{ and } x^T I x > 0 \quad \forall x \neq 0$$

then

$$x^T M^\theta x = x^T I x + \frac{1}{M_n} x^T M^r x > 0 \quad \forall x \neq 0$$

Which implies that M^θ is positive definite. ■

Property A.1.2
The matrix M^v is positive definite.

Proof:
Since the matrix M^θ is positive definite then the determinant of each principal minor of M^θ must be positive. This is a necessary and sufficient condition for a matrix to be positive definite [62].

There exist a theorem in [63 p. 313] that states if any column of a matrix A is multiplied by a constant α then the new determinant of this modified matrix is $\alpha \cdot det(A)$.

The matrix M^{θ} was defined earlier in this section, is given in (A.10) if the each element of the i^{th} column of matrix M^{θ} is multiplied by D_i then the resulting matrix is M^{v} as given in matrix equation (A.10).

For $i = [1, \ldots, n\text{-}1]$ multiply each element of the i^{th} column of the matrix M^{θ} by D_i. The resultant matrix as stated above is M^{v}. Since $D_i > 0$ the determinant of each principal minor of M^{v} remains positive which shows that M^{v} is positive definite. ■

A.3 Proof of Theorem 3.3.3

The proof is given in [64] but needs a slight modification. The proof is based on Theorem 1 from [65].

Let H be the symmetric matrix

$$H = \begin{bmatrix} J_{gs}^{-1} & 0 \\ 0 & -N^{-1} \end{bmatrix}$$

where $N = M^{\theta} M$ is symmetric and is shown below to be positive definite.

The matrix M^{θ} is defined in Section A.2.1 of this chapter and the matrix N can be written as

$$N_{ij} = \begin{cases} M_i \left(1 + \dfrac{M_i}{M_n}\right) & \text{if } i = j \\ \dfrac{M_i M_j}{M_n} & \text{if } i \neq j \end{cases}$$

This matrix can be manipulated to be

$$N = M + \frac{1}{M_n} M^T U M = M + M^{\theta}$$

where the matrix U is defined as

$$U_{ij} = \begin{cases} 1 \text{ if } i = j \\ 1 \text{ if } i \neq j \end{cases}$$

The matrix U has n-2 eigenvalues that are zero and one eigenvalue that is equal to $(n-1)$. Therefore it is easily seen that the matrix M^q is positive semi - definite and since the matrix M is positive definite the matrix N is also positive definite.

From Chapter 3 the Jacobian matrix of the swing system is

$$J_{ss} = \begin{bmatrix} 0 & I \\ M^{-1}\dfrac{\partial g}{\partial \theta} & -M^{-1}D \end{bmatrix}$$

and note that the lower left partition of the matrix J_{ss} is

$$M^{-1}\frac{\partial g}{\partial \theta}$$

Since

$$M^{-1} = N^{-1} M^{\theta}$$

the lower left partition can be written as

$$N^{-1} M^{\theta}\frac{\partial g}{\partial \theta} = N^{-1} J_{gs}$$

Substituting this into the J_{ss} matrix

$$J_{ss} H + H J_{ss}^{T} = \begin{bmatrix} 0 & -N^{-1} \\ N^{-1} & M^{-1} D N^{-1} \end{bmatrix} \begin{bmatrix} 0 & [N^{-1}]^{T} \\ -N^{-1} & N^{-1} D M^{-1} \end{bmatrix}$$

$$= \begin{bmatrix} 0 & 0 \\ 0 & M^{-1} D N^{-1} + N^{-1} D M^{-1} \end{bmatrix}$$

Theorem 1 from [65] states that if H is nonsingular and has no eigenvalues on the imaginary axis and if $[J_{ss} H + H J_{ss}^T]$ is positive semi - definite then $n_u(H) = n_u(J_{ss})$. Where $n_u(H)$ is the number of eigenvalues of H which have a positive real part. J_{gs}^{-1} is nonsingular since J_{gs} is nonsingular and $-N^{-1}$ is negative definite since N is positive definite. The eigenvalues of H are the eigenvalues of J_{gs}^{-1} together with the eigenvalues of $-N^{-1}$. The eigenvalues of $-N^{-1}$ all have negative real part since $-N^{-1}$ is negative definite. Also, a well known fact is that since J_{gs} is nonsingular $n_u(J_{gs}) = n_u(J_{gs}^{-1})$. Therefore, $n_u(H) = n_u(J_{gs})$.

In order to show that $[J_{ss} H + H J_{ss}^T]$ is positive semi - definite it must be shown that $[M^{-1} D N^{-1} + N^{-1} D M^{-1}]$ is positive semi - definite.

Let

$$M^D = [M^{-1} D N^{-1} + N^{-1} D M^{-1}]$$

An explicit form for N^{-1} can be found in [66] and is

$$N_{ij}^{-1} = \frac{1}{M_T} \begin{cases} \frac{M_T - M_i}{M_i} & \text{if } i = j \\ -1 & \text{if } i \neq j \end{cases}$$

Since uniform damping is assumed (i.e., $D_i/M_i = c$)

$$M^D = c N^{-1} + N^{-1} c = 2 c N^{-1}$$

Since N is positive definite and $c > 0$, $2 c N^{-1}$ is also positive definite. Therefore, $[J_{ss} H + H J_{ss}^T]$ is positive semi - definite and $n_u(H) = n_u(J_{gs})$. ■

A.4 Derivation of $dg((\theta^r - \theta^s)\,\alpha + \theta^s)/d\alpha$

From Section 3.1 the equation for g_i is

$$g_i(\theta) = P_i - \sum_{\substack{j=1 \\ j \neq i}}^{n-1} C_{ij} \sin\left(\theta_i - \theta_j\right)$$

$$- C_{in} \sin\left(\theta_i + \frac{1}{M_n}\left(M_1\theta_1 + M_2\theta_2 + \cdots + M_{n-1}\theta_{n-1}\right)\right)$$

Let

$$\Omega_{ij} = (\theta_i^r - \theta_j^r + \theta_i^s - \theta_j^s)$$

$$\Delta_i = (\theta_i^r - \theta_i^s) + \frac{1}{M_n} \sum_{j=1}^{n-1} M_j(\theta_j^r - \theta_j^s)$$

$$m^s = \frac{1}{M_n} \sum_{j=1}^{n-1} M_j\theta_j^s$$

Substituting $\theta = (\theta^r - \theta^s)\,\alpha + \theta^s$, $\alpha \geq 0$, the equation g_i becomes

$$g_i((\theta^r - \theta^s)\,\alpha + \theta^s) = P_i - \sum_{\substack{j=1 \\ j \neq i}}^{n-1} C_{ij} \sin\left(\Omega_{ij}\,\alpha + \theta_i^s - \theta_j^s\right)$$

$$- C_{in} \sin\left(\Delta_i\,\alpha + \theta_i^s + m^s\right)$$

The derivative with respect to α becomes

$$dg_i((\theta^r - \theta^s)\,\alpha + \theta^s)/d\alpha = - \sum_{\substack{j=1 \\ j \neq i}}^{n-1} \Omega_{ij}\, C_{ij} \cos\left(\Omega_{ij}\,\alpha + \theta_i^s - \theta_j^s\right)$$

$$- \Delta_i\, C_{in} \cos\left(\Delta_i\,\alpha + \theta_i^s + m^s\right)$$

APPENDIX B

B.1 Presentation of the 3-machine Power System

This section is a description of the 3-machine system which is taken from [30]. There is a small difference in that the bus numbering in this system is not the same as the bus numbering in the system in [30]. Figure B.1 is an one-line diagram of the 3-machine system. This system consists of 3 generators, 9 buses, 6 transmission lines, 3 transformers and 3 loads. The data for this system based on a system base of *100 MVA* is shown on the one-line diagram and is the base case of the system. The data that is present are

- line impedances in pu,
- line capactive charging suseptances in pu,
- transformer reactances in pu,
- real and reactive loads in pu,
- real and reactive generation in pu at the terminal of each generator,
- voltage magnitude in pu and angle in degrees at each bus. The voltages represent the system at equilibrium and are a result of a power flow calculation,
- buses 1 and 2 are PV buses and bus 3 is the slack bus.

Table B.1 contains generator data, namely the normalized inertia constant H, the corresponding M constant and the transient reactance x'_d; damping is not consisdered.

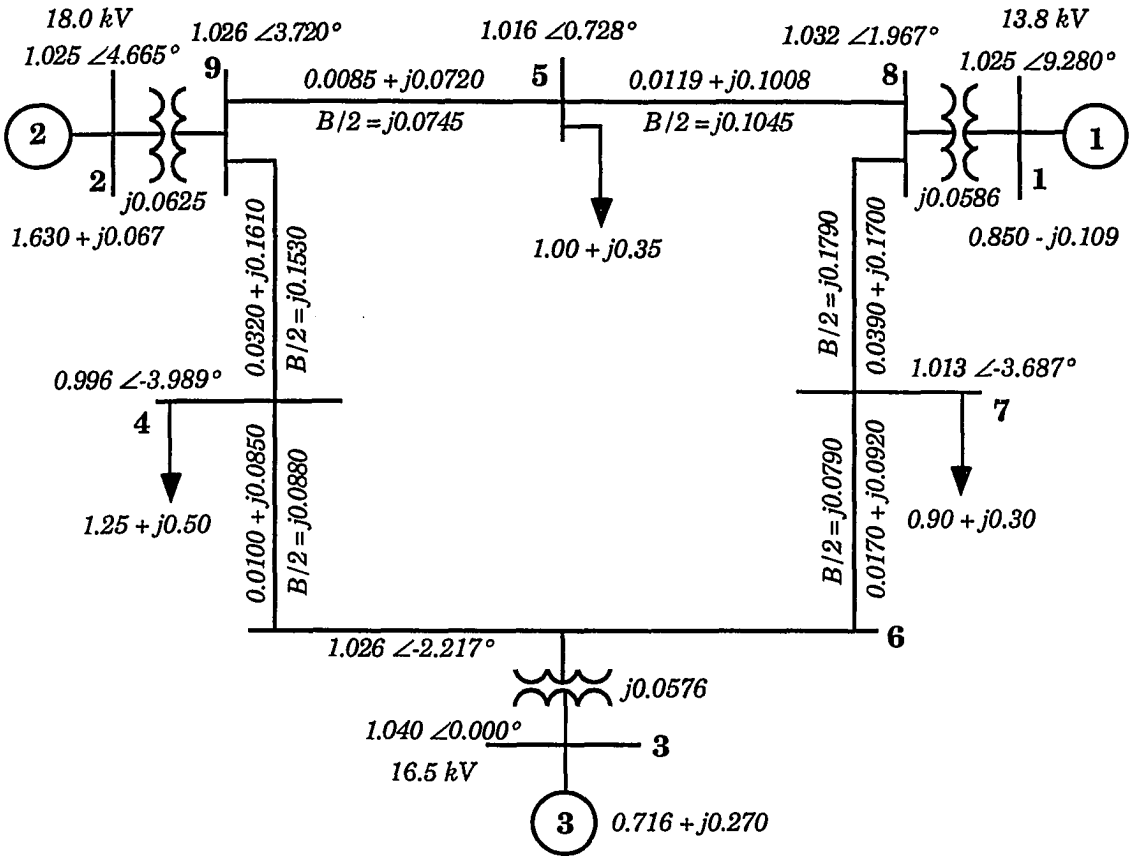

Figure B.1 One-line diagram for the base case of the 3-machine system

Table B.1 Machine data for the 3-machine system

Generator	H (seconds)	M (second^2)	x'_d (pu)
1	*3.01*	*0.0160*	*0.1813*
2	*6.40*	*0.0340*	*0.1198*
3	*23.64*	*0.1254*	*0.0608*

All values are based on a system base of *100 MVA*

The values of M are calculated on asystem frequency of *60 Hz*

B.2 Reduced 3-machine Power System

In this section the data for the reduced 3-machine system is presented. The 3-machine is reduced to the internal generator bus which is the fictitious bus behind the transient reactance x'_d. The internal generator voltage E_i can be calculated since the voltage and the real and reactive power at the generator terminal bus is known. The terminal buses in the system are buses 1, 2 and 3 and after the internal voltage is calculated the terminal bus is removed and the corresponing internal bus is given the same bus number. Table B.2 contains the values of the reduced admittance matrix (Y_{bus}) and these values are of the form $Y_{ij} = G_{ij} + jB_{ij}$. Table B.3 contains the values of the internal bus voltage of each generator. Tables B.4 and B.5 contain the values of $C_{ij} = E_iE_jB_{ij}$ and $D_{ij} = E_iE_jG_{ij}$ respectively.

Table B.2 Admittance matrix data for the base case of the reduced 3-machine system

Generator	1	2	3
1	*0.2770 - j2.3681*	*0.2133 + j1.0879*	*0.2069 + j1.2256*
2	*0.2133 + j1.0879*	*0.4200 - j2.7239*	*0.2871 + j1.5129*
3	*0.2069 + j1.2256*	*0.2871 + j1.5129*	*0.8455 - j2.9883*

All values are in pu

Table B.3 Internal generator voltages for the base case of the reduced 3-machine system

Generator	Voltage (pu)
1	$1.0170 \angle 13.1665°$
2	$1.0502 \angle 19.7317°$
3	$1.0566 \angle 2.2716°$

Table B.4 Values of C_{ij} for the base case of the reduced 3-machine system

Generator	1	2	3
1	*-2.4492*	*1.1619*	*1.3170*
2	*1.1619*	*-3.0042*	*1.6789*
3	*1.3170*	*1.6789*	*-3.3364*

All values are in pu

Table B.5 Values of D_{ij} for the base case of the reduced 3-machine system

Generator	1	2	3
1	*0.2865*	*0.2278*	*0.2252*
2	*0.2278*	*0.4632*	*0.3186*
3	*0.2252*	*0.3186*	*0.9440*

All values are in pu

B.3 Unloaded, Reduced 3-machine Power System

This system is a modification of the reduced 3-machine system and is quite simple and unrealistic. The modification are

- line resistances are set to zero,
- all real and reactive loads are set to zero,
- real power generation is set to zero for each generator.

Since there are no real power loads and no line resistances there are no transfer conductances in the resultant reduced admittance matrix and hence, there are no real losses in the system. Also, since buses 1 and 2 are PV buses and bus 3 is a slack the terminal voltages are set before a power flow calculation is made. These terminal voltages where changed and are shown in Table B.6. Data that is simliar to the data given for the reduced 3-

machine system in Section B.2 is given for this system. Table B.7 contains the values of the reduced admittance matrix (Y_{bus}) and these values are of the form $Y_{ij} = G_{ij} + jB_{ij}$. Since there are no transfer conductances all G_{ij} are zero and thus, so are all D_{ij}. Table B.8 contains the values of the internal bus voltage of each generator. Tables B.9 contains the values of $C_{ij} = E_iE_jB_{ij}$.

Table B.6 Terminal bus voltages for the unloaded, reduced 3-machine system

Generator	Voltage (pu)
1	$1.0550 \angle 0.00°$
2	$1.0350 \angle 0.00°$
3	$1.0400 \angle 0.00°$

Table B.7 Admittance matrix data for the unloaded, reduced 3-machine system

Generator	1	2	3
1	*-j2.2668*	*j1.2252*	*j1.4241*
2	*j1.2252*	*-j2.5398*	*j1.7754*
3	*j1.4241*	*j1.7754*	*-j2.5646*

All values are in pu

Table B.8 Internal generator voltages of the unloaded, reduced 3-machine system

Generator	Voltage (pu)
1	$0.9830 \angle 0.000°$
2	$0.9724 \angle 0.000°$
3	$1.0069 \angle 0.000°$

Table B.9 Values of C_{ij} for the unloaded, reduced 3-machine system

Generator	1	2	3
1	*-2.1904*	*1.1712*	*1.4096*
2	*1.1712*	*-2.4016*	*1.7384*
3	*1.4096*	*1.7384*	*-2.6002*

All values are in pu

APPENDIX C

Table C.1 Machine data and initial generating conditions for the IEEE 50-generator system

Gen. num.	Bus num.	Bus name	Initial real power generation (MW)	Inertia constant H (seconds)	Transient reactance (pu)
1	60	LAK 187A 100	51.0	1.41	0.4769
2	67	BEC 287A 100	1486.0	52.18	0.0213
3	79	MCK1032 100	250.2	6.65	0.1292
4	80	HIG1036S 100	47.0	1.29	0.6648
5	82	CHF1262 100	70.0	2.12	0.5291
6	89	CAN1751T 100	673.0	20.56	0.0585
7	90	AGU1752T 100	22.0	0.76	1.6000
8	91	ARN1754T 100	64.0	1.68	0.3718
9	93	BRU1771318.5	700.0	115.04	0.0240
10	94	CAM17761 100	300.0	17.34	0.0839
11	95	CAR1777T 100	131.0	5.47	0.1619
12	96	CHE17801 100	60.0	2.12	0.4824
13	97	DEC1782T 100	140.0	5.49	0.2125
14	98	DES17831 100	426.0	13.96	0.0795
15	99	DOU1793T 18	200.0	17.11	0.1146
16	100	HOL17961 100	170.0	7.56	0.1386
17	101	LAK18068 100	310.9	12.28	0.0924
18	102	LAM18071 100	2040.0	78.44	0.0135
19	103	LON1815T 100	135.0	8.16	0.1063
20	104	NAN18205 100	2000.0	73.85	0.0122
21	105	PIC18252 100	1620.0	84.39	0.0208
22	106	PIC18263 100	1080.0	56.26	0.0312
23	108	SAU18311 100	800.0	30.43	0.0248
24	109	STW18435 100	52.0	2.66	0.2029
25	110	BRU1853118.5	700.0	115.04	0.0240
26	111	NAN18563 100	2000.0	73.85	0.0122
27	112	LAK18637 100	300.0	12.28	0.0924
28	115	18C2007E 100	2493.0	97.33	0.0024
29	116	18H2016O 100	2713.0	105.50	0.0022
30	117	19B2051R 100	2627.0	102.16	0.0017
31	118	19M20792 100	4220.0	162.74	0.0014
32	119	AK 2152 100	8954.0	348.22	0.0002
33	121	CHA2184G 100	2997.0	116.54	0.0017
34	122	DUN22033 100	1009.0	39.24	0.0089
35	124	HNT2264G 100	3005.0	116.86	0.0017
36	128	BR.24593 100	12963.0	503.87	0.0001
37	130	BER26011 100	5937.0	230.90	0.0010
38	131	CLV2609F 100	28300.0	1101.72	0.0001
39	132	ERI2616. 100	3095.0	120.35	0.0016
40	134	ALL2651 100	20626.0	802.12	0.0003
41	135	BD 26524 100	5982.0	232.63	0.0008
42	137	CAP2655 100	12068.0	469.32	0.0004
43	140	SPP2669H 100	23123.0	899.19	0.0003
44	142	01A2679R 100	24449.0	950.80	0.0003
45	143	03D2699E 100	5254.0	204.30	0.0023
46	144	3BR2719 100	11397.0	443.22	0.0004
47	145	8BO2739 100	14118.6	518.08	0.0018
48	136	CAL26541 100	51950.0	2018.17	0.0001
49	141	VER2674N 100	37911.0	1474.33	0.0001
50	139	SPP2666N 100	56834.0	2210.20	0.0001

Per-unit quantities are based on a *100 MVA* system base

Table C.2 Machine data and initial generating conditions for the NSP 161-generator system

Gen. num.	Bus num.	Bus name	Initial real power generation (MW)	Inertia constant H (seconds)	Transient reactance (pu)
1	39	COOPER1G22.0	772.0	34.60	0.0437
2	53	GENTLM2G24.0	564.1	23.51	0.0297
3	55	GENTLM1G23.0	581.3	29.27	0.0322
4	283	FT CA31G22.0	465.0	28.59	0.0559
5	284	NEBRC31G18.0	585.0	20.67	0.0544
6	287	SUB1253G13.8	90.7	4.25	0.1797
7	288	SUB1254G15.0	239.0	15.69	0.0628
8	415	FTPECK5G13.8	42.0	1.43	0.7891
9	458	GARISN2G13.8	96.0	5.55	0.2322
10	459	GARISN3G13.8	96.0	5.55	0.2322
11	460	GARISN4G13.8	80.0	3.18	0.3815
12	542	BGBND12G13.8	118.0	3.66	0.2624
13	543	BGBND34G13.8	118.0	3.66	0.2624
14	545	BGBND78G13.8	40.4	3.66	0.2624
15	547	FTRDL34G13.8	261.0	9.32	0.1447
16	556	OAHE2-3G13.8	196.0	10.26	0.1189
17	557	OAHE4-5G13.8	196.0	10.26	0.1189
18	575	GAVINS1G13.8	92.0	3.38	0.3850
19	603	ANTEL31G24.0	373.0	15.95	0.0540
20	607	ANTEL32G24.0	380.0	15.95	0.0540
21	611	LELAN32G20.0	235.0	21.91	0.0801
22	618	LARAM31G24.0	424.6	18.98	0.0377
23	748	CENTER2G20.0	309.0	15.95	0.0583
24	749	CENTER1G22.0	234.0	6.90	0.0950
25	815	COYOTE1G24.0	305.0	15.10	0.0633
26	845	HESKET2G13.8	59.8	3.14	0.3639
27	912	BIGSTN1G24.0	379.0	15.10	0.0644
28	1365	THOMSON7 115	64.0	2.20	0.2511
29	1474	BOSWE43G20.9	267.0	11.06	0.0531
30	1475	BOSWE44G22.8	510.6	15.19	0.0515
31	1476	BOSWE71G14.4	45.0	3.06	0.2561
32	1477	BOSWE72G14.4	45.0	3.06	0.2561
33	1521	COAL 41G22.0	531.3	13.21	0.0420
34	1522	COAL 42G22.0	357.4	13.21	0.0420
35	1523	STANT41G18.0	158.1	7.12	0.1302
36	1618	PR IS31G20.0	530.0	20.96	0.0546
37	1619	PR IS32G20.0	530.0	20.96	0.0546
38	1680	MNTCE31G22.0	559.0	23.32	0.0578
39	1681	SHERC31G24.0	707.5	20.08	0.0356
40	1682	SHERC32G24.0	707.5	20.08	0.0356
41	1683	SHERC33G26.0	817.0	24.57	0.0256
42	1780	KING 31G20.0	500.0	24.96	0.0494
43	1781	BLK D71G13.8	39.2	3.41	0.2677
44	1782	BLK D72G13.8	128.9	4.20	0.2000
45	1784	BLK D74G18.0	171.5	7.51	0.2005
46	1785	HIBRD75G13.8	94.7	5.34	0.1855
47	1786	HIBRD76G18.0	170.4	6.89	0.1198
48	1787	RIVRS77G14.0	117.0	2.62	0.2632
49	1788	RIVRS78G22.0	226.8	9.29	0.0996
50	1831	BAYFRNT888.0	62.6	3.94	0.2266

Table C.2 Continued

Gen. num.	Bus num.	Bus name	Initial real power generation (MW)	Inertia constant H (seconds)	Transient reactance (pu)
51	2016	FOXLK53G13.8	60.0	3.04	0.2290
52	2057	LANS5 4G22.0	200.0	8.08	0.1062
53	2058	LANS5 3G22.0	61.0	5.40	0.1370
54	2085	BVRCH52G20.0	165.0	9.02	0.1342
55	2122	GENOA53G24.0	310.0	14.40	0.0840
56	2140	ALMA5 5G14.4	60.0	3.74	0.1990
57	2142	ALMA5 6G24.0	330.0	15.18	0.0772
58	2343	NEAL 3G22.0	1016.5	32.53	0.0206
59	2446	ARNOLD1G22.0	499.0	29.59	0.0535
60	2454	PR CRK4G18.0	100.0	6.65	0.1131
61	2591	CBLUF33G24.0	675.0	19.76	0.0298
62	2605	BURLIN1G20.0	772.0	26.41	0.0231
63	2710	LOUIS31G24.0	764.3	29.20	0.0286
64	2901	MPW 9G20.0	199.2	8.38	0.0710
65	3001	BD 1G14.4	43.0	4.29	0.3604
66	3002	BD 2G14.4	43.0	4.29	0.3732
67	3003	BD 3G16.0	110.0	4.52	0.1464
68	3004	BD 4G16.0	117.0	4.52	0.1464
69	3005	BD 5G15.0	134.0	5.45	0.1236
70	3006	BD 6G18.0	205.4	10.40	0.0840
71	3010	POPLAR1G18.0	575.0	21.87	0.0398
72	3030	SQUAW 1G14.4	290.0	15.14	0.0822
73	3032	SQUAW 5G14.4	60.0	8.08	0.1335
74	3588	JNPG1-6G4.00	244.0	6.67	0.0845
75	3590	KLSY1-7G13.8	200.0	10.76	0.0929
76	3591	GRSTC12G13.8	290.0	25.35	0.0437
77	3595	PNFL1-6G13.8	69.0	2.53	0.4043
78	3596	GTFL1-6G11.0	106.0	3.06	0.2460
79	3598	7SIS1-6G11.0	100.0	5.47	0.1861
80	3600	SLFL1-8G6.90	48.0	2.49	0.4075
81	4015	QUAD Y1G18.0	1538.0	69.57	0.0192
82	4850	HAVANA 138	8889.9	517.56	0.0025
83	4852	EDGEWATE 345	3452.8	191.59	0.0064
84	4885	GRAND TW 138	315.0	24.67	0.0514
85	4888	MARION 69.0	188.6	14.78	0.0859
86	4889	JOPPA N 161	1014.5	79.47	0.0160
87	4890	JOLIET 345	2168.0	169.82	0.0075
88	4891	CRAWFORD 345	773.5	60.59	0.0209
89	4892	WAUKEGAN 138	750.0	58.75	0.0216
90	4894	TECHE 4 138	8820.9	703.46	0.0018
91	4903	ZION 345	1040.0	45.12	0.0417
92	4905	BRAIDWD 345	1090.0	56.75	0.0276
93	4949	ROCK RIV 138	11594.5	714.39	0.0027
94	4963	NELSON D 138	185.0	15.94	0.4122
95	4964	PULLIAM 115	199.0	69.10	0.2986
96	4966	WESTON 345	386.0	21.26	0.0664
97	4970	DRESDEN 138	772.0	170.08	0.0553
98	4971	DRESDEN 138	773.0	170.08	0.0470
99	4972	NEWTON 138	648.0	85.04	0.0209
100	4986	ZION 345	1040.0	45.12	0.0417

Table C.2 Continued

Gen. num.	Bus num.	Bus name	Initial real power generation (MW)	Inertia constant H (seconds)	Transient reactance (pu)
101	4987	POWERTON 345	1358.0	51.58	0.0126
102	4993	BRAIDWD 345	1090.0	56.75	0.0276
103	4994	POINT BE 345	1500.0	62.11	0.0277
104	5007	IATAN 7 345	11565.3	786.72	0.0019
105	5870	DOLHIL 6 230	3053.2	231.03	0.0053
106	5871	LEWIS 4 138	4627.8	351.18	0.0035
107	5872	CON-W 5 161	1543.0	116.75	0.0105
108	5873	LKPAUL 269.0	41.2	3.12	0.3930
109	5874	PENSA 269.0	2354.8	180.71	0.0068
110	5875	RIVSIDE4 138	4133.9	312.81	0.0039
111	5876	NC 230 6 230	1223.8	92.60	0.0132
112	5877	SOONR4 138	2587.6	195.80	0.0063
113	5878	ARSHILL4 138	3068.1	257.38	0.0048
114	5879	OZARK S269.0	764.0	57.80	0.0212
115	5880	HUGO PP4 138	496.0	37.53	0.0327
116	5882	STOCKTN5 161	60.0	4.54	0.2700
117	5883	BULL SH5 161	891.0	67.42	0.0182
118	5884	SIKESTN5 161	177.0	13.39	0.0915
119	5888	PARSONS4 138	172.8	14.03	0.0874
120	5891	OZ DAM 5 161	386.0	31.02	0.0395
121	5892	NEWMAD 5 161	600.0	45.40	0.0270
122	5960	NEASN 7 345	900.0	135.31	0.0223
123	5961	GILL 4 138	195.4	83.99	0.0689
124	5970	SOONR7 345	1014.4	125.98	0.0151
125	5971	NEWMAD 7 345	592.0	121.32	0.0616
126	5977	LAKE RD5 161	203.0	30.33	0.1525
127	5981	NEASN 4 138	630.0	116.65	0.0519
128	5984	ISES 8 500	790.0	165.64	0.0357
129	5985	WH BLF 8 500	1580.0	132.98	0.0179
130	5986	ARKNU 8 500	1628.1	177.31	0.0255
131	5987	GGULF 8 500	2424.0	298.62	0.0176
132	5988	WILSON 8 500	601.0	291.62	0.0644
133	5989	CAJUN2 8 500	1554.7	279.96	0.0163
134	6534	LAMBTON 220	1040.0	78.37	0.0135
135	6536	BECK2 DK 220	863.0	40.43	0.0284
136	6552	ST LAWRE 220	832.0	30.43	0.0245
137	6609	ATIKOKAN18.0	171.0	15.85	0.1000
138	6900	8BROWNFR	4449.2	207.92	0.0051
139	6935	06KYGER	15388.5	1041.38	0.0010
140	6936	10CULLEY	3249.4	215.13	0.0049
141	6937	07MEROM	16372.6	1075.13	0.0010
142	6939	04ASHTBL	5519.3	362.44	0.0029
143	6940	05OPOSSC	13638.2	935.52	0.0011
144	6941	05DUMONT	5273.9	366.44	0.0029
145	6942	18ALCONA	14820.0	973.18	0.0011
146	6944	LINDEN G	4886.4	320.87	0.0033
147	6945	8BOWEN8	16486.9	1085.91	0.0010
148	6946	8HATCH8	10663.1	700.21	0.0015
149	6947	6BARRY	5328.4	349.90	0.0030
150	6948	6CAPE K	11348.7	745.22	0.0014

Table C.2 Continued

Gen. num.	Bus num.	Bus name	Initial real power generation (MW)	Inertia constant H (seconds)	Transient reactance (pu)
151	6949	6A M WIL	6893.3	453.39	0.0023
152	6950	ALLEN	15871.1	1142.92	0.0009
153	6951	3CAROLNA	13154.9	917.04	0.0012
154	6952	5PARADIS	10007.0	678.13	0.0016
155	6953	ORRINGTN	13883.6	911.69	0.0012
156	6954	ESSEX	6894.6	452.75	0.0023
157	6955	E RIVER	7461.0	503.91	0.0021
158	6956	BRDR CTY	9733.1	640.30	0.0017
159	6502	PINARD J 220	15507.3	1271.19	0.0013
160	6938	01FTMART	24269.5	1596.32	0.0007
161	6943	PEACH BT	35308.8	2329.88	0.0005

Per-unit quantities are based on a *100 MVA* system base